STUDIES OF FOIL WOUND COMPONENTS

by

NICHOLAS JAMES WALKER

A Doctoral Thesis
Submitted in partial fulfilment of the
requirements for the award of
Doctor of Philosophy of the Loughborough
University of Technology
July 1979

Supervisor: Dr.P.N.Murgatroyd
Department of Electronic and
Electrical Engineering

List of Contents

Acknowledgements

My sincere thanks goes to my supervisor Dr. P. N. Murgatroyd for his inspiration and encouragement. My thanks also goes to the staff of the Electronic and Electrical Engineering Department and the Computer Centre for their assistance.

The work was supported by the Science Research Council.

Chapter 1 Introduction

1) Aluminium in Transformers

Copper has long been the traditional material used in the winding of transformers. Copper wire has a high conductivity, second only to Silver, and being malleable is easily wound. These factors combine to make Copper an obvious choice for the majority of electrical applications.

Copper forms an estimated 0.007% of the earth's crust, about 70% of this occuring in a limited number of deposit types in a few locations. The major producers are the United States with 21% of the world's production; the Soviet Union with 15%, Zambia with 10%, Chile with 10%, and Zaire with 6%. Thus 16% of the world production of Copper is concentrated in central Africa, which has been beset with serious political upheavals since the early nineteen sixties. These upheavals have interrupted production of Copper and led to wildly fluctuating world prices. Poor labour relations also disrupt the supply of Copper, strikes accounting for shortness of supply more so with Copper than with any other of the non-ferrous metals (1). Another factor adversly affecting the supply of Copper is that it is a "strategic material" used in munitions, so that Government stockpiling during military emergencies has often caused major fluctuations in demand (2).

By contrast Aluminium forms an estimated 8% of the earth's crust. The principal Aluminium ore, Bauxite, occurs in large deposits in: United States, Caribbean, Northern South America, Hawaii, Australia, India, Indonesia, Malaysia, China, Soviet

Union, Ghana, Greece, Yugoslavia, Hungary, Italy and France. The wide distribution of Aluminium ore together with the fact that 97% of the smelting of the ore is carried out in the Developed countries (3) make the world price of Aluminium much more stable than that of Copper. Fig. 1-1 shows the variation in the price of Aluminium and Copper during the twenty year period from 1947 to 1967 (4). This graph does not tell the whole story. Although Aluminium has only 60% of the conductivity of Copper, Copper is 300% denser, thus Aluminium can be twice the price of Copper by weight and still be competitive in terms of its electrical conductivity. The graph in Fig. 1-1 shows that the price of Aluminium by weight was approximately the same or less than the price of Copper over the twenty year period.

Despite this price advantage Aluminium has been regarded as an inferior substitute for Copper. The first recorded instances of the use of Aluminium for transformer winding were in Germany in 1917 (5) and in France about the same time (6). This use of Aluminium was due to the shortage of Copper during the First World War. A similar shortage occured during the Second World War when Aluminium was again used as a substitute (7,8). After the war when Copper again became available transformers wound with Aluminium were often rewound with Copper.

Despite this attitude research continued into the use of Aluminium for transformer winding. The basic problem is that Aluminium has only 60% of the conductivity of Copper therefore a transformer wound in the traditional manner using round Aluminium wire in place of round Copper wire has to be larger to achieve the same performance. This increase in size offsets the initial cost advantage of Aluminium. However, methods have

Figure 1-1

Variation in the price of Aluminium and Copper
1947-1967

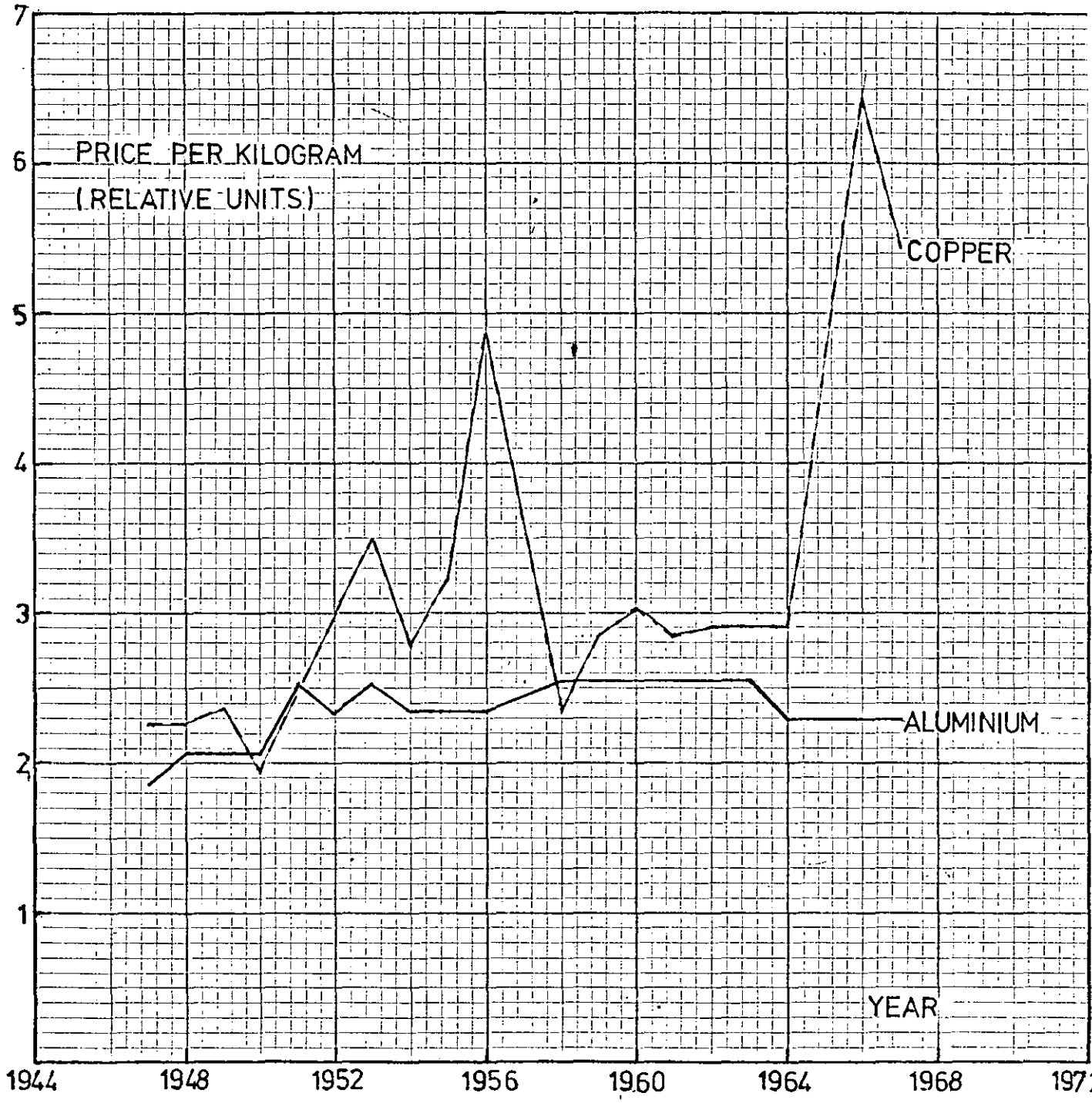

been evolved which reduce the size disadvantage of Aluminium. The principal method is the use of Aluminium foil or strip in place of wire (9,10). Fig. 1-2 illustrates how this is achieved. With strip or foil superfluous insulation within the winding is eliminated, also the thickness of the inter-foil insulation can be reduced because the insulation need only withstand the turn-to-turn voltage. Wire wound transformers are wound in layers therefore the insulation on the wire has to withstand the maximum layer-to-layer voltage, which is equal to the turn-to-turn voltage times twice the number of turns per layer, or alternatively layer insulation may be used. The use of strip or foil eliminates the need for layer insulation.

The space-factor or ratio of the conductor cross-section to the total cross-section is approximately 90% for a strip or foil wound transformer compared with 50% to 60% for a wire wound transformer (10). This improvement in the space-factor increases as the ratio of insulation thickness to conductor thickness decreases, so that the use of Aluminium strip or foil as a replacement for Copper wire tends to be more competitive for large transformers than for small ones.

In addition foil or strip windings are almost self-supporting therefore the bobbin flanges are not needed in some cases, also the bobbin former need not be as strong.

Heat generated within a strip or foil wound transformer is dispersed efficiently. Each turn has its own heat path to the surface of the winding and more of the winding is metal ensuring a more even temperature distribution and the elimination of "hot spots", which effectively increases the rating of the winding.

Figure 1-2

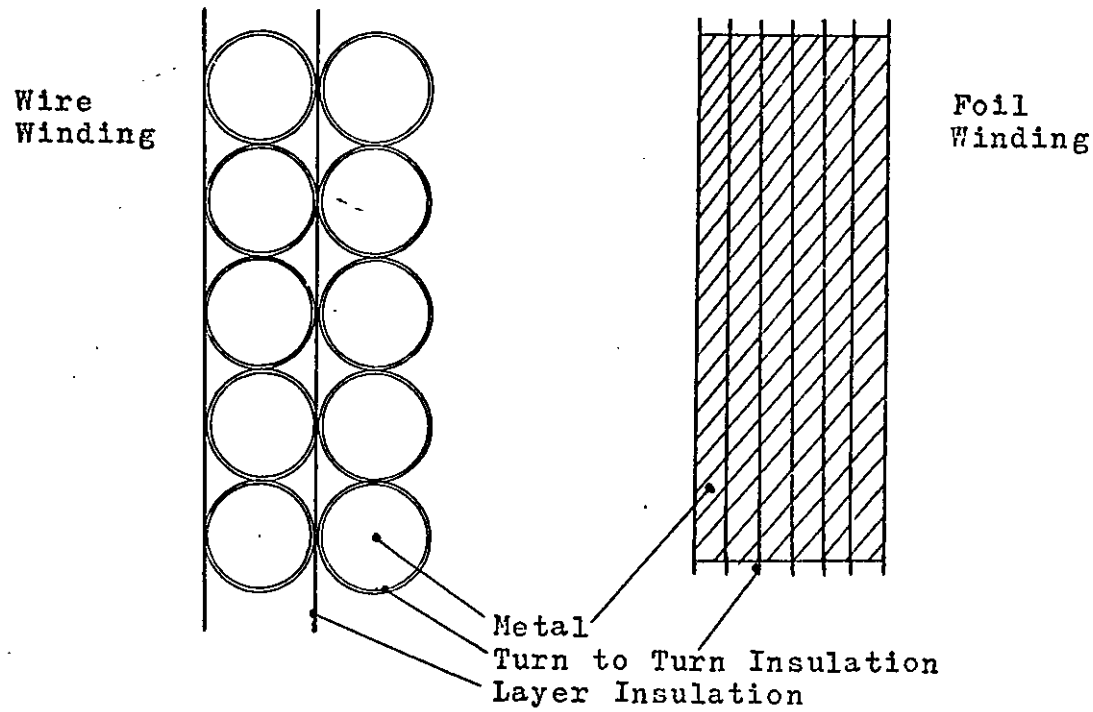

Comparison: Showing the difference between wire and foil windings.

Figure 1-3

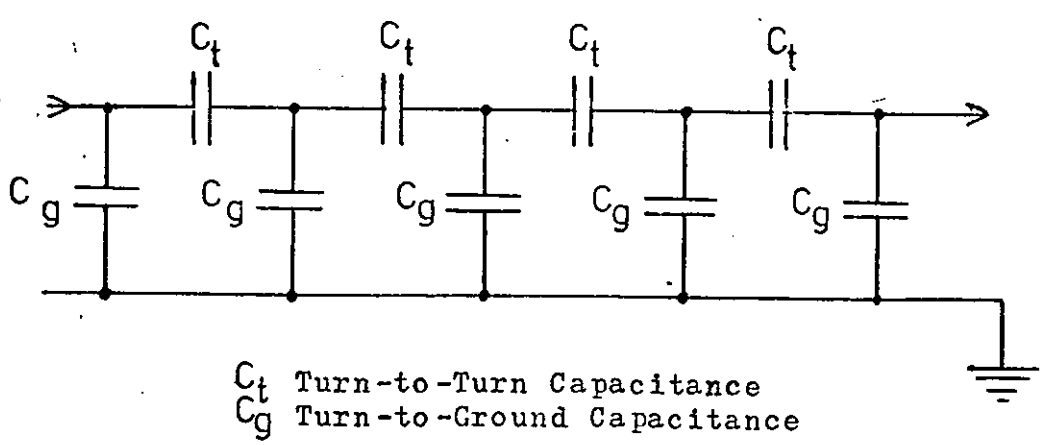

C_t Turn-to-Turn Capacitance
C_g Turn-to-Ground Capacitance

The capacitances of a single layer wire wound coil.

Insulation in a foil or strip wound transformer may be a paper or polymer film interleaved with the metal during winding or a layer of varnish, resin or oxide on the Aluminium foil itself (11,12,13,14). After winding, the paper or film insulation is impregnated with varnish to prevent moisture penetration. Varnish or resin can be applied to the foil before winding and after winding can be heated to make the winding one solid mass. Anodising increases the thickness of the oxide layer on the Aluminium strip or foil until it is usable as insulation. This is the thinnest insulation and will withstand high temperatures.

The use of strip or foil windings has two technical advantages. The first is that transformers wound with strip or foil are more resistant to impulse breakdown (4,12,14). Fig. 1-3 represents the capacitances of either a single layer wire winding or a multi-layer strip or foil winding. C_t is the turn-to-turn capacitance and C_g the turn-to-ground capacitance. These capacitances form a ladder network. When an impulse voltage is applied to the beginning of the network it will travel down the ladder. The degree of attenuation it undergoes is determined by the ratio of C_t to C_g . A foil or strip wound transformer has a large ratio while a wire wound transformer has a smaller ratio. Thus in a wire wound transformer an impulse voltage will be attenuated more severely than in a strip or foil wound transformer and consequently the insulation on the turns at the beginning of the winding will be subject to more dielectric stress than the turns in a strip or foil wound transformer.

The second technical advantage is that strip or foil

wound transformers are not so susceptible to short circuit current damage as wire wound transformers (4,12,15,16). A comparison of the axial forces generated in a transformer with a wire secondary and in a transformer with a strip or foil secondary is shown in Fig. 1-4. Under short circuit conditions the helicity of the wire secondary generates axial forces which can damage the winding whereas in the foil secondary the current can flow at whatever axial position is required to balance the ampere turns of the other winding.

For many years one of the biggest problems facing the designer was that of making joints and connections to the Aluminium winding. This problem has now largely been solved and a variety of methods evolved: clamping; crimping, cold-pressure welding; soldering; brazing; inert-gas welding; ultra-sonic bonding (4,11,14,15,17,18,19,20,21,22).

Figure 1-4

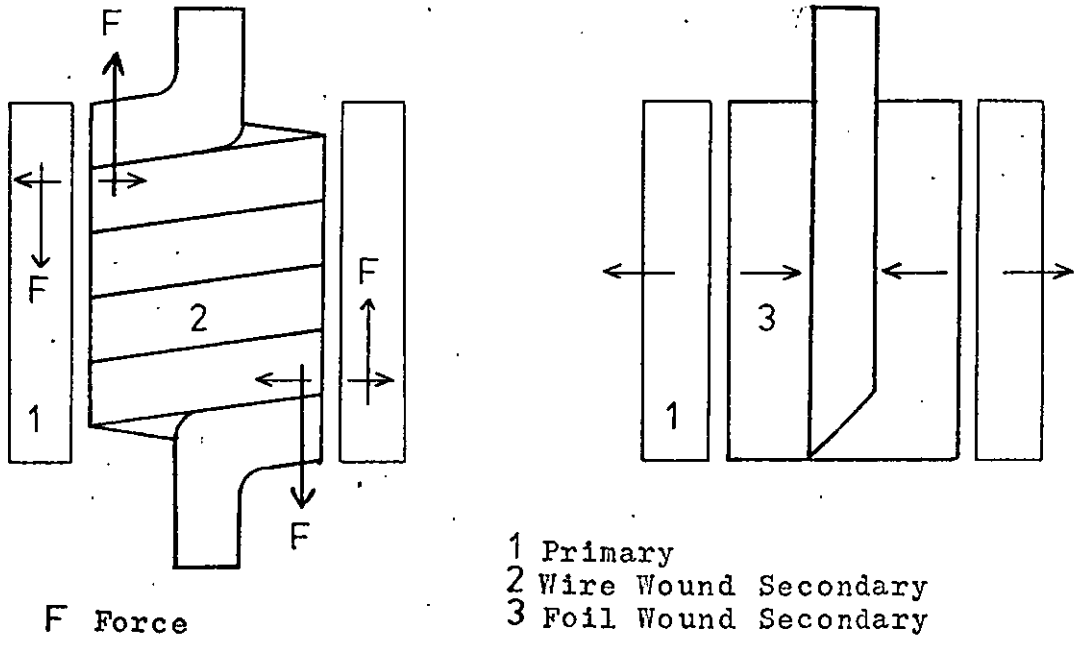

F Force

1 Primary
2 Wire Wound Secondary
3 Foil Wound Secondary

Comparison: Showing the different short circuit forces on coils with wire wound secondaries and with foil wound secondaries.

Chapter 2 Self-Resonance in Small Foil-Wound Inductors

1) Introduction

Research into the properties of small air-cored, foil-wound inductors began at the Plessey Company in 1972. This interest began as part of a study of the inductance of foil-wound capacitors. The high-frequency response of filters and suppressors using these capacitors could not be predicted from simple theories that neglected this inductance. It was thought that an understanding of the inductance of foil-wound inductors would provide a basis for an understanding of the inductance of foil-wound capacitors. The work (23) resulted in a computer evaluated formula which could accurately predict the low-frequency inductance of a foil wound inductor. The work also included an experimental investigation of the variation of inductance with frequency for several air-cored, foil-wound inductors. This investigation showed that with increasing frequency the inductance at first declined by approximately ten percent from the low frequency value then increased rapidly to a maximum value. The maximum in the inductance can be accounted for using the high-frequency equivalent circuit of Welsby (24). This equivalent circuit is shown in Fig. 2-1 and consists of an inductor in series with a resistor, with both shunted by an effective capacitance. The circuit has an impedance maximum at the resonant frequency. Below resonance the circuit behaves as an inductance and above as a capacitance. The drop in inductance at lower frequencies is due to a combination of skin effect and proximity effect acting within the turns of the coil. This effect is discussed in detail in chapter 3.

Figure 2-1

Normal high-frequency equivalent circuit of a wire wound inductor.

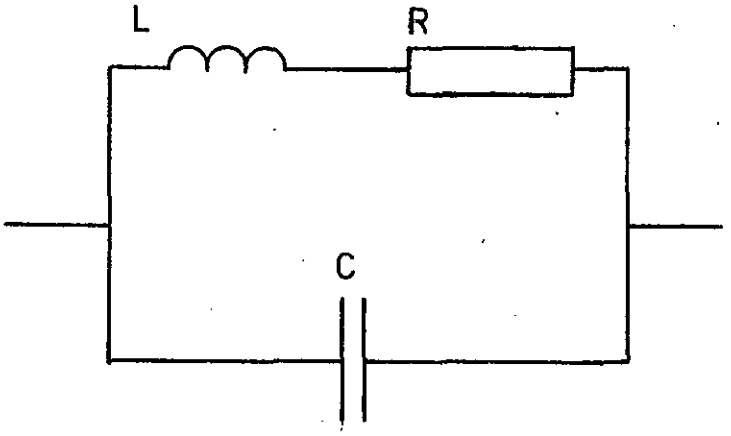

The resonant frequency is given by

$$F_o = \frac{1}{2\pi\sqrt{LC}}$$

The Q of the circuit is given by

$$Q = \frac{1}{R}\sqrt{\frac{L}{C}}$$

The experimental investigation at the Plessey Company also showed that some foil-wound inductors had a second resonance at a higher frequency. This behaviour cannot be explained using the simple equivalent circuit of Welsby, although Welsby does state that some types of single layer coil can exhibit secondary resonances or multiple resonance, which he considers is due to the inductor behaving as a transmision line.

2) Manufacture of Small Foil Wound Inductors (FWI)

Four small foil wound inductors are shown in the photograph in Fig. 2-2. These coils are wound from Aluminium foil with a width of 3.9 cm and a thickness of 5.0 μm, and a polypropylene film with a thickness of 12.5 μm. These coils were wound on the converted capacitor winding machine shown in the photograph in Fig. 2-3. Most of the small foil wound devices investigated in this thesis were wound on this machine. The cores of these devices were made by winding up the plastic insulation to the required depth at which point the Aluminium foil was inserted. The contacts were made from strips of 50 μm Aluminium foil which were inserted at the appropriate points during winding and were held in place by the pressure of the winding. Several FWI were manufactured using 50 μm thick Aluminium foil and the contacts to these coils were made by cutting and folding the metal foil in the manner shown in Fig. 2-4.

All the small FWI manufactured were heat treated in an electric oven at 120°C for 1 hour. This treatment causes the plastic foil to shrink preventing any creepage of the winding under its own tension. Heat treatment also reduces the air gap between the plastic film and the metal foil. The effect of this

Figure 2-2

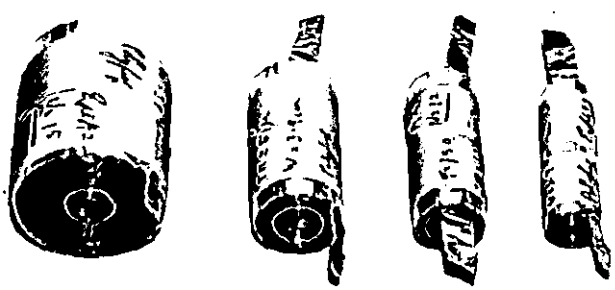

Four Foil Wound Inductors with, from left to right, 1000 Turns, 200 Turns, 50 Turns and 10 Turns
The line on the photograph is 10 cm long.

Figure 2-3

Capacitor Winding Machine Converted to a Coil Winding Machine

Figure 2-4

Method of cutting and folding foil to form a terminal

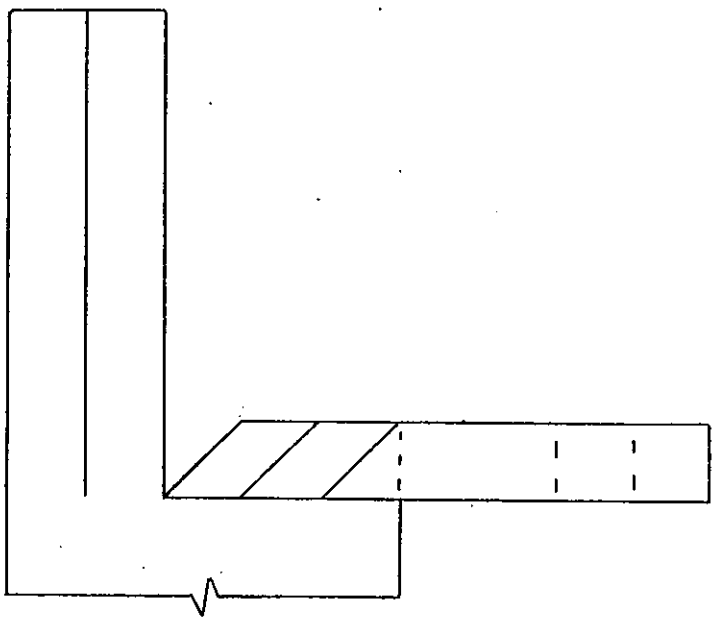

Figure 2-5

a/ Method of impedance/frequency spectrum measurement

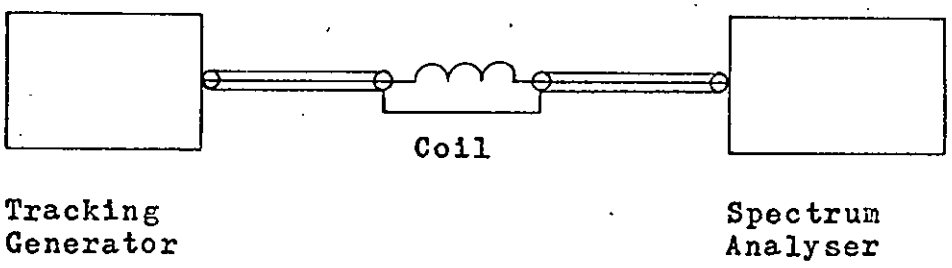

b/ Voltages and impedances associated with Fig. 2-5a

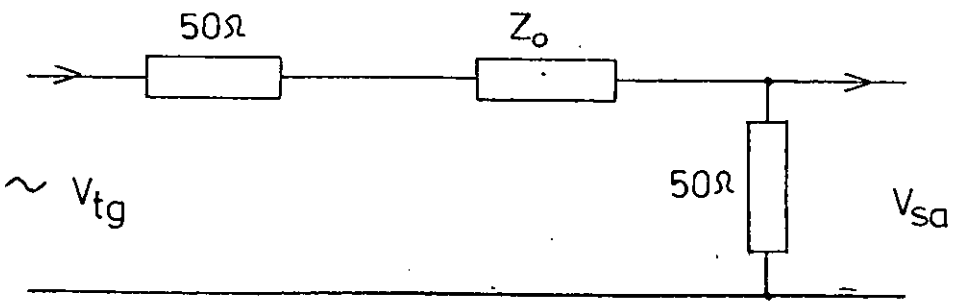

heat treatment on the capacitance of the FWI's is discussed in section 2-8.

3) Methods of Impedance Spectrum Measurement

One of the quickest methods of measuring the impedance/frequency spectrum of a wire or foil wound inductor is to use a spectrum analyser in conjunction with a tracking generator. The coil is connected in series between the tracking generator and the spectrum analyser in the manner shown in Fig. 2-5a. The photograph in Fig. 2-6 shows this equipment in use. The frequency of the output from the tracking generator is locked to the swept frequency of the spectrum analyser so that they can be swept in synchronism from 100 KHz to 110 MHz with an accuracy of ±50 Hz. This arrangement has a dynamic range of 190 dB. The impedances associated with the tracking generator, coil and spectrum analyser are shown in Fig. 2-5b. The output impedance of the tracking generator is 50Ω as is the input impedance of the spectrum analyser. The impedance of the coil is Z_o, the output voltage from the tracking generator is V_{tg} and the input voltage to the spectrum analyser is V_{sa}. V_{sa} is related to V_{tg} by

$$V_{sa} = \frac{50 V_{tg}}{100 + Z_o} \qquad 2\text{-}3\text{-}1$$

The photograph in Fig. 2-7 shows the impedance/frequency spectrum of a 100 μH wire wound inductor from 100 KHz to 10 MHz. The flat trace at the top of the photograph is the spectrum obtained with the coil shorted out, the lower trace is the spectrum with the coil in circuit. The spectrum has a minimum at 3.311 MHz and as the spectrum analyser measures power

Figure 2-6

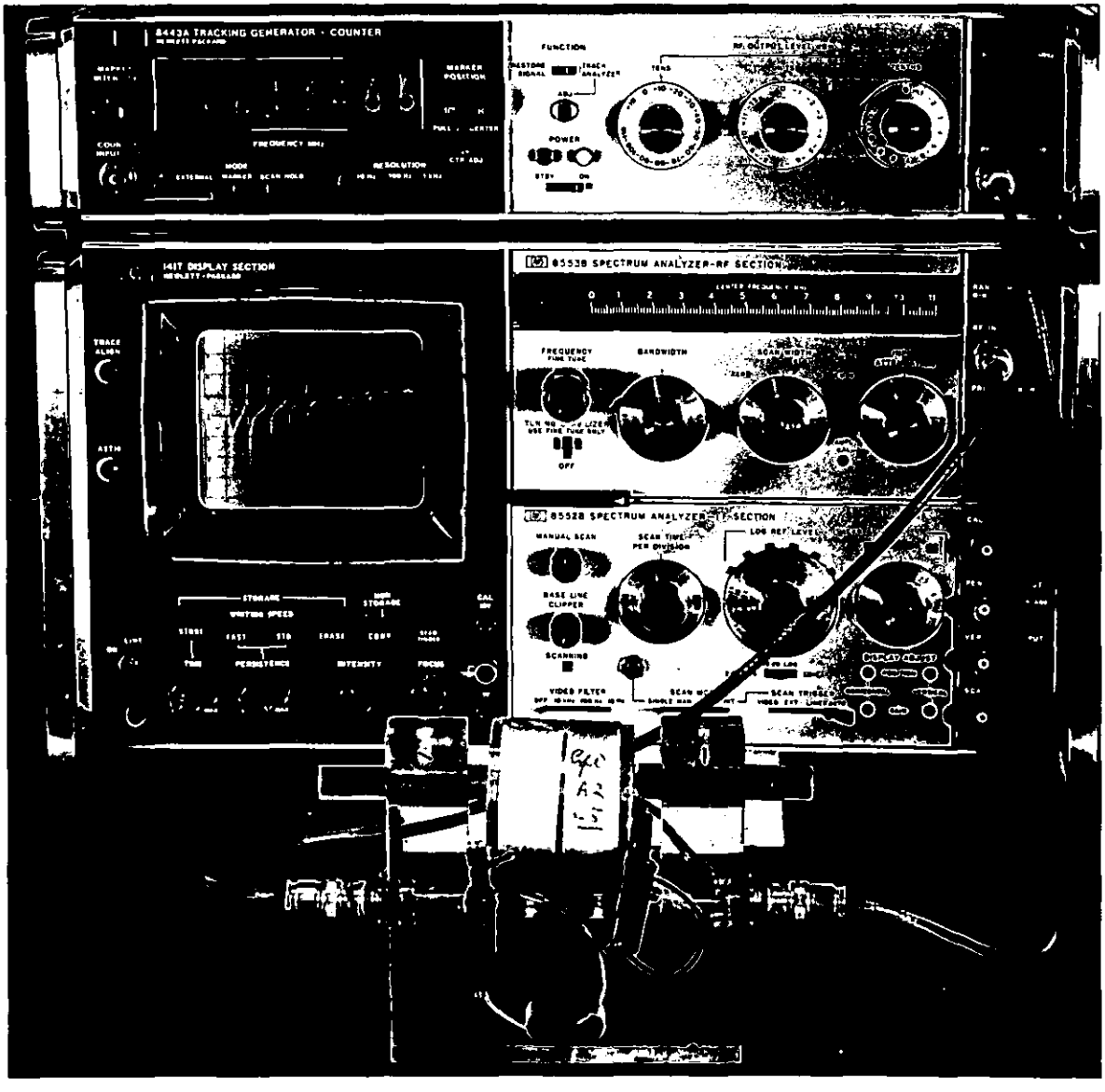

Tracking Generator and Spectrum Analyser Measuring the Impedance/Frequency Spectrum of a 1000 Turn Foil Wound Inductor

Figure 2-7

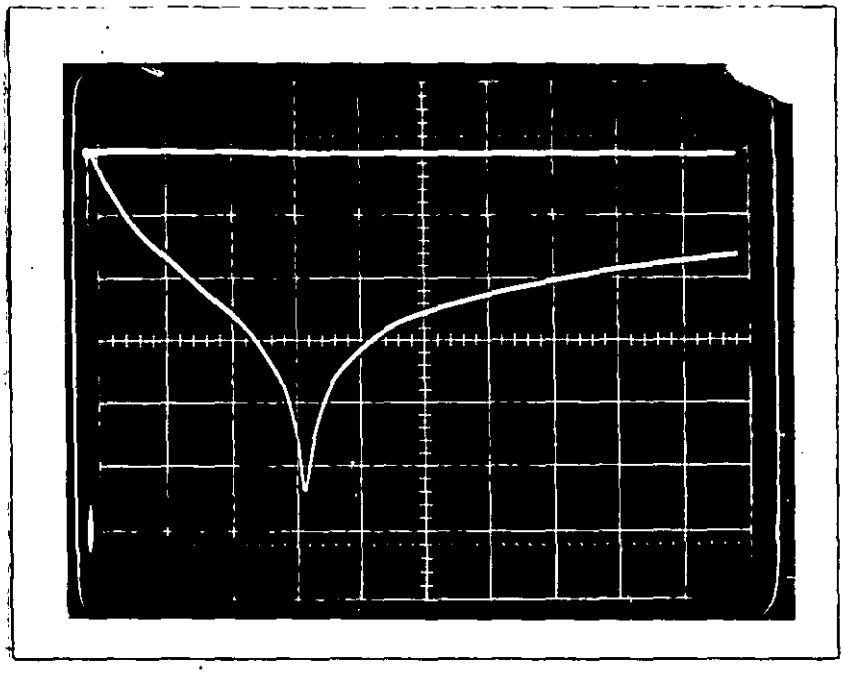

Impedance/frequency spectrum of a 100 μH wire wound inductor
Abscissa: 1 MHz per square, range 100KHz-10MHz
Ordinate: 10 dB attenuation per square, zero at top

Figure 2-8

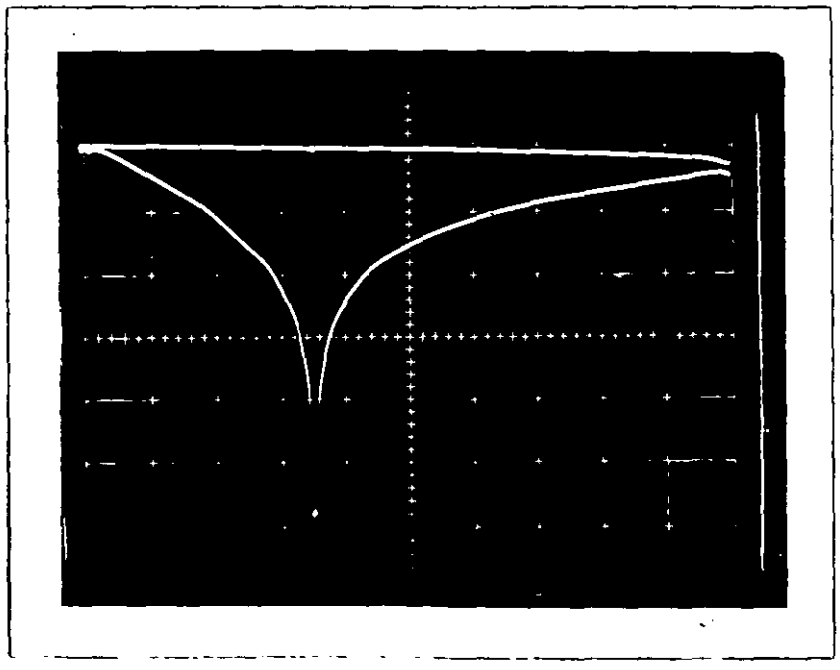

Impedance/frequency spectrum of a 50 turn foil wound inductor
Abscissa: 2 MHz per square, range 100KHz-20MHz
Ordinate: 10 dB attenuation per square, zero at top

the impedance of the coil has a maximum at this frequency. This resonance is due to the self-capacitance of the wire wound inductor resonating with the inductance.

The spectrum analyser measures power in dBm, therefore if the input voltage to the spectrum analyser is $\frac{1}{2} V_{tg}$ when the coil is shorted out and V_{sa} when it is in circuit, then the difference in the power levels measured by the spectrum analyser with the coil in circuit and with it shorted out is given by

$$V_m = 20\text{Log}\left(\frac{|V_{tg}|}{2\,|V_{sa}|}\right) \qquad 2\text{-}3\text{-}2$$

Where V_m is the difference in the power levels measured in dBm. Combining equations 2-3-1 and 2-3-2 gives

$$V_m = 20\text{Log}\left(\frac{|100 + Z_o|}{100}\right) \qquad 2\text{-}3\text{-}3$$

Assuming that $Z_o \gg 100$ gives the impedance of the coil as

$$|Z_o| = 10^{\frac{V_m}{20}} \times 100 \qquad 2\text{-}3\text{-}4$$

The impedance/frequency spectrum of the 50 turn foil wound inductor shown in Fig. 2-2 is shown in the photograph in Fig. 2-8. This spectrum only shows one resonance at 7.073 MHz. However, the impedance/frequency spectrum of the 1000 turn FWI shown in the photograph in Fig. 2-9 is markedly different. There are impedance maxima at 0.514 MHz, 1.344 MHz, 2.232 MHz and 3.218 MHz, and impedance minima at 1.240 MHz, 2.165 MHz, 3.150 MHz. This form of behaviour has been termed "multiple resonance" Wire wound inductors do not exhibit this form of behaviour

Figure2-9

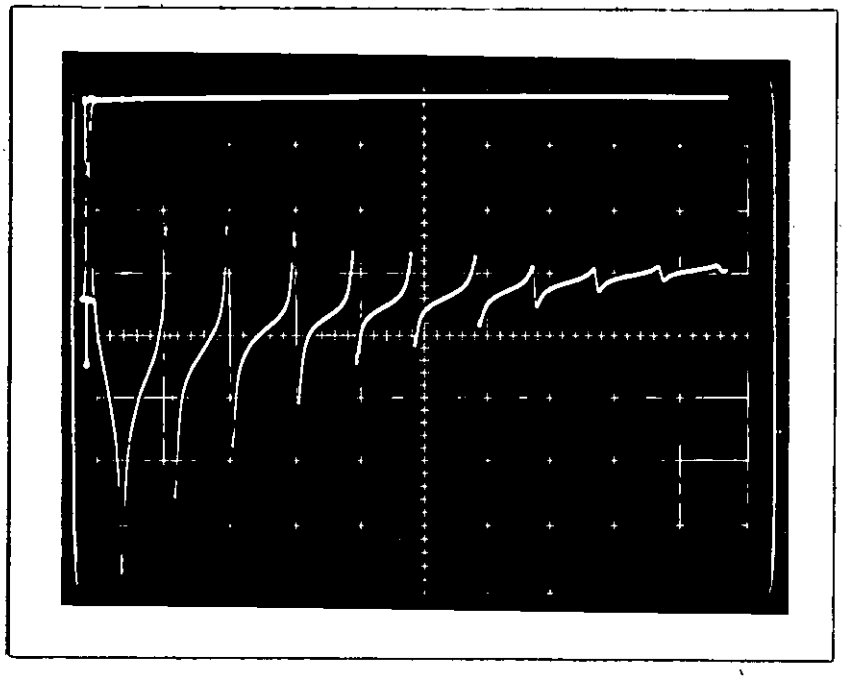

Impedance/frequency spectrum of a 1000 turn foil wound inductor
Abscissa: 1 MHz per square, range 100KHz--10MHz
Ordinate: 10dB attenuation per square, zero at top

normally, except for the particular type of single layer coil described by Welsby.

4) Computer Model of a Foil Wound Inductor

A field theory solution may seem the most direct method of solving this problem, but the difficulties involved can be illustrated by considering the size of the matrix required for a finite difference scheme using the vector potential $\underline{A}$. If each turn is divided into a mesh of size 10 round the circumference and 10 across the width, a 1000 turn foil wound inductor would require a matrix of size 10^5, and as $\underline{A}$ is a vector each cycle of the iteration would require 3×10^5 calculations. An iteration would require anything up to 100 cycles to complete and would only give one point on the impedance/frequency spectrum. In view of these diffulties an equivalent circuit model was adopted.

The lumped element equivalent circuit of a foil wound inductor is based on the assumption that each turn has a self-inductance L^t, a resistance R^t, a turn-to-turn capacitance C^t and mutual-inductance to all other turns. The arrangement of the inductances, resistances and capacitances is shown in Fig. 2-10a, and by considering the way they are arranged around the point A in Fig. 2-10a the linear circuit of Fig. 2-10b can be derived. In Fig. 2-10a and 2-10b the turn self inductances and resistances have been split into two to make the derivation of Fig. 2-10b clear.

For an N turn foil wound inductor there will be N-1 turn-to-turn capacitances, therefore the equivalent circuit should consist of N-1 resonant circuits, each consisting of a turn-

Figure 2-10

a/

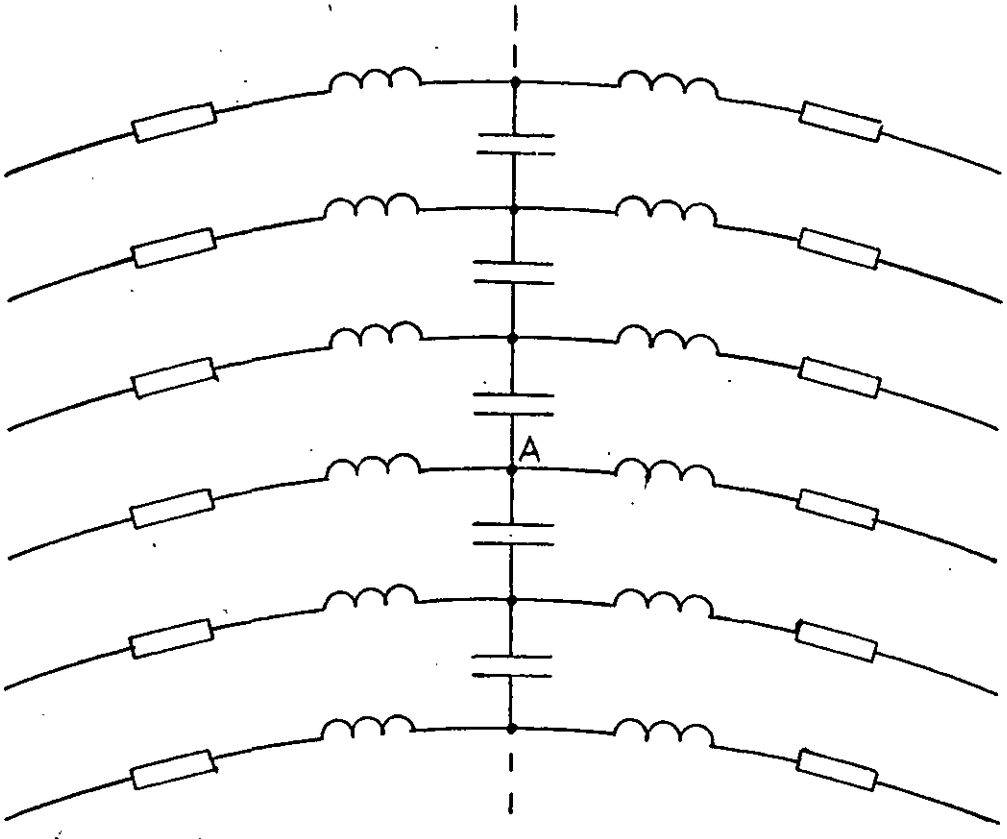

Arrangement of the turn inductances, capacitances and resistances within a foil wound inductor.

b/

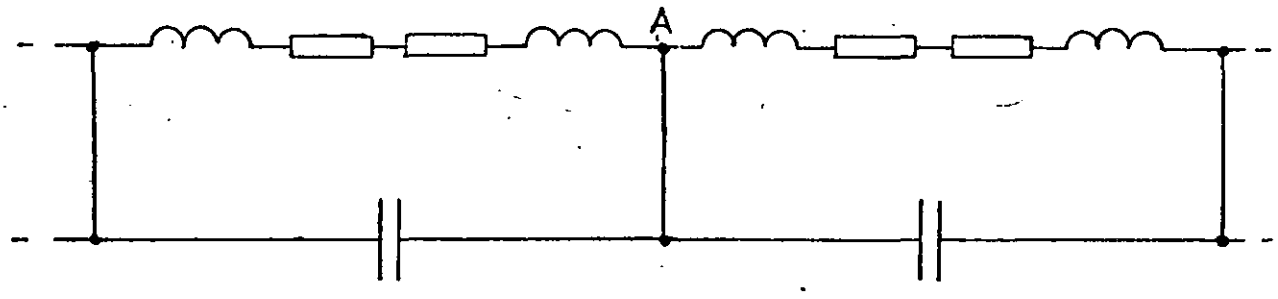

Alternative arrangement of the turn inductances, capacitances and resistances.

inductance in series with a turn-resistance paralled by a turn-to-turn capacitance, plus a half-turn section at each end. All the resonant circuits are coupled by mutual-inductances. To simplify the theory the equivalent circuit will be taken to consist of N resonant circuits and not N-1 , for a foil wound inductor with a large number of turns this represents a small error.

This model of a foil wound inductor is based on the following assumptions; that any capacitances other than the immediate turn-to-turn capacitances can be neglected, and that for the frequencies under consideration the system is "electrically short", meaning that the time for light to cross the FWI is short compared with the period of the excitation. There are also problems connected with the definition of the self-inductance of a foil turn, due to non-uniform current flow across the width of the foil (25). This effect is discussed in detail in chapter 3 and only appears to have a marginal effect on the inductances used in the model.

It has been shown by Murgatroyd (26) that by making suitable approximations the lumped element equivalent circuit can be derived as an approximation to the field theory approach, starting from the vector potential $\underline{A}$. The basis of this approximation is the assumption that the phase gradient, which must be continuous through the coil, is zero round each turn. This can be done provided there is a suitable discontinuity of phase between adjacent turns.

However, the equivalent circuit of Fig. 2-10b is still too large to be manipulated satisfactorily. It can be reduced

by dividing it into S sections each with d turns (N=Sd), and making the following assumptions: that the current throughout each section is uniform in magnitude and phase; that L^t , R^t and C^t are uniform throughout each section; that the mutual-inductance linking any two turns within a section are equal to the turn-inductance of that section; that the mutual-inductance linking each turn of one section with each turn of another section are all equal.

L_i^t , R_i^t and C_i^t are the turn-inductance, turn-resistance and turn-to-turn capacitance of the ith section based on its mean radius. Given the above approximations these are related to the self-inductance, resistance and capacitance of the ith section by

$$L_i = d^2 L_i^t \qquad 2\text{-}4\text{-}1$$

$$R_i = d R_i^t \qquad 2\text{-}4\text{-}2$$

$$C_i = \frac{C_i^t}{d} \qquad 2\text{-}4\text{-}3$$

If the mutual-inductance linking the average turn of the ith section to the average turn of the kth section is $M_{i,k}^t$ then the mutual-inductance linking the ith and kth sections is given by

$$M_{ik} = d^2 M_{i,k}^t \qquad 2\text{-}4\text{-}4$$

The S section equivalent circuit is shown in Fig. 2-11. This circuit results in S mesh equations of the form

Figure 2-11

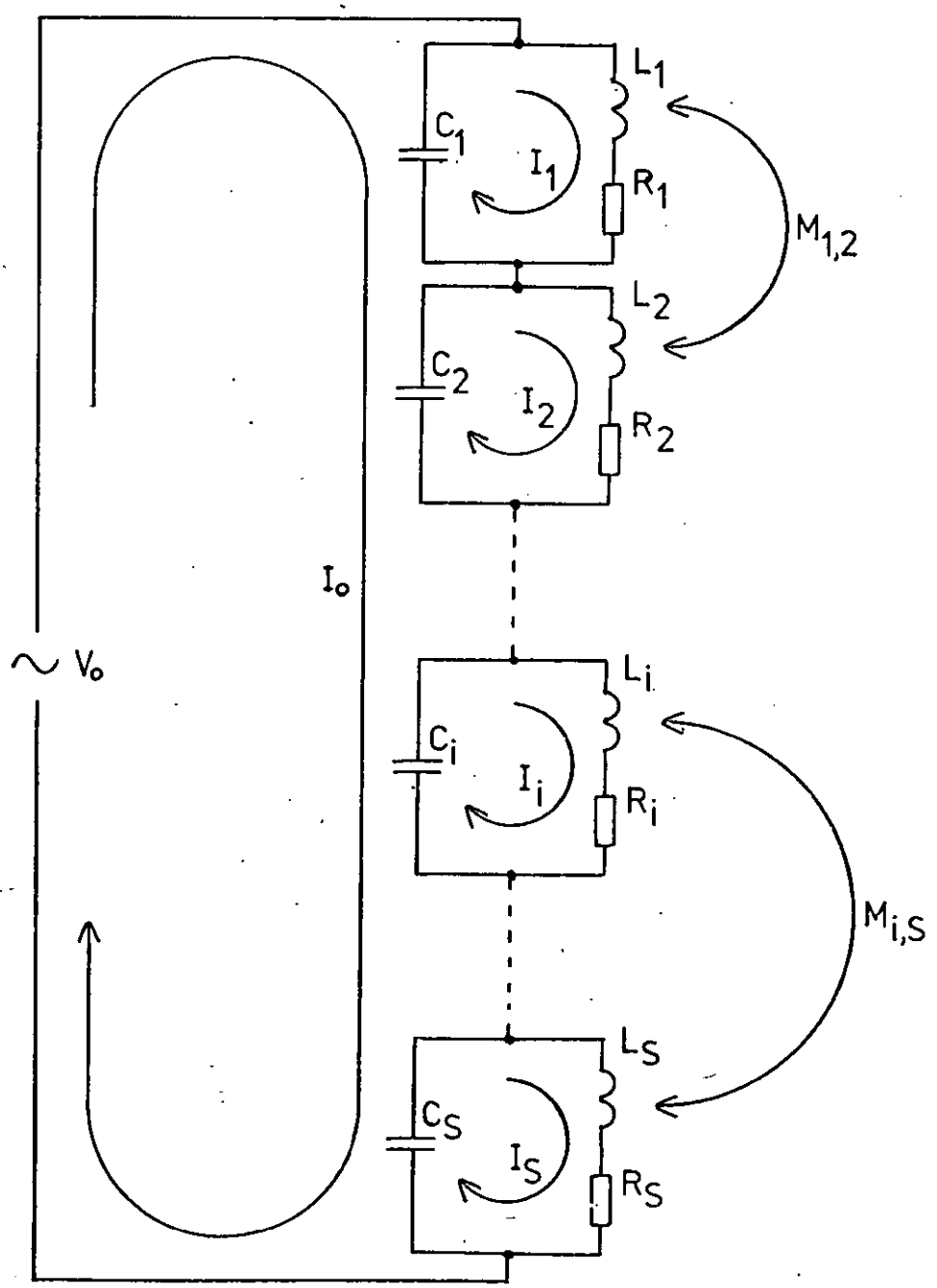

Equivalent Circuit of a Foil Wound Inductor

All inductors are mutually coupled

$$j\omega M_{i,1}q_1 + j\omega M_{i,2}q_2 + - - - - + (R_i + j\omega L_i + \frac{1}{j\omega C_i})q_i +$$

$$- - - - - - - + j\omega M_{i,s}\, q_s = \frac{1}{j\omega C_i} \qquad 1 \leq i \leq S \qquad 2\text{-}4\text{-}5$$

Where ω is the angular frequency and $q_i = \frac{I_i}{I_o}$ is the ratio of the current in the i th section I_i to the external current I_o.

For the external circuit

$$\frac{V_o}{I_o} = Z_o = \sum_{i=1}^{S} \frac{(1 - q_i)}{j\omega C_i} \qquad 2\text{-}4\text{-}6$$

If all the q_i are equal in magnitude and phase then equation 2-4-5 reduces to

$$q_i = \left\{ j\omega C_i (R_i + j\omega L_i + \frac{1}{j\omega C_i} + \sum_{k \neq i}^{S} j\omega M_{i\,k}) \right\}^{-1} \qquad 2\text{-}4\text{-}7$$

Inserting this expression for q_i into equation 2-4-6 gives

$$Z_o = \sum_{i=1}^{S} \left\{ \frac{1}{j\omega C_i} + \frac{1}{\omega^2 C^2 (R_i + j\omega L_i + \frac{1}{j\omega C_i} + \sum_{k \neq i}^{S} j\omega M_{i,k})} \right\} \qquad 2\text{-}4\text{-}8$$

This expression for the input impedance of a foil wound inductor is valid at low frequencies where the radial current distribution is uniform. A simpler form of equation 2-4-8 is possible when it is applied to a foil wound inductor with a radius much larger than the winding depth. Here L_i , R_i and C_i can be considered to have the same value throughout the FWI. Given this assumption equation 2-4-8 reduces to

$$Z_o = \frac{N R^t + j\omega N^2 L^t}{1 - \omega^2 N L^t C^t + j\omega R^t C^t} \qquad 2\text{-}4\text{-}9$$

This expression represents the impedance of a single resonant circuit with inductance N^2L^t in series with resistance NR^t and paralled by capacitance $\frac{C^t}{N}$. A resonant circuit of this type will resonate at a frequency, approximately, of $\omega=\frac{1}{\sqrt{NL^tC^t}}$. This expression is useful for predicting the resonant frequency of small foil wound inductors with small turn-numbers.

The S equations of the form 2-4-5 can be written in matrix form as

$$[A][Q] = [B] \qquad 2\text{-}4\text{-}10$$

Where [A] is the complex matrix of the coefficients from the left-hand side of equation 2-4-5. [Q] is the complex vector of the unknowns and [B] is the vector of the terms $\frac{1}{j\omega C_i}$. Equation 2-4-10 can be expanded into a $2S \times 2S$ real matrix equation of the form

$$\begin{bmatrix} \mathrm{Re}[A] & - & \mathrm{Im}[A] \\ \mathrm{Im}[A] & + & \mathrm{Re}[A] \end{bmatrix} \begin{bmatrix} \mathrm{Re}[Q] \\ \mathrm{Im}[Q] \end{bmatrix} = \begin{bmatrix} \mathrm{Re}[B] \\ \mathrm{Im}[B] \end{bmatrix} \qquad 2\text{-}4\text{-}11$$

5) Numerical Solution Methods

Investigation showed that the best method of solving equation 2-4-11 was the method of Gaussian Elimination (27). This method, although not ideally suited to the solution of large matrices, was used because problems were encountered with the convergence of iterative methods. Most iterative methods depend on the matrix equation being diagonally dominant and the diagonal terms of equations 2-4-5 are dominant at low frequencies, but become relatively small when $\omega=\frac{1}{\sqrt{L_iC_i}}$. Details of the Gaussian Elimination program are given in Appendix 1.

Two tests were applied to the Gaussian Elimination. The first was a truncation test. This test involves truncating the elements of the matrix to be solved to the first four figures; ie, any figures after the first four are set to zero. The truncated matrix and the normal matrix are then solved and the two answers compared, these should not differ in the first four figures of each element of the vector [Q] . If the two answers differ then the solution of the matrix equation is unstable and the answer is unreliable.

The truncation test was too lengthy to be used while the impedance/frequency program was running, and was only employed when a new type of matrix equation had to be solved. When the program was running a back substitution test was used. This involves substituting the answers obtained from the elimination back into the left-hand side of the matrix equation (2-4-11) and comparing the answer so obtained with the right-hand side of the matrix equation. The two vectors should not differ to a high degree of accuracy.

The truncation test showed that the Gaussian Elimination method was sufficiently accurate for the particular type and size of matrix equation encountered, whereas the complex matrix solving subroutine in the NAG library (28) was not accurate.

The Gaussian Elimination method requires approximately $\frac{8S^3}{3}$ calculations to solve a matrix equation of size S , thus the computer time required to provide one point on the impedance/frequency spectrum of the FWI rises as the cube of the size of the matrix. Therefore the number of sections which can be used in the theory is limited by the amount of computer time that is available.

6) Calculation of Lumped Inductance Values

To calculate the self-inductance L_i^t and the mutual-inductance $M_{i,k}^t$ is not a simple task, for all the standard formulae apply to filamentary conductors, and the current distribution is not uniform across the width of the foil at AC. However, useful approximations can be derived for the required inductances.

To calculate the self-inductance L_i^t a suitable starting point is the standard formula for the magnetic field on the axis of a circular current filament (29) of radius a, where a is the mean radius of the i th section. If the width of the foil is W then the filament of width dV will carry a current $\frac{I dV}{W}$, where I is the total current flowing in the foil turn and is uniformly distributed over the foil width. If the current filament is distance V from the origin then the magnetic field H'_z at a distance Z from the origin, and on the axis of the foil turn as shown in Fig. 2-12, is given by

$$H'_z = \frac{I a^2 dv}{2W\left\{(z-v)^2 + a^2\right\}^{3/2}} \qquad 2\text{-}6\text{-}1$$

The total magnetic field H_z, due to the total current I, can be found by integrating over the whole foil with respect to V

$$H_z = \int_{-\frac{W}{2}}^{\frac{W}{2}} \frac{I a^2 dv}{2W\left\{(z-v)^2 + a^2\right\}^{3/2}} \qquad 2\text{-}6\text{-}2$$

This is a standard integral that can be found in Petit-Bois (30). This integral gives H_z as

$$H_z = \frac{I}{2W}\left\{\frac{W/2 - z}{\left[(z-\frac{W}{2})^2 + a^2\right]^{1/2}} + \frac{W/2 + z}{\left[(z+\frac{W}{2})^2 + a^2\right]^{1/2}}\right\} \qquad 2\text{-}6\text{-}3$$

Figure 2-12

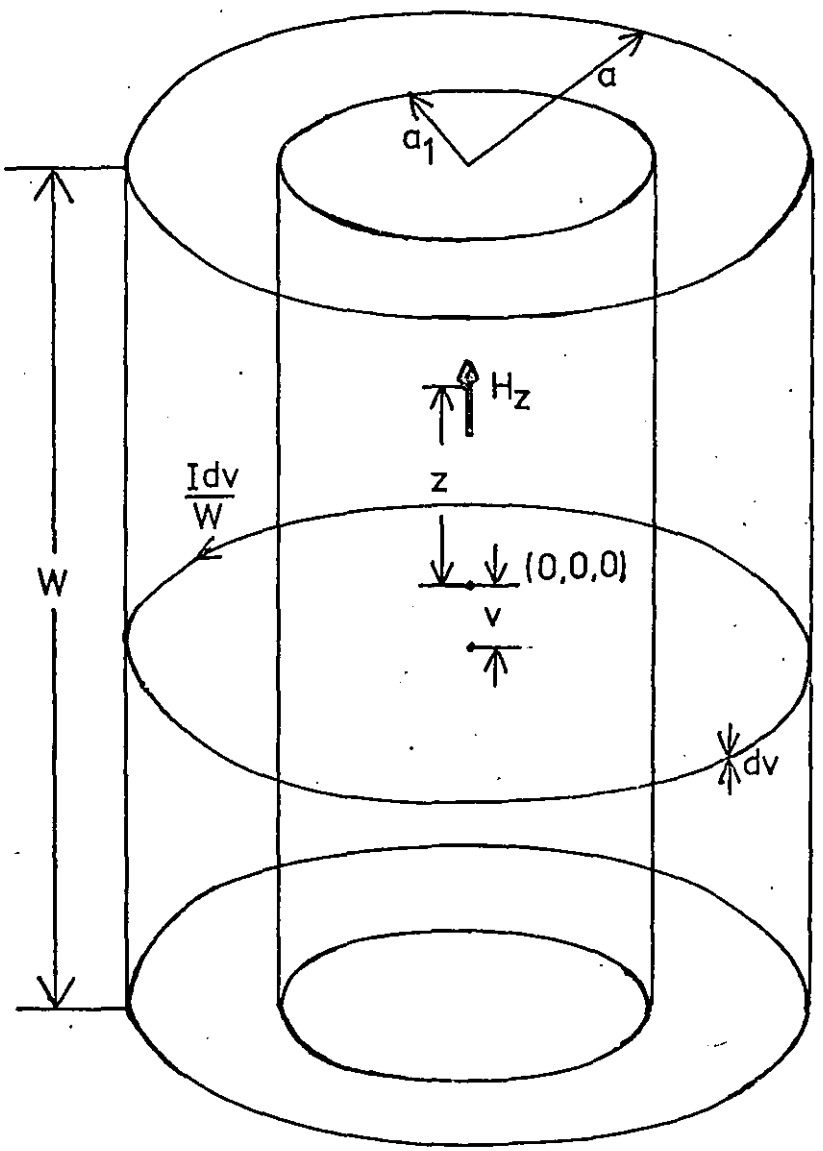

Two Coaxial Turns of Foil

The average magnetic field $\overline{H_z}$ along the axis of the foil turn is given by

$$\overline{H_z} = \frac{I}{2W^2} \int_{-\frac{W}{2}}^{+\frac{W}{2}} \left\{ \frac{\frac{W}{2} - z}{[(z - \frac{W}{2})^2 + a^2]^{1/2}} + \frac{\frac{W}{2} + z}{[(z + \frac{W}{2})^2 + a^2]^{1/2}} \right\} dz \qquad 2\text{-}6\text{-}4$$

This is also a standard integral found in Petit-Bois and results in an expression for $\overline{H_z}$ of the form

$$\overline{H_z} = \frac{I}{W^2} \left\{ (W^2 + a^2)^{1/2} - a \right\} \qquad 2\text{-}6\text{-}5$$

An approximate expression for the self-inductance L_i^t of a foil turn can be found by assuming that the magnetic field across the foil turn section is uniform and equal in magnitude to the magnetic field at the axis of the foil turn and by assuming that the turn can be treated as a filamentary current I linked to a flux $\overline{\Phi_a}$, given by

$$\overline{\Phi_a} = \pi a^2 \mu_0 \overline{H_z} \qquad 2\text{-}6\text{-}6$$

Thus L_i^t can be derived by combining equations 2-6-5 and 2-6-6 with the definition of inductance. This gives

$$L_i^t = \frac{\overline{\Phi_a}}{I} = \frac{\pi a^2 \mu_0}{W^2} \left\{ (W^2 + a^2)^{1/2} - a \right\} \qquad 2\text{-}6\text{-}7$$

An approximate expression for the mutual-inductance $M_{i,k}^t$ linking the average turn of the i th section to the average turn of the k th section can be found by treating the two turns as filaments of radius a and a_1 linked by a flux $\overline{\Phi_{a_1}}$. It is assumed that a_1 is less than a. The expression for the flux will have the form

$$\overline{\Phi_{a_1}} = \pi a_1^2 \mu_0 \overline{H_z} \qquad 2\text{-}6\text{-}8$$

Combining equations 2-6-5 and 2-6-8 with the definition of mutual-inductance gives an expression for $M^{t}_{i,k}$ of the form

$$M^{t}_{i,k} = \frac{\overline{\Phi_{a_1}}}{I} = \frac{\pi a_1^2 \mu_0}{W^2} \left\{ (W^2 + a^2)^{\frac{1}{2}} - a \right\} \qquad 2\text{-}6\text{-}9$$

Combining equations 2-4-1 and 2-6-7 gives an expression for the self-inductance of the ith section of the form

$$L_i = \frac{\pi a^2 d^2 \mu_0}{W^2} \left\{ (W^2 + a^2)^{\frac{1}{2}} - a \right\} \qquad 2\text{-}6\text{-}10$$

In a similar manner, combining equations 2-4-4 and 2-6-9 gives an expression for the mutual-inductance coupling the ith and kth sections of the form

$$M_{i,k} = \frac{\pi a_1^2 d^2 \mu_0}{W^2} \left\{ (W^2 + a^2)^{\frac{1}{2}} - a \right\} \qquad 2\text{-}6\text{-}11$$

To test the inductance formulae derived in section 2-6 a set of five 150 turn foil wound inductors were manufactured with core radii varying from 0.7 cm to 1.5 cm. The other relevant physical parameters and dimensions are given in the table in Fig.2-13. Three of these inductors are the same, enabling an estimate of the manufacturing tolerances.

The theoretical self-inductance of a foil wound inductor at low frequency, where self-resonance has little effect, can be found by summing the sectional self and mutual inductances. This gives an expression for L of the form

Figure 2-13

Dimensions of the set of 150 turn foil wound inductors used in section 1-5.

Coil 1:	Thickness of Al. foil	5.0 μm
	Width of Al. foil	2.52 cm
	Type of insulating film	Polypropylene
	Thickness of insulating film	25.0 μm
	Dielectric constant of the insulating film	2.2
	Radius of the core	1.5 cm
Coil 2:	Thickness of Al. foil	5.0 μm
	Width of Al. foil	2.52 cm
	Type of insulating film	Polypropylene
	Thickness of insulating film	25.0 μm
	Dielectric constant of the insulating film	2.2
	Radius of the core	0.7 cm
Coil 3, Coil 4 and Coil 5:	Thickness of Al. foil	5.0 μm
	Width of Al. foil	3.9 cm
	Type of insulating film	Polypropylene
	Thickness of insulating film	12.5 μm
	Dielectric constant of the insulating film	2.2
	Radius of the core	0.7 cm

Figure 2-14

Inductances of the set of 150 turn foil wound inductors used in section 2-6.

	Theoretical Inductance μH	Measured Inductances μH			
		40.Hz	1.KHz	10.KHz	100.KHz
Coil 1	495.95	550.2 ±.3%	550.5 ±.3%	526.2 ±.3%	620. ±1%
Coil 2	175.3	184.6 ±.6%	184.4 ±.6%	177.4 ±.6%	175. ±1%
Coil 3		117.8 ±.6%	117.4 ±.6%	113.9 ±.6%	113. ±1%
Coil 4	113.4	117.3 ±.6%	116.8 ±.6%	113.2 ±.6%	113. ±1%
Coil 5		117. ±.6%	116.8 ±.6%	112.9 ±.6%	113. ±1%
Average of coils 3 to 5		117.4	117.	113.3	113.

$$L = \sum_{i=1}^{S} \left(L_i + \sum_{k \neq i}^{S} M_{i,k} \right) \qquad 2\text{-}6\text{-}12$$

The calculated inductances, with S set to ten, for the set of FWI are given in the table in Fig. 2-14.

The inductances of the set were measured at 40 Hz, 1 KHz and 10 KHz on the Maxwell inductance bridge described in chapter 3, and at 100 KHz on a Wayne Kerr Universal Bridge (Sections B602 and SR268). These measured values are given in the table in Fig. 2-14.

In the case of coil 1 the calculated inductance is in error by -9.9% at 40 Hz, -5.7% at 10 KHz and then rises to -20% at 100 KHz. The large error at 100 KHz is probably due to the FWI self-resonating, resulting in an apparent rise in the inductance. In the case of coil 2 the error in the calculated inductance decreases from -5% at 40 Hz to +0.2% at 100 KHz. In the case of coils 3 to 5 the error in the calculated inductance decreases from -3.4% at 40 Hz to +0.4% at 100 KHz.

This set of measurements indicates that there is little point in deriving a more exact inductance formula since this will only be accurate at low frequency. The simple formulae derived appear to be reasonably accurate at the frequencies involved and with the type and size of FWI involved. The decrease in the inductance at low frequency is probably due to the "width effect" and is investigated in chapter 3.

7) Calculation of the DC Resistance

The DC resistance of the average turn, radius a, of the ith section is given by

$$R_i^t = \frac{2\pi a \rho}{W t} \qquad 2\text{-}7\text{-}1$$

Where ρ is the resistivity and t the thickness, of the metal foil. This formula will be valid only at very low frequencies. At higher frequencies the width effect, skin effect and proximity effect will combine to increase the resistance of the foil turn by several orders of magnitude. However, as the increase in the resistance with frequency can only at present be predicted for certain types of foil wound inductor over a limited frequency range, the DC resistance formula was used, although this will give rise to errors in the predicted Q values of the resonances.

Combining equations 2-4-2 and 2-7-1 gives an expression for the DC resistance of the i th section of the form

$$R_i = \frac{2\pi a d \rho}{W t} \qquad 2\text{-}7\text{-}1$$

8) Calculation of the Capacitance

Neglecting end-effects and the curvature of the foil the parallel-plate formula can be used for the turn-to-turn capacitance of the i th section

$$C_i^t = \frac{2\pi a \varepsilon \varepsilon_o W}{h} \qquad 2\text{-}8\text{-}1$$

Where h is the thickness, and ε the dielectric constant, of the plastic insulation film. All the turns of the section are assumed to have the same radius a. Combining equations 2-4-3 and 2-8-1 gives an expression for the capacitance of the i th section of the form

$$C_i = \frac{2\pi a \epsilon \epsilon_o W}{dh} \qquad 2\text{-}8\text{-}2$$

The problem with this expression is not that it is fundamentally wrong, but that variations in the winding tension and side slip of the metal foil when the FWI is wound, together with variations in the thickness and dielectric constant of the plastic film, make the parameters a, W, d and ϵ inaccurate. Also to prevent the plastic film creeping under tension, once the FWI has been wound, the coils have to be heat treated. This shrinks the plastic, decreasing the foil separation.

To test equation 2-8-2 directly would be difficult, if not impossible. The capacitance of a FWI cannot be separated from its inductance. Therefore, an indirect method of testing equation 2-8-2 was adopted. A 30 turn capacitor was wound using the same materials used to manufacture the FWI. The dimensions of this capacitor, which are approximately the same as that of the FWI investigated, are given in the table in Fig. 2-15.

As the core radius of the capacitor is relatively large the depth of the winding can be neglected and an average radius of 1.053 cm used to calculate the capacitance. Inserting values into equation 2-8-1 yields a value for the turn-to-turn capacitance of 4.021 nF. The total capacitance will be 59 times this, or 237.2 nF. The experimental value of the capacitance, measured on a Hewlett Packard Universal Bridge (Type 4265A) at 1 KHz, was 213. nF before heat treatment and 230. nF ± 2. nF after heat treatment. The difference between the theoretical and experimental values is -3.1%. This error is not excessive, considering that the tolerance of normal commercial capacitors

Figure 2-15

Dimensions of the test capacitor used in section 1-7	
Thickness of Al. foil	5.0 μm
Width of Al. foil	3.9 cm
Type of insulating film	Polypropylene
Thickness of insulating film	12.5 μm
Dielectric constant of the insulating film	2.2
Radius of the core	1.0 cm

Figure 2-16

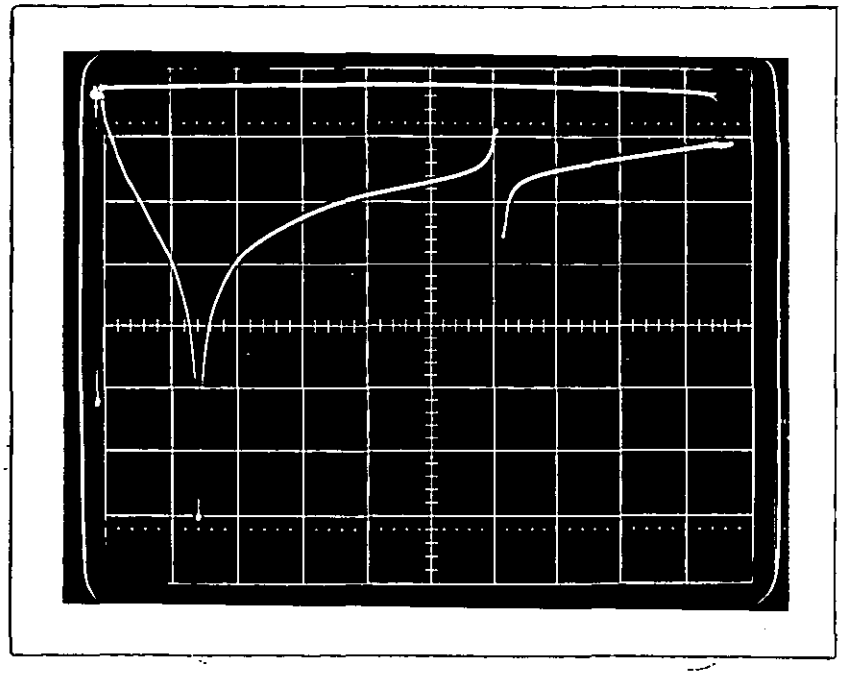

Impedance/frequency spectrum of a 150 turn foil wound inductor.

Abscissa: 2 MHz per square, range 100 KHz to 20 MHz

Ordinate: 10 dB attenuation per square, zero at top

is in the region of ±10%.

9) Comparison of the Theoretical and Experimental Impedance/Frequency Spectra of Two Foil Wound Inductors

The experimental impedance/frequency spectrum of a 150 turn FWI, coil 4 in the tables in Figs. 2-13 and 2-14, is shown in the photograph in Fig. 2-16 and has two maxima and one minimum. The theoretical sectional inductances, resistances and capacitances for this FWI were calculated with S set at ten, and inserted as data to the Gaussian Elimination program. The theoretical variation of the magnitude of the input impedance with frequency is shown in Fig. 2-17. This graph has maxima at 3.201 MHz and 12.47 MHz. The experimental impedance/frequency spectrum shows maxima in the input impedance at 3.24 MHz ±1.6% and 12.87 MHz ±0.9%, giving a difference respectively, of -1.2% and -3.3% between the theoretical and experimental values.

The theoretical input impedance locus of the 150 turn FWI is shown in Fig. 2-18. This shows that the input impedance maxima and mimimum occur at points where the phase of the impedance is almost zero, indicating that the resonances behave like normal series or parallel L, C resonances.

The experimental impedance/frequency spectrum of the 1000 turn FWI, with the dimensions shown in Fig. 2-19, is shown in the photograph in Fig. 2-9 and as an x-y recorder plot in Fig. 2-20. The theoretical impedance/frequency spectrum is shown in Fig. 2-20. The input impedance locus is shown in Fig. 2-21. This shows again that the maxima and minima behave like normal series or parallel L, C resonances. A direct comparison is made between the theoretical and experimental impedance/frequency spectra in Fig. 2-22. The experimental impedance/frequency spectrum

Figure 2-17

The Theoretical Variation of the Input Impedance with Frequency for a 150 Turn Foil Wound Inductor (S set to 10)

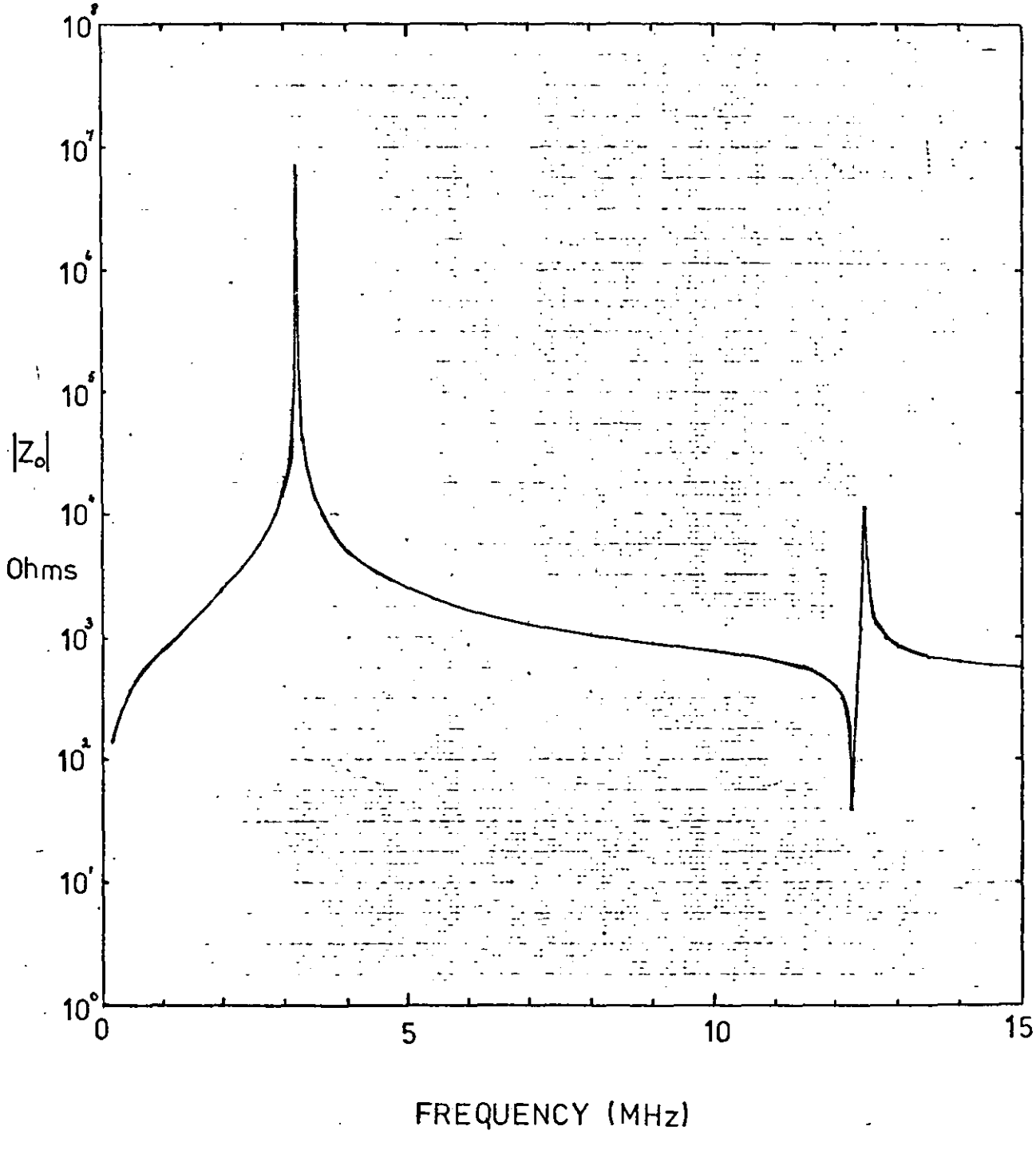

Figure 2-18

The Theoretical Input Impedance Loci of a 150 Turn Foil Wound Inductor from 0 to 15 MHz (S = 10)

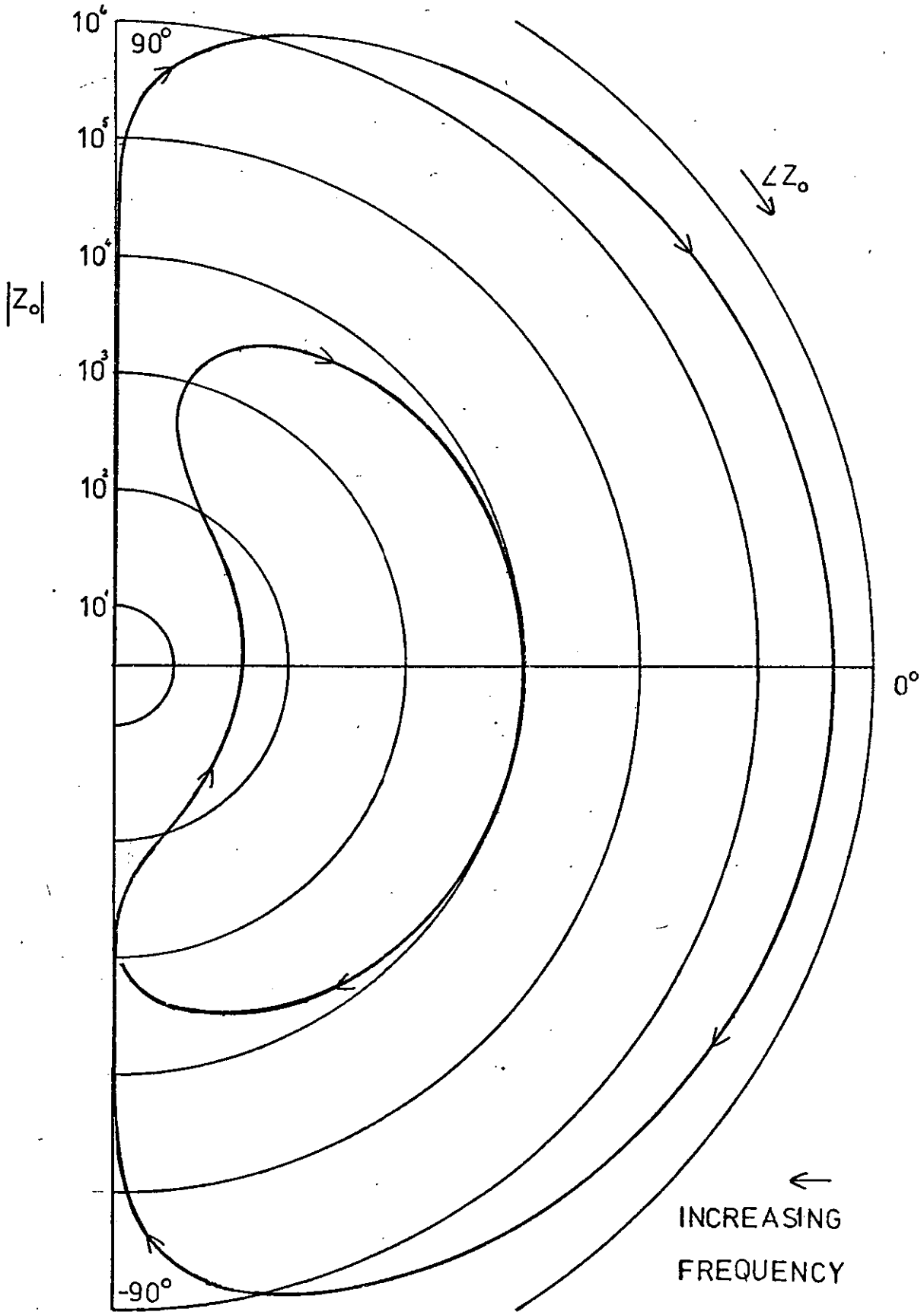

Figure 2-19

Dimensions of the 1000 turn foil wound inductor used in section 2-9

Thickness of Aluminium foil	5.0 μm
Width of Aluminium foil	3.9 cm
Type of insulating film	Polypropylene
Thickness of insulating film	12.5 μm
Dielectric constant of the insulating film	2.2
Radius of the core	0.7 cm

Figure 2-20

The Theoretical Variation of the Input Impedance with Frequency for a 1000 turn Foil Wound Inductor (S set to 10)

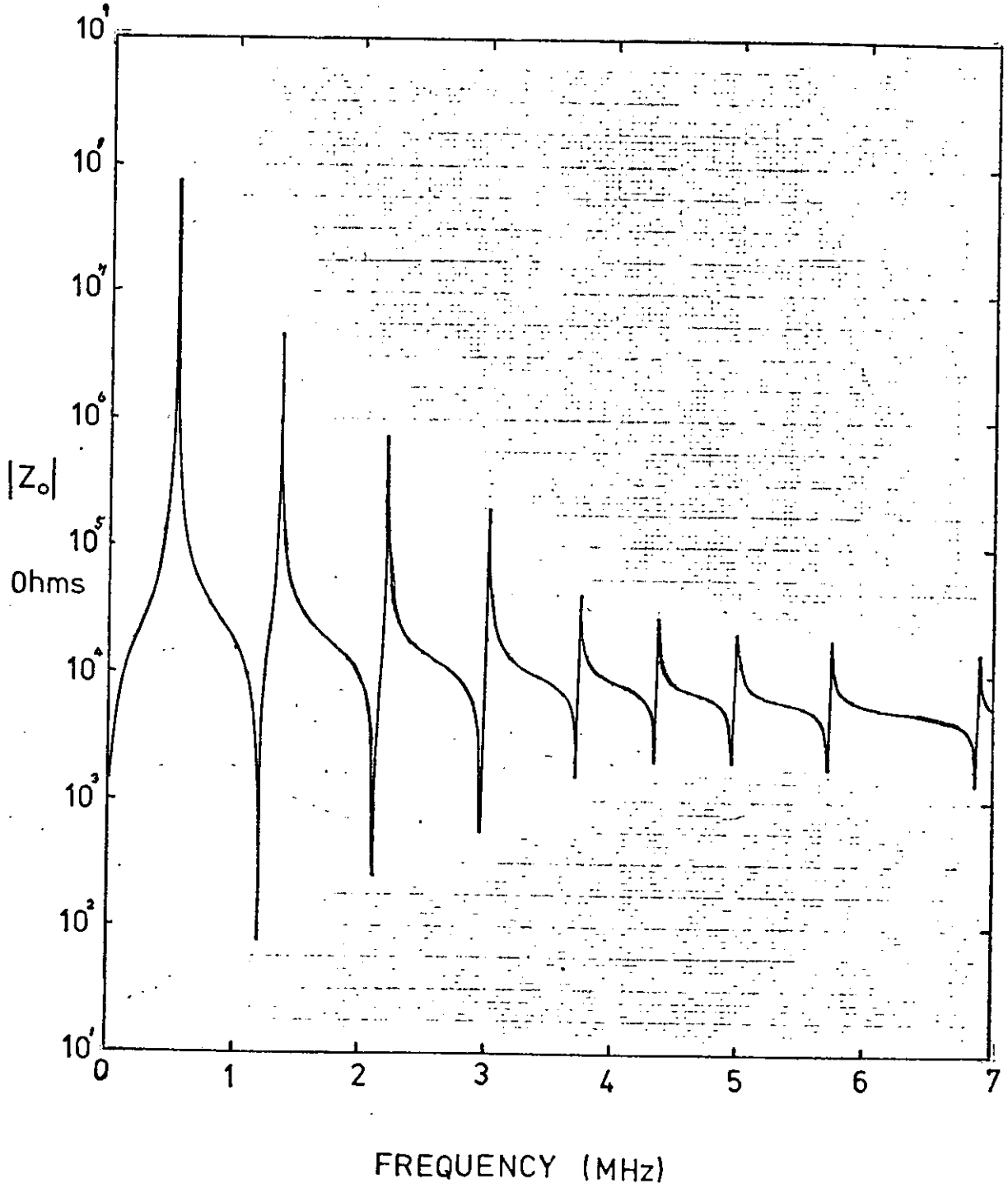

Figure 2-21

The Theoretical Input Impedance Loci of a 1000 Turn Foil Wound Inductor from 0 to 3.5 MHz (S = 10)

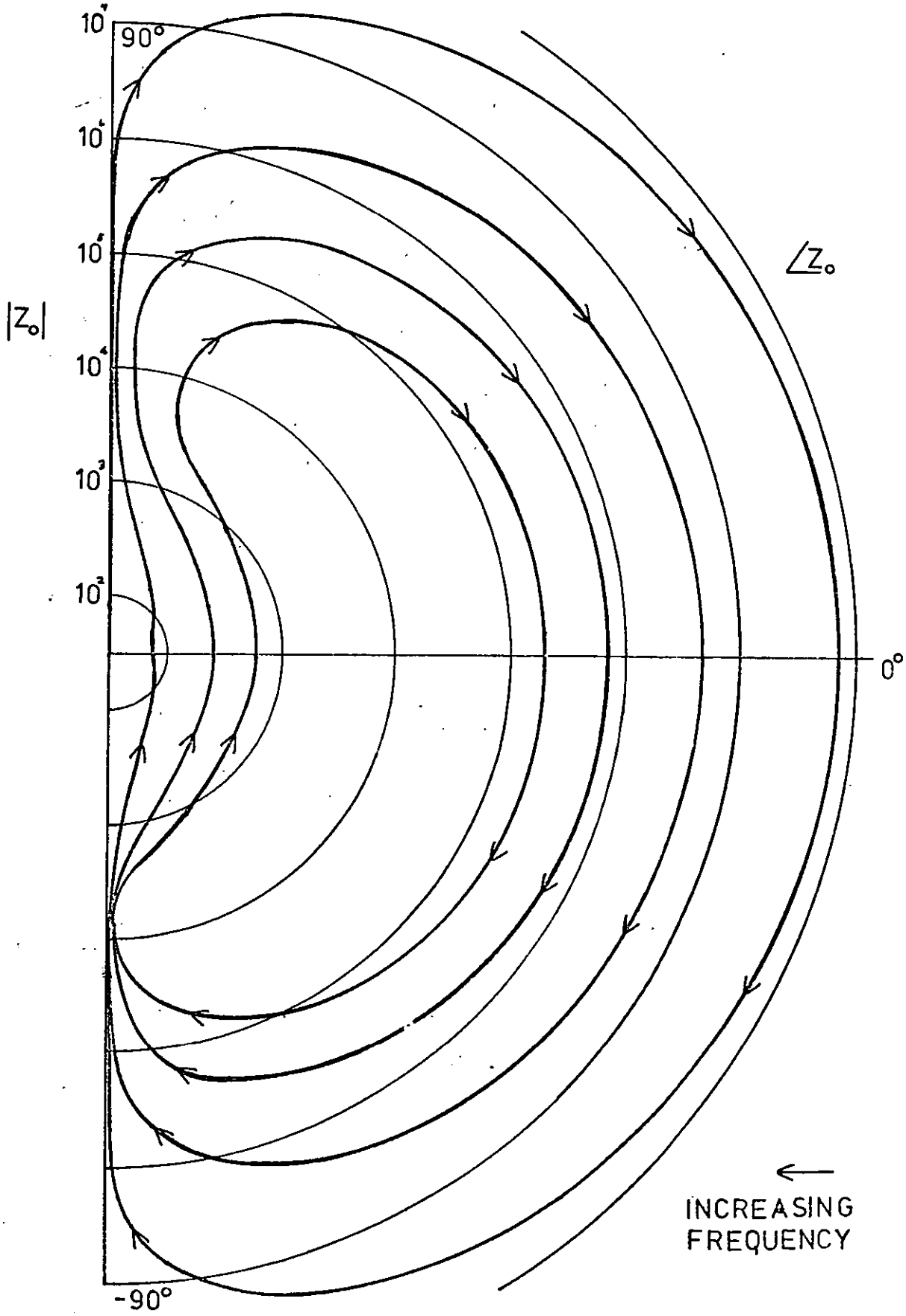

Figure 2-22 Theoretical and Experimental Variations of Vm with Frequency for the 1000 Turn Foil Wound Inductor
The 0 level of dBm is the output power from the tracking generator.

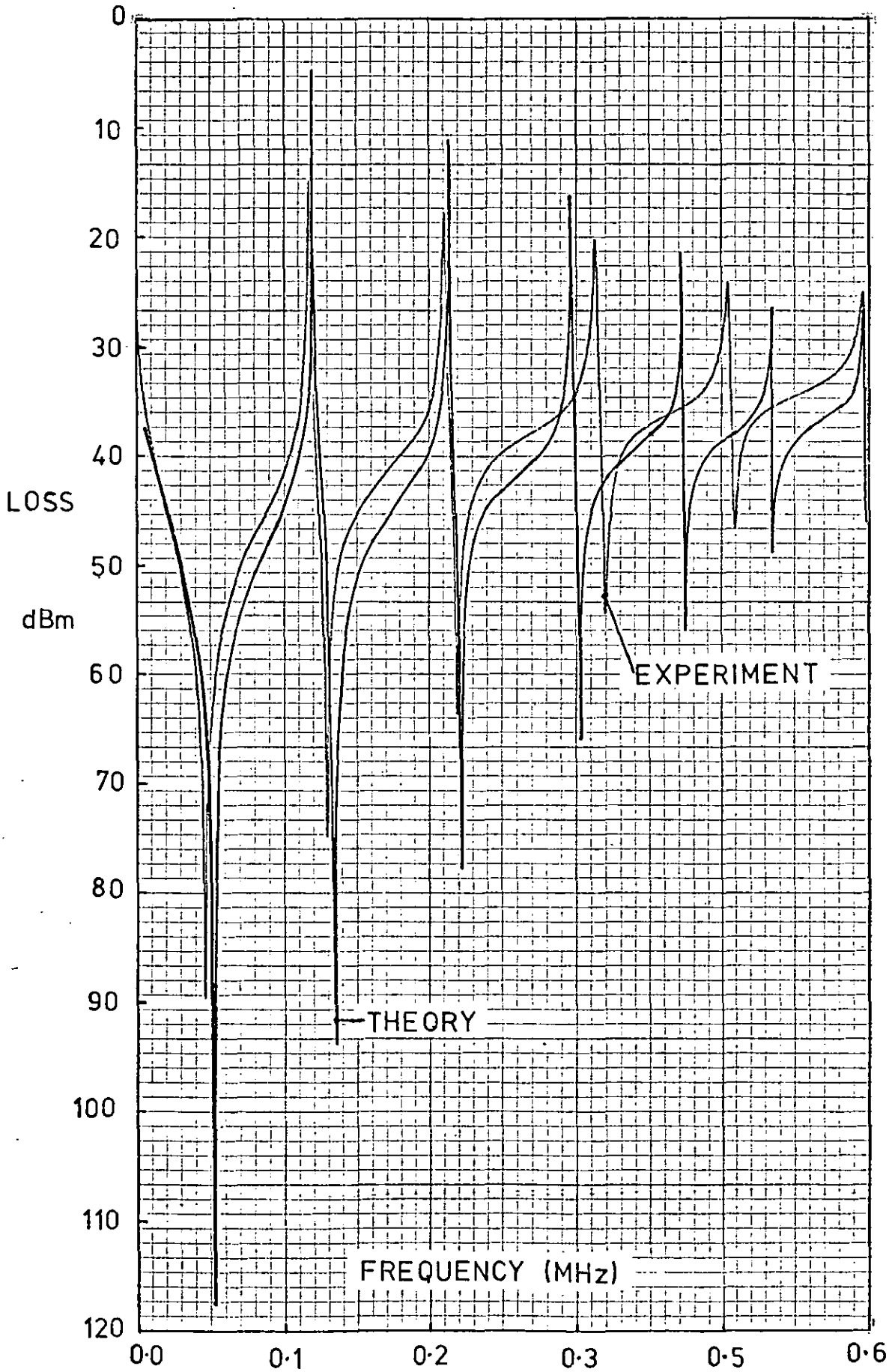

is the output level from the spectrum analyser recorded on an X-Y plotter. The 0 dBm level on the graph corresponds to the power level with the coil shorted out. The theoretical impedance/frequency spectrum was plotted using equation 2-3-3, which relates the input impedance Z_o to the dBm level.

These graphs show two main effects: the theoretical and experimental dBm levels at the maxima and minima differ by large amounts, and the frequencies of the resonances correspond quite well up to the third impedance minimum at 3 MHz. The difference in the dBm levels at resonance is clearly due to the use of DC resistance values in the computer calculations. For more accurate calculations a method of calculating the AC resistance would be required. The differences between the theoretical and experimental resonant frequencies shown in the table in Fig. 2-23 are in part due to the limited number of sections used in the model. This limitation is examined in section 2-10.

The paper by Kemp, Murgatroyd and Walker summarizes the theory of self-resonance in FWI and is reproduced as Appendix 2.

10) Current and Voltage Standing Waves

The theoretical equivalent circuit of Fig. 2-11 is essentially a set of coupled resonators and as such will behave in the same manner as any set of coupled resonators, such as a system of coupled pendula. A set of coupled resonators, whether mechanical or electrical, has a number of modes of resonance in which the amplitude and phase of the oscillation varies from resonator to resonator. Thus it is possible for the equivalent circuit to resonate at many frequencies.

Figs. 2-24a to 2-30a show the relative voltage, relative

Figure 2-23

Comparison of Theoretical and Experimental Resonant Frequencies for a 1000 Turn Foil Wound Inductor, Maximum Impedance Resonances only.		
Experimental Resonant Frequencies MHz	Theoretical Resonant Frequencies MHz	Percentage Difference
0.514 ±0.39%	0.5167	+0.52%
1.344 ±0.15%	1.366	+1.65%
2.232 ±0.09%	2.216	-0.72%
3.218 ±0.06%	3.022	-6.1%
4.101 ±0.07%	3.748	-8.6%
5.005 ±0.08%	4.375	-12.6%
6.008 ±0.17%	4.979	-17.2%
6.888 ±0.15%	5.740	-16.7%

Figure 2-24

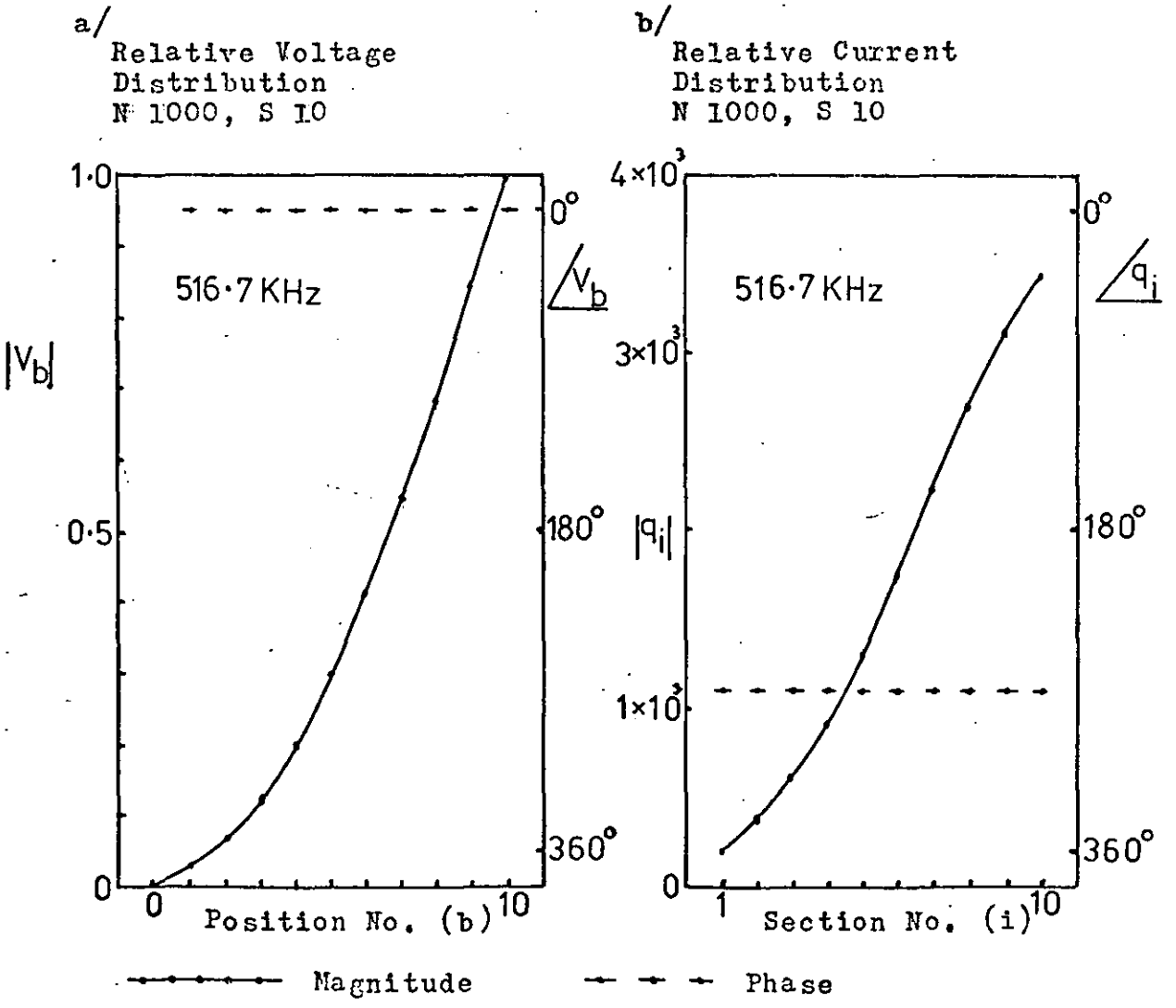

Figure 2-25

a/ Relative Voltage Distribution N=1000, S=10

b/ Relative Current Distribution N=1000, S=10

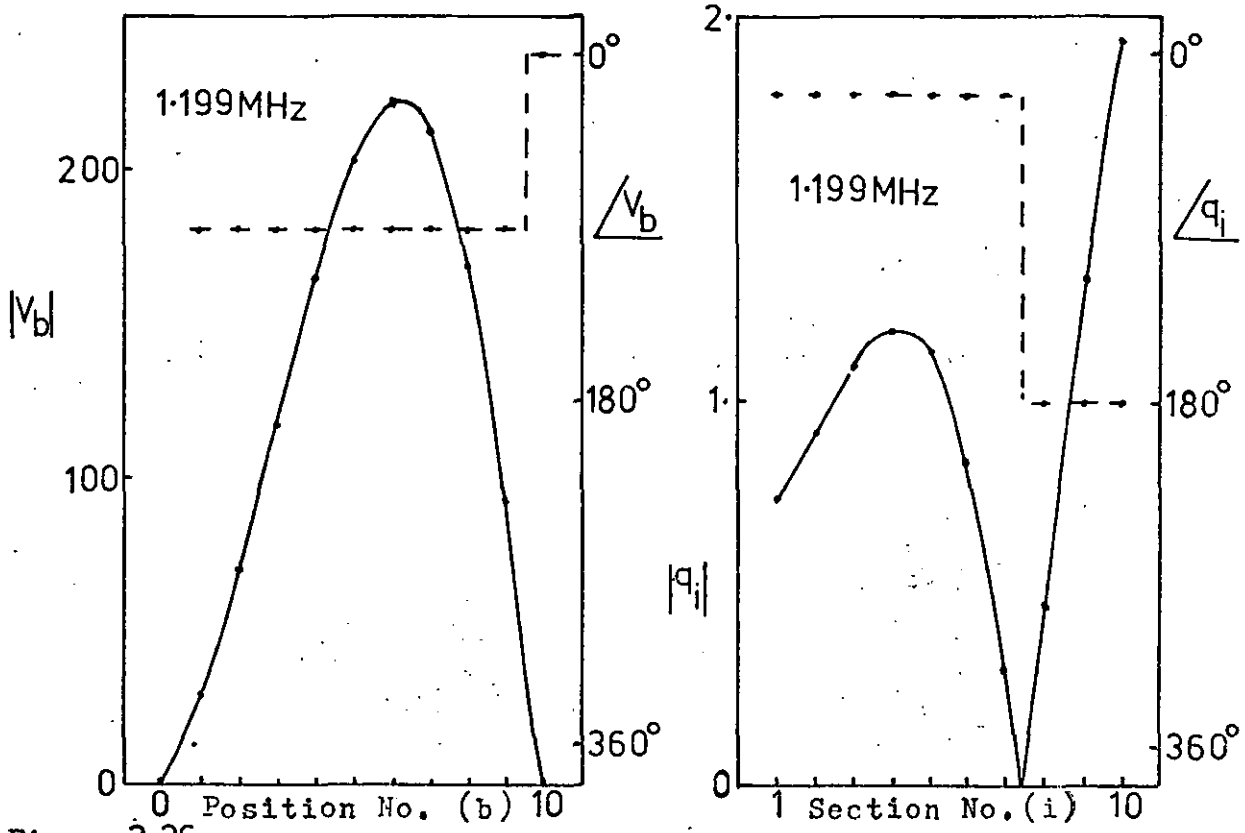

Figure 2-26

a/

b/

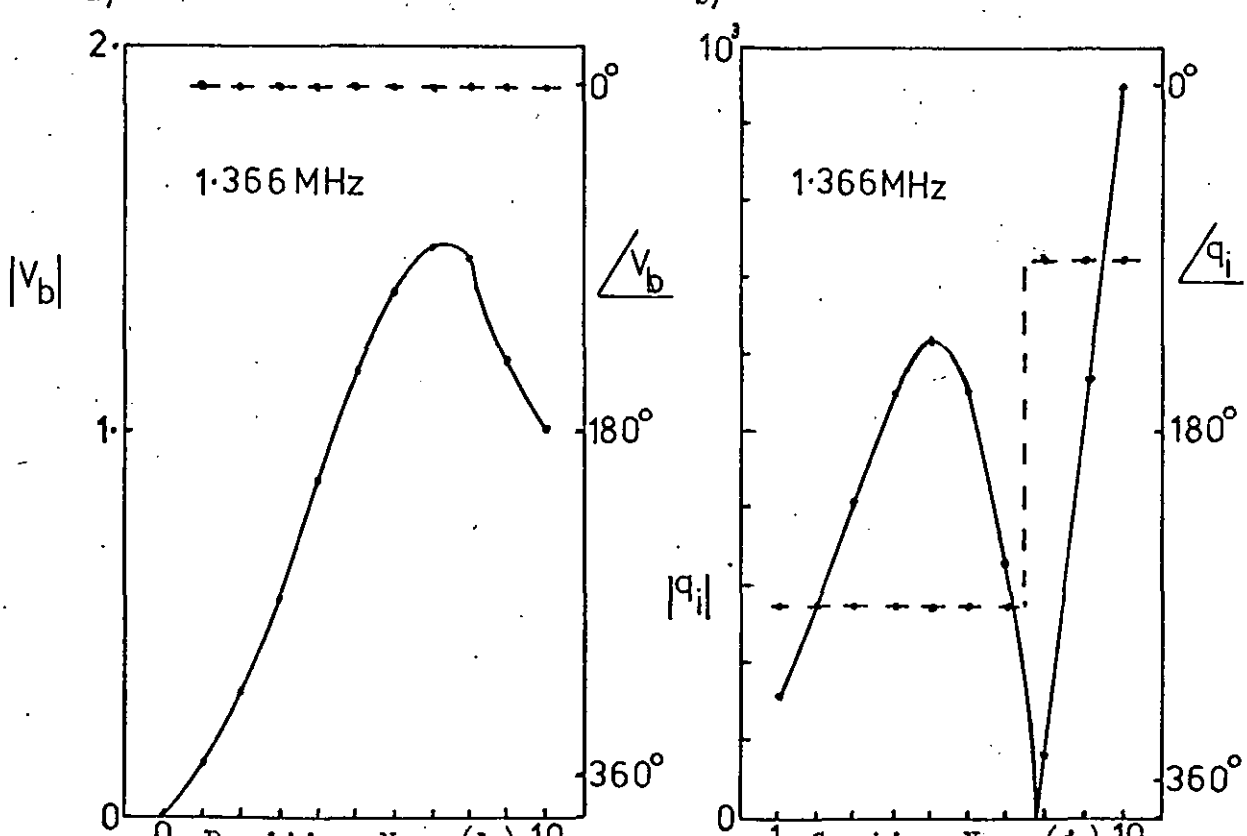

Relative Voltage Distribution N=1000, S=10

Relative Current Distribution N=1000, S=10

Magnitude ——— Phase

Figure 2-27

a/ Relative Voltage Distribution N=1000, S=10

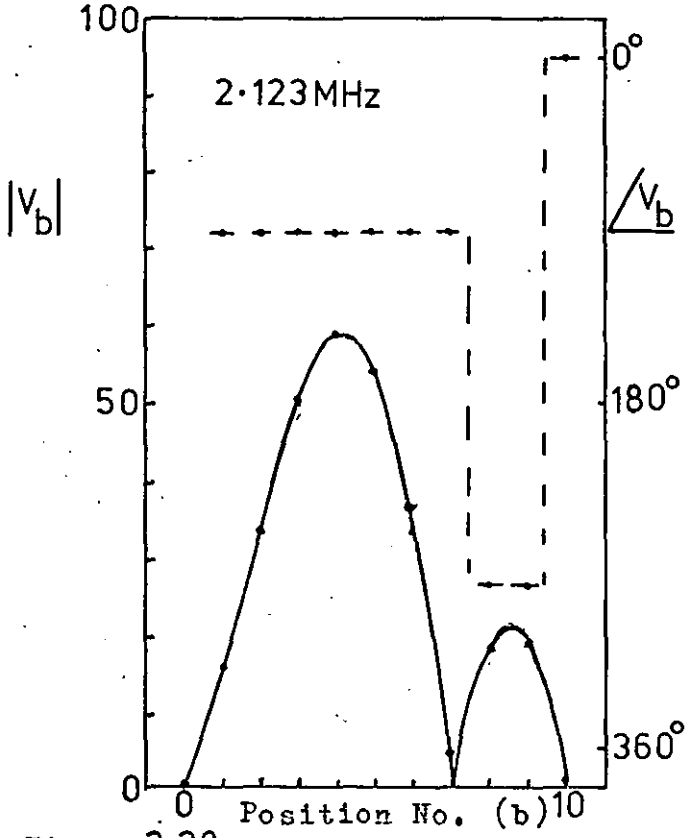

b/ Relative Current Distribution N=1000, S=10

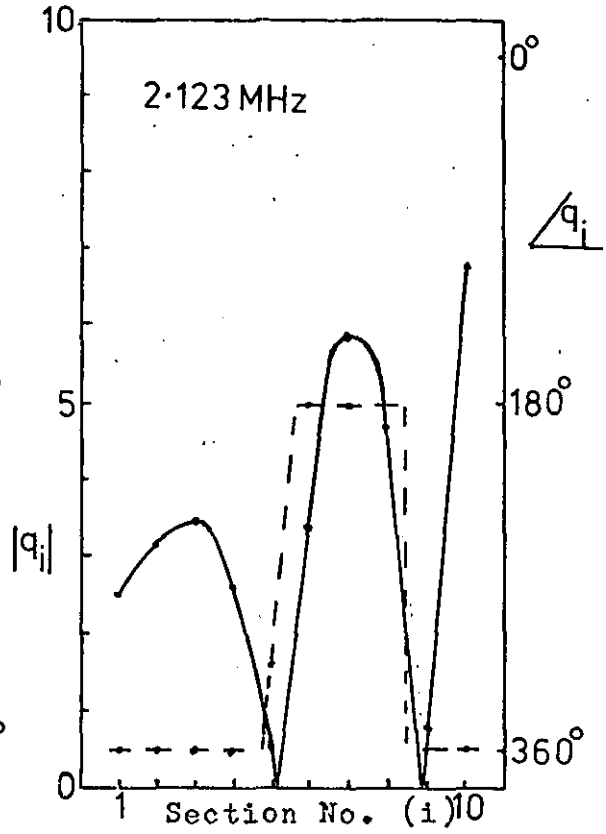

Figure 2-28

a/

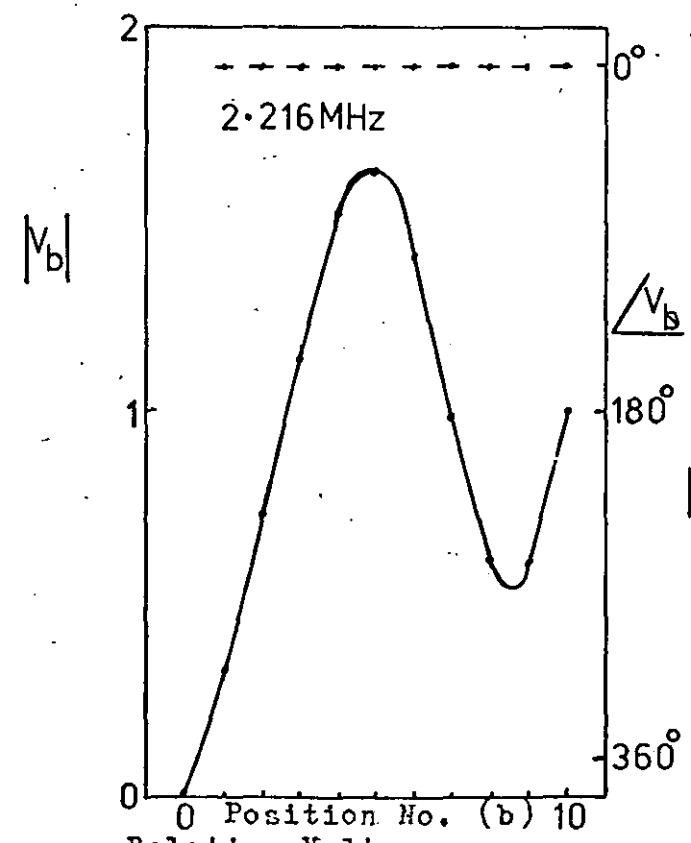

Relative Voltage Distribution N=1000, S=10

b/

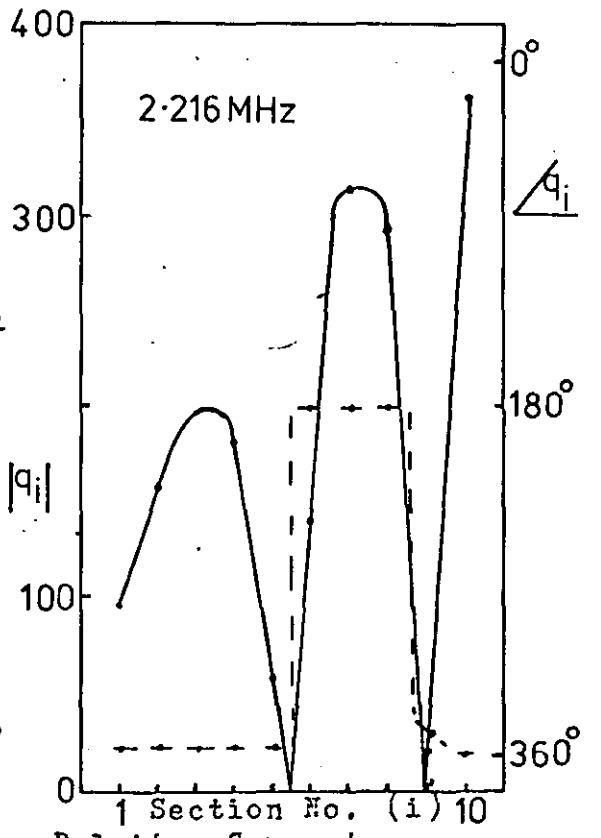

Relative Current Distribution N=1000, S=10

——●——●—— Magnitude — — — — Phase

Figure 2-29

a/ Relative Voltage Distribution N=1000, S=10

b/ Relative Current Distribution N=1000, S=10

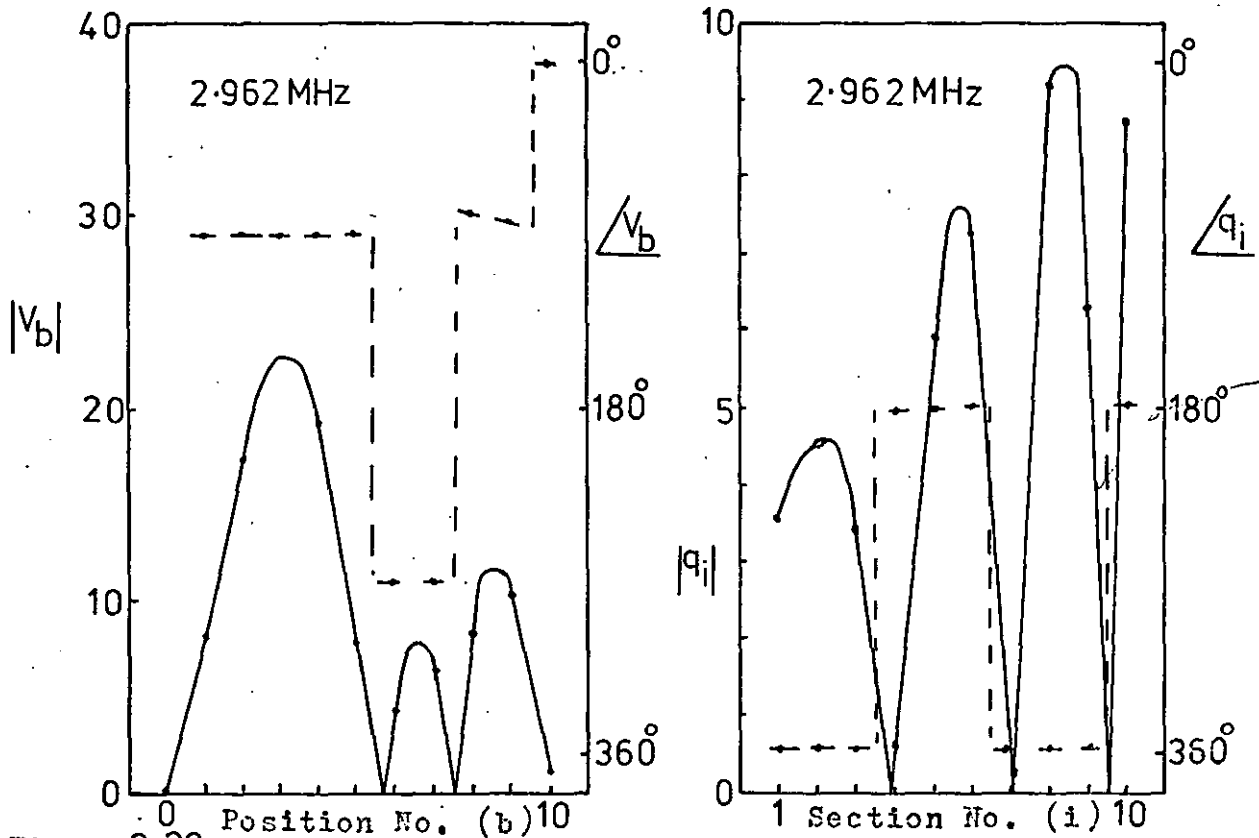

Figure 2-30

a/ b/

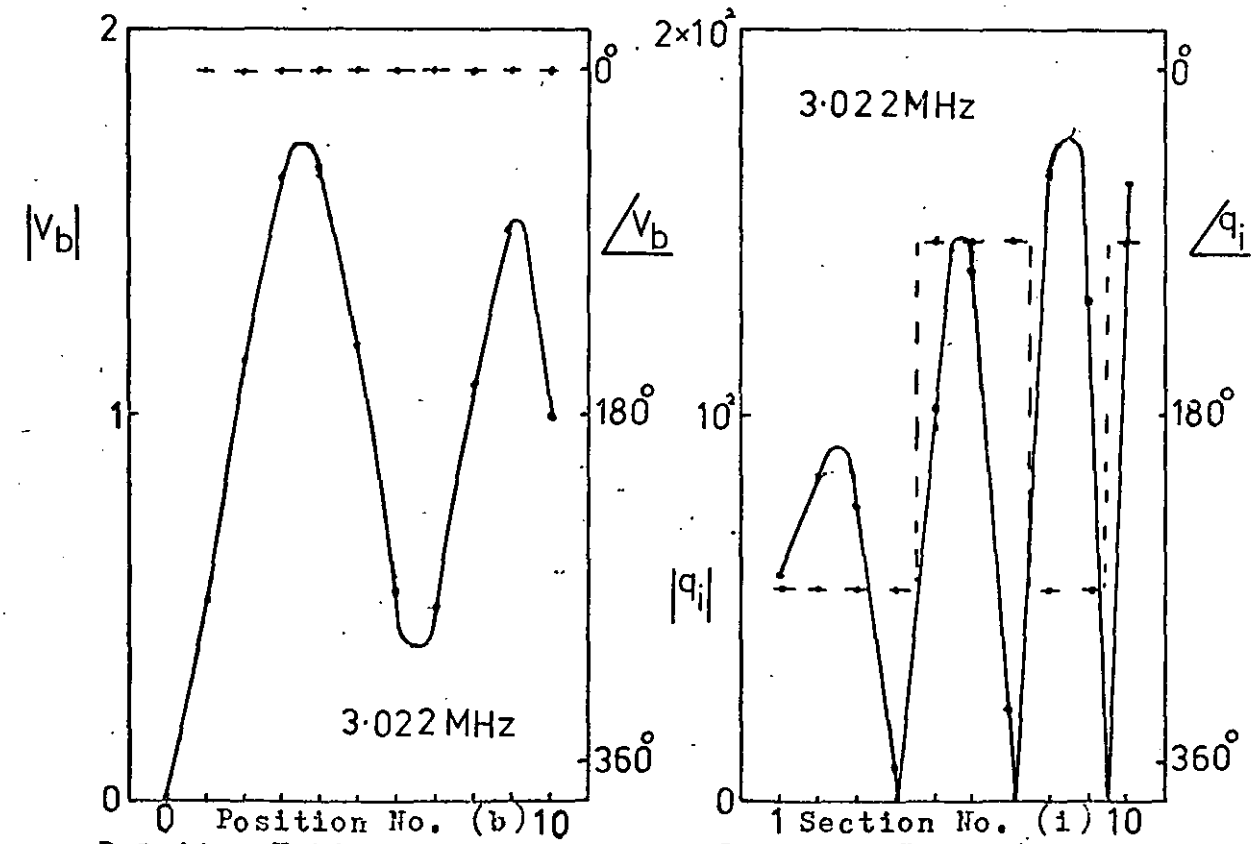

Relative Voltage Distribution N=1000, S=10

Relative Current Distribution N=1000, S=10

Magnitude ——— Phase - - - -

to the input voltage, distribution within the 1000 turn FWI, and Figs. 2-24b to 2-30b show the relative current, relative to the input current, distribution within the FWI at the frequencies of 516.7 KHz, 1.366 MHz, 2.216 MHz and 3.022 MHz, which are the frequencies of maximum impedance resonances, and at the frequencies of 1.199 MHz, 2.123 MHz, and 2.962 MHz, which are the freqencies of minimum impedance resonances. These distributions are theoretical ones.

V_b the relative voltage, relative to the input voltage, at the end of the b th section can be derived from equation 2-4-6, and has the form

$$V_b = \sum_{i=1}^{b} \frac{(1 - q_i)}{j\omega C_i Z_o} \qquad 2\text{-}10\text{-}1$$

Position $b=0$ lies at the beginning of the first section, which is at the start of the winding, and position $b=10$ lies at the end of the tenth section, which is at the end of the winding at the edge of the coil.

Fig. 2-31 shows the amplitude and phase of the first four orders of resonance of an idealised set of coupled resonators. In a first order resonance the phase of the amplitude does not change. In a second order resonance the phase of the amplitude changes phase by 180° once. In a third order resonance the phase changes by 180° twice. In the N th order resonance the phase changes by 180° $N-1$ times.

Fig. 2-24b, 2-26b, 2-28b and 2-30b show respectively the characteristics of first, second, third and fourth order current resonances. The current distribution at 516.7 KHz does not change phase, the distribution at 1.366 MHz changes phase by

Figure 2-31 General Forms of the First Four Orders of Resonance

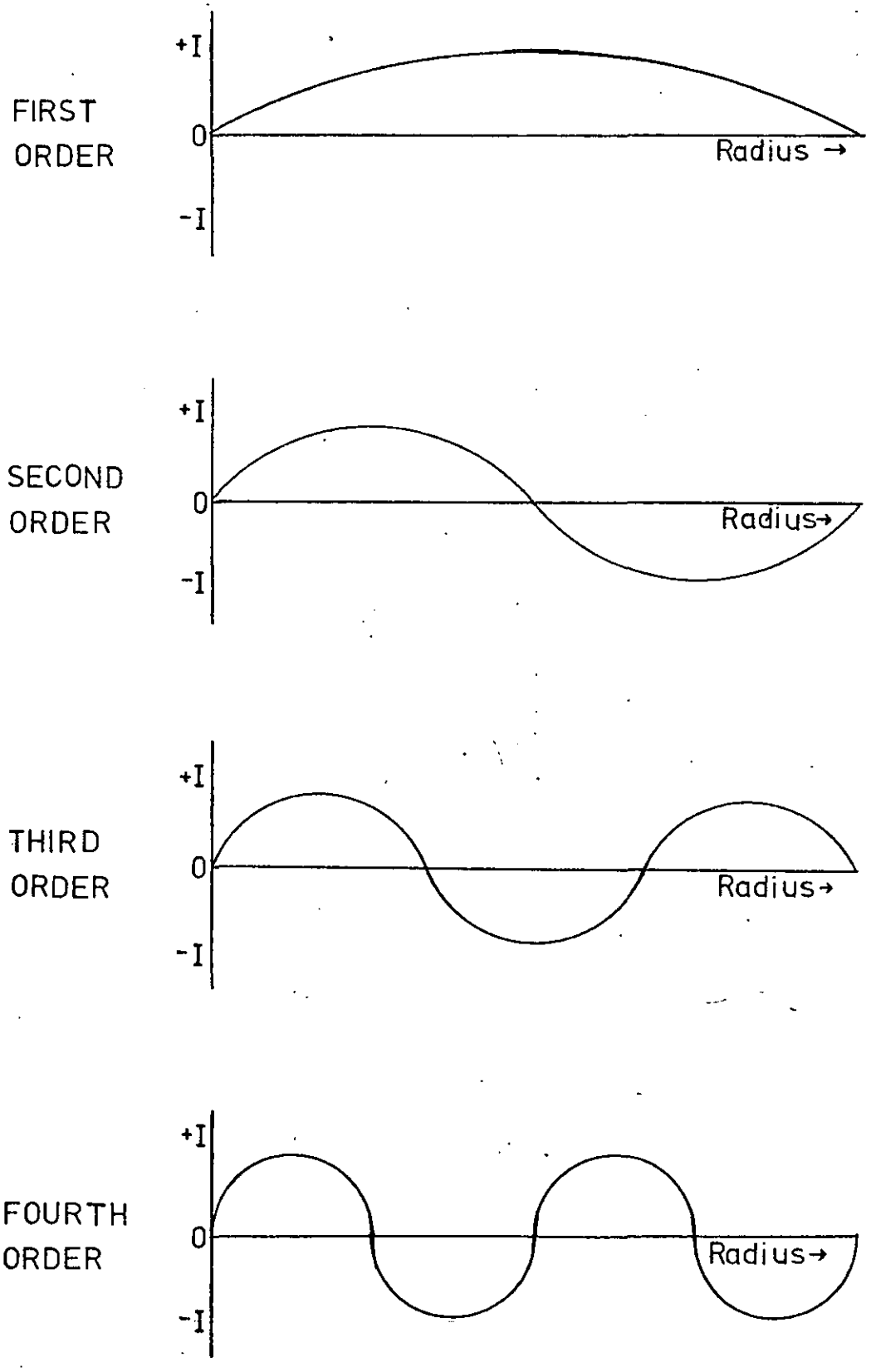

180° once, the distribution at 2.216 MHz changes phase by 180° twice and the distribution at 3.022 MHz changes phase by 180° three times. At each of these frequencies the amplitudes of the relative currents are large. These resonances correspond to parallel L, C resonances, in that in an ideal parallel L, C resonant circuit the input impedance is infinite at resonance, as is the relative current flowing in the circuit (relative current: current flowing in the resonant circuit divided by the input current).

Figs. 2-25, 2-27 and 2-29 show respectively the characteristics of first, second and third order voltage resonances, despite the 90° phase change between position 9 and 10, which is necessary to bring the phase of the voltage distribution back to the phase of the input voltage. The voltage distribution at 1.199 MHz does not change phase, the distribution at 2.123 MHz changes phase by 180° once, and the distribution at 2.962 MHz changes phase by 180° twice. At each of these frequencies the amplitudes of the relative voltages are large. These resonances correspond to series L, C resonances. In an ideal series L, C resonant circuit the input impedance is zero at the resonant frequency, while the relative voltage across either the L or the C is infinite (relative voltage: voltage across either L or C divided by the input voltage).

It can be seen from Fig. 2-30b that with only ten sections in the equivalent circuit the theory has difficulty in following the variations within the current distribution. Therefore, the theory cannot be expected to predict the resonant frequencies of higher orders of resonance with any accuracy, as the results shown in the table in Fig. 2-23 confirm. The results of this

table show that theory can with reasonable accuracy predict the resonant frequency up to the order given by the number of sections used in the theory divided by three.

11) Experimental Evidence for Current Standing Waves

Current standing waves have been shown to exist in a qualitative manner by Kemp (32) and in a semi-quantitative manner by Walker (33). This was done by detecting the AC magnetic field profile using a small search coil. However, it was not possible to show that voltage standing waves exist. An attempt to measure the voltage distribution across a foil wound inductor using a high-impedance FET probe was not successful. The capacitance of the probe was not low enough not to load the resonant circuit. An indirect method of showing that voltage standing waves exist was therefore adopted. This method is discussed in detail in chapter 4.

It has been shown that a lumped-element equivalent-circuit can describe with some accuracy, apart from the Q values of the resonances, the impedance/frequency spectrum of a small, air-cored, foil-wound inductor, up to an order of resonance determined by the number of sections used in the theoretical model. The model can also give some indication of the internal mechanism which generates the secondary resonances.

Chapter 3 Width Effect in Air-Cored, Foil-Wound Inductors

1) Introduction

The lumped-element, equivalent circuit of a foil wound inductor examined in chapter 2 contains the inductance of an individual turn L^t . An approximate formula has been derived but it is not clear how an exact calculation may be made. Standard formulae apply only to filamentary conductors. In order to calculate the axial field inside a foil turn and hence the inductance, some assumption is needed about the distribution of current across the width of the foil turn. At DC this will be uniform, but at AC some other distribution may be expected, created by a combination of skin and proximity effects, and requiring a field theory solution. This problem has been examined by Reeves (34), who obtained results for a single turn of foil using a complex numerical field-theory solution. The alternative method presented here is much simpler and has been extended to thin multi-turn foil-wound inductors.

2) Equivalent Circuit of a Single Turn of Foil

The single turn of foil shown in Fig. 3-1 is made from material of uniform thickness t , width W , and has a mean radius a . It is assumed that t is much less than a . It is also assumed that the connections to the foil turn have zero resistance, so that the connexions form equipotentials. It is then expected that the current flow in the foil turn is purely circumferential.

To examine the variation of current density across the width of the foil turn, we now divide it into strips in the

Figure 3-1

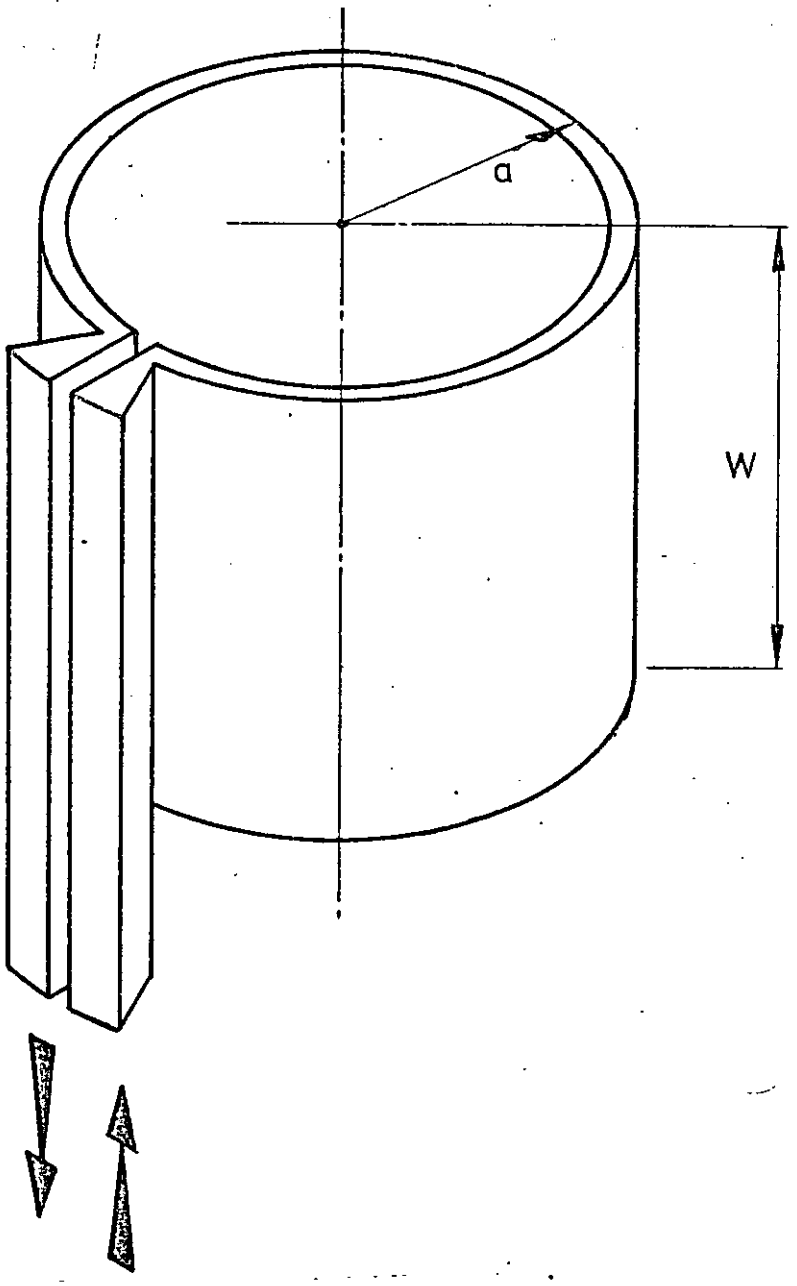

A Single Foil Turn of Radius a and Width W, with Equipotential Bus-Bars

axial direction, as shown in Fig. 3-2. It is convenient to have P strips of equal width c . Although in principle all strip widths could be different. c must be chosen so that the expected variation of current density within c is small.

The DC resistance of a foil turn is R_t , which is given by equation 2-7-1. The strips all have equal widths therefore the resistance of a strip is PR_t .

The inductance of a strip(L_r) with a uniformly distributed current flowing in it, is given by Grover (35) as

$$L_r = \mu_o a D \quad \text{Henries} \qquad 3-2-1$$

Where D is a dimensionless factor given by

$$D = \text{Ln}(8\beta) - 0{\cdot}5 + \frac{(\text{Ln}(8\beta) + \frac{1}{8})}{32\beta^2} + \frac{(\text{Ln}(8\beta) - \frac{2}{3})}{1024\beta^4}$$

$$+ \frac{(\text{Ln}(8\beta) - \frac{109}{120})}{13107{\cdot}2\,\beta^6} + \text{-----} \qquad 3-2-2$$

β is the ratio of the radius of the foil turn to the width of a strip.

By approximating the strips to filamentary conductors the formula given by Grover for mutual-inductance of two coaxial circular filaments can be used for the mutual-inductance of two strips. This expression has the form

$$M_{k,i} = \mu_o a F \quad \text{Henries} \qquad 3-2-3$$

Where F is a dimensionless factor dependent on the ratio α, which is the ratio of the radius of the foil turn to the separation of the two strips subscripted k and i .

Figure 3-2

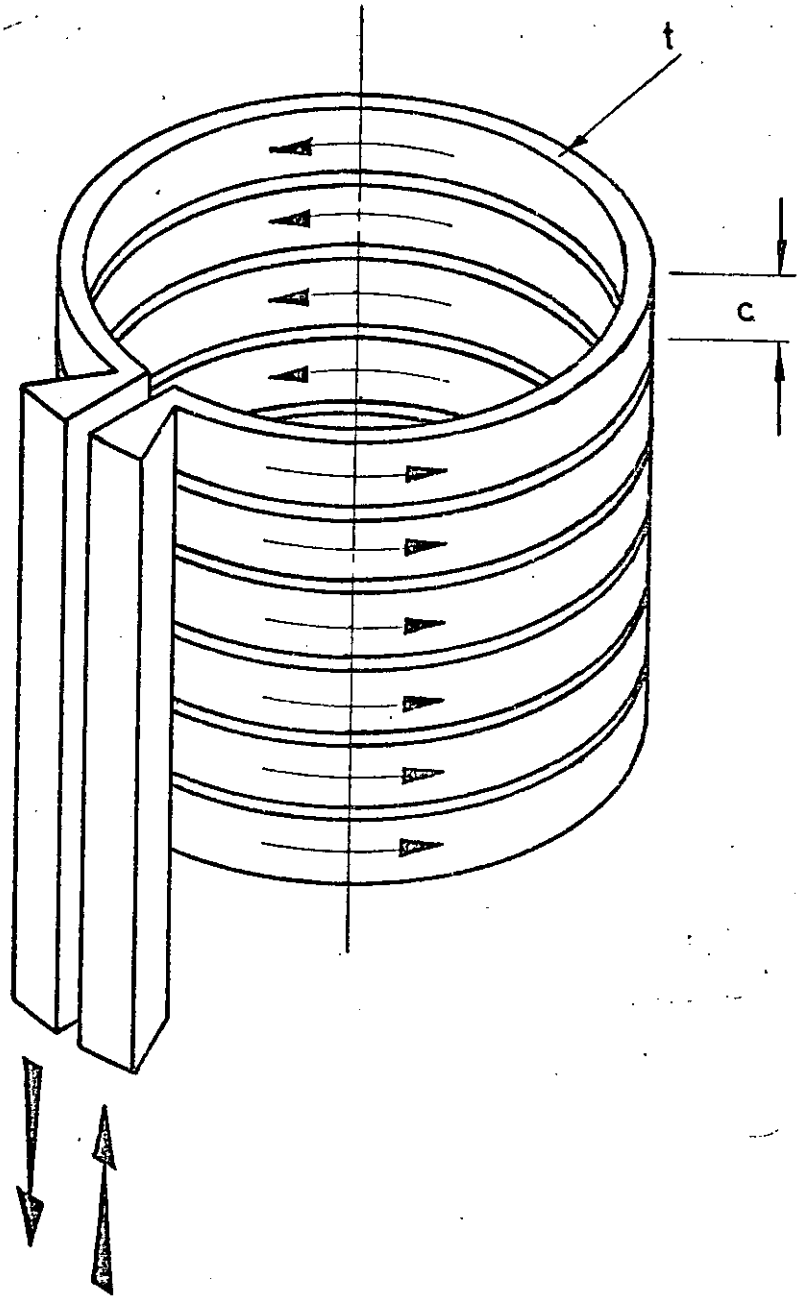

A Single Turn of Foil Thickness t cut into P Strips of Width c

F can be obtained from tables in Grover. Since the separation of the strips is constant and the strips are of equal width the mutual-inductances coupling the P strips can be characterised by P values of F .

The complete foil turn is represented by the equivalent circuit shown in Fig. 3-3. Each strip has a constant DC resistance in series with an inductance, which is coupled by mutual-inductances to all the other strips. The current flowing at the centre will at AC be less than the current flowing at the edges. This can be shown by first assuming that the currents in all the strips are equal. Each current has the same applied EMF, but a different back EMF. A strip near the centre will have a larger back EMF than a strip near the edge, as the strips near the centre are on average nearer their neighbours than the strips near the edge. Therefore towards the centre the back EMF will be larger, and as a first correction the currents near the centre will be smaller than those near the edge.

3) Computer Solution of the Equivalent Circuit

The equivalent circuit of Fig. 3-3 has to be analysed. The external current I_t is the sum of the strip currents I_k .

$$I_t = \sum_{k=1}^{P} I_k \qquad 3\text{-}3\text{-}1$$

The applied voltage is V_t , therefore the impedance will be given by

$$Z_t = \frac{V_t}{I_t} \qquad 3\text{-}3\text{-}2$$

The currents can be found by solving the P simultaneous equations of the form

Figure 3-3

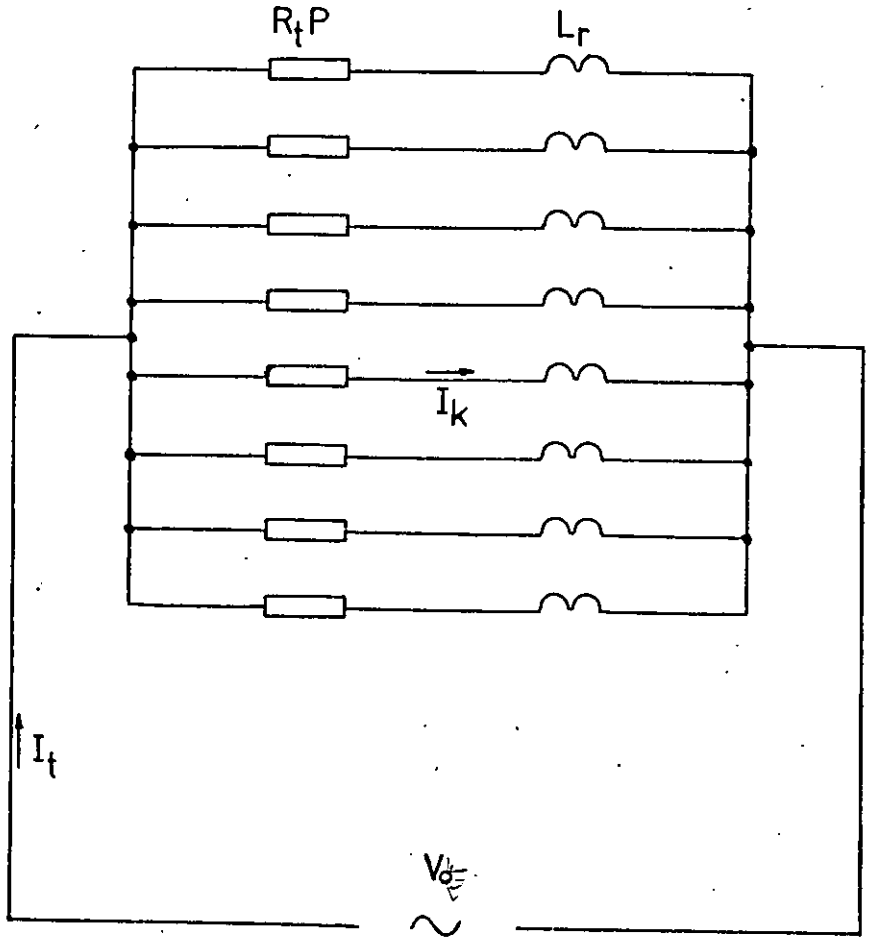

Equivalent Circuit of a Foil Turn Divided into P Strips

All the inductors are mutually coupled.

$$(PR_t + j\omega L_r)I_k + \sum_{i \neq k}^{P} j\omega M_{k,i} I_i = V_t \qquad 1 \leq k \leq P \qquad 3\text{-}3\text{-}3$$

To solve these equations it is convenient to reduce the problem to a dimensionless form as follows. A generalised frequency is defined by

$$\beta = \frac{\omega L_r}{PR_t} \qquad 3\text{-}3\text{-}4$$

A generalised admittance t_k for the strip k is defined to be

$$t_k = \frac{P R_t I_k}{V_t} \qquad 3\text{-}3\text{-}5$$

The matrix of mutual-inductances $[M_{k,i}]$ is replaced by a matrix of coupling coefficients $[K_{k,i}] = [M_{k,i}]/L_r$. For coils having the same ratio of length to radius and divided into the same number of strips the matrix of the elements $K_{k,i}$ is the same. This means that turns of foil of differing size but the same shape are characterised by the same set of generalised equations.

With the above transformations the P simultaneous equations become

$$(1 + j\beta)t_k + j\beta \sum_{i \neq k}^{P} t_i K_{k,i} = 1 \qquad 1 \leq k \leq P \qquad 3\text{-}3\text{-}6$$

The admittance of the complete foil will be given by

$$\frac{1}{Z_t} = \sum_{k=1}^{P} \frac{t_k}{R_t P} \qquad 3\text{-}3\text{-}7$$

The matrix $[K_{k,i}]$ is composed of the P^2 elements $K_{k,i}$. There are only P distinct values of the coupling coefficients $K_{k,i}$ when the strips are equally spaced, and these can be

derived from the set:

$$1, K_2, K_3, -----, K_\delta, ----, K_P \qquad 3\text{-}3\text{-}8$$

Where δ is given by

$$\delta = |k - i| + 1 \qquad 3\text{-}3\text{-}9$$

The matrix [K] is dimensionless and its elements are obtained by combining equations 3-2-1 and 3-2-3 to give

$$K_{k,i} = \frac{M_{k,i}}{L_r} = \frac{F}{D} \qquad 3\text{-}3\text{-}10$$

F and D are dependent on the ratios α and β, which are dimensionless.

Since the t_k are complex the set of equations 3-3-6 were organised as a complex matrix equation and solved in the same manner as the set of equations 2-4-5. The complex matrix equation was expanded into a $2P \times 2P$ real matrix equation and solved using the Gaussian Elimination described in Appendix 1.

4) Theoretical Results for a Foil Turn with $a = W$

The width effect in the set of foil turns with $\gamma = 1$ was calculated up to the frequency of $\xi = 1$. Where γ is the ratio of the radius of the foil turn to the foil width. The non-uniformity of the current distribution and its dependence on frequency are shown in Fig. 3-4. For this particular example the magnitude of the current flowing in the midfoil strips is well below half that flowing in the edge strips at $\xi = 1$, so a significant increase in the resistance of the foil at AC is expected. There is a variation in the phase of the current across the foil width. This can be seen in the Argand diagram

Figure 3-4

Plot of Relative Magnitude of Current Density across the Foil Width as a Function of Frequency ($a = W$).

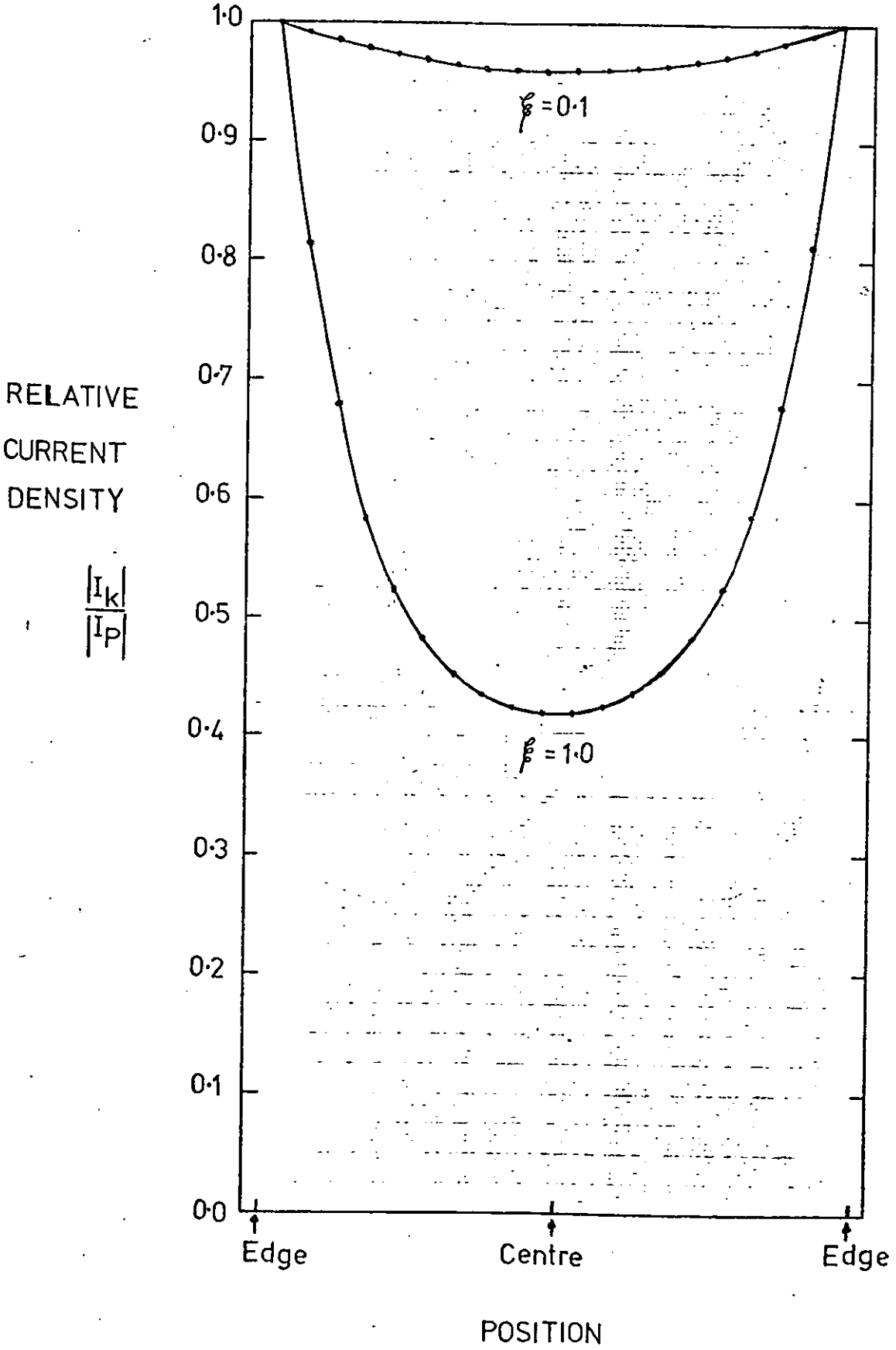

of Fig. 3-5; each solid line represents the fan of vectors at one value of β . As β increases the weighted average phase of the fan (which is the phase of I_t relative to V_t) shows increasing lag and the currents near the midfoil always lag the larger currents near the edges.

The effective resistance of the foil turn can be obtained from equation 3-3-7. The real part of Z_t is the effective resistance, which is composed of a DC resistance plus an AC resistance. As the DC resistance is unknown at this point the effective resistance is best expressed as a ratio of the DC resistance. This ratio, for the foil turn with $\alpha=1$, is shown against generalised frequency in Fig. 3-6. At $\beta=1$ the effective resistance has risen by 15% over the DC value. This rise is large enough to be significant in the design of foil chokes. The variation of the ratio of the AC resistance to the DC resistance with generalised frequency is shown in Fig. 3-7 on a logarithmic scale. This shows that at frequencies below $\beta=0{\cdot}1$ the increase in the effective resistance is closely proportional to the square of the frequency. This dependence is observed in a wide range of eddy current and proximity loss problems.

The imaginary part of Z_t is the product of the inductance with the angular frequency. To preserve generality the inductance is best expressed as the ratio of the inductance at AC to the inductance at DC. For simplicity the inductance at DC is taken to be that at $\beta=0{\cdot}001$. The variation of inductance with generalised frequency is shown in Fig. 3-6. At $\beta=1$ the fall in the inductance is only 3% and for many purposes could be neglected.

Figure 3-5

Argand Diagram Showing the Phase and Amplitude of the Current Density Across the Foil Width, as a Function of Frequency (α=W).

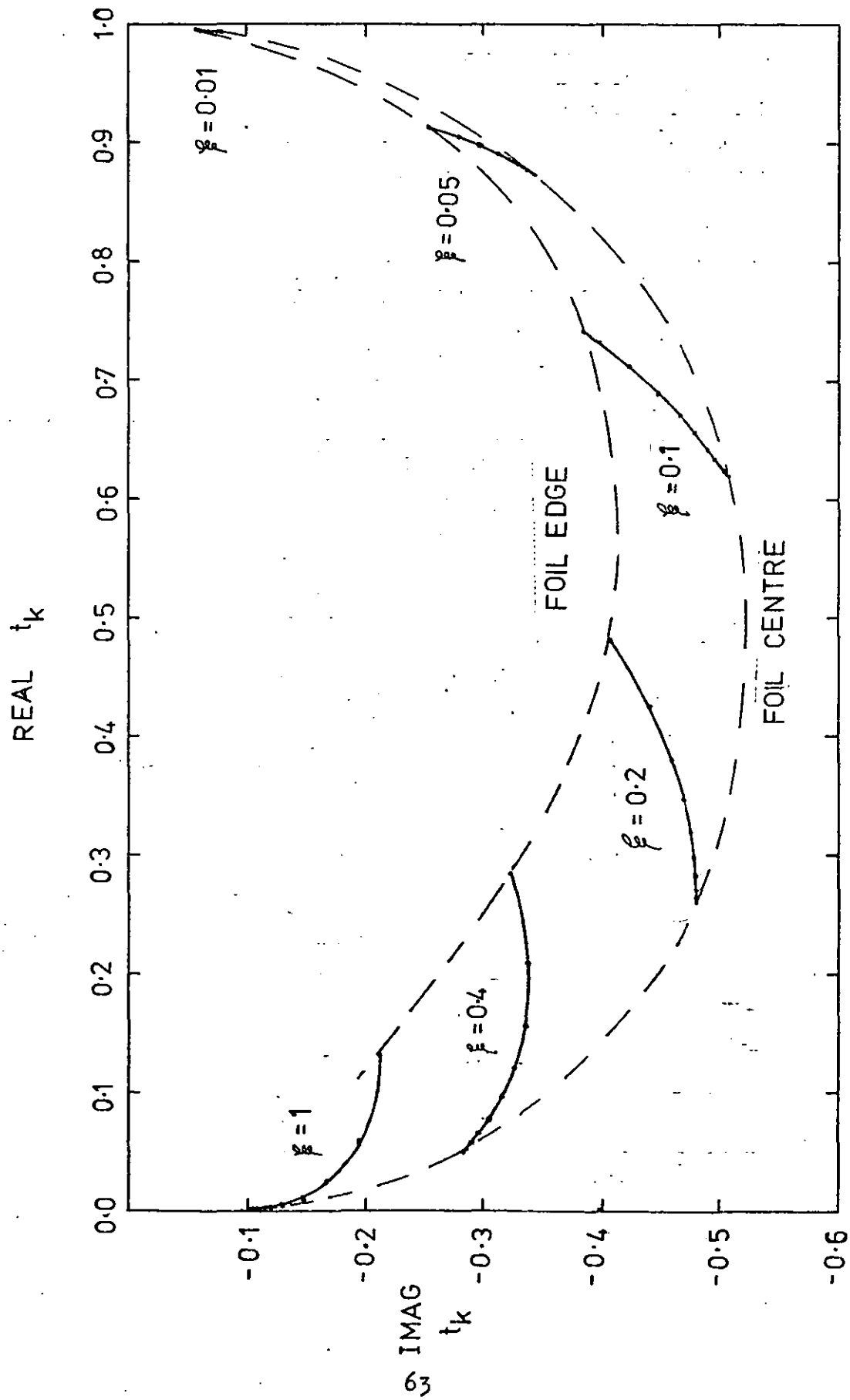

Figure 3-6

Frequency Dependence of Resistance and Inductance for a Single Foil Turn with $\alpha = W$.

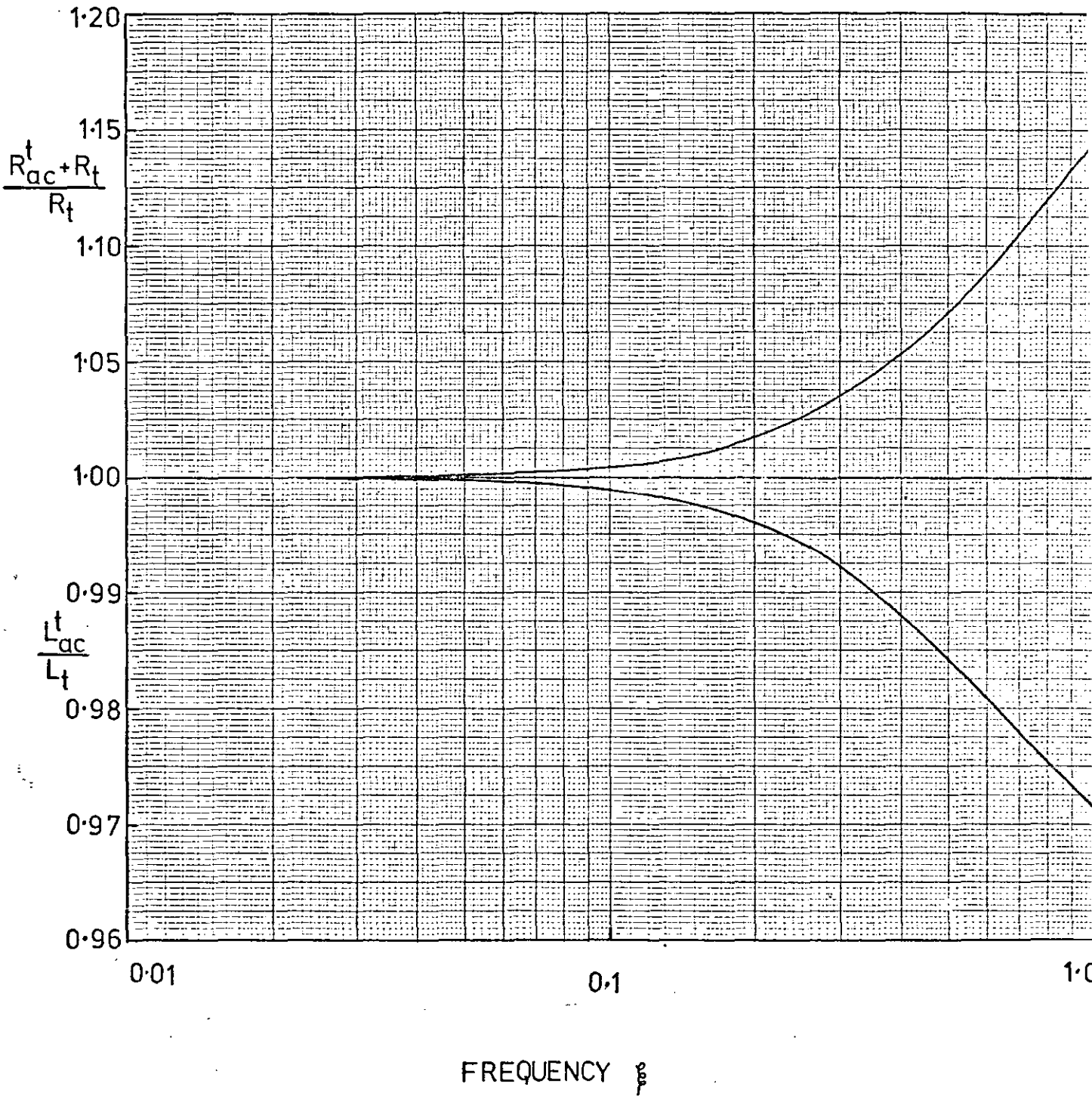

Figure 3-7

Approximate Square Law Dependence of the Excess A.C. Resistance R_{ac}^{t}.

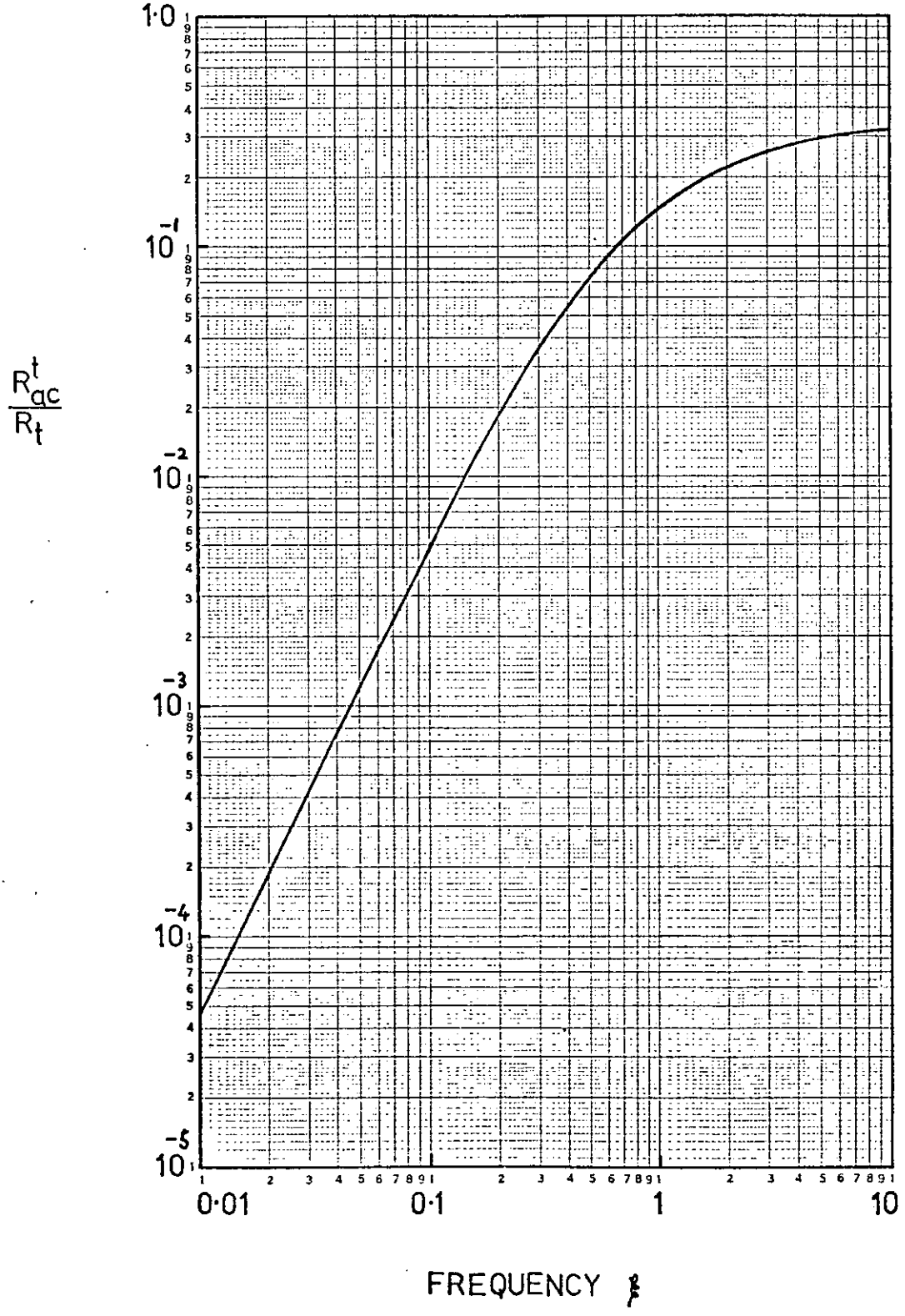

As the current profile changes with increasing frequency we would expect the shape of the magnetic field within the foil turn to change. The calculations show this effect. The strip k is threaded by a flux Φ_k , which is given by

$$\Phi_k = L_r I_k + \sum_{i \neq k}^{P} I_i M_{k,i} \qquad 3\text{-}4\text{-}1$$

$$1 \leqslant k \leqslant P$$

Fig. 3-8 shows the profile of Φ_k , as a ratio to the value of Φ_k at the centre of the turn, for two values of β . The profile becomes flatter with increasing frequency; at $\beta = 1$ the profile is virtually flat over more than three-fifths of the turn length. If we examine equation 3-3-3 in the limit of large frequencies and neglect the resistive term, we may then substitute from equation 3-4-1 and obtain

$$V_t = j\omega \Phi_k \qquad 3\text{-}4\text{-}2$$

$$1 \leqslant k \leqslant P$$

The limit gives equal flux through all the strips. This implies that the current distribution has a limiting profile at high frequency.

The variation of the flux profile with frequency can be shown experimentally. The experiment involves the use of a foil wound inductor with two search coils wound into it, one at the centre and one at the edge. The physical dimensions of this coil are given in the table shown in Fig. 3-9. The voltages from the search coils are directly proportional to the fluxes through them, therefore the ratio of the two voltages $|V_{outer}|$ to $|V_{centre}|$ will be the ratio of the magnitudes of the two fluxes. The graphs shown in Fig. 3-8 show that theoretically

Figure 3-8

The Dependence of the Flux Φ_k on Axial Position and Frequency ($a = W$).

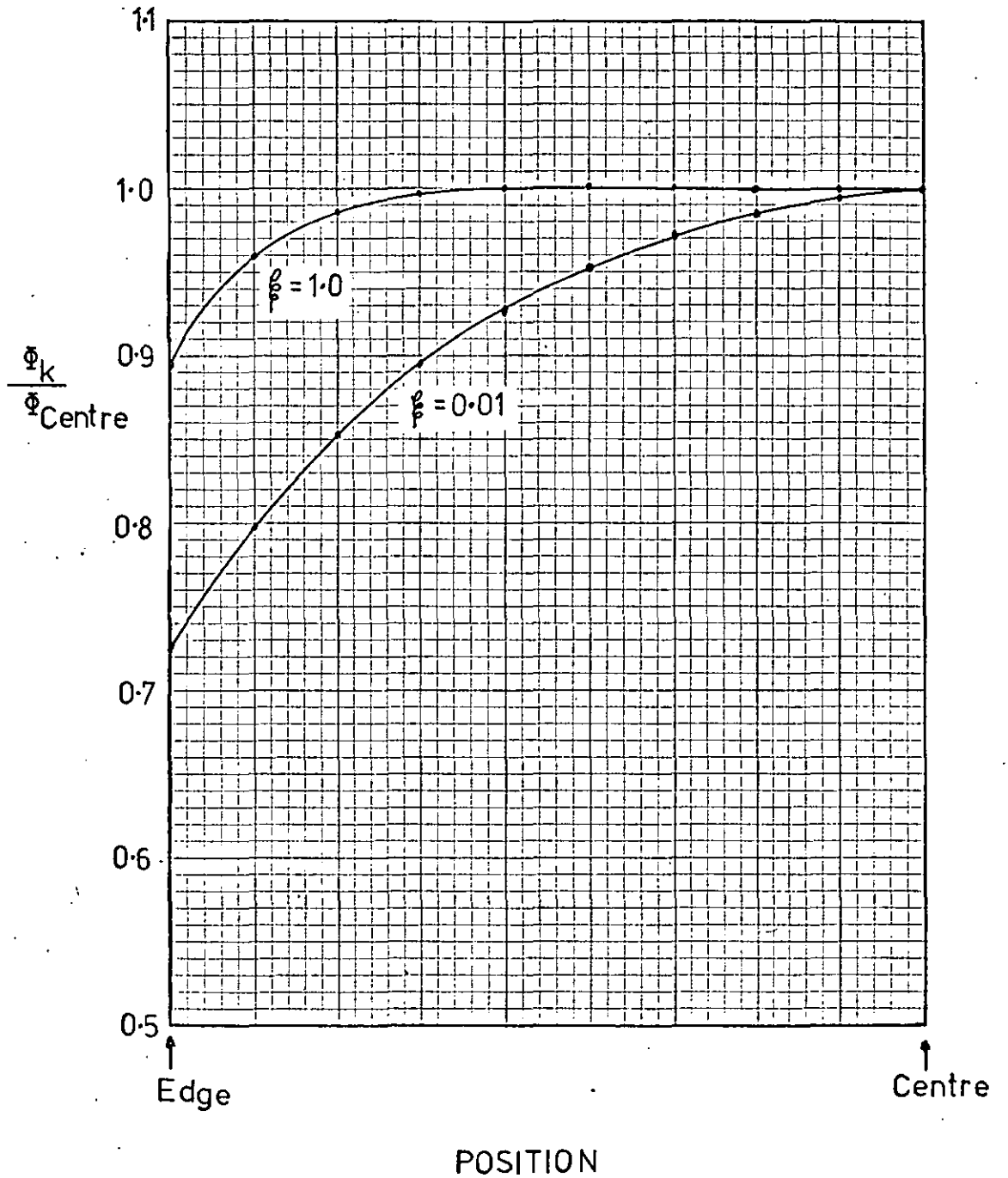

Figure 3-9

Dimensions of the Foil Wound Inductor with Search Coils.	
Core Radius	0.6 cm
Type of Metal Foil	Aluminium
Thickness of Metal Foil	5.0 μm
Width of Metal Foil	3.8 cm
Thickness of Plastic Film	15.0 μm
Number of Turns	725 Turns
Search Coils Begin at	530 th Turn
Search Coils End at	710 th Turn

Figure 3-10

Experimental Apparatus Used to Measure the Ratio $|V_{outer}| / |V_{centre}|$

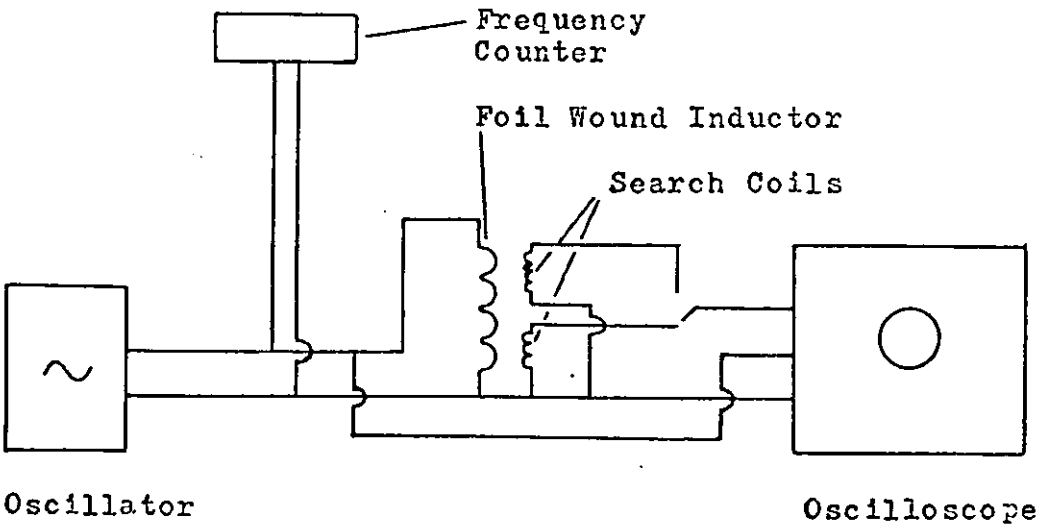

the ratio of the voltages should tend towards equality at high frequencies.

The experimental apparatus is shown in Fig. 3-10. The frequency of the input voltage was measured using a frequency counter, while its amplitude was measured using one beam of the oscilloscope. The frequency of the input was varied from 50 Hz to 100 KHz. The voltages from the two search coils were measured using the other beam of the oscilloscope.

The results are shown in Fig. 3-11. The ratio of $|V_{outer}|$ to $|V_{centre}|$ rises from approximately 0.5 at 50 Hz to 1.02 at 100 KHz. This confirms in an empirical manner that there is a "width effect".

5) Width Effect in Thin Multi-Turn Coils

The extension of the equivalent circuit from single turns of foil to multi-turn foil coils is not a simple matter, because the possibility of axial current flow must be considered. One possible equivalent circuit which takes this into consideration is shown in Fig. 3-12. In this model the N turns of the coil are divided axially into P strips in the same manner as the single turn, except that each strip now has N turns. The l^{th} turn of the k^{th} strip has an inductance L'_r and a resistance PR'_r. The strips are cross linked by resistances to represent axial current flow. The principal disadvantage of this circuit is that there are $N\times(P-1)$ currents that have to be calculated: a 50 turn coil sub-divided into 20 strips would have 950 currents that have to be calculated. Clearly the computer power and time required to calculate the impedance/frequency spectrum would be prodigious.

Figure 3-11 Variation of $|V_{outer}|/|V_{centre}|$ with Frequency

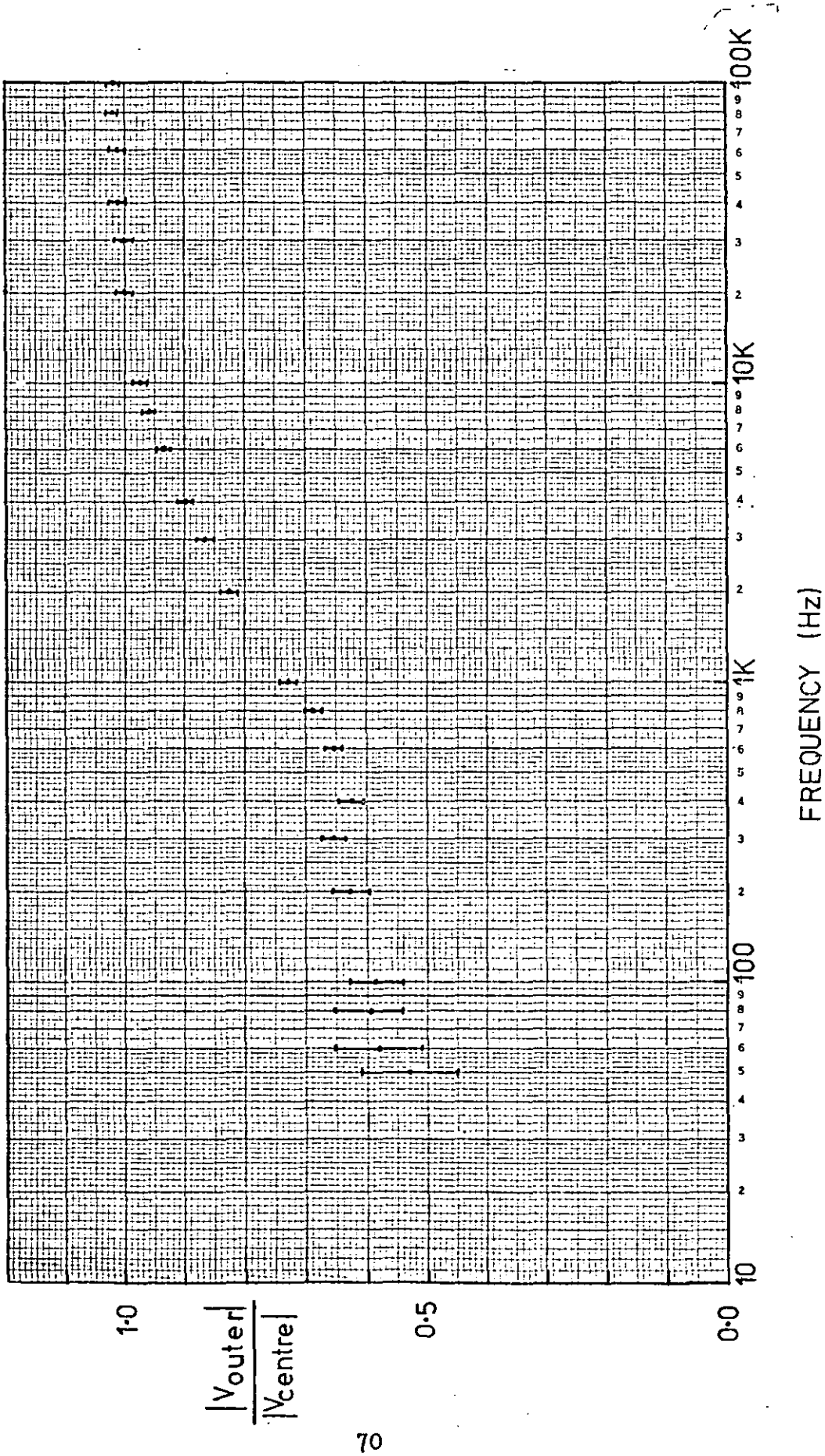

Figure 3-12 General Low-Frequency Equivalent Circuit of an N Turn Foil Wound Inductor with P Strips Each of N Turns

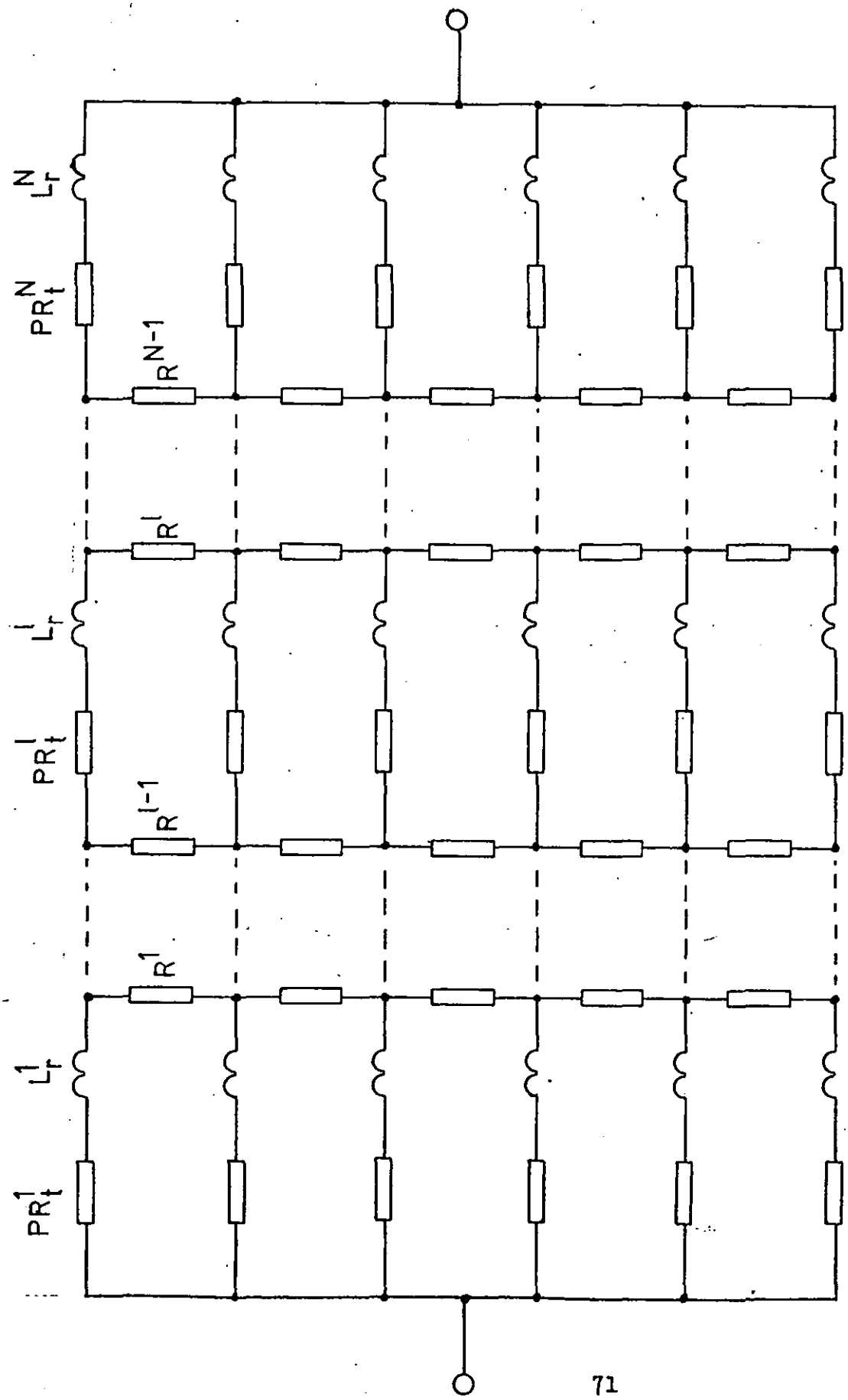

However, by restricting the application of the multi-turn model to one particular class of foil wound inductor a manageable theory can be derived. For foil wound inductors where the build-up of the winding is much less than either the radius of the winding or the width of the metal foil it can be assumed that all the strip turns are identical. This means that all the turn inductances are the same, as are all the turn resistances, and that all the turn inductances within a strip are perfectly coupled. This implies that the self-inductance of a strip is N^2L_r and the resistance NPR_t . This approximation also means that all the mutual-inductances coupling two strips are the same. Therefore the mutual-inductance from the k^{th} strip to the i^{th} strip is equal to $N^2M_{k,i}$.

Now we consider one particular strip-turn. This strip-turn is now perfectly coupled to all the other strip-turns on the same strip and mutual-inductances from this strip-turn to all the strip-turns of another strip are the same. Therefore all the strip-turns on a strip are identical and the voltage drop across each must be the same. This argument can be applied to all the strips. Thus the voltage across the cross-linking resistances is zero and they can be removed from the equivalent circuit.

The equivalent circuit is now that shown in Fig. 3-13. This circuit can be analysed using P equations of the form

$$(NPR_t + j\omega N^2 L_r)I_k + \sum_{i \neq k}^{P} j\omega N^2 M_{k,i} I_i = V_o \qquad 3\text{-}5\text{-}1$$

The generalised frequency p can be redefined as

Figure3-13

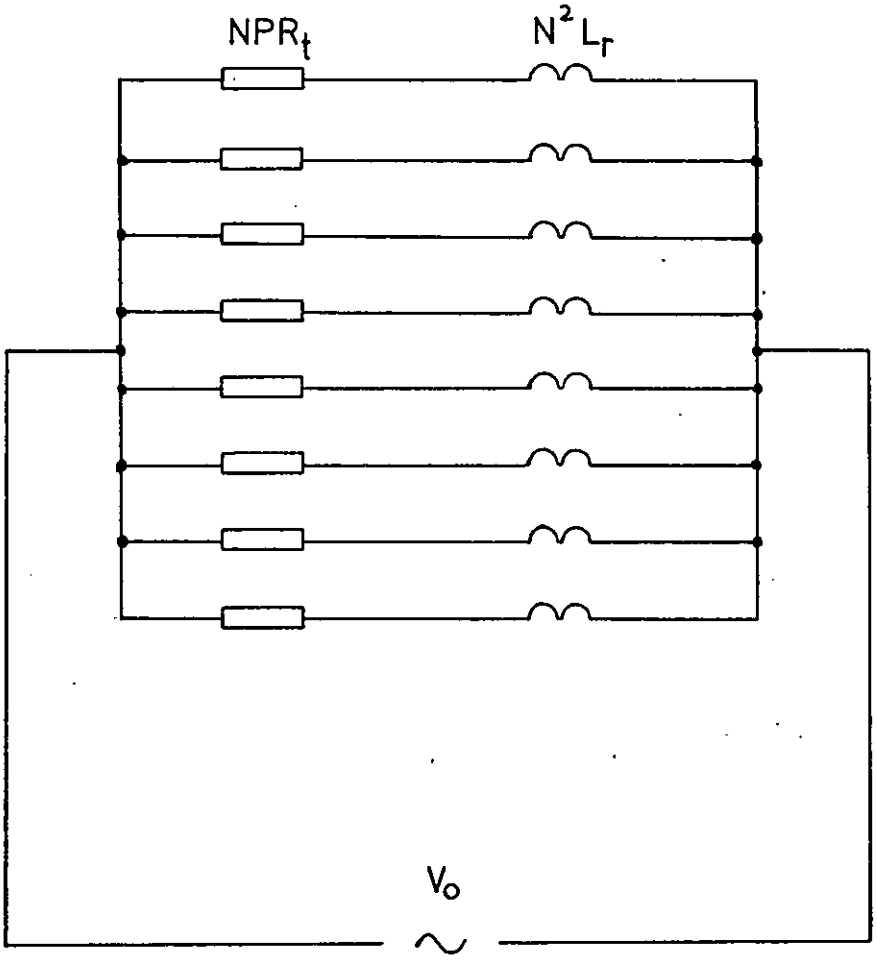

Equivalent Circuit of a Multi-Turn Foil Wound Inductor (build-up << a, << W) Divided into P Strips

All the inductors are mutually coupled.

$$\beta = \frac{\omega N L_r}{P R_t} \qquad 3\text{-}5\text{-}2$$

Also the generalised admittance t_k can be redefined as

$$t_k = \frac{N P R_t I_k}{V_o} \qquad 3\text{-}5\text{-}3$$

The previous definitions of β and t_k , equations 3-3-4 and 3-3-5 are now the special case of $N = 1$.

With the new definitions of β and t_k equation 3-5-1 reduces to equation 3-3-6, which previously applied only to a single turn of foil, but can now be applied to a whole set of coils.

6) Experimental Technique and Apparatus

The most important aspect of the theory of the thin multi-turn coil is that both β and t_k scale with N . Thus if a set of coils of equal width and radius but varying N meet the conditions regarding the build-up of the coils, then the variation of the inductance and resistance should be the same for all the coils of the set when plotted on a scale of turns times frequency.

To test the theory against the number of turns on the coil and the width of the coil six special foil wound inductors were manufactured §. These coils were designed as two sets, each comprising one coil of 100 turns, one of 50 turns and one of 25 turns. The two sets differed in one respect only; one set had a width of 14 cm and the other a width of 6 cm. The dimensions of the foil wound inductors are shown in Fig. 3-14.

§ Manufactured by Aluminium Inductors Ltd, Croydon, Surrey

Figure 3-14

Physical Parameters and Dimensions of the 14 cm Wide Set of Foil wound inductors	
Core Radius (Outer Diameter)	3.175 cm
Type of Metal Foil	Aluminium
Thickness of Metal Foil	50.0 um
Width of Metal Foil	14.0 cm
Type of Plastic Foil	Polyester
Thickness of Plastic Foil	25.0 um
Number of Turns	100 50 25

Physical Parameters and Dimensions of the 6 cm Wide Set of Foil Wound Inductors	
Core Radius (Outer Diameter)	3.175 cm
Type of Metal Foil	Aluminium
Thickness of Metal Foil	50.0 um
Width of Metal Foil	6.0 cm
Type of Plastic Foil	Polyester
Thickness of Plastic Foil	25.0 um
Number of Turns	100 50 25

The coils are shown in the photograph in Fig. 3-15.

In the worst case, the build-up of the 100 turn coils is 0.75 cm compared with an internal coil radius of 3.175 cm and a width of either 14 cm or 6 cm.

The connections to the coils were made with copper strips 1 cm wide and 1mm thick, with the exception of the 50 turn, 14 cm wide coil; the copper strips in this case were 1.9 cm wide and 1.5 mm thick.

These foil wound inductors have D.C. resistances in the order of 0.1 Ohm and inductances in the order of 0.1 milli-Henry. To measure this low impedance in the audio frequency range a suitable bridge had to be built. Although several types of bridge are suitable a form of the Maxwell inductance bridge was chosen, because the necessary high accuracy resistance and capacitance boxes were available. This particular form of the Maxwell inductance bridge is shown in Fig. 3-16. Where R_x and L_x represent the resistance and inductance of the unknown impedance and R_1 , R_2 , R_3 and C have known values. The balance condition for this bridge is given by

$$\frac{R_x + j\omega L_x}{R_1} = R_2\left(\frac{1}{R_3} + j\omega C\right) \qquad 3\text{-}6\text{-}1$$

Separating the real and imaginary parts of this equation gives

$$R_x = \frac{R_1 R_2}{R_3} \qquad 3\text{-}6\text{-}2$$

$$L_x = R_1 R_2 C \qquad 3\text{-}6\text{-}3$$

The expressions for R_1 and R_2 fulfill two important criteria; the balance conditions for the resistance and inductance are

Figure 3-15

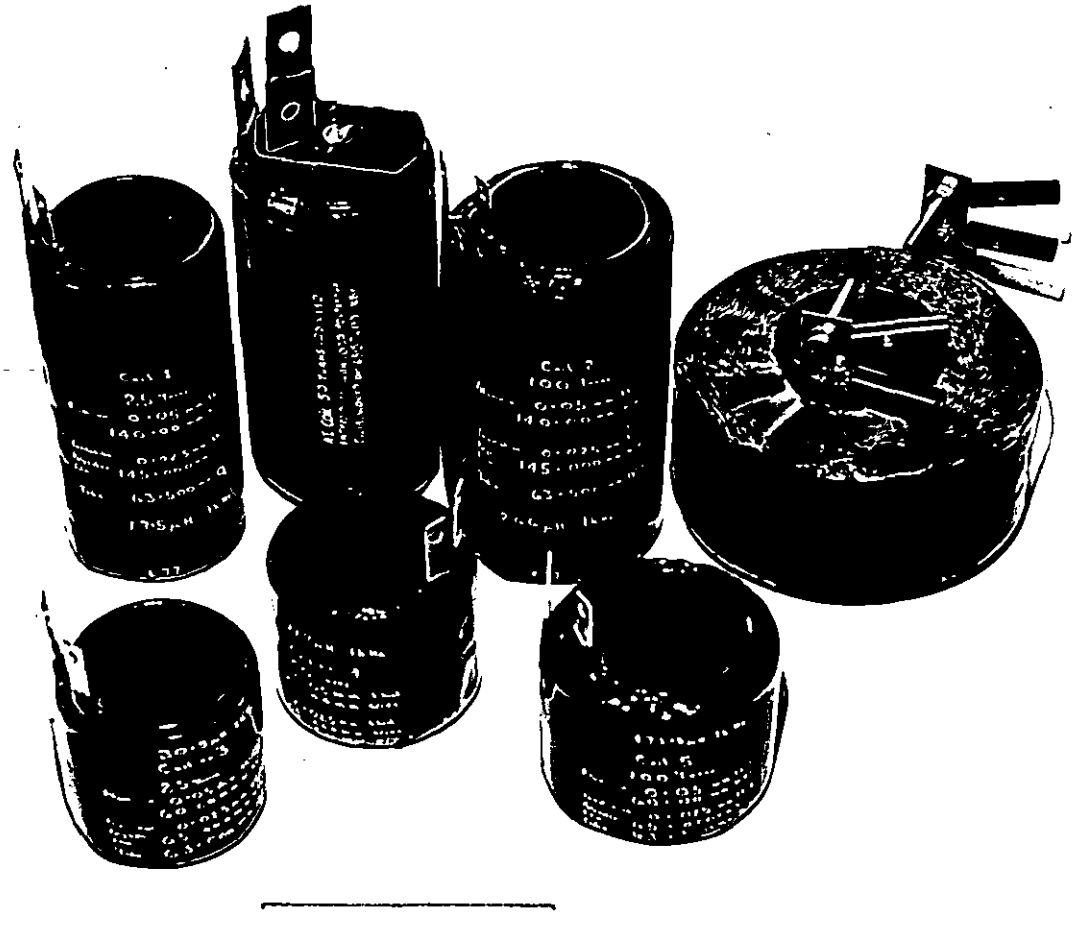

Seven Foil Wound Inductors Used to Test the Width Effect Theory
The line on the photograph is 10 cm long.

Figure 3-16

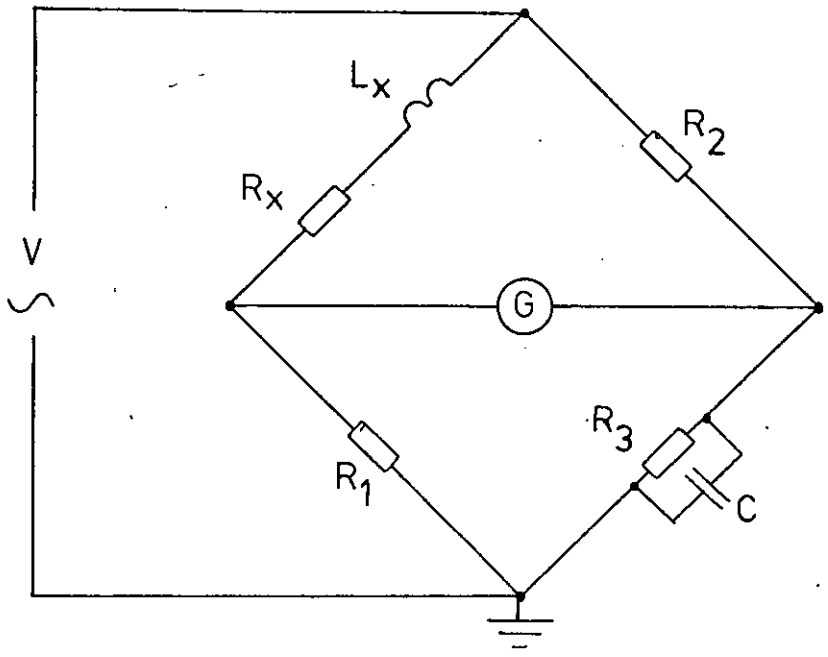

Maxwell bridge used to measure the inductance and resistance of the Foil Wound Inductors.

L_x and R_x represent the impedance of the Foil Wound Inductor. R_1, R_2 and R_3 are 0.05% accuracy resistance boxes and C is a 0.1% accuracy capitance box.

G is the Scalamp Galvanometer used to measure the D.C. resistance of the Foil Wound Inductor.

Figure 3-17

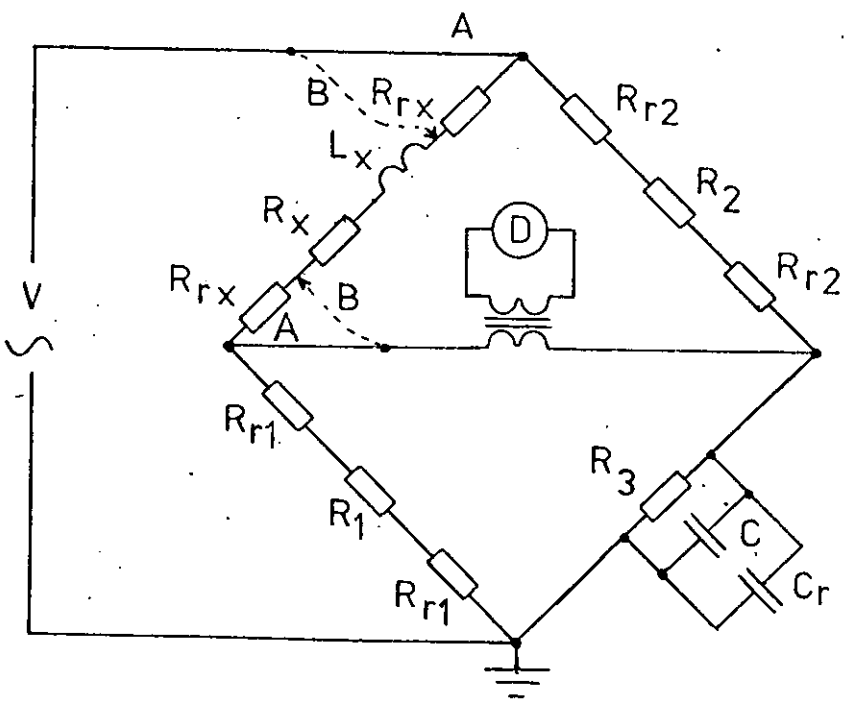

Maxwell bridge of Fig. including relevent residual resistances and the residual capitance of the capacitance box.

Arrangement A is the two terminal method and arrangement B is the four terminal method of measuring the unknown inductance

D is a General Radio Tuned Amplifier and Null Detector (Type 1232-A)

The transformer is a Sullivan Type A.C. 300/A

separate and they are independent of frequency.

Both R_1 and R_2 are common to the expressions for R_x and L_x . Therefore R_3 was varied to obtain the value of R_x and C was varied to obtain the value of L_x . Resistance boxes with an accuracy of 0.05% were used for R_1 and R_2 . With the foil wound inductors investigated the optimum value for both R_1 and R_2 was found to be 10 Ohms. R_3 was a 5 decade resistance box with an accuracy of 0.05% and C was a 5 decade low-loss mica capacitance box with an accuracy of 0.1%.

It was found that because the foil wound inductors present a low impedance at audio frequencies, the residual resistances of the bridge have to be taken into consideration. These residual resistances are composed of wire resistances, contact resistances and the residual resistances of the resistance boxes R_1 and R_2 . Fig. 3-17 shows the residual resistances R_{rx} , R_{r1} and R_{r2} together with the residual capacitance of the capacitance box, which was 110 pF. Because the capacitance box used mica capacitors the leakage resistance was neglected. The residual resistance connected with R_3 was small enough compared with the value of R_3 to be neglected. It has been assumed that the residual resistances were distributed equally on either side of the associated resistance.

Arrangement A in Fig. 3-17 is the normal two terminal bridge method of measuring the unknown impedance. Arrangement B in Fig. 3-17 is the four terminal bridge method employed to minimise the effect of the residual resistance R_{rx} . With the four terminal method the balance condition equations 3-6-2 and 3-6-3 become

$$R_x = \frac{(R_1 + 2R_{r1} + R_{rx})(R_2 + 2R_{r2} + R_{rx})}{R_3} \qquad 3\text{-}6\text{-}4$$

$$L_x = (R_1 + 2R_{r1} + R_{rx})(R_2 + 2R_{r2} + R_{rx})(C + C_r) \qquad 3\text{-}6\text{-}5$$

A first order value for R_{r1} was obtained by taking one set of measurements R_1 , R_2 and R_3 , then altering R_1 to R_1' , and taking another set of measurements R_1' , R_2 and R_3' . Neglecting the other residual resistances the first order value of R_{r1} can be obtained from

$$R_x = \frac{(R_1 + 2R_{r1})R_2}{R_3} = \frac{(R_1' + 2R_{r1})R_2}{R_3'} \qquad 3\text{-}6\text{-}6$$

Solving this equation for R_{r1} gives

$$R_{r1} = \frac{(\frac{R_1'}{R_3'} - \frac{R_1}{R_3})}{2(\frac{1}{R_3} - \frac{1}{R_3'})} \qquad 3\text{-}6\text{-}7$$

A similar procedure taking two sets of measurements R_1, R_2 R_3 and R_1 , R_2'' , R_3'' will yield a value for R_{r2} given by

$$R_{r2} = \frac{(\frac{R_2''}{R_3''} - \frac{R_2}{R_3})}{2(\frac{1}{R_3} - \frac{1}{R_3''})} \qquad 3\text{-}6\text{-}8$$

Neglecting the other residual resistances the two terminal bridge method yields a first order value for $R_x + 2R_{rx}$ given by

$$R_x + 2R_{rx} = \frac{R_1 R_2}{R_3'''} \qquad 3\text{-}6\text{-}9$$

Subtracting this equation from equation 3-6-2 and solving for R_{rx} gives

$$R_{rx} = \frac{R_1 R_2}{2}\left(\frac{1}{R'''_3} - \frac{1}{R_3}\right) \qquad 3\text{-}6\text{-}10$$

The first order value of the residual resistance R_{rx} was found by taking one set of measurements R_1 , R_2 , R_3 using the four terminal bridge method, then changing to the two terminal bridge method and taking another set of measurements R_1 , R_2 , R'''_3 .

Altogether 4 sets of readings are needed to derive the values of R_{rx} , R_{r1} , R_{r2} , which were typically of the order of 0.1 Ohm. Each time a foil wound inductor was connected to the bridge new sets of readings were taken to determine the residuals. These readings were taken at D.C. although in principle they could have been taken using the A.C. source and detector.

The D.C. calibration of the bridge was performed using Sulivan precision standard resistances with values of 0.5 Ohm, 0.1 Ohm and 0.01 Ohm. The four terminal bridge method alone gave values for these resistors of 0.4955Ω ±0.05%, 0.09607Ω ±0.05% and 0.008432Ω ±0.05%. Taking the residual resistances into account increased these values to 0.5008Ω ±0.05%, 0.10052Ω ±0.05% and 0.010166Ω ±0.05%. These values are in error by +0.16%,+0.52% and +1.7%. As these errors decrease with increasing resistance it can be assumed that the D.C. error for resistances greater than 0.5 Ohm will be less than +0.16% ±0.05%, for resistances between 0.5 Ohm and 0.1 Ohm the D.C. error will be less than +0.52% ±0.05% and for resistances between 0.1 Ohm and 0.01 Ohm the D.C. error will be less than +1.7% ±0.05%.

The A.C. resistance calibration of the bridge was performed using Sullivan low-inductance resistance boxes calibrated in hundredths of an Ohm. Two resistances with nominal values of 0.5 Ohm and 0.05 Ohm were formed with these resistance boxes. The A.C. resistance of these resistances were measured, as a fraction of the D.C. resistance, at frequencies between 40 Hz and 20 KHz. The results are shown graphically in Fig. 3-18 and show that the error is less than ±1% at frequencies below 4 KHz and is less than ±3% at frequencies between 4 KHz and 20 KHz.

The A.C. inductance calibration of the bridge was performed using three inductors wound from 38 SWG copper wire. This gauge of wire has a diameter of 0.152 mm and it can be seen from Fig. 3-27 that this is approximately three times less than the skin depth at 20 KHz of copper at room temperature. Therefore the inductance of these inductors should not vary significantly within the frequency range of the bridge.

The three inductors had values of 243.2 μH ±0.1%, 108.1 μH ±0.1% and 49.14 μH ±1.0% measured on a Sullivan-Griffiths inductance bridge at 1 KHz. The corresponding values on the Maxwell bridge at 1 KHz were 243.04 μH ±0.2%, 107.4 μH ±0.2% and 48.53 μH ±0.2%. These values are in error by -0.06%, -0.6% and -1.3%. As the error decreases with increasing inductance the error in any measured inductance value at 1 KHz will be -0.06%±0.22% for inductances greater than 243 μH, less than -0.6% ±0.22% for inductances between 107 and 243 μH and -1.3% ±1.02% for inductances between 49 and 107 μH.

The inductances of these inductors were measured at frequencies bewteen 40 Hz and 20 KHz. These measurements

Figure 3-18 Maxwell Bridge A.C. Resistance Calibration Curves

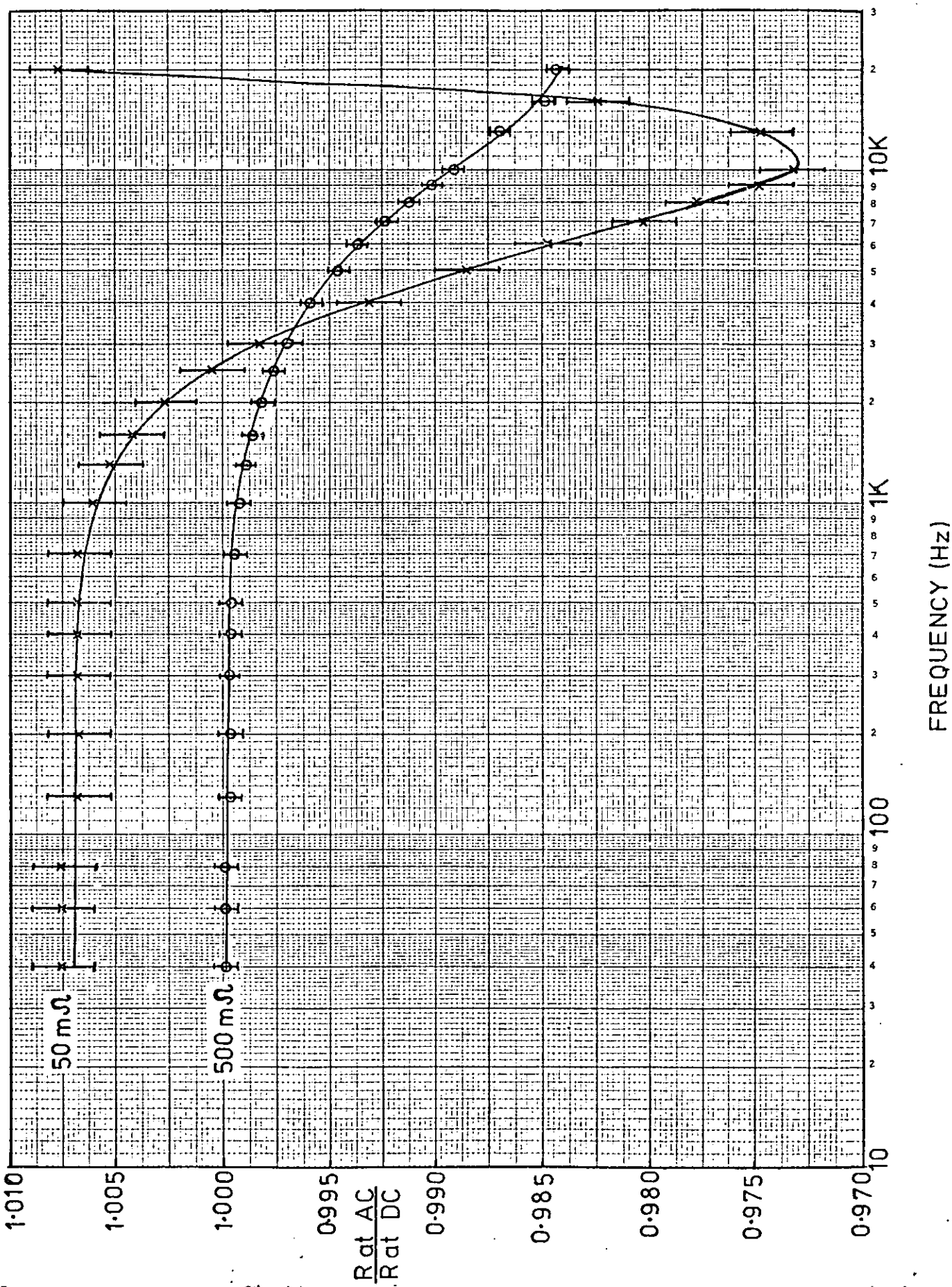

showed that the accuracy, relative to the 1 KHz inductance, was ±0.2% at frequencies between 40 Hz and 10 KHz and ±0.4% between 10 KHz and 20 KHz.

7) Resistance and Inductance Measurements

For convenience the impedance Z_o of the foil wound inductor is represented by

$$Z_o = R_{dc} + R_{ac} + j\omega L \qquad 3\text{-}7\text{-}1$$

Where R_{dc} is the D.C. resistance of the foil wound inductor; R_{ac} its frequency dependent excess A.C. resistance, which is zero at D.C.; and L its frequency dependent inductance.

For each of the two sets of foil wound inductors the resistance $(R_{dc} + R_{ac})$ and the inductance (L) were measured at frequencies between 40 Hz and 20 KHz, then the D.C. resistances (R_{dc}) and the residual resistances were measured at D.C.

The bridge could not be used at frequencies below 40 Hz due to the limitations of the detector or at frequencies above 20 KHz due to the increasing frequency dependence of the resistance boxes R_1 , R_2 , and R_3 .

Fig. 3-19 shows the D.C. resistances, the 1 KHz inductances and the 10 KHz inductances of the two sets of foil wound inductors. Fig. 3-20 gives the percentage increase in the resistance $(R_{dc} + R_{ac})$ at 1 KHz and 10 KHz over the D.C. resistance (R_{dc}) . The results of Fig. 3-19 show that the self-inductance decreases with increasing frequency. The results of Fig. 3-20 show that the increase in the resistance increases with the number of turns.

Figure 3-19

The D.C. resistance, the 1 KHz self-inductance and the 10 KHz self-inductance of the two sets of foil wound inductors.

Coil Width: 14. cm			
Number of Turns	D.C. Resistance Ohms	1 KHz Self-Inductance μH	10 KHz Self-Inductance μH
100	0.08969 ±1.7%	267.7 ±0.28%	263.1 ±0.47%
50	0.04307 ±1.7%	64.49 ±2.3%	62.8 ±2.3%
25	0.02049 ±1.7%	15.39 ±2.3%	15.01 ±2.3%
Coil Width: 6. cm			
Number of Turns	D.C. Resistance Ohms	1 KHz Self-Inductance μH	10 KHz Self-Inductance μH
100	0.2039 ±0.57%	479.3 ±0.28%	464.7 ±0.47%
50	0.09608 ±1.7%	117.6 ±0.82%	113.7 ±1.1%
25	0.04734 ±1.7%	28.98 ±2.3%	27.85 ±2.3%

Figure 3-20

Percentage increase of the A.C. resistance at 1 KHz and 10 KHz over the D.C. resistance.

Coil Width: 14. cm		
Number of Turns	1 KHz	10 KHz
100	32.5 ±1.%	239. ±3.%
50	20.7 ±1.%	201. ±3.%
25	10.1 ±1.%	110. ±3.%
Coil Width: 6. cm		
Number of Turns	1 KHz	10 KHz
100	40.1 ±1.%	220. ±3.%
50	21.7 ±1.%	154. ±3.%
25	10.8 ±1.%	105. ±3.%

The variation of the resistance with frequency for the 14 cm wide set is shown in Fig. 3-21 and for the 6 cm wide set in Fig. 3-22. The variation is expressed fractionally as the total resistance divided by the D.C. resistance. These graphs show that over the full frequency range from 40 Hz to 20 KHz the increase in the resistance increases with the number of turns. This result follows from equation 3-5-2. β is proportional to N; so, all other things being equal, the width effect will be more severe in a coil with a greater number of turns.

The variation of the inductance with frequency for the 14 cm wide set is shown in Fig. 3-23 and for the 6 cm wide set in Fig. 3-24. The variation is expressed fractionally as the inductance divided by the 1 KHz inductance. Of the results shown in these two Figures the most significant are those of the 25 turn coils. Both of these graphs show the same form of behaviour below 1 KHz as the theoretical variation of inductance shown in Fig. 3-6. This provides a useful point for starting the comparison of theory and experiment.

For an N turn foil wound inductor β has the form

$$\beta = \frac{\omega N L_f}{P R_t} \qquad 3\text{-}5\text{-}2$$

For the 14 cm wide foil wound inductor; $N = 25$, $L_f = 0.1236$ μH (derived from equations 3-2-2 and 3-2-3), $P = 20$, $R_t = 0.8196$ milli-Ohms (derived from the measured resistance given in Fig. 3-19). With these values $\beta = 1.885\ 10^{-4}\omega$.
For the 6 cm wide foil wound inductor; $N = 25$, $L_f = 0.1236$ μH, $R_t = 1.8936$ milli-Ohms, $P = 20$. With these values $\beta = 8.1547\ 10^{-5}\omega$.

Figure 3-21

Variation of Resistance with Frequency for the set of Foil Wound Inductors with Width 14. cm

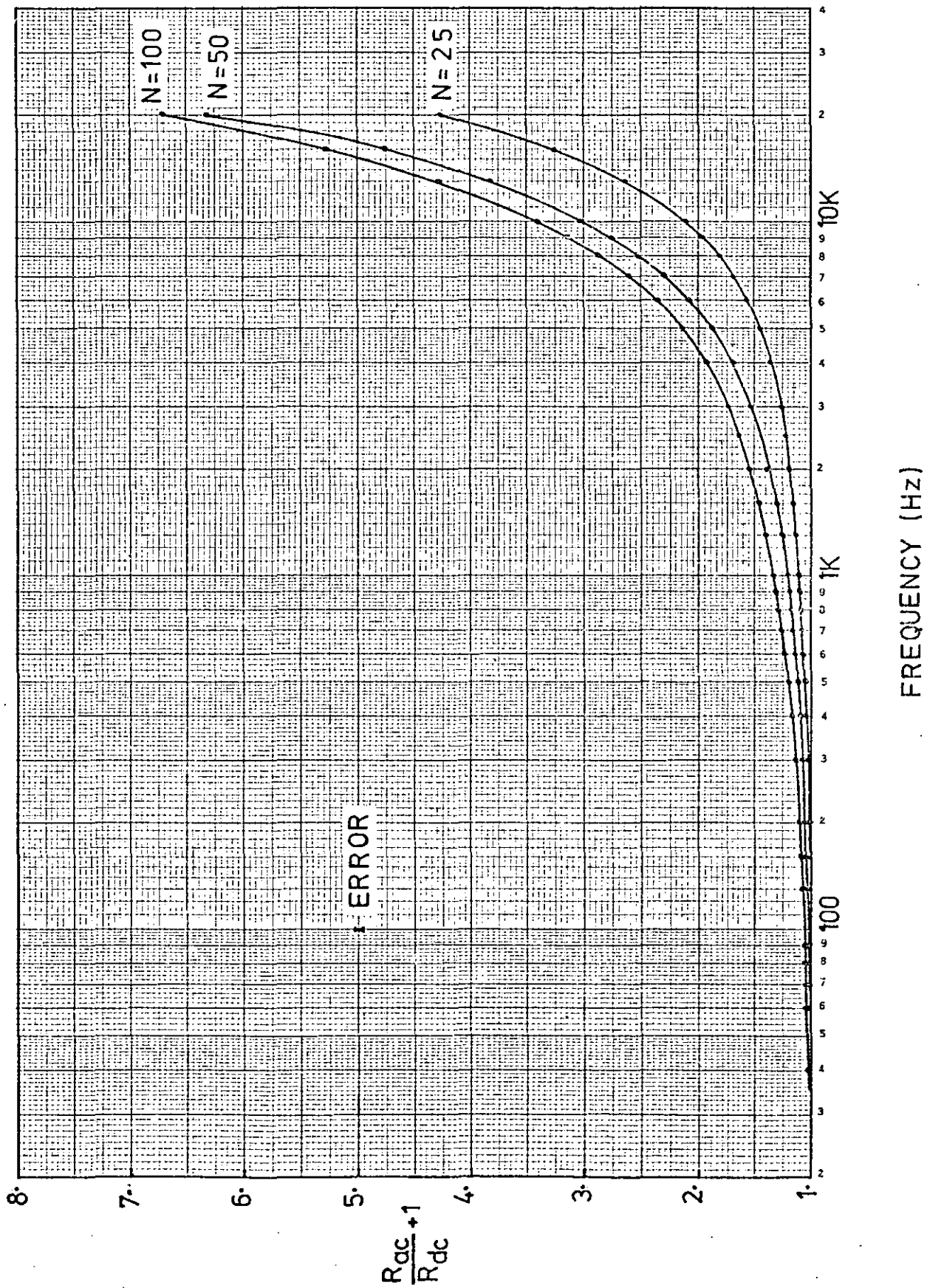

Figure 3-22

Variation of Resistance with Frequency for the set of Foil Wound Inductors with Width 6. cm

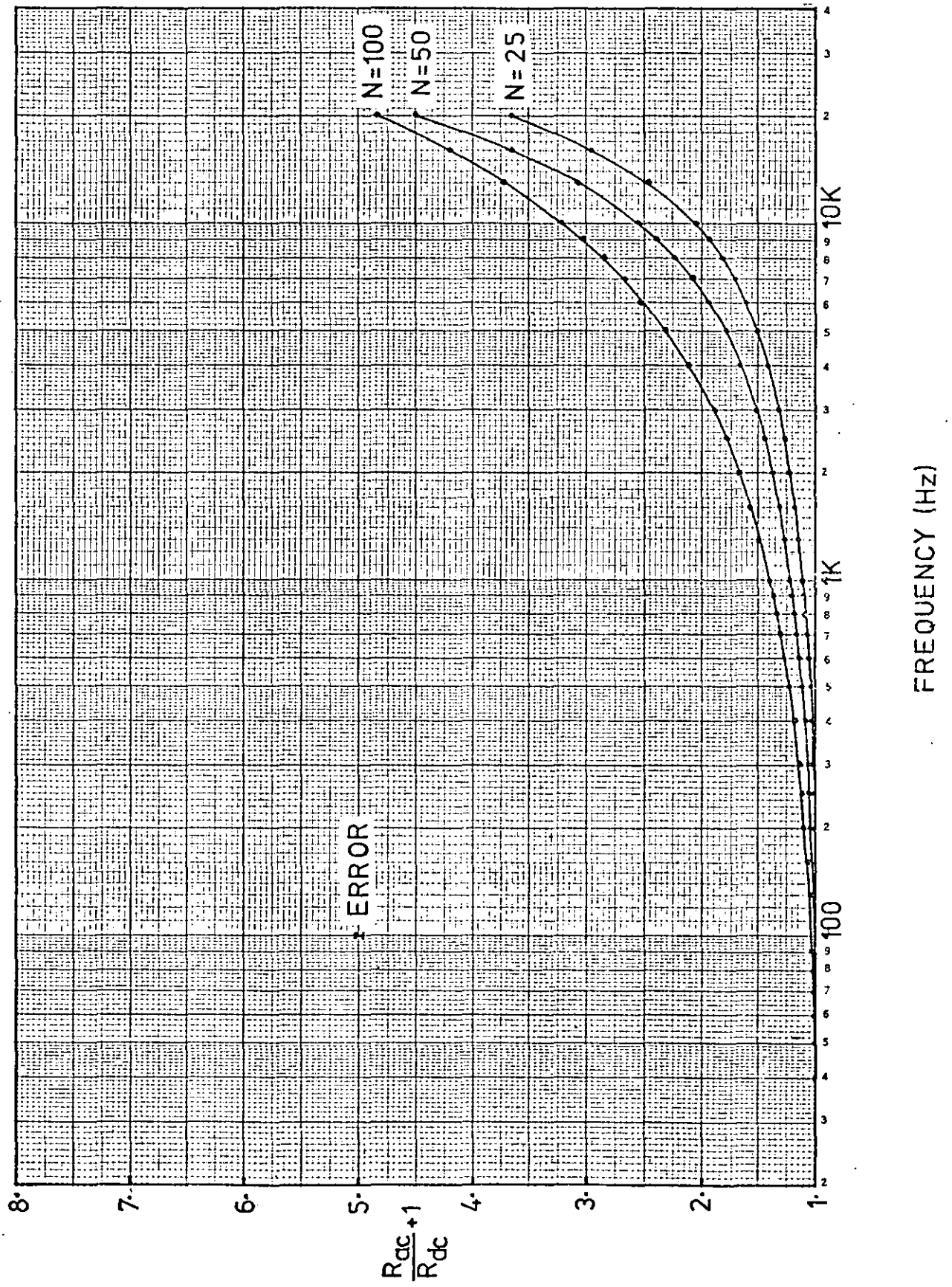

Figure 3-23

Variation of Inductance with Frequency for the Set of Foil Wound Inductors with Width 14. cm

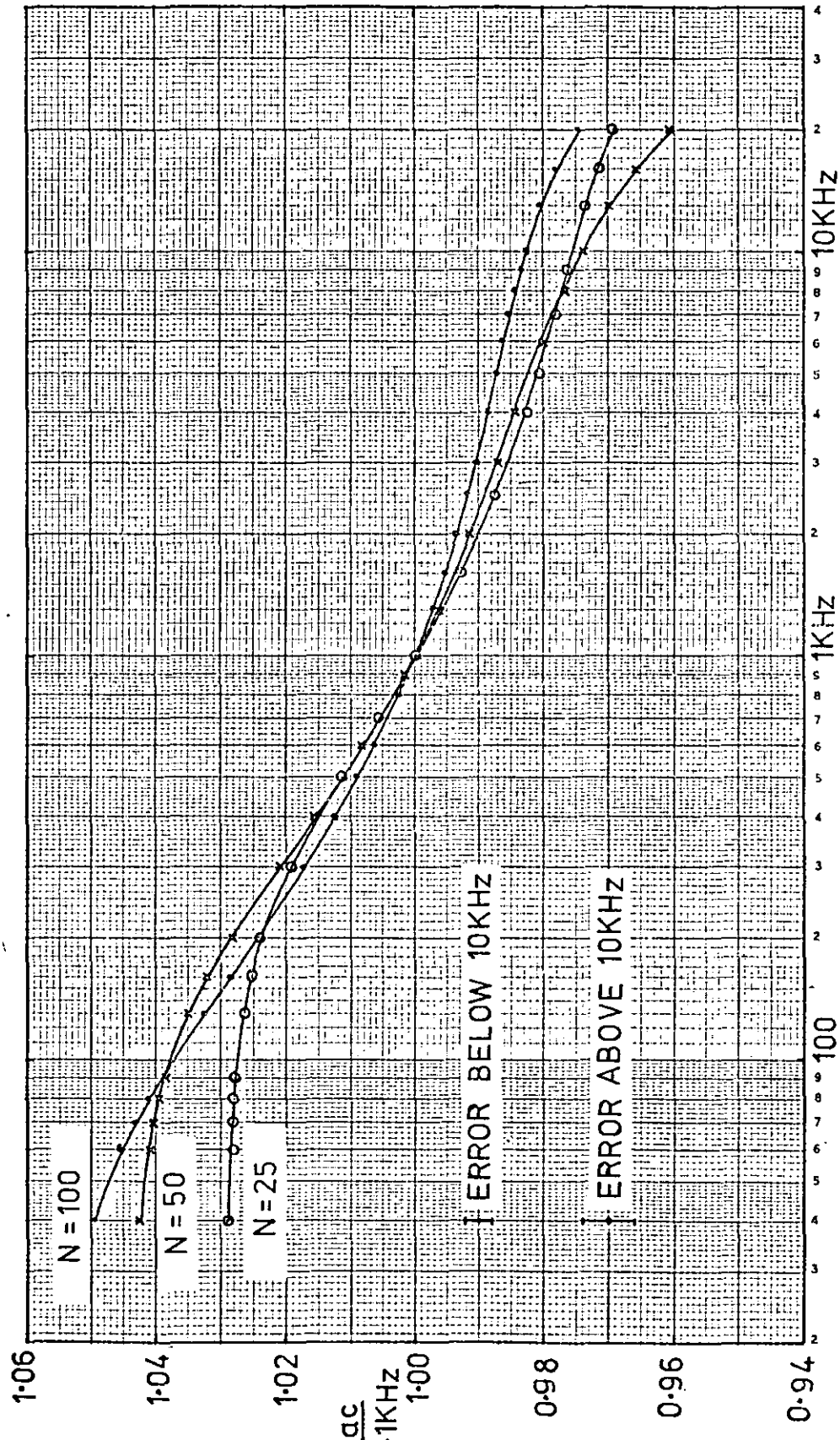

Figure 3-24

Variation Of Inductance with Frequency for the Set of Foil Wound Inductors with Width 6. cm

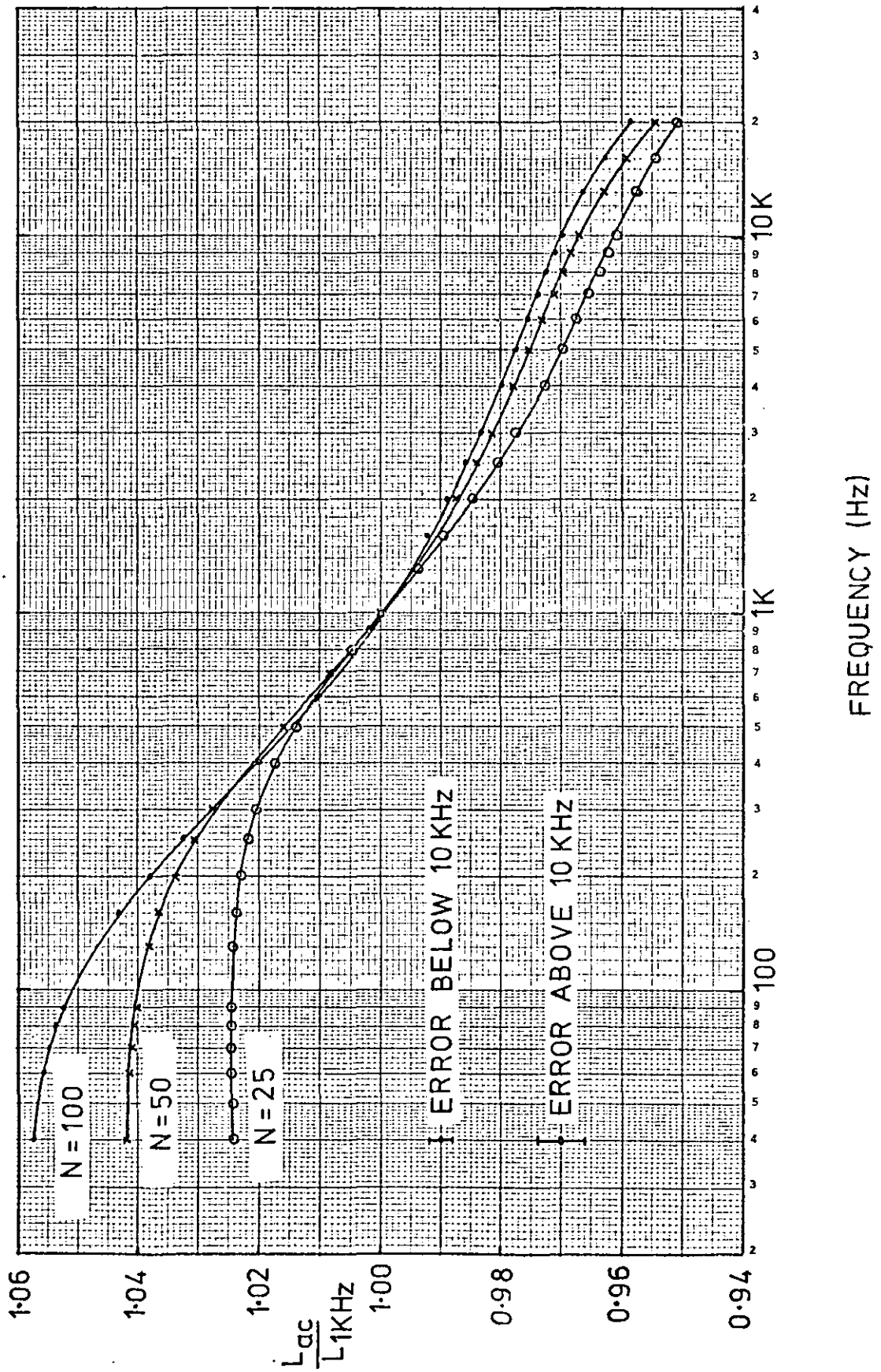

Using the above data the theoretical impedance/frequency spectra for both the sets of foil wound inductors were calculated. The values of β given above were used to draw the comparisons of the theoretical and experimental results shown in Figs. 3-25 and 3-26. The comparison shown in Fig. 3-25 is that of the 14 cm, 25 turn foil wound inductor. This shows that the theoretical and experimental variations of inductance with frequency correspond within the experimental error up to a frequency of 500 Hz. The comparison shown in Fig. 3-26 is that of the 6 cm, 25 turn foil wound inductor, in this case the theoretical and experimental variations of inductance correspond up to a frequency of 400 Hz.

One method of setting an upper limit to the validity of the width effect theory is to say that the strip width C should not be greater than the skin depth δ , which has the form

$$\delta = \sqrt{\frac{2\rho}{\mu_0 \omega}} \qquad 3\text{-}7\text{-}2$$

The variation of the skin depth with frequency for Aluminium at 20° centigrade is shown in Fig. 3-27.

The above limit suggests that the upper limit for the theory in the case of the 14 cm, 25 turn FWI is 138 Hz compared with an experimental limit of 500 Hz. The upper limit to the theory in the case of the 6 cm, 25 turn foil wound inductor is 751 Hz compared with an experimental of 400 Hz.

Another method of testing the theory is to plot either the variation of resistance with frequency or the variation of inductance with frequency on a scale of turns times frequency.

Figure 3-25

Comparison of the Theoretical and Experimental Inductance Variations with Frequency for the 25 Turn, 14. cm Wide Foil Wound Inductor (P = 20)

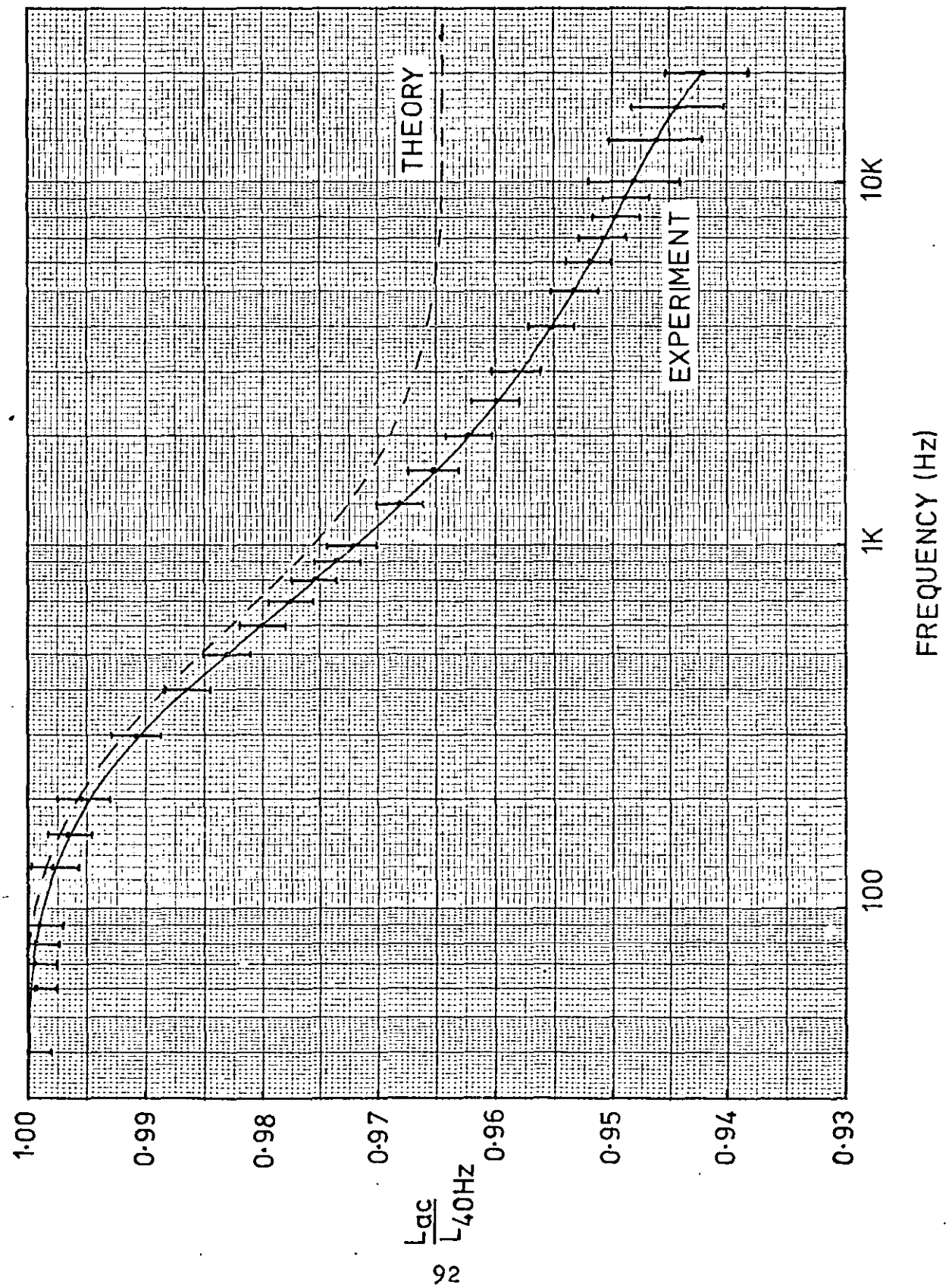

Figure 3-26

Comparison of the Theoretical and Experimental Inductance Variation with Frequency for the 25 Turn, 6. cm Wide Foil Wound Inductor (P = 20)

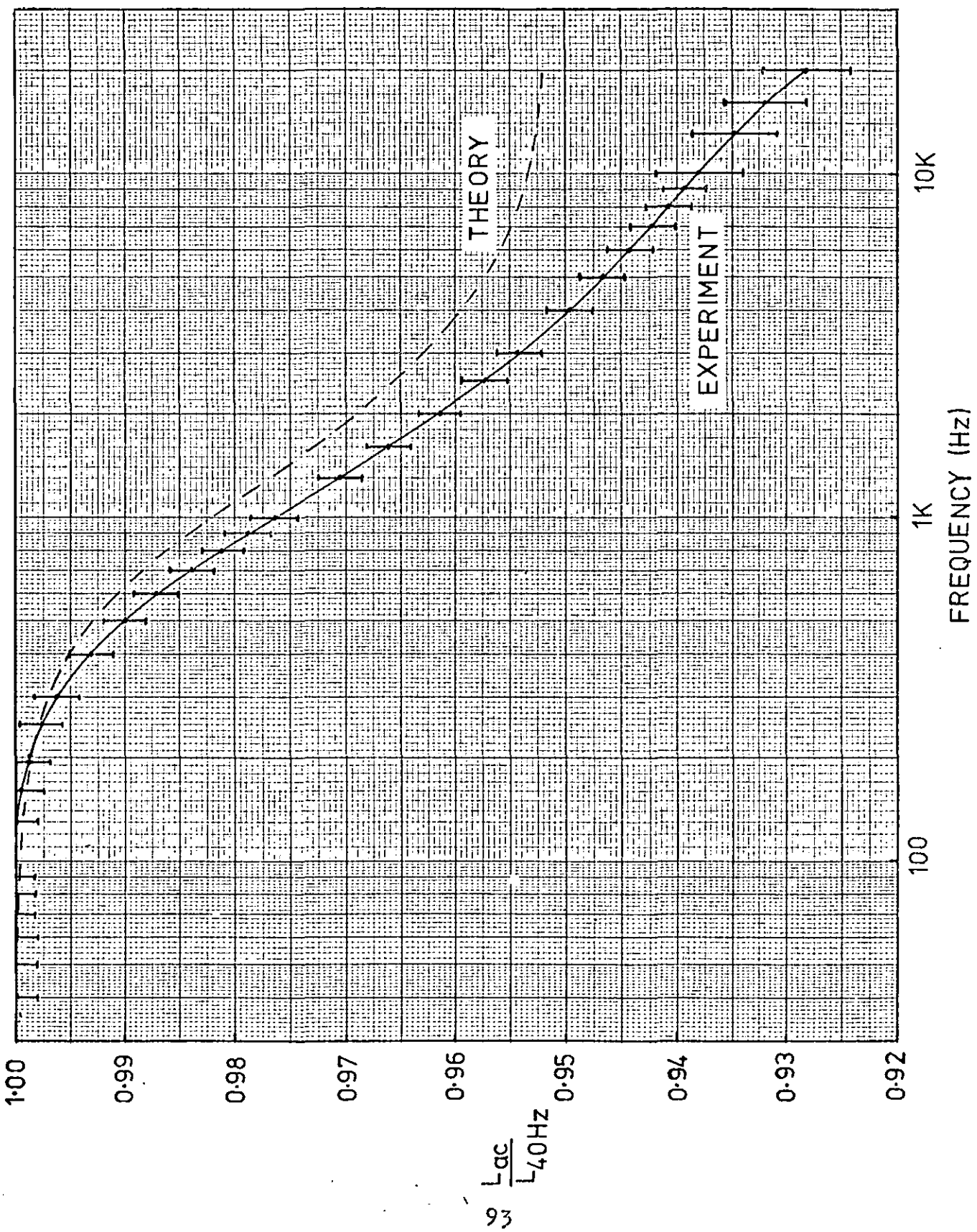

Figure 3-27

Variation of the Skin Depth with Frequency for Aluminium and Copper at 20 Centigrade

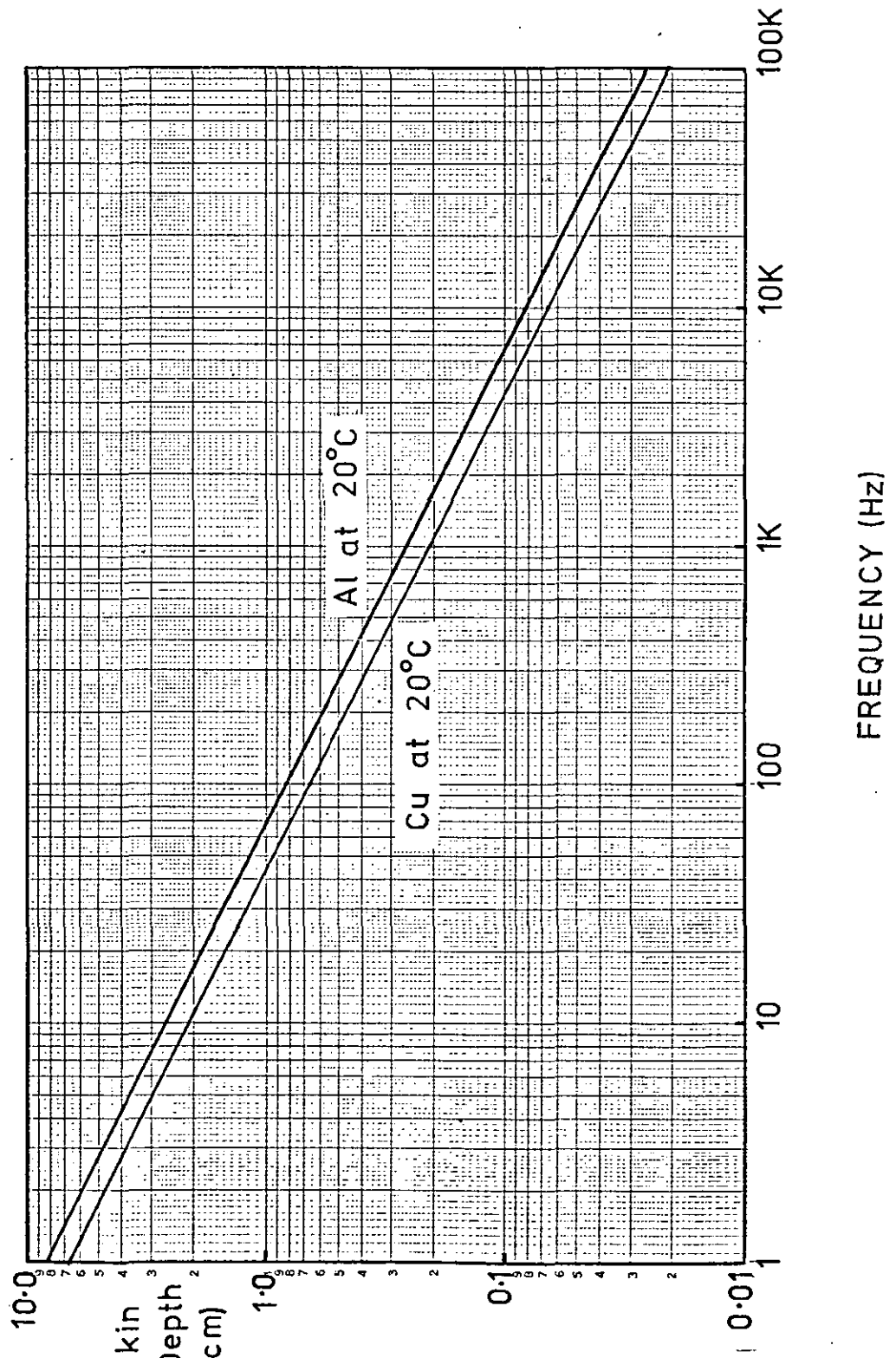

On this scale the variations of all the coils within a set should follow the same curve. The variation of resistance is easier to plot on this scale because the D.C. value is known. Fig. 3-28 shows the relative variation of the resistance of the 14 cm wide set of foil wound inductors plotted on the scale of turns×frequency. It is clear from this graph that the curves follow the same line up to a turn-frequency of 75,000 turn-Hertz. At higher turn-frequencies the curves diverge with the 25 turn coil having the steepest gradient and the 100 turn coil having the lowest gradient. Fig. 3-29 shows the relative variation of the resistance of the 6 cm wide set of foil wound inductors plotted on the scale of turns×frequency. This graph also shows that the curves for the three different coils follow the same line, although this time they diverge at a turn-frequency of 65,000 turn-Hertz. Again the curves diverge at high turn-frequencies with the 25 turn coil having the steepest gradient and the 100 turn coil having the lowest gradient.

Plotting the results shown in Figs. 3-28 and 3-29 as the variation of the relative A.C. resistance against a scale of turns×frequency on a log-log graph gives the best comparison of the theoretical and experimental curves. Fig. 3-30 compares the theoretical and experimental results for the variation of the relative A.C. resistance of the 14 cm wide set of foil wound inductors. These curves show that the theory agrees with the experimental results only at turn-frequencies below 10,000 turn-Hertz. Fig. 3-31 shows the same comparison for the 6 cm wide set of foil wound inductors, again the theory agrees with experimental results up to an approximate turn-frequency of

Figure 3-28

Variation of Resistance with Turns x Frequency for the 14.cm Wide Set of Foil Wound Inductors,

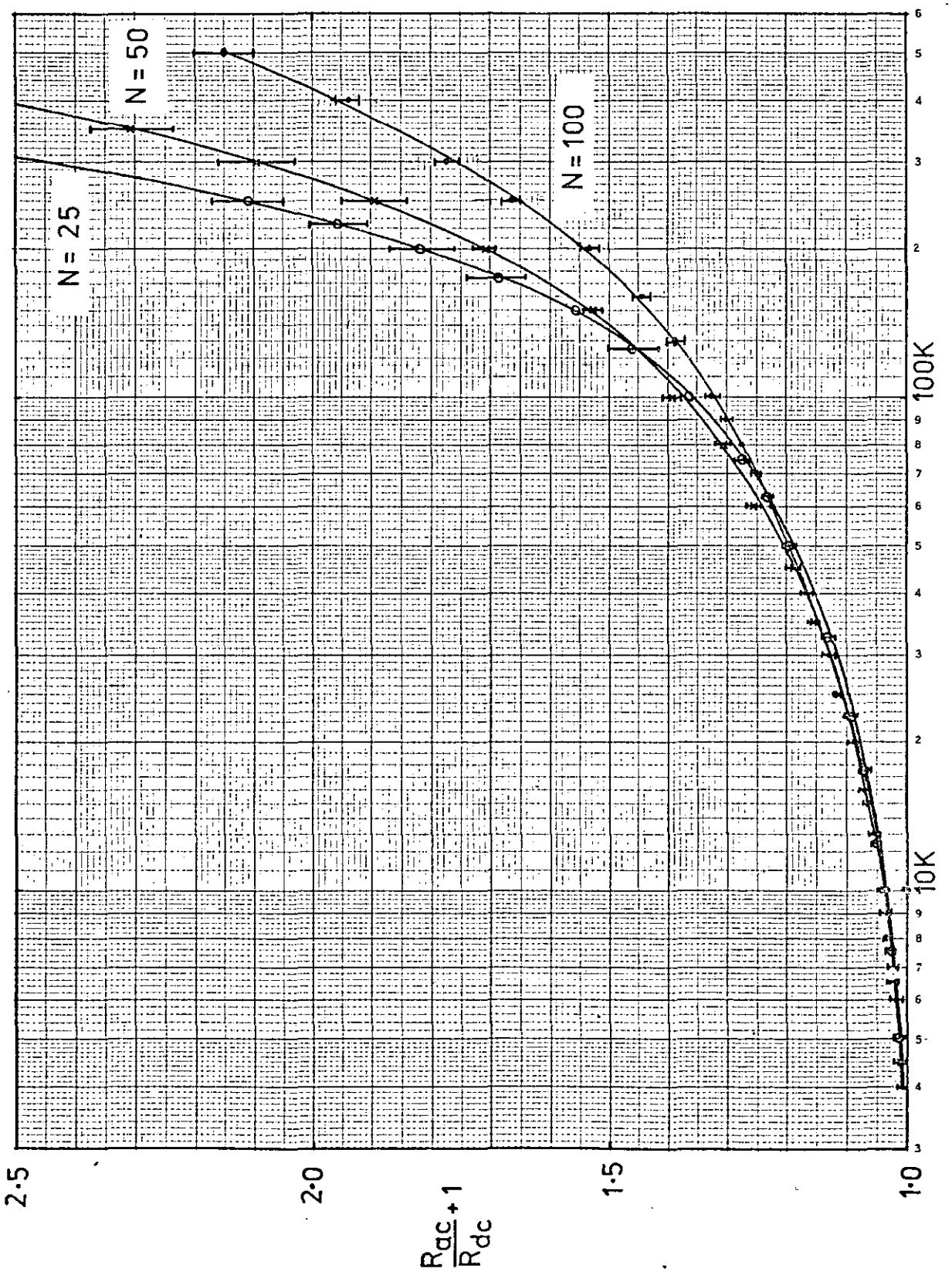

Figure 3-29

Variation of Resistance with Turns × Frequency for the 6.cm Wide Set of Foil Wound Inductors

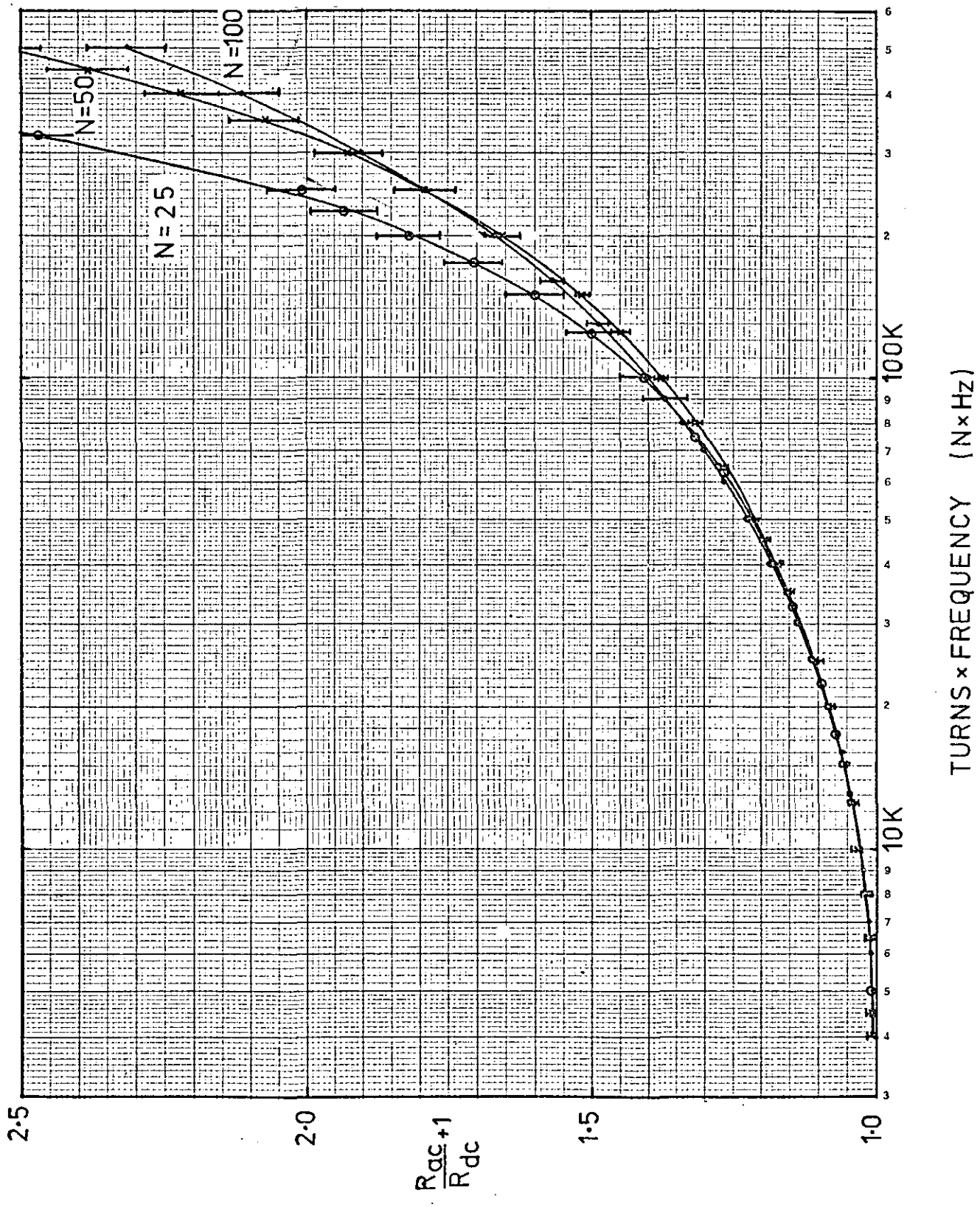

Figure 3-30

Comparison of the Theoretical and Experimental Variation of A.C. Resistance with Turns x Frequency for the Set of 14.cm Wide Foil Wound Inductors

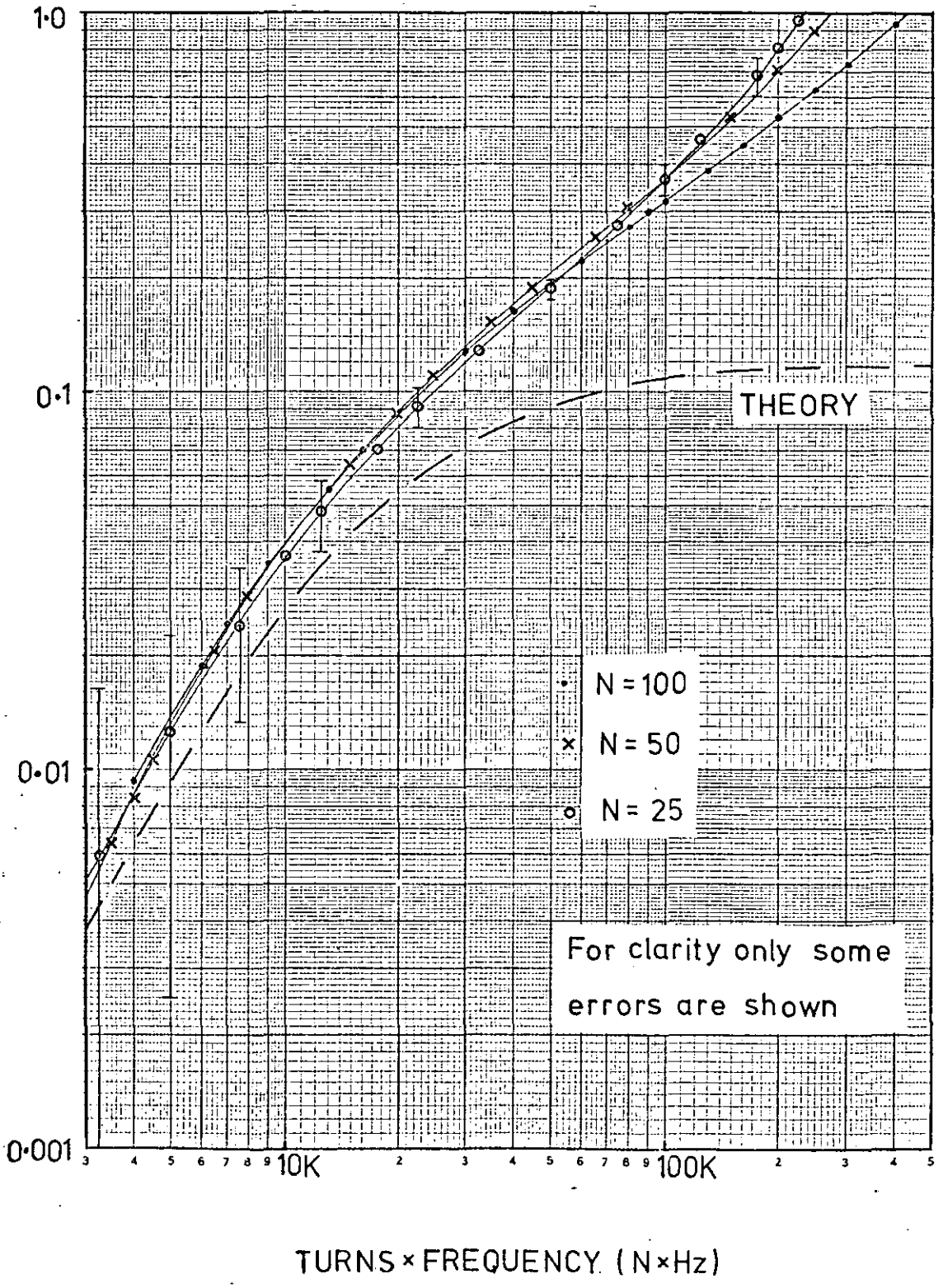

Figure 3-31

Comparison of the Theoretical and Experimental Variation of A.C. Resistance with Turns x Frequency for the Set of 6.cm Wide Foil Wound Inductors

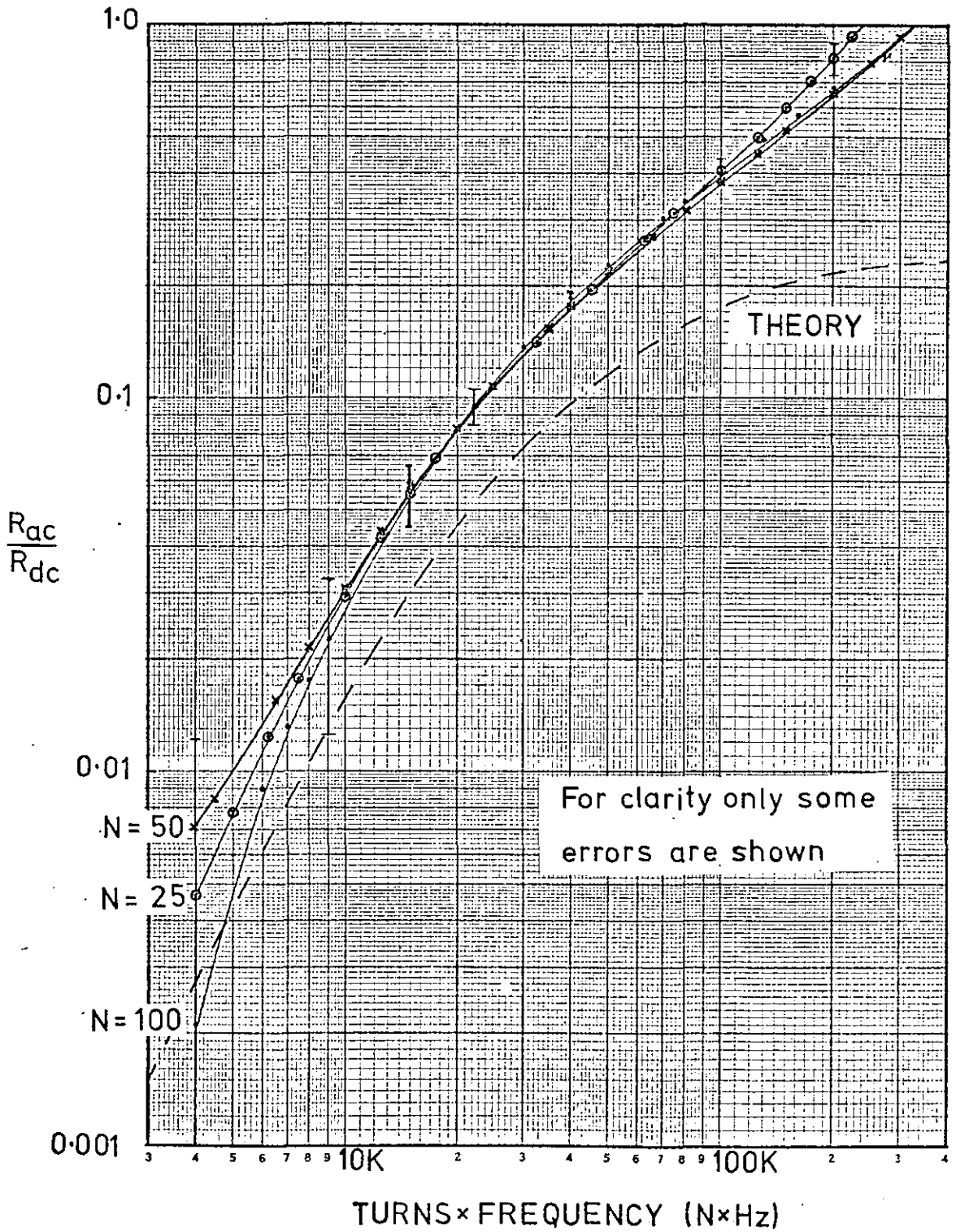

10,000 turn-Hertz.

Analysis of the results suggests three things; the width effect theory is valid up to a turn-frequency of approximately 70,000 turn-Hertz for the six foil wound inductors studied, the theoretical calculations using twenty strips are valid up to a turn-frequency of approximately 10,000 turn-Hertz for both sets of foil wound inductors and the method of setting an upper limit to the theoretical calculations using the skin depth as a criteria for the strip width is invalid.

Above 70,000 turn-Hertz the foil thickness is probably becoming significant. Further analysis would have to take into account the current distribution across the thickness of the foil as well as that across the width.

By increasing the number of strips it should be possible to improve the upper limit to the validity of the theory in the turn-frequency domain.

8) Variation of the Flux Profile with Frequency

It is possible with both sets of foil wound inductors to repeat the experiment described in section 3-4, in which the variation of the flux profile with frequency was measured. To repeat this experiment four search coils were wound onto a plastic former with an outside diameter of 5.7 cm, which fitted smoothly down the inside of the coil formers. The search coils consisted of 300 turns of 46 SWG copper wire and were wound into grooves 3 mm wide by 1 mm deep cut into the plastic former. This gives the search coil an average radius of 2.8 cm.

The theoretical calculations are based on a model with twenty strips. Therefore to ensure the maximum correspondence

with the theory the outer search coils were centred on the first strip and the centre search coils were centred on the tenth strip. Thus the search coils for the 14 cm wide set of coils were separated by 6.3 cm and the search coils for the 6 cm wide set of coils were separated by 2.7 cm.

The experimental arrangement was basically the same as that shown in Fig. 3-10 although with certain alterations; the output from the oscillator was reinforced with an Amcron DC 300A power amplifier and an 8 Ohm, 100 Watt resistor was inserted in series with the foil wound inductor to increase the load impedance across the output of the power amplifier. To negate the capacitive coupling between the search coils and the foil wound inductor, the inner terminal of the foil wound inductor was earthed and 33K Ohm resistors were connected in parallel with the search coils.

All other things being equal the ratio of V_{centre} to V_{outer} is equal to the ratio Φ_{centre} to Φ_{outer}. This ratio was measured at frequencies between 40 hz and 20 KHz for both sets of foil wound inductors. The values of Φ_k for $k=1$ and $k=10$ were calculated within the computer program using equation 3-4-1 and the magnitude of the ratio Φ_{outer} to Φ_{centre} derived. The theoretical and experimental results are compared in Figs. 3-32 and 3-33 plotted on a scale of turns×frequency. The experimental curves in Fig. 3-32 follow the same line, showing that the effect scales with the turns on the coil and have the same trend as the theoretical curve although there is not an exact correspondence. The experimental curves for the 6 cm wide set of coils in Fig. 3-33 do not follow the same

Figure 3-32

Comparison of the Theoretical and Experimental Variation of the Ratio Φ_{outer} to Φ_{centre} with Turns × Frequency for the 14.cm Wide Set of Foil Wound Inductors

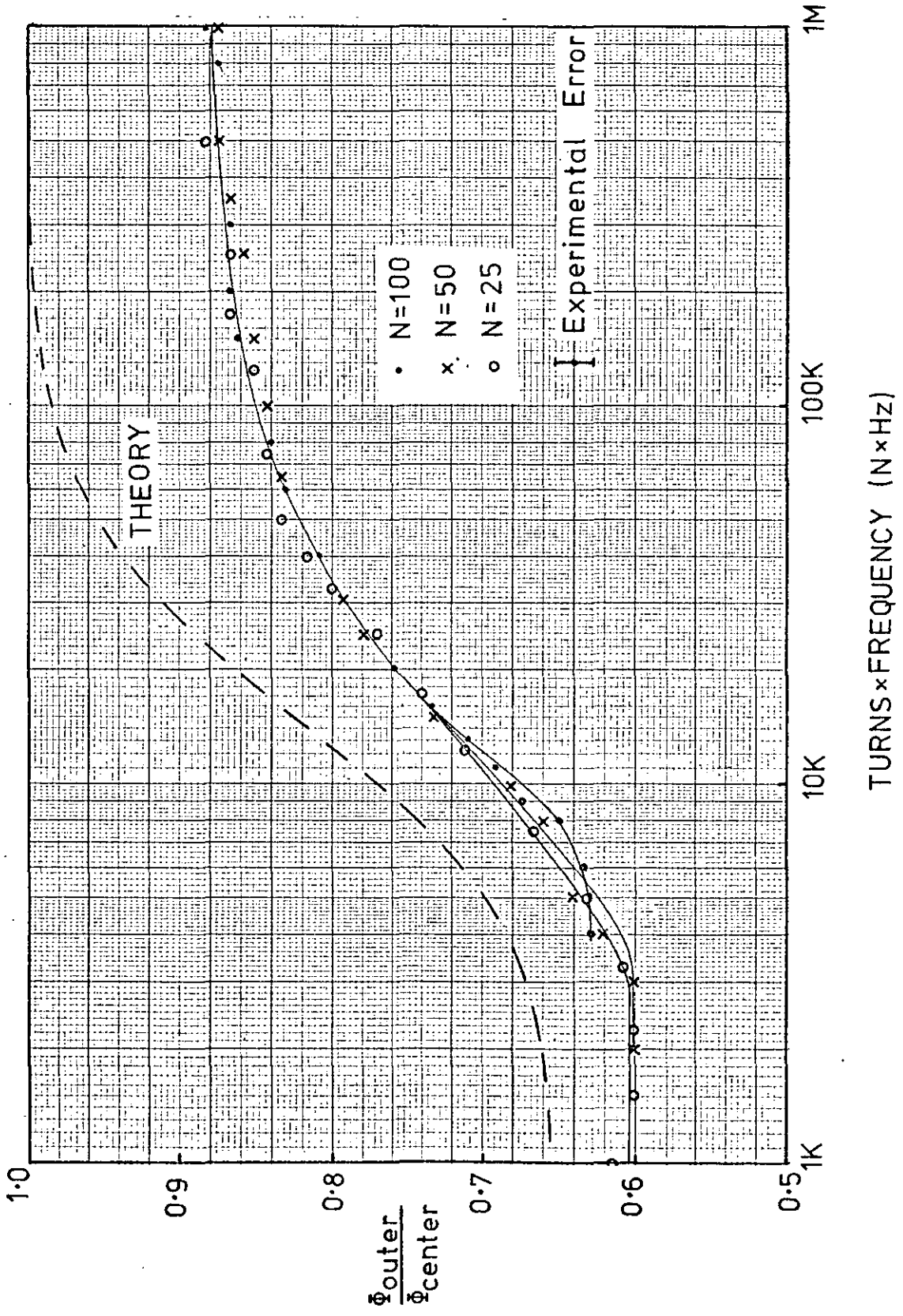

Figure 3-33

Comparison of the Theoretical and Experimental Variation of the Ratio Φ_{outer} to Φ_{centre} with Turns × Frequency for the 6.cm Wide Set of Foil Wound Inductors

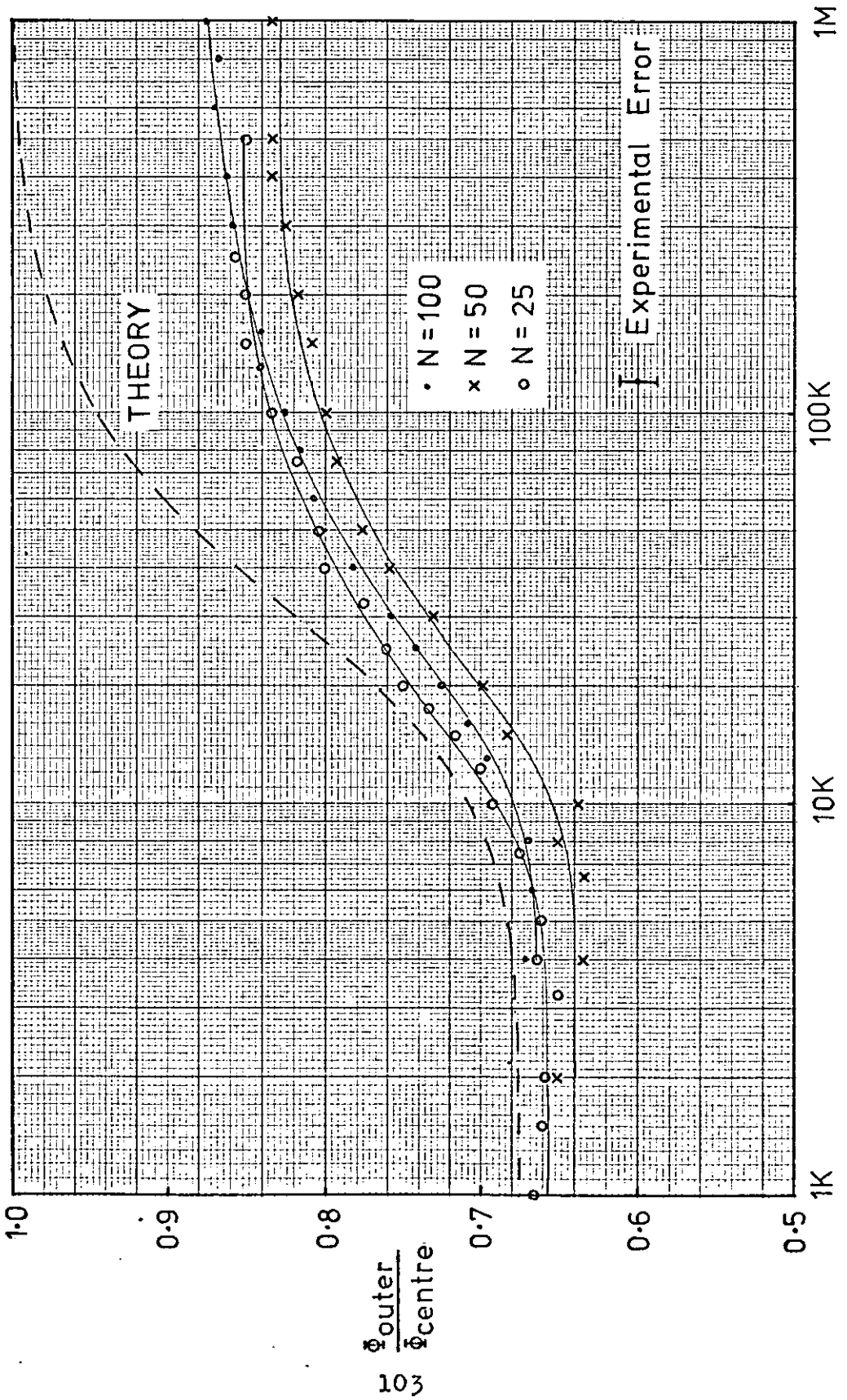

line quite so closely as the experimental curves for the 14 cm wide set of coils, although the correspondence with the theoretical curve is better at low turn-frequencies.

Although the correspondence between the theoretical and experimental resulte is not exact, the results clearly show that the current flow tends towards the edges of the foil wound inductor at increased frequencies. The discrepancy at low turn-frequencies between the theoretical and experimental ratios may be due to the fact that the search coils do not cut all of the flux Φ . It is impossible to say what the discrepancy at high turn-frequencies is due to at this stage.

9) Conclusion

The equivalent circuit model of the width effect predicts basically that the current through a foil wound inductor will tend to flow at the edges of the coil as the frequency of the current is increased. As a consequence of the current redistribution with increased frequency, four effects are predicted; the resistance of the foil wound inductor will increase, its self-inductance will decrease, its axial flux distribution will tend towards equality and for one particular class of foil wound inductor these effects will scale with the number of turns on the foil wound inductor.

Experimentation has shown that at low frequencies the changes in the resistances and self-inductances with frequency of the two sets of foil wound inductors do correspond with the predicted changes and that the changes in the resistance scale with the number of turns on the foil wound inductor over a limited frequency range. It has also been possible to confirm experimentally, using the axial flux distribution, that the

current does tend to flow at the edges of the foil wound inductor as the frequency of the current is increased.

However most foil wound inductors of interest to the coil designer have appreciable build-up, which renders the simple model developed in this chapter invalid. Also the increasing use of foil wound inductors in thyristor switching circuits means that the frequency range of interest to the designer extends beyond the frequencies at which the width effect theory is valid. The results shown in Figs. 3-34 and 3-35 for two industrial foil wound inductors illustrate the need for a theory that can accommodate coils of appreciable build-up and a current distribution that varies across the thickness as well as the width of the foil.

The width effect theory only applies to air-cored foil wound inductors. In a cored coil the axial flux is mainly determined by the core material and shape. In the case of an ideal core, with no air gap between the core and the winding, the axial flux distribution will be uniform, in which case there would be no width effect. However with a real core there will be a form of current redistribution, due to the radial flux leakage from the core (36).

The width effect theory is summarised in the papers by Murgatroyd and Walker which appear as Appendices 3 and 4.

Figure 3-34

Variation of Resistance and Inductance with Frequency for an Industrial 111.5 Turn Foil Wound Inductor

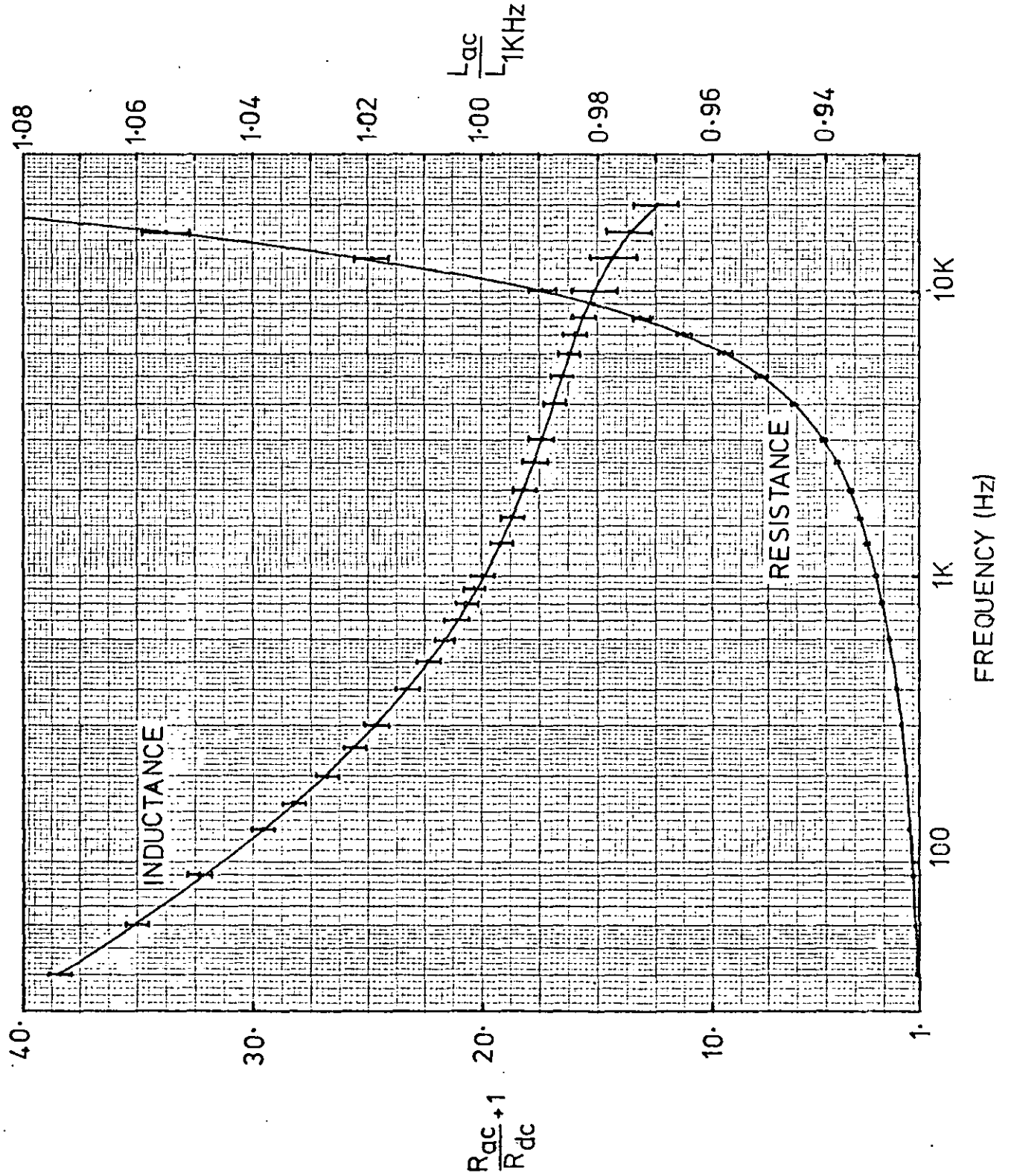

Figure 3-35

Variation of Resistance and Inductance with Frequency for an Industrial 55.5 Turn Foil Wound Inductor

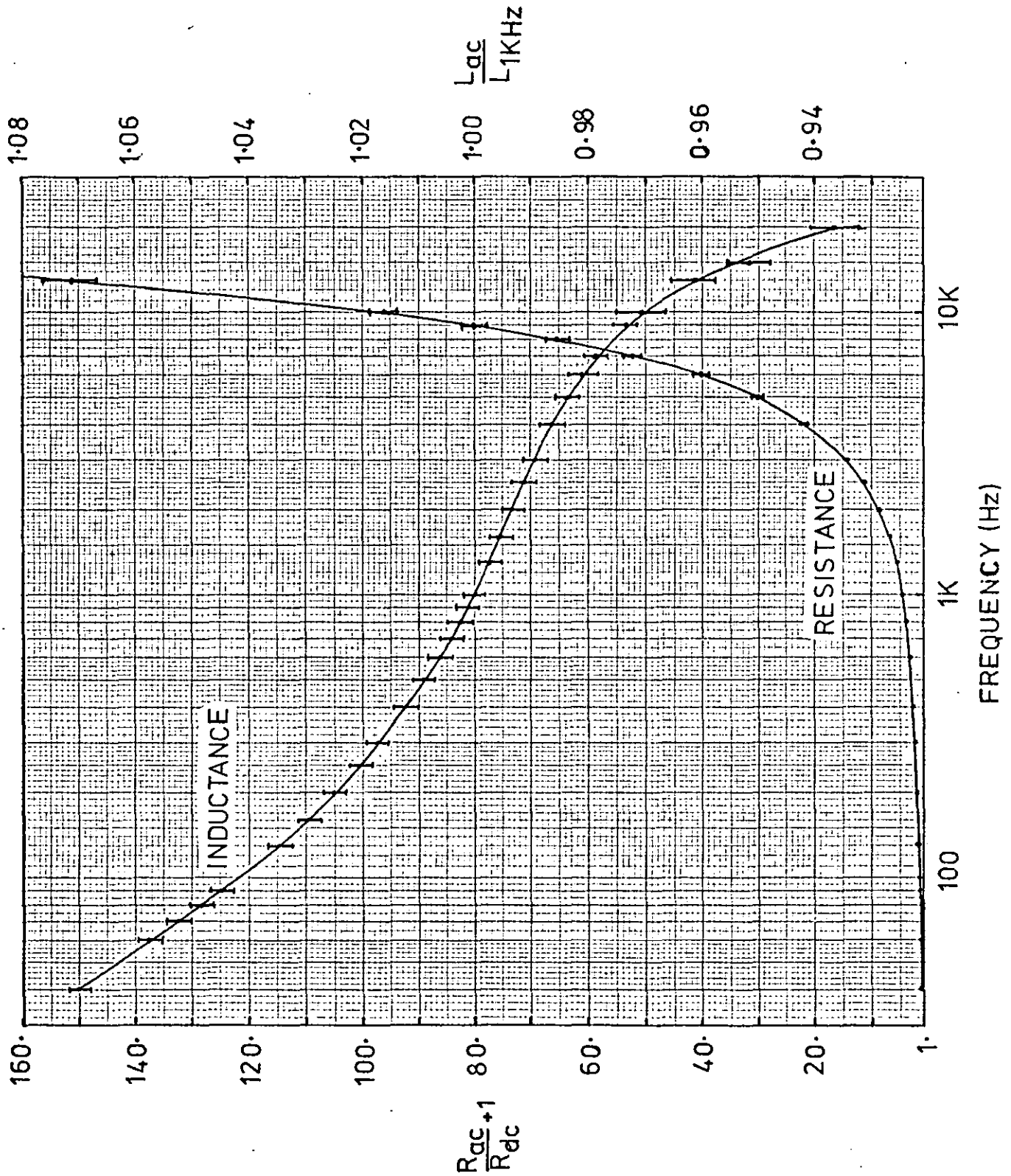

Chapter 4 Voltage Resonances in Tapped Foil Wound Inductors

1) Introduction

The lumped-element equivalent-circuit analysis of foil wound inductors analysed in chapter 2 predicts that current and voltage standing waves can exist within a foil wound inductor at frequencies above the first resonance. The author has shown experimentally (33) that current standing waves exist by examining the external A.C. magnetic field of a foil wound inductor using a search coil. However the voltage standing wave pattern which must occur with the current standing wave pattern cannot be examined in a direct manner, because any probe will have sufficient capacitance to disrupt the standing wave pattern. But if the problem is approached in an indirect manner by examining the output of a tapped foil wound inductor, then the effects of the voltage standing wave may become apparent.

2) Experimental Arrangement

Three tapped foil wound inductors were wound with taps placed at regular turn-intervals on the winding; a 1000 turn coil with taps at intervals of 100 turns, a 250 turn coil with taps at intervals of 50 turns and a 200 turn coil with taps at intervals of 50 turns. The taps were strips of 50 μm aluminium foil held in place by the pressure of the winding. The other physical dimensions of the coils are given in Figs. 4-1, 4-2 and 4-3. The coils were heat treated in the manner described in chapter 2.

Figure 4-1

Physical Parameters and Dimensions of the 1000 Turn Tapped Foil Wound Inductor	
Core Radius	0.7 cm
Type of Metal Foil	Aluminium
Thickness of Metal Foil	5.0 μm
Width of Metal Foil	3.9 cm
Type of Plastic Foil	Polypropylene
Thickness of Plastic Foil	12.5 μm
Taps at	0 Turns, 100 " , 200 " , 300 " , 400 " , 500 " , 600 Turns, 700 " , 800 " , 900 " , 1000 "

Figure 4-2

Physical Parameters and Dimensions of the 250 Turn Tapped Foil Wound Inductor	
Core Radius	0.7 cm
Type of Metal Foil	Aluminium
Thickness of Metal Foil	5.0 μm
Width of Metal Foil	3.9 cm
Type of Plastic Foil	Polypropylene
Thickness of Plastic Foil	12.5 μm
Taps at	0 Turns, 50 " , 100 " , 150 " , 200 " , 250 "

Figure 4-3

Physical Parameters and Dimensions of the 200 Turn Tapped Foil Wound Inductor	
Core Radius	0.7 cm
Type of Metal Foil	Aluminium
Thickness of Metal Foil	5.0 μm
Width of Metal Foil	3.9 cm
Type of Plastic Foil	Polypropylene
Thickness of Plastic Foil	12.5 μm
Taps at	0 Turns, 50 " , 100 " , 150 " , 200 "

The experimental arrangement used is shown in Fig. 4-4a. The output from the oscillator was fed into a matching transformer, which was necessary due to the low input impedance of the tapped foil wound inductor at certain frequencies. The transformer consisted of a Mullard FX 2242 ferrite core with 5 turns of 30 SWG copper wire as the primary and 1 turn of 30 SWG copper wire as the secondary. The maximum usable frequency of this transformer was 9 MHz. An F.E.T. probe with an input impedance of 1M Ohm in parallel with 3.5 pF was connected to one channel of the oscilloscope and used to measure the output voltage of the tapped foil wound inductor. The other channel of the oscilloscope was used to measure the input voltage.

The connections to the tapped foil wound inductor are shown in Fig. 4-4b. The input voltage V_o was applied between turn 0 at the centre of the coil and the tap at turn T . The tap at turn 0 is earthed. The output voltage is taken across the whole coil of N turns. A normalised relative output voltage V_r is defined as

$$V_r = \frac{V_l T}{V_o N} \qquad 4\text{-}2\text{-}1$$

Where V_l is the output voltage and V_o the input voltage.

The input voltage V_o and the output voltage V_l of the 200 turn tapped foil wound inductor were measured from 500 KHz to 8 MHz with $T = 50$, 100 and 150. The results in terms of V_r are plotted on a log-log scale against frequency in Fig. 4-5. In each case V_r has a low frequency value of 1, then rises to a maximum value at an intermediate frequency and falls off at high frequencies. The maximum values of V_r , the resonant

Figure 4-4

a/ Experimental Arrangement used to Measure the Output Voltage Response of the Tapped Foil Wound Inductors

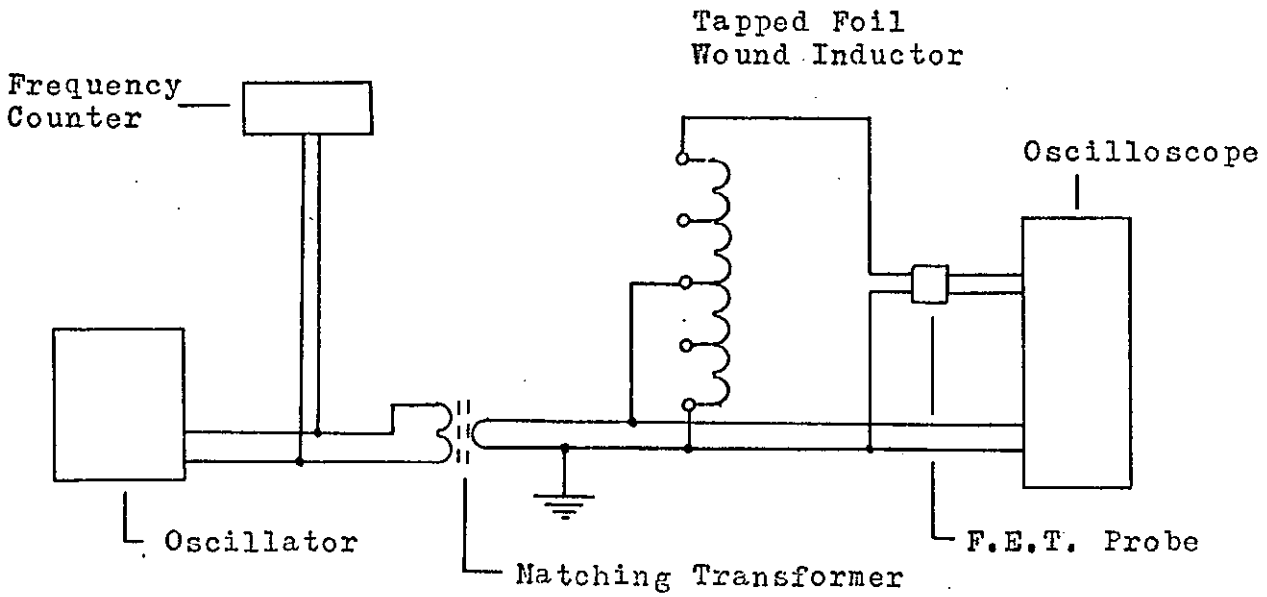

b/ Connections to the Tapped Foil Wound Inductor

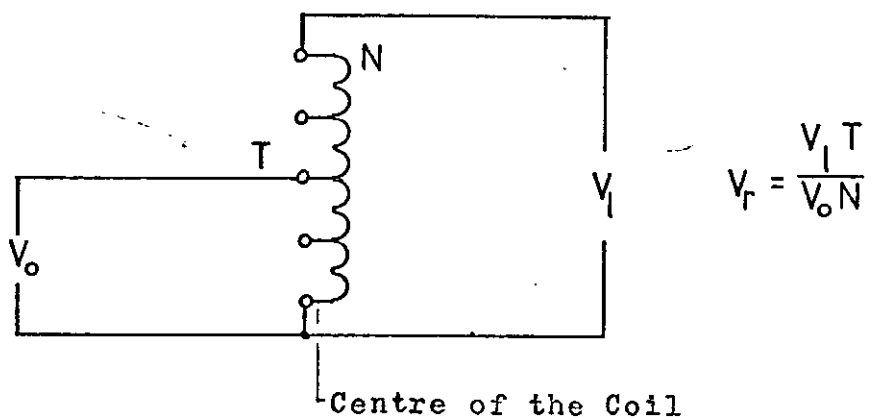

Figure 4-5

Output Voltage Response of a 200 Turn Tapped Foil Wound Inductor with T = 50,100 and 150

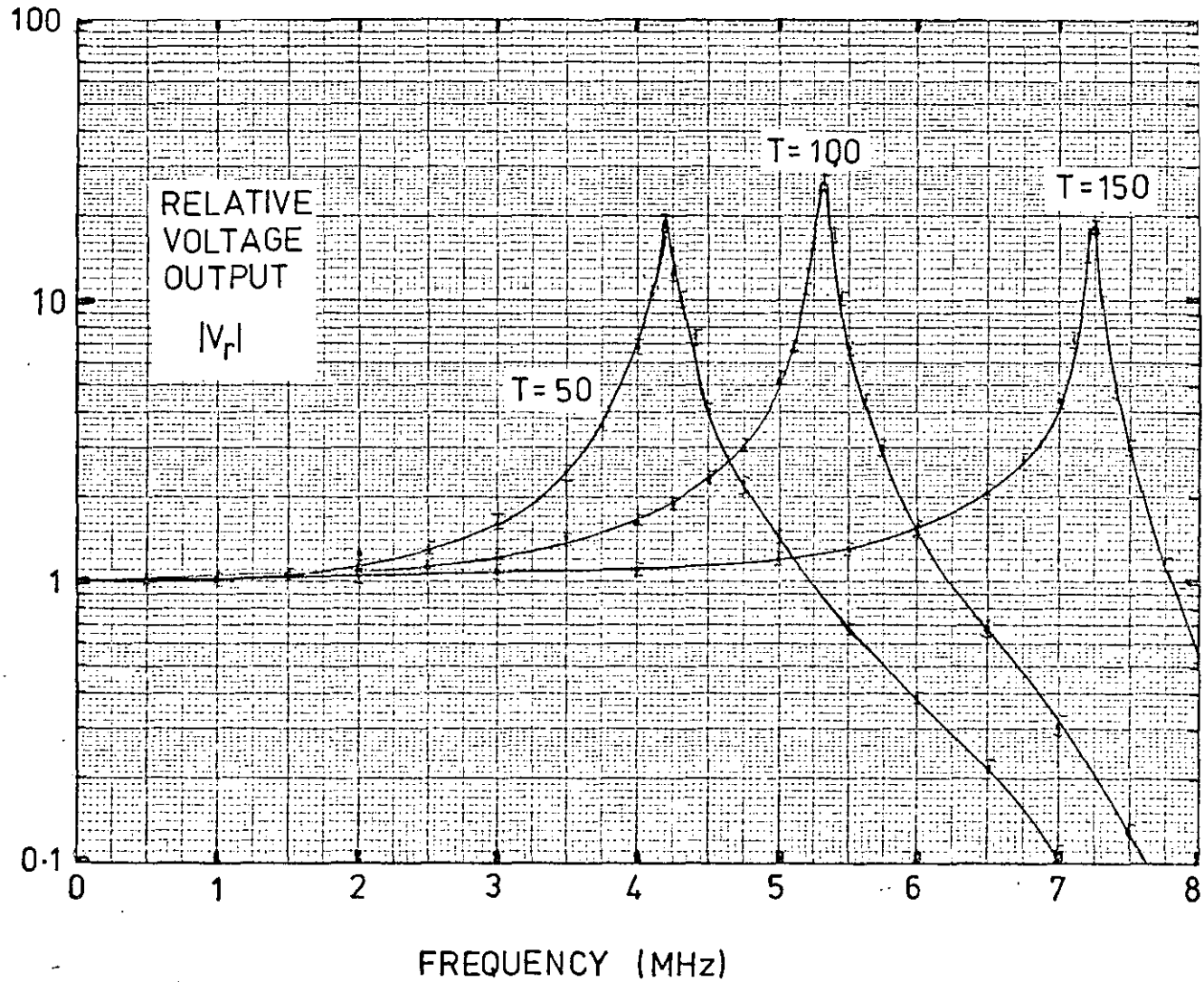

frequencies and the approximate Q values of these resonances are given in Fig. 4-6. This table shows that the resonant frequency increases with increasing T .

Clearly the observed resonances in the output voltage of the tapped foil wound inductor must be due to a non-uniform voltage distribution within the coil.

3) Analysis of the Equivalent Circuit

The proposed lumped element equivalent circuit is shown in Fig. 4-7. This circuit is based on the equivalent circuit of the foil wound inductor analysed in section 2-4. A load impedance Z_l is included in this analysis in case it is necessary to take account of the impedance of the probe. To facilitate the comparison of theory and experiment, the numbers of turns in the experimental and theoretical models were arranged so that the physical taps appear at nodes of the equivalent circuit. Other situations could be included in the analysis but this would entail the use of sections with unequal numbers of turns.

The theoretical model is composed of S sections, with the input tap placed at the end of the u^{th} section. There will be $S+2$ circuit equations for this model. u of these will have the form

$$(R_i + j\omega L_i)(I_i - I_l) + \sum_{k \neq i}^{S} j\omega M_{i,k}(I_k - I_l) + \frac{(I_i - I_o)}{j\omega C_i} = 0 \qquad 4\text{-}3\text{-}1$$

$$1 \leq i \leq u$$

Where i and k are dummy suffixes with the limits indicated. $S-u$ equations have the form

Figure 4-6

The Experimental Resonant Frequencies, Maximum Values of V_r and Q Values for the 200 Turn Tapped Foil Wound Inductor

Input Connection	Resonant Frequency MHz	Maximum Value of V_r	Q Value
T = 150	7.25 ±0.02	18.0 ±0.4	40
T = 100	5.3 ±0.01	24.5 ±0.5	26
T = 50	4.2 ±0.01	19.0 ±0.4	17

Figure 4-7

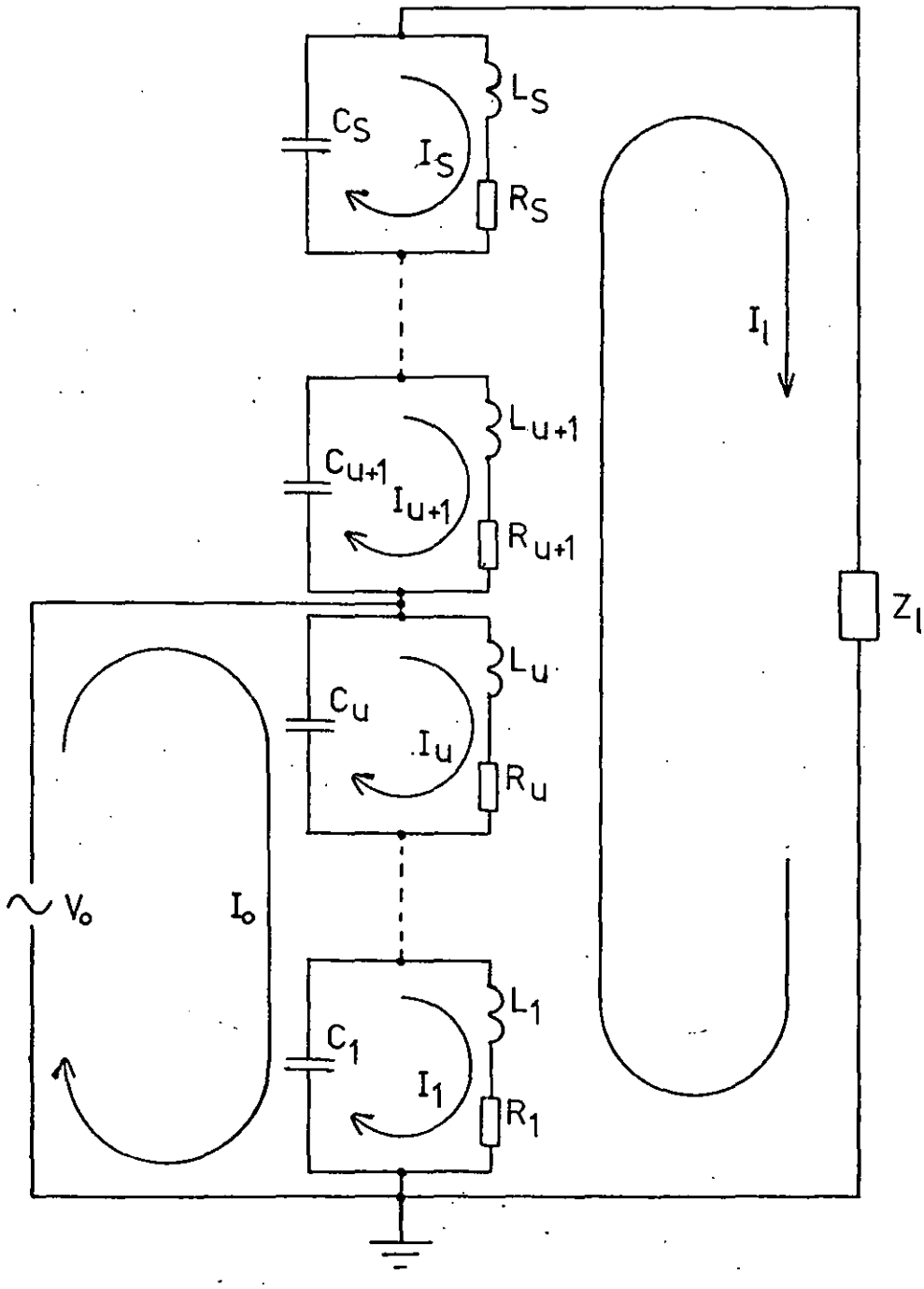

Equivalent Circuit of a Tapped Foil Wound Inductor

All inductors are mutually coupled.

$$(R_i + j\omega L_i)(I_i - I_l) + \sum_{k\neq i}^{S} j\omega M_{i,k}(I_k - I_l) + \frac{I_i}{j\omega C} = 0 \qquad 4\text{-}3\text{-}2$$

$$u < i \leq S$$

The circuit equation round the input loop is

$$V_o = \sum_{i=1}^{u} \frac{(I_o - I_i)}{j\omega C_i} \qquad 4\text{-}3\text{-}3$$

The circuit equation round the load loop is

$$I_l Z_l - \sum_{i=1}^{S} \{(R_i + j\omega L_i)(I_i - I_l) + \sum_{k\neq i}^{S} j\omega M_{i,k}(I_i - I_l)\} = 0 \qquad 4\text{-}3\text{-}4$$

The $S + 2$ circuit equations can be reduced to $S + 1$ equations by dividing by I_o and substituting $q_i = \frac{I_i}{I_o}$, $q_k = \frac{I_k}{I_o}$ and $q_{S+1} = \frac{I_l}{I_o}$. With these substitutions equation 4-3-1 becomes

$$(R_i + j\omega L_i + \frac{1}{j\omega C_i})q_i + \sum_{k\neq i}^{S} j\omega M_{i,k} q_k$$

$$- (R_i + j\omega L_i + \sum_{n\neq i}^{S} j\omega M_{i,n})q_{S+1} = \frac{1}{j\omega C_i} \qquad 4\text{-}3\text{-}5$$

$$1 \leq i \leq u$$

Equation 4-3-2 becomes

$$(R_i + j\omega L_i + \frac{1}{j\omega C_i})q_i + \sum_{k=i}^{S} j\omega M_{i,k} q_k$$

$$- (R_i + j\omega L_i + \sum_{n\neq i}^{S} j\omega M_{i,n})q_{S+1} = 0 \qquad 4\text{-}3\text{-}6$$

$$u < i \leq S$$

The input loop equation becomes

$$\frac{V_o}{I_o} = Z_o = \sum_{i=1}^{U} \frac{(1 - q_i)}{j\omega C_i} \qquad 4\text{-}3\text{-}7$$

The load loop equation becomes

$$Z_l q_{S+1} - \sum_{i=1}^{S} \left\{ (R_i + j\omega L_i)(q_i - q_{S+1}) + \sum_{k \neq i}^{S} j\omega M_{i,k}(q_k - q_{S+1}) \right\} = 0 \qquad 4\text{-}3\text{-}8$$

Equations 4-3-5, 4-3-6 and 4-3-8 form a matrix equation of the same type as equation 2-4-5. Although there are S + 1 unknowns, the matrix equation has the same form as equation 2-4-11 and can be solved in the same manner using the Gaussian Elimination. In this matrix equation [Q] is composed of the S+1 complex unknowns. [B] is composed of the right hand sides of equations 4-3-5, 4-3-6 and 4-3-8. Re[A] has the form

$$\begin{bmatrix} R_1 & \cdot & \cdot & -R_1 \\ \cdot & — & \cdot & — \\ \cdot & \cdot & R_S & -R_S \\ -R_1 & — & -R_S & Ra_{S+1,S+1} \end{bmatrix} \qquad 4\text{-}3\text{-}9$$

Where

$$Ra_{S+1,S+1} = Re(Z_l) + \sum_{i=1}^{S} R_i \qquad 4\text{-}3\text{-}10$$

Im[A] has the form

$$\begin{bmatrix} \omega L_1 - \frac{1}{\omega C_1} & , - & , \omega M_{1,S} & , -\omega L_1 - \sum_{i\neq 1}^{S} \omega M_{1,i} \\ - & , - & , - & , - \\ \omega M_{S,1} & , - & , \omega L_S - \frac{1}{\omega C_S} & , -\omega L_S - \sum_{i\neq S}^{S} \omega M_{S,i} \\ -\omega L_1 - \sum_{i\neq 1}^{S} \omega M_{1,i} & , - & , -\omega L_S - \sum_{i\neq S}^{S} \omega M_{S,i} & , Ia_{S+1,S+1} \end{bmatrix} \qquad 4-3-11$$

Where

$$Ia_{S+1,S+1} = Im(Z_l) + \sum_{i=1}^{S}(\omega L_i + \sum_{k\neq i}^{S} \omega M_{i,k}) \qquad 4-3-12$$

$Re(Z_l)$ and $Im(Z_l)$ are respectively the real and imaginary parts of the load impedance.

Once the matrix equation has been solved then the unknowns can then be inserted into equation 4-3-7 to obtain the input impedance of the coil. This value of Z_o can then be used to obtain a value for V_r . Remembering that $V_o = I_o Z_o$ and $V_l = I_l Z_l$ equation 4-2-1 reduces to

$$V_r = \frac{V_l T}{V_o N} = \frac{q_{S+1} Z_l T}{Z_o N} \qquad 4-3-13$$

Or alternatively equation 4-3-8 can be modified to obtain a value for V_r of the form

$$V_r = \frac{T}{Z_o N} \sum_{i=1}^{S} \left\{ (R_i + j\omega L_i)(q_i - q_{S+1}) + \sum_{k\neq i}^{S} j\omega M_{i,k}(q_k - q_{S+1}) \right\} \qquad 4-3-14$$

If the load impedance Z_l is large the load current can be neglected. With this approximation equations 4-3-1 and 4-4-2

reduce to

$$(R_i + j\omega L_i + \frac{1}{j\omega C_i}) q_i + \sum_{k \neq i}^{S} j\omega M_{i,k} q_k = \frac{1}{j\omega C_i} \qquad 4\text{-}3\text{-}15$$

$$1 \leq i \leq u$$

and

$$(R_i + j\omega L_i + \frac{1}{j\omega C_i}) q_i + \sum_{k \neq i}^{S} j\omega M_{i,k} q_k = 0 \qquad 4\text{-}3\text{-}16$$

$$u+1 \leq i \leq S$$

Equations 4-3-15 and 4-3-16 form a matrix equation that is only slightly different from that formed by equation 2-4-5. Thus the computer program used to calculate the input impedance of foil wound inductors can be used to calculate the relative output voltage response of tapped foil wound inductors with very few modifications.

When the load impedance can be neglected V_l will be given by

$$V_l = \sum_{i=1}^{u} \frac{1}{j\omega C_i} (I_o - I_i) - \sum_{k=u+1}^{S} \frac{1}{j\omega C_k} I_k \qquad 4\text{-}3\text{-}17$$

Inserting this expression into equation 4-2-1 and remembering that $V_o = I_o Z_o$ gives an expression for V_r of the form

$$V_r = \frac{T}{Z_o N} \left\{ \sum_{i=1}^{u} \left(\frac{1 - q_i}{j\omega C_i} \right) - \sum_{k=u+1}^{S} \frac{q_k}{j\omega C_k} \right\} \qquad 4\text{-}3\text{-}18$$

Once the matrix equation has been solved then the unknowns can be inserted into equation 4-3-17 to obtain the input impedance. The input impedance together with the relative currents can then be inserted into equation 4-3-18 to obtain the relative

output voltage.

4) Theoretical Results

The theoretical output voltage response and the input impedance were calculated for the 250 turn tapped foil wound inductor described in section 4-2. The simplified model, which neglects the load impedance, was easier to implement, therefore it was used initially. In this model with 10 sections each of 25 turns $u = 4$, which corresponds with $T = 100$.

The theoretical output voltage and input impedance are shown in Fig. 4-8, plotted on a log scale against frequency from 500 KHz to 6 MHz. The input impedance has a maximum at 2.181 MHz and a minimum at 4.165 MHz, which corresponds exactly with the maximum in the relative output voltage. This is to be expected if power is to be conserved. Providing the input voltage is constant the input impedance must decrease to compensate for the increase in the output voltage.

In the theoretical model of the foil wound inductor analysed in chapter 1 the maxima in the input impedance were associated with resonances in the current distribution within the coil and the minima in the input impedance were associated with resonances in the voltage distribution.

The relative voltage at the junctions of sections p and $p+1$ will, when p is less than or equal to u, be given by

$$V_r^p = \frac{T}{Z_o N} \sum_{i=1}^{p} \frac{(1 - q_j)}{j\omega C_i} \qquad 4-4-1$$

If p is greater than u the relative voltage at p will be given by

Figure 4-8

Theoretical Relative Output Voltage and Input Impedance of the 250 Turn Foil Wound Inductor with T=100

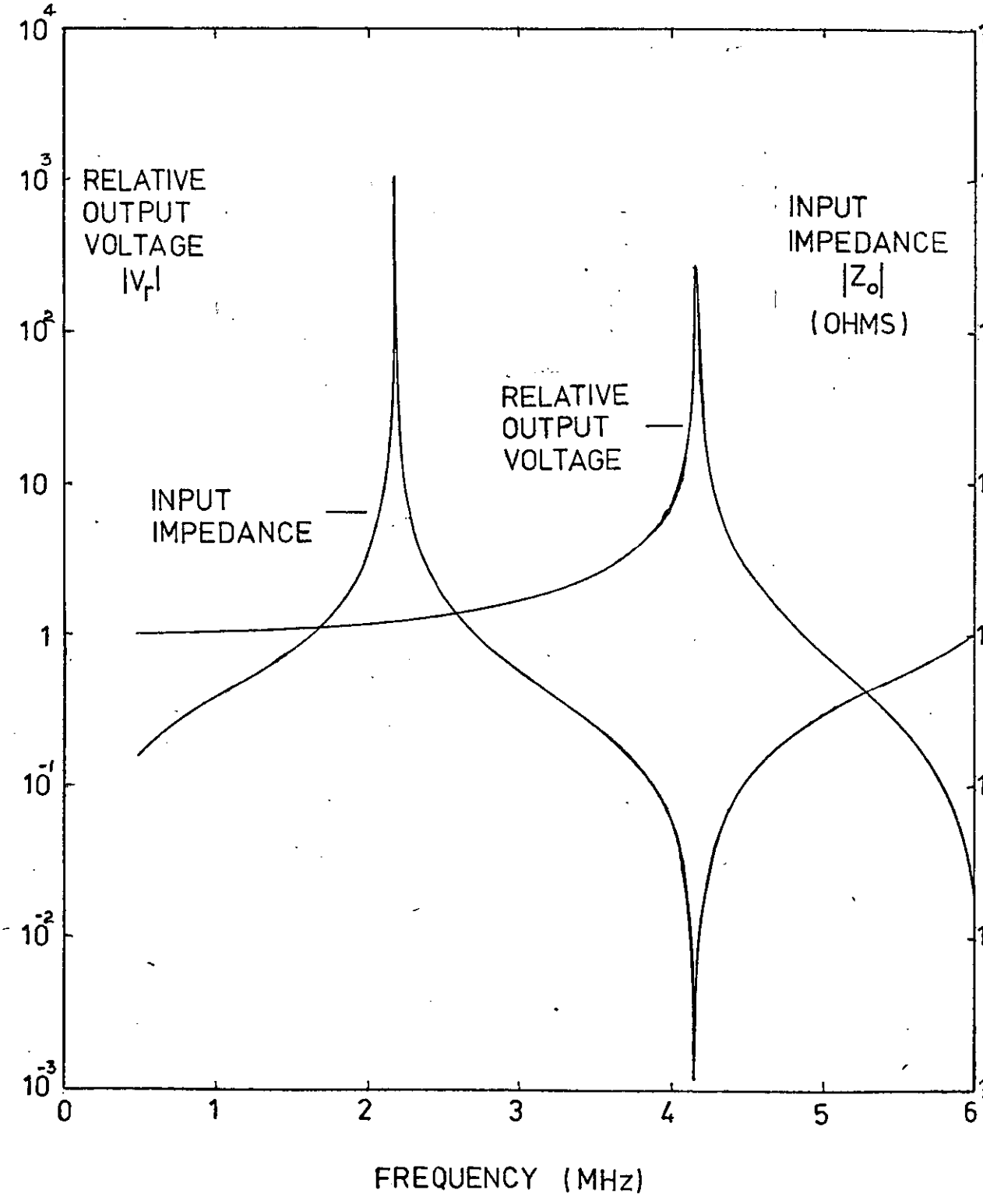

Figure 4-9

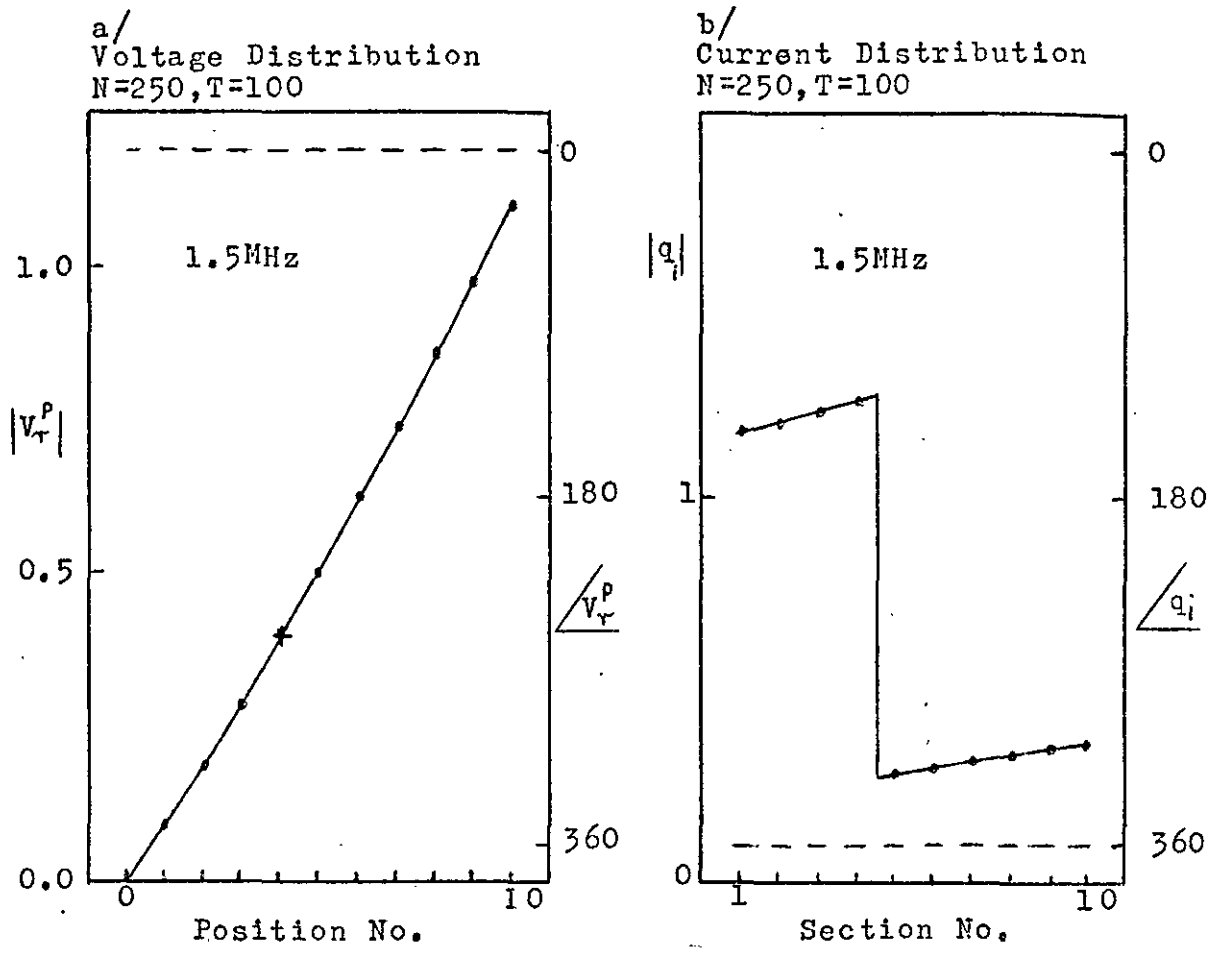

Figure 4-10

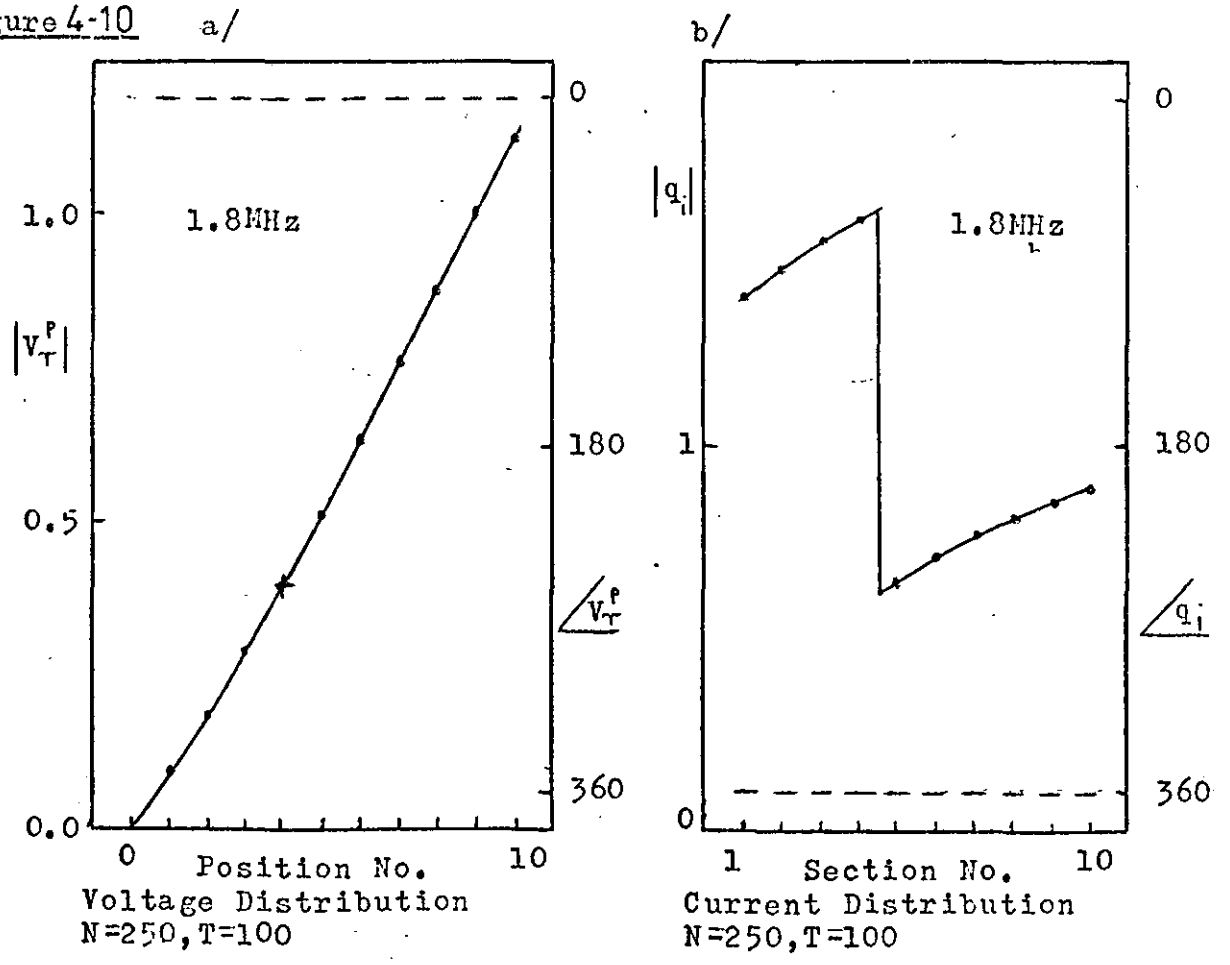

+ Input Voltage ——— Magnitude — — — Phase

Figure 4-11

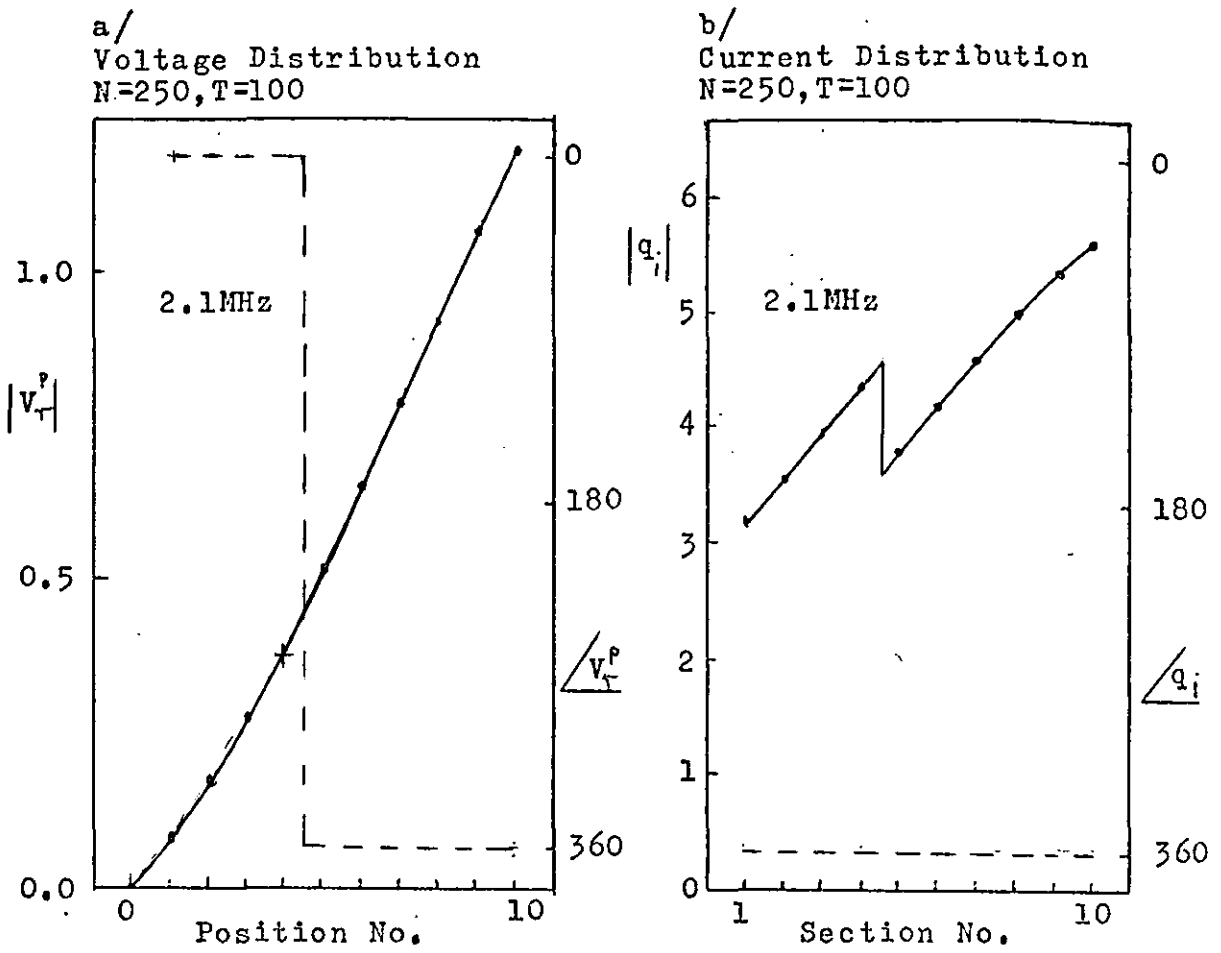

Figure 4-12

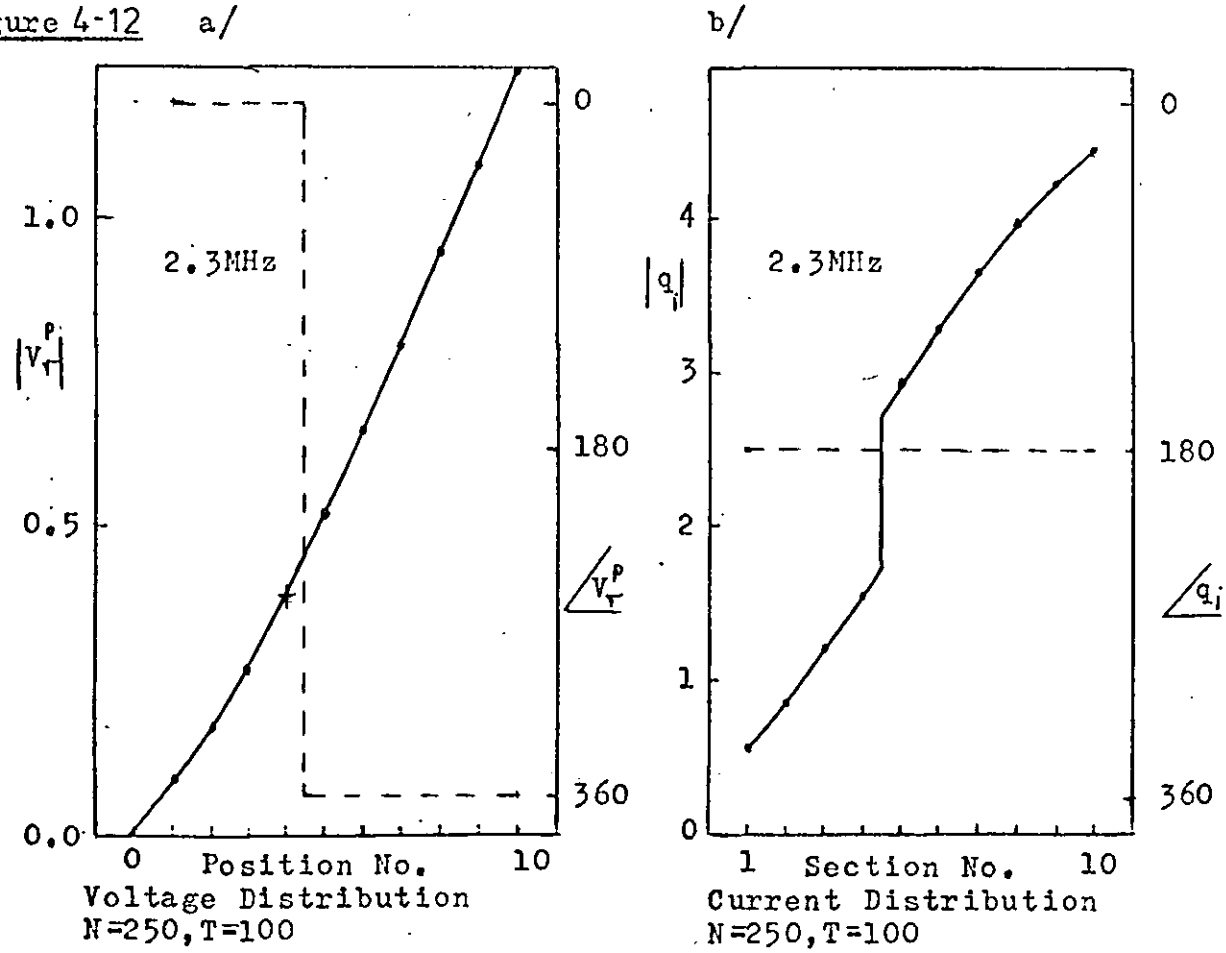

+ Input Voltage —— Magnitude — — — Phase

Figure 4-13

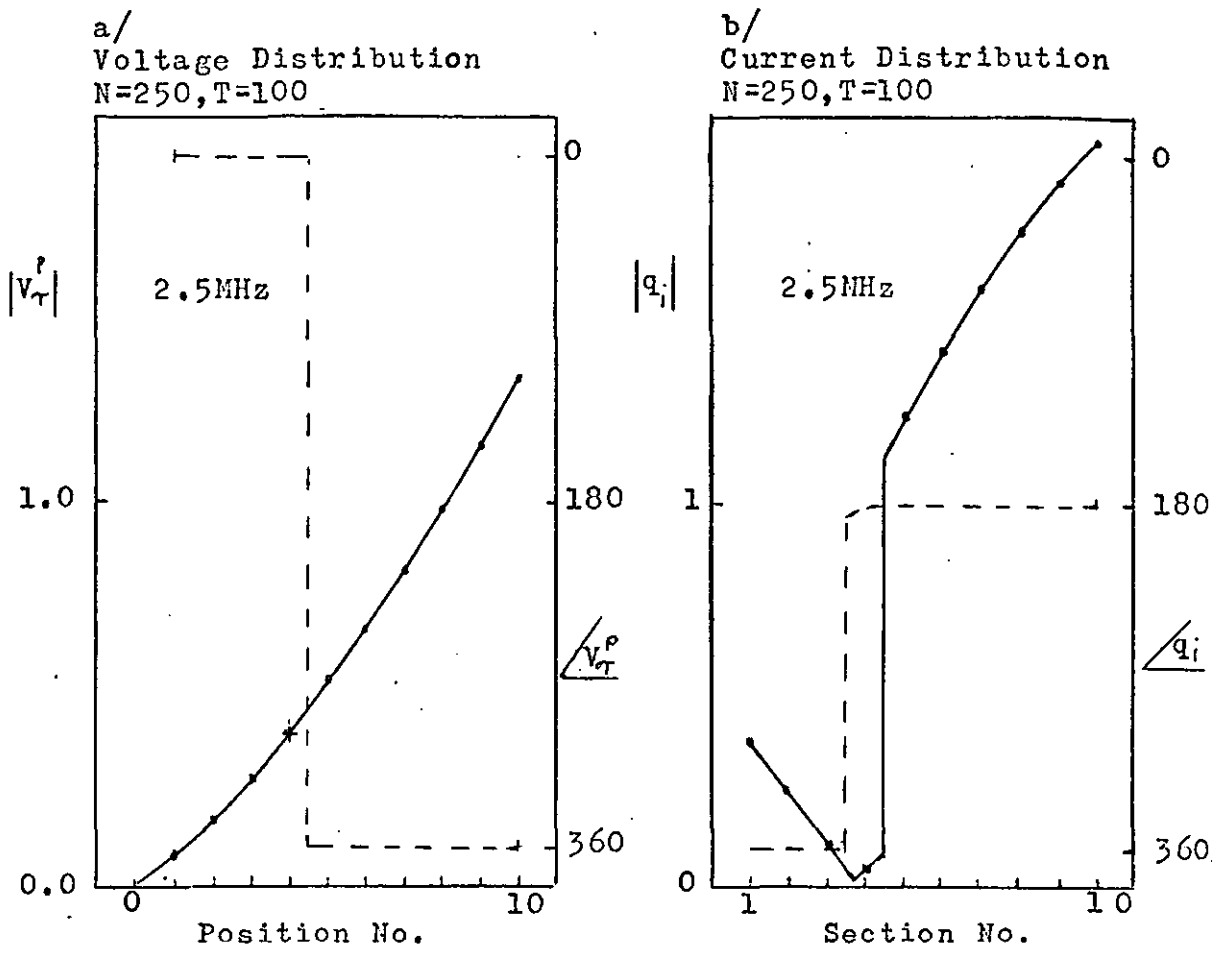

Figure 4-14

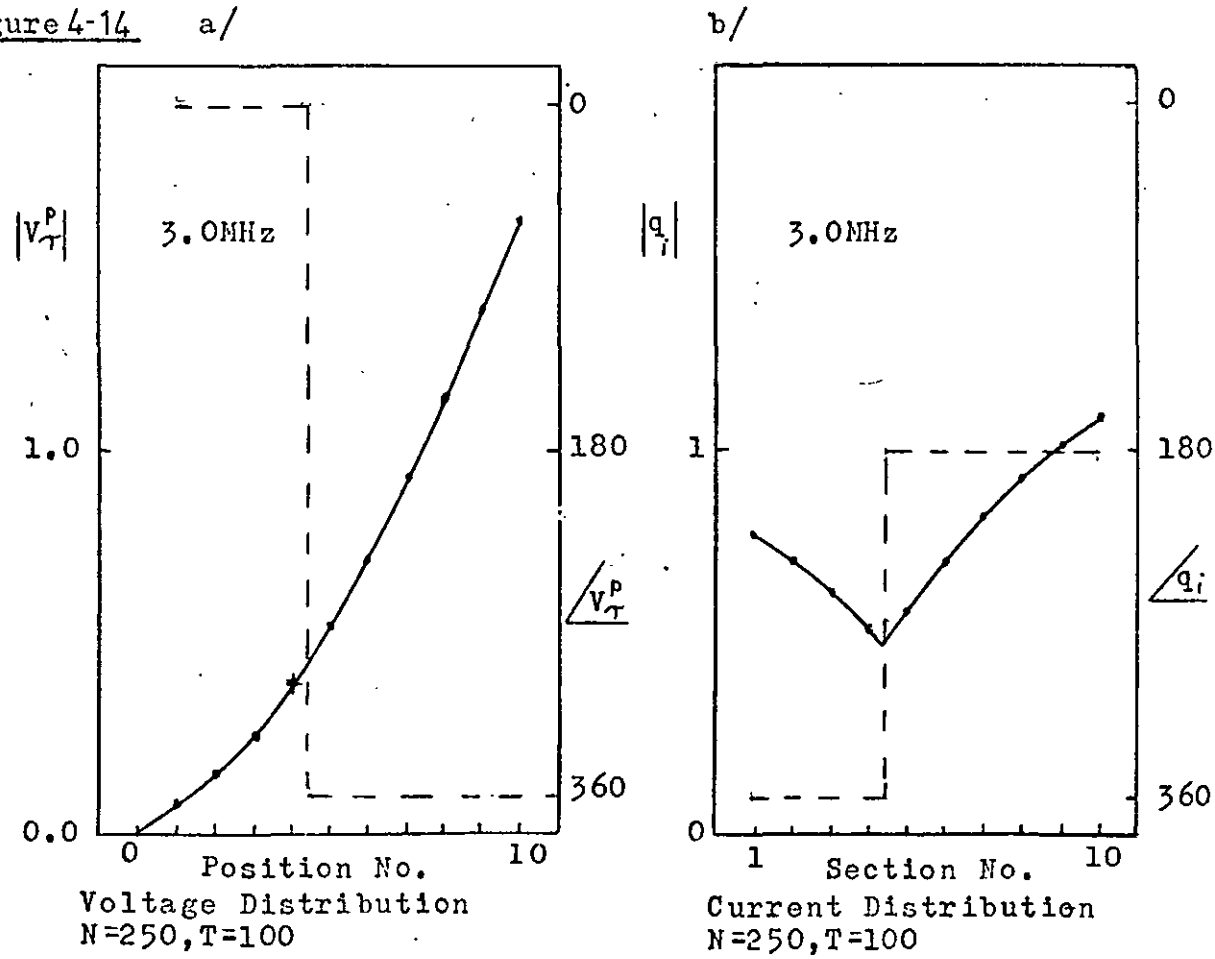

+Input Voltage ——— Magnitude — — — Phase

Figure 4-15

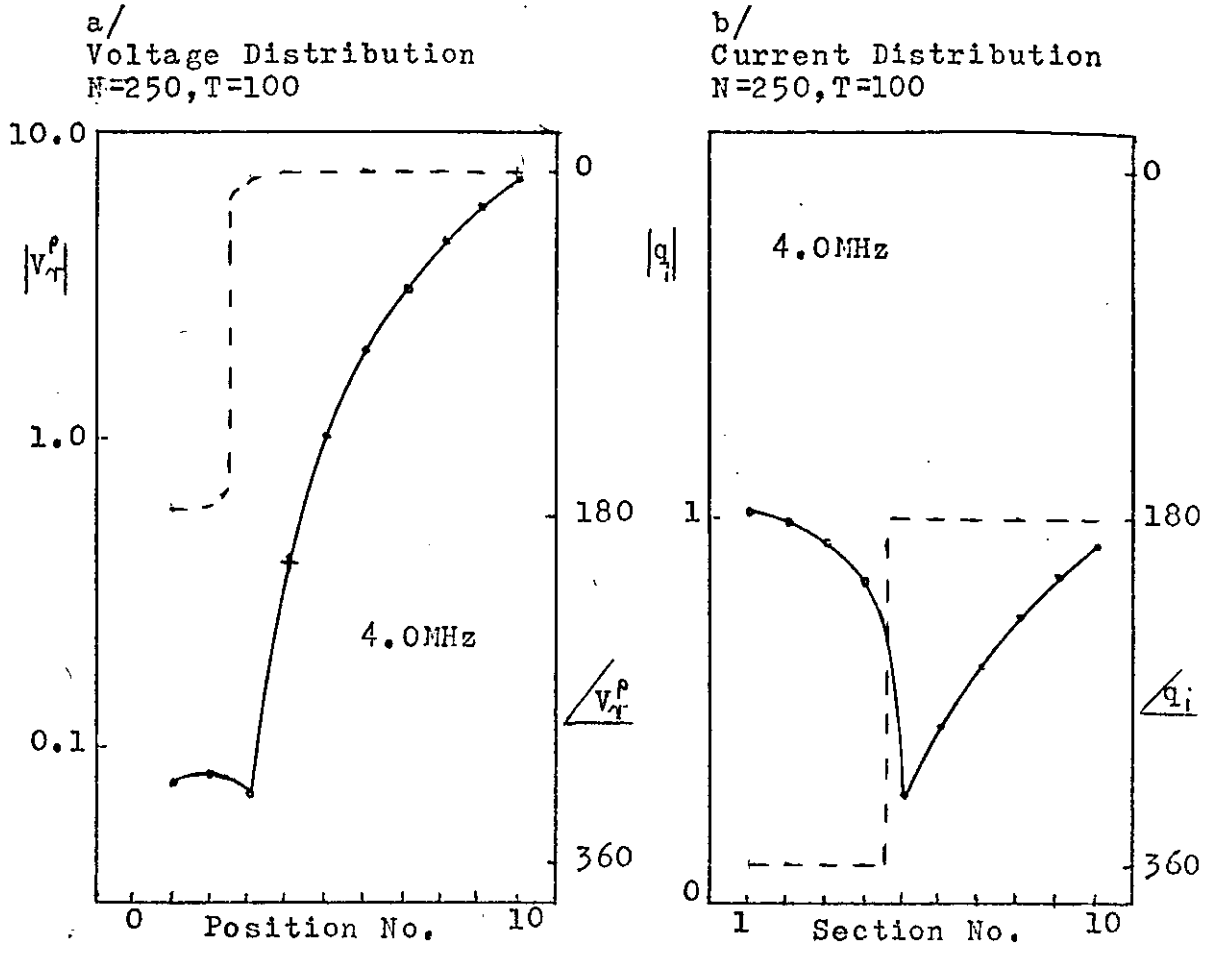

Figure 4-16

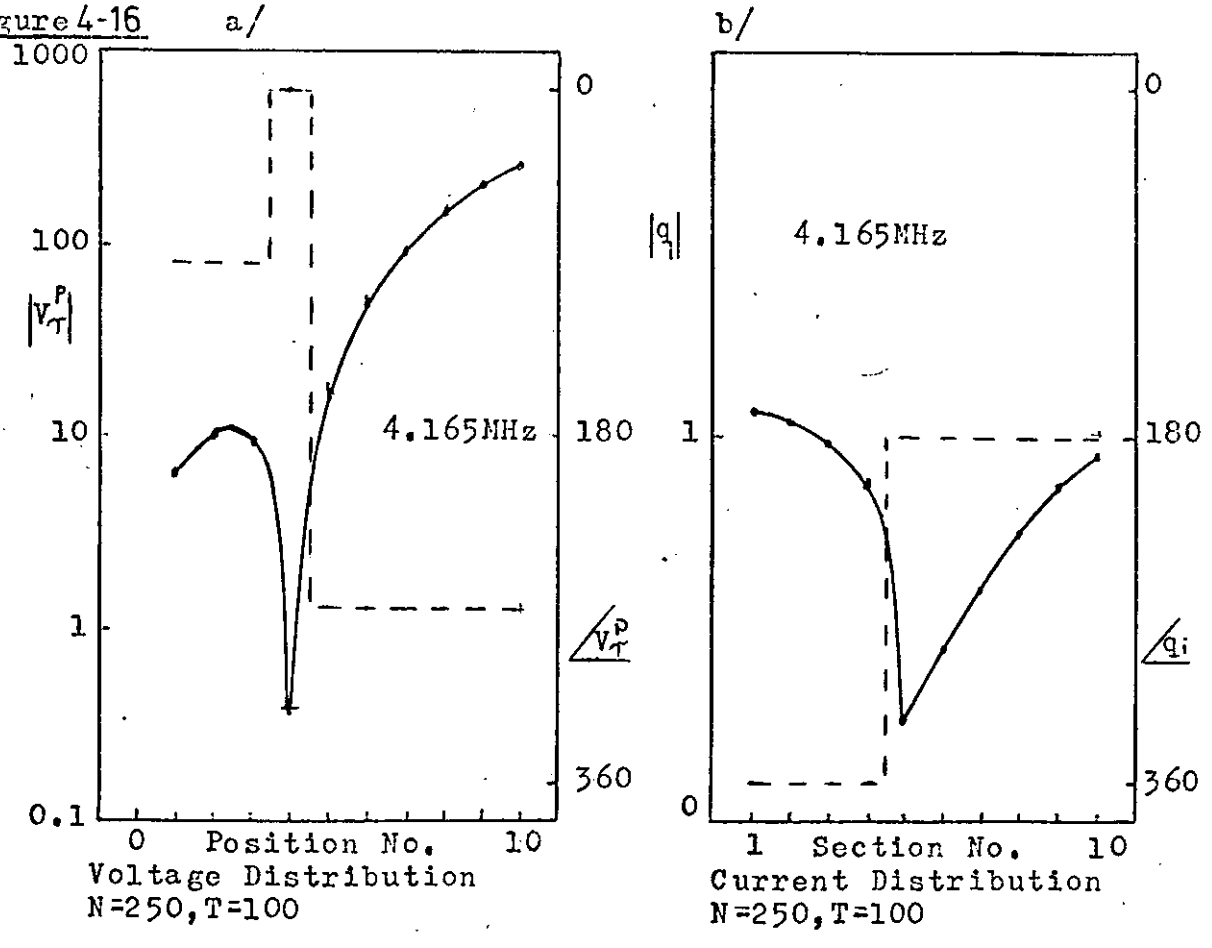

+Input Voltage ——— Magnitude — — — Phase

Figure 4-17

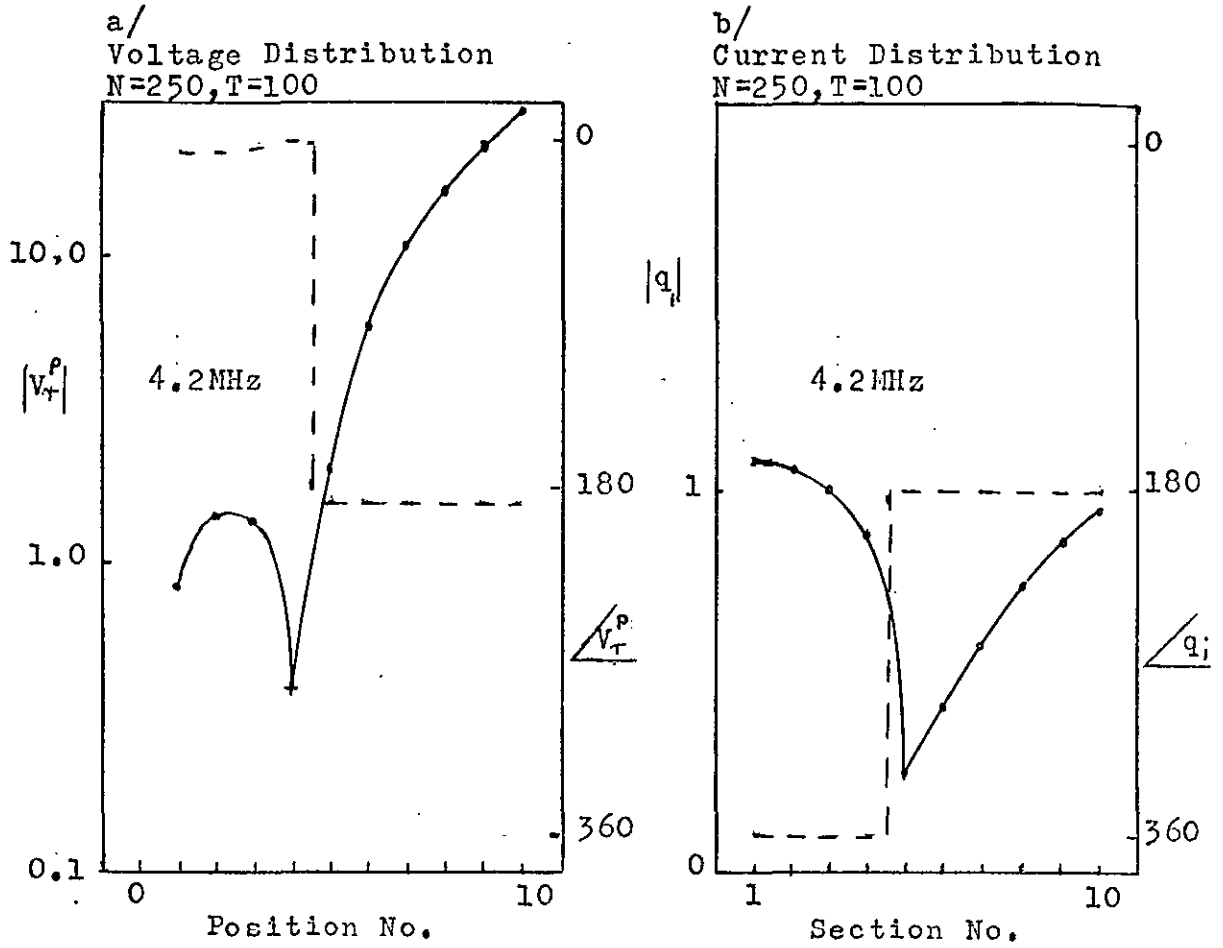

Figure 4-18

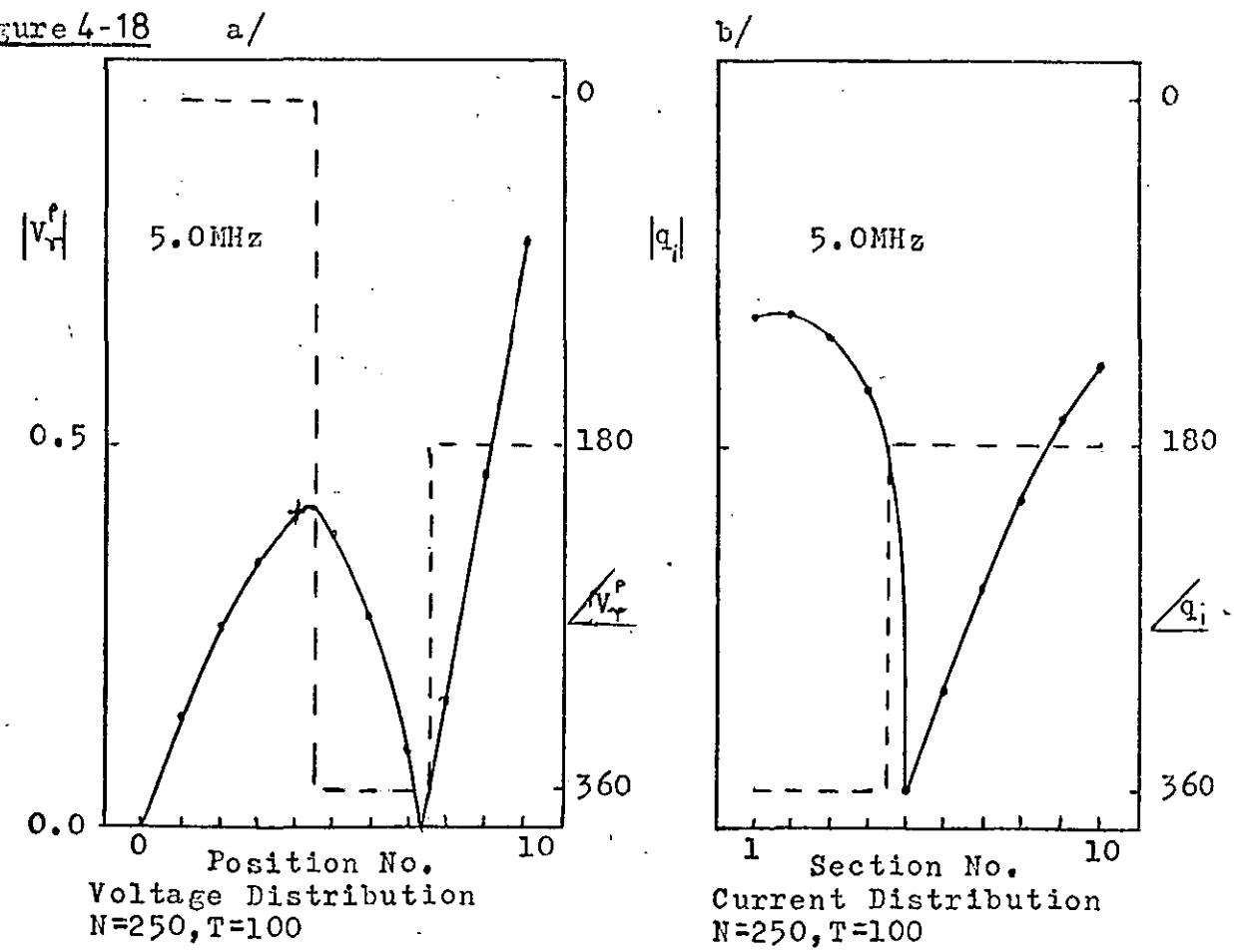

+Input Voltage ——— Magnitude — — — Phase

$$V_r^p = \frac{T}{Z_o N} \left\{ \sum_{i=1}^{u} \frac{(1-q_i)}{j\omega C_i} - \sum_{k=u+1}^{p} \frac{q_k}{j\omega C_i} \right\} \qquad 4\text{-}4\text{-}2$$

Both of these equations are derived from equation 4-3-18. Ten sections were used in this model. Therefore in the same manner as in chapter 1 the beginning of section 1, which is at the centre of the coil, will be labeled position 0 and the end of section 10, which is at the edge of the coil, will be labeled position 10.

The evolution of the theoretical relative voltage distribution within the 250 turn tapped foil wound inductor ($T = 100$) from 1.5 MHz to 5.0 MHz is shown in Figs. 4-9 to 4-18. Figs. 4-9a to 4-18a show the voltage V_r^p plotted against position number, while Figs. 4-9b to 4-18b show the relative current q_i plotted against section number. At 1.5 MHz the relative voltage distribution is almost linear and the relative output voltage at position 10 is just above 1. Then with increasing frequency the distribution becomes increasingly non-linear and the relative output voltage increases, until at 4.0 MHz the voltages at positions 1 to 3 have reversed phase, with respect to the rest of the distribution, and the relative output voltage has reached almost 10. The maximum in the relative output voltage occurs at 4.165 MHz. The relative voltage distribution at this frequency changes phase by 180° once, allowing for the phase of the input voltage, which is fixed. This resonance has the characteristic of a second order resonance, suggesting that the first order resonance has been suppressed by the method of exciting the coil. The first order current resonance that occurs

between 2.1 MHz and 2.3 MHz has no appreciable effect on the relative voltage distribution. The discontinuity in the relative current distributions is due to the input current of magnitude 1.

5) Comparison of Theory and Experiment

A comparison of the theoretical and experimental relative output voltage responses for the 250 turn tapped foil wound inductor with $T = 100$ is shown in Fig. 4-19, plotted on a log scale against frequency. Experimentally the resonance in the output voltage response occurs at 3.77 MHz, while theoretically it occurs at 4.165 MHz; a difference of -9.5%. The difference between the maximum experimental value of V_r and the theoretical value is a factor of 6.8 times.

The theoretical and experimental resonant frequencies for $T = 50$, 150 and 200 were also found and are shown tabulated in Fig. 4-20. The difference between the theoretical and experimental resonant frequencies increases from +2.2% when $T = 200$ to +19.1% when $T = 50$.

It has been shown theoretically that the maximum in the relative output voltage is associated with a second order voltage resonance, so it is reasonable to assume that there are maxima associated with the third and higher orders of resonance. With the 1000 turn tapped foil wound inductor described in section 4-2 the first three maxima in the relative output voltage fall within the usable frequency range of the experimental apparatus.

The theoretical relative output voltage and input impedance of the 1000 turn tapped foil wound inductor with $T = 500$

Figure 4-19

Comparison of the Theoretical and Experimental Voltage Responses of the 250 Turn Tapped Foil Wound Inductor With T = 100

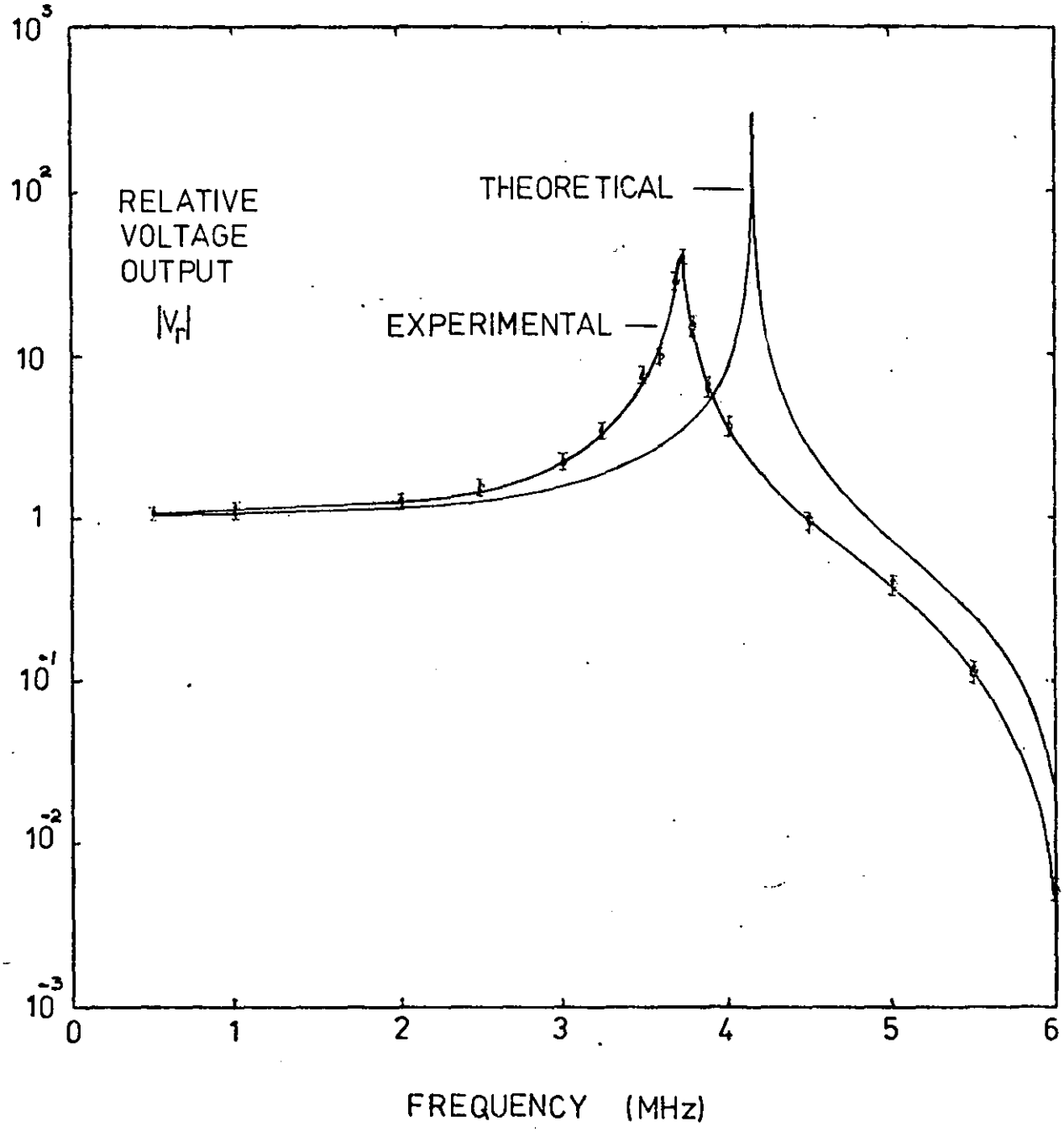

Figure 4-20

Comparison of the Theoretical and Experimental Resonant Frequencies of the 250 Turn Tapped Foil Wound Inductor

Input Connection	Experimental Resonant Frequency MHz	Theoretical Resonant Frequency MHz	Percentage Difference
T = 200	5.88 ±0.05	6.011 ±1KHz	+2.2
T = 150	4.52 ±0.05	4.945 ±1KHz	+8.6
T = 100	3.77 ±0.05	4.165 ±1KHz	+9.5
T = 50	2.93 ±0.05	3.62 ±1KHz	+19.1

are shown in Fig. 4-21 plotted on a log scale against frequency from 200 KHz to 3 MHz. This graph clearly shows three maxima and two minima in the output voltage response. The minima in the input impedance correspond in frequency with the maxima in the relative output voltage, while the maxima in the input impedance do not correspond in frequency with the minima in the output voltage response.

The theoretical resonant frequencies for the first three maxima and minima in the relative output voltage response are tabulated in Figs. 4-29 and 4-30. The relative current and voltage distributions within the tapped foil wound inductor at these frequencies are shown in Figs. 4-22 to 4-27. Figs. 4-22a to 4-27a show the relative voltage plotted against position number and Figs. 4-22b to 4-27b show the relative current plotted against section number. These graphs do not present a very clear picture. The voltage distribution at the first maximum (0.6975 MHz) changes phase by 180° once, the voltage distribution at the second maximum (1.886 MHz) changes phase by 180° once and the voltage distribution at the third maximum (2.924 MHz) changes phase by 180° three times. The current distributions at these frequencies change phase by 180° once, twice and three times respectively. It appears that the first order voltage resonance has been suppressed and the third order voltage resonance at 1.886 MHz appears to be a second order resonance. However the equivalent circuit is a complexly linked resonant system therefore it will not necessarily show the same resonant patterns as a simple system.

A comparison of the theoretical and experimental relative

Figure 4-21

Theoretical Relative Output Voltage and Input Impedance of the 1000 Turn Tapped Foil Wound Inductor with T=500

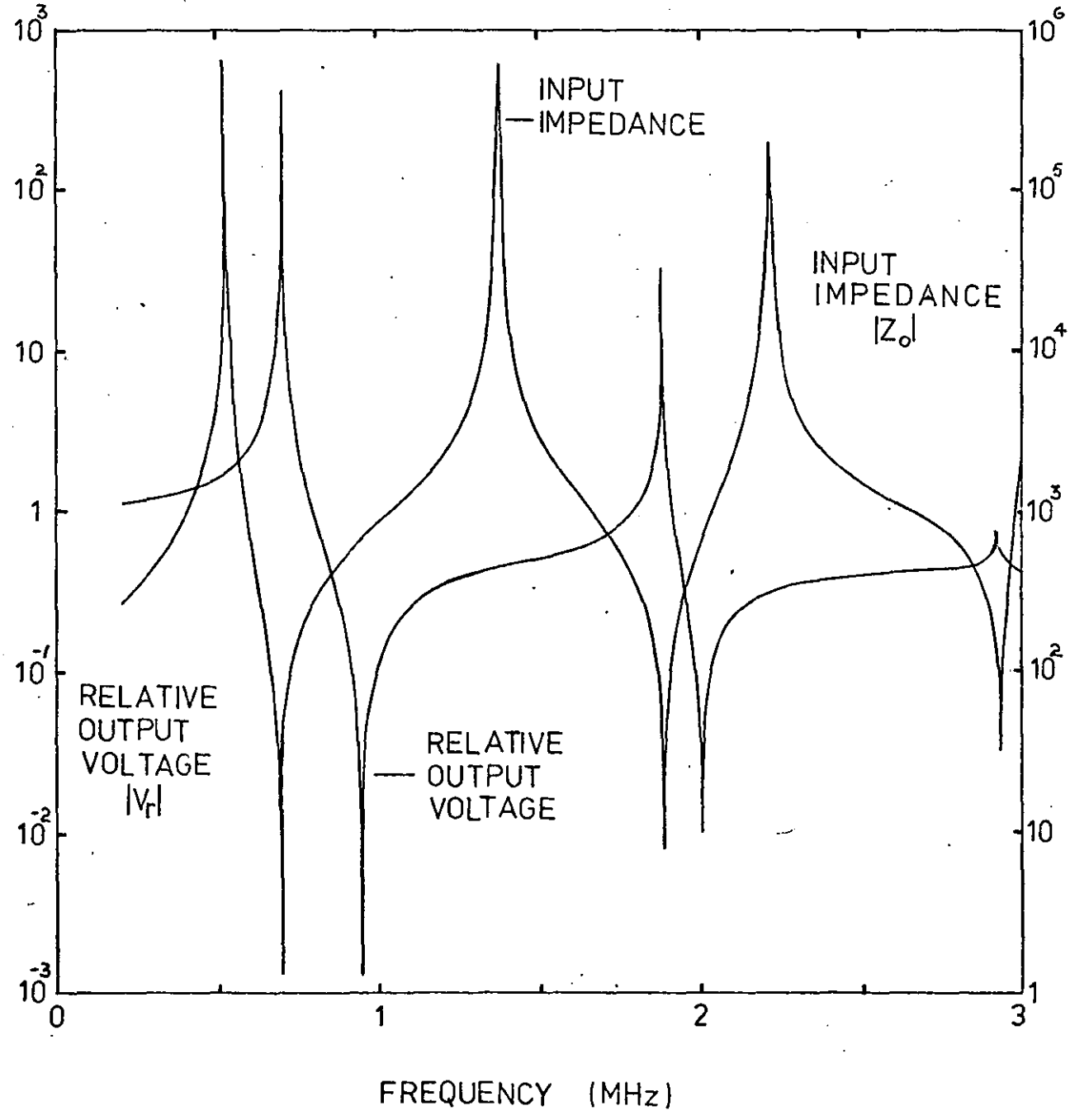

Figure 4-22

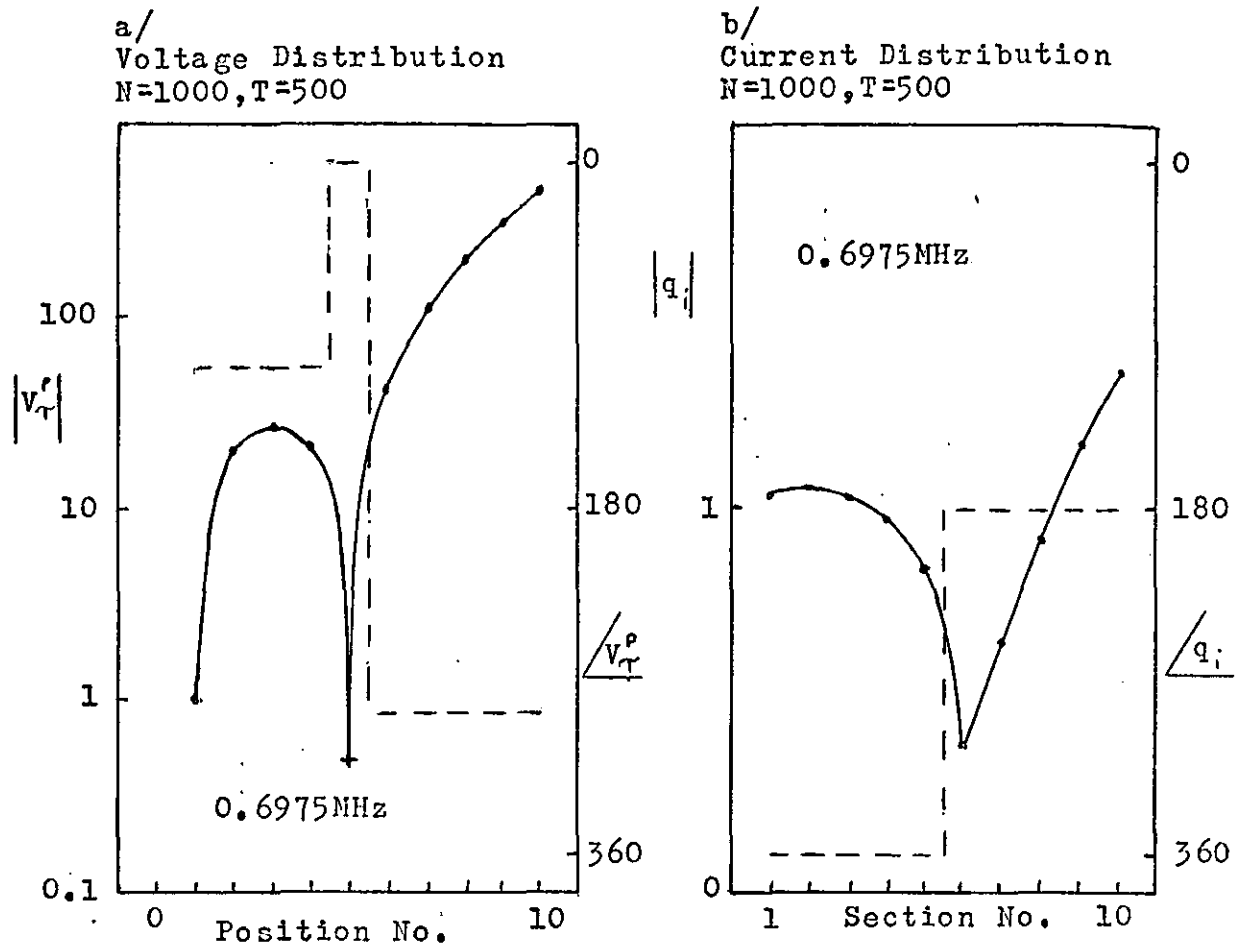

Figure 4-23 a/

b/

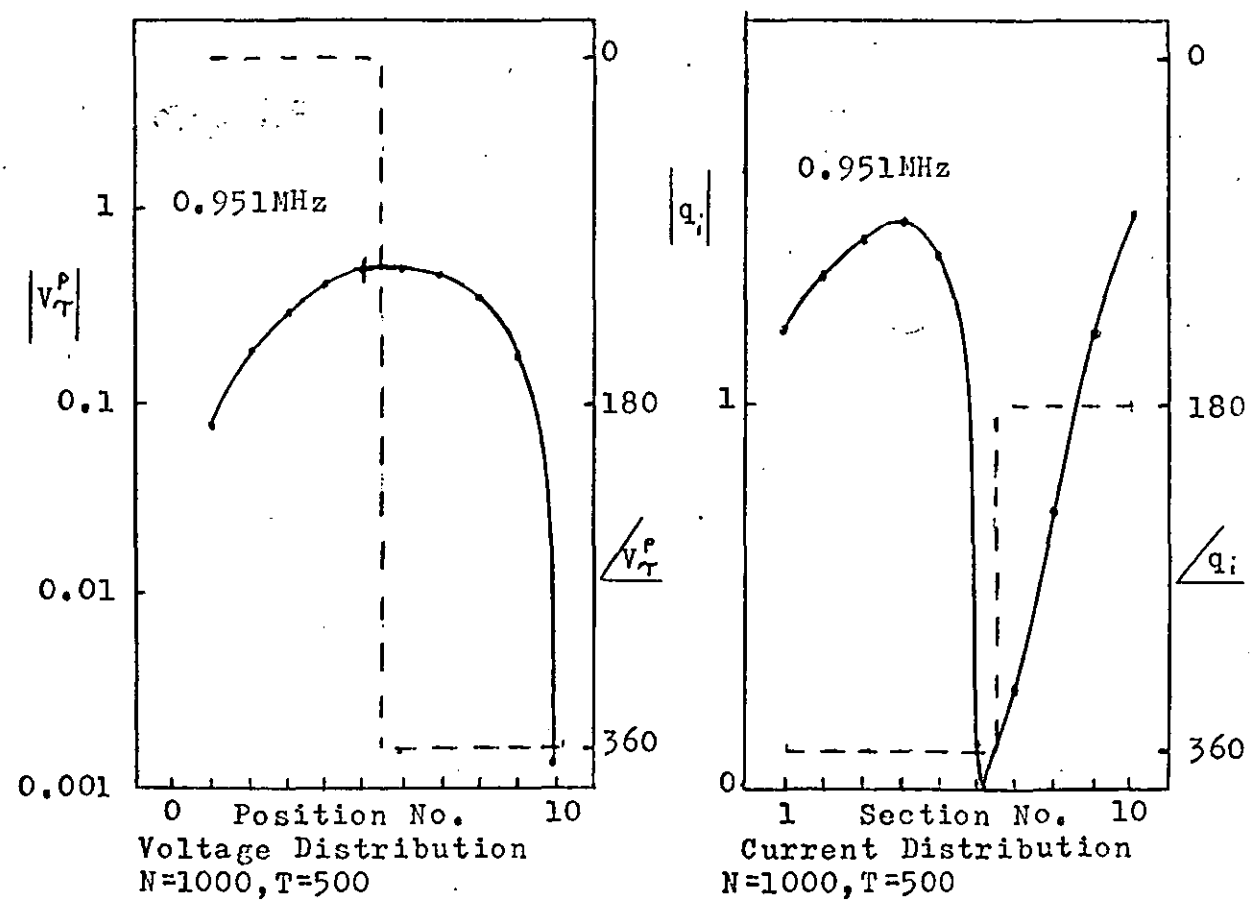

+Input Voltage —— Magnitude - - - - Phase

Figure 4-24

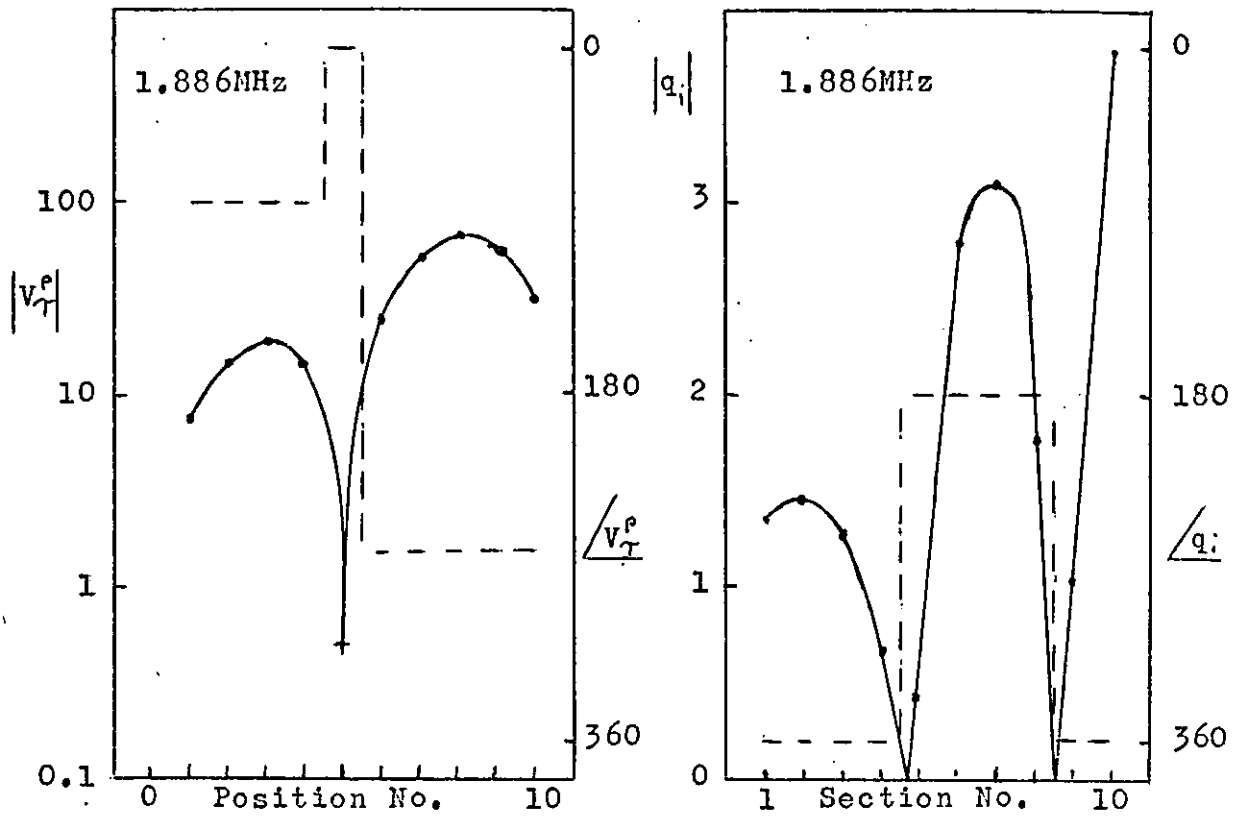

Figure4-25 a/

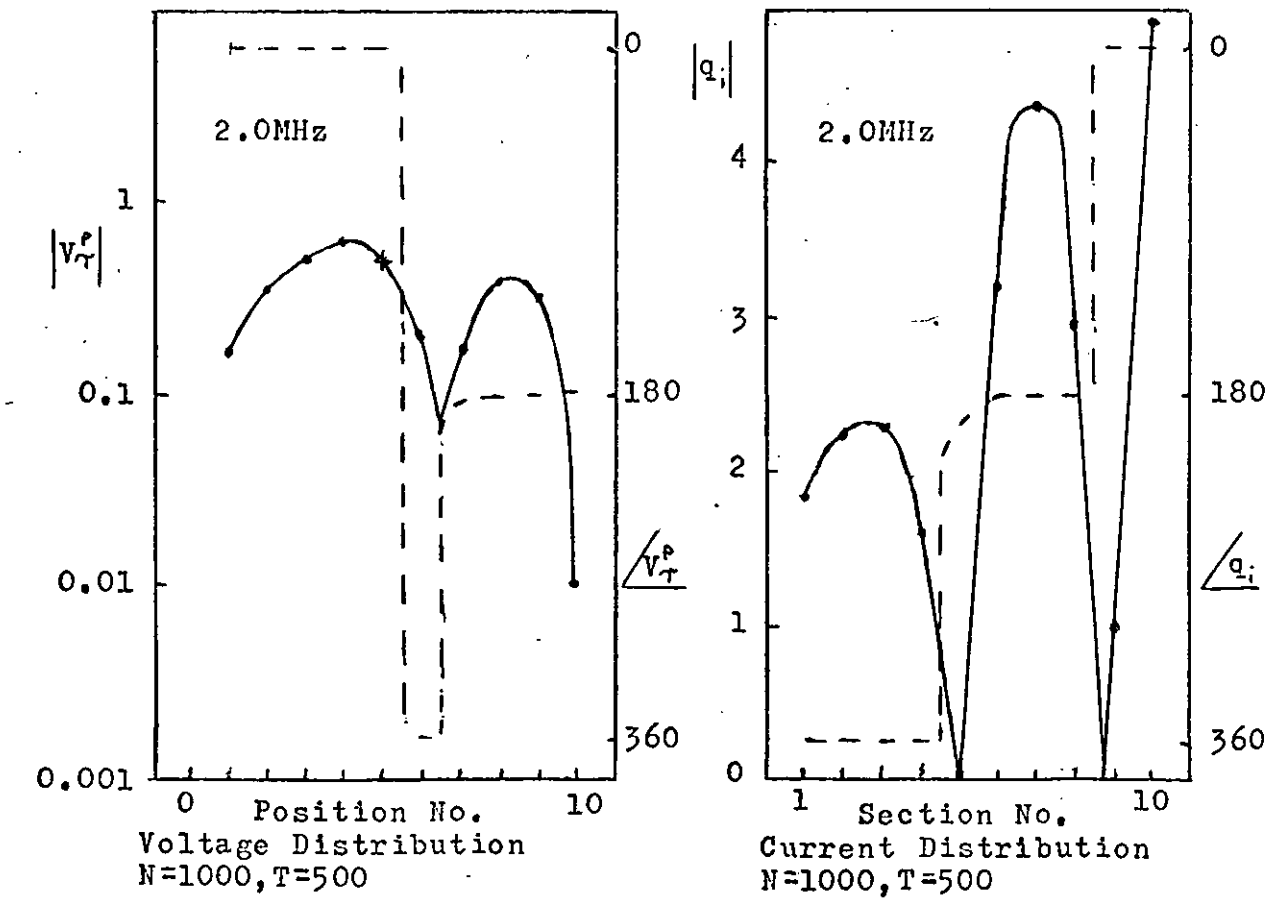

+Input Voltage ——— Magnitude - - - - Phase

Figure 4-26

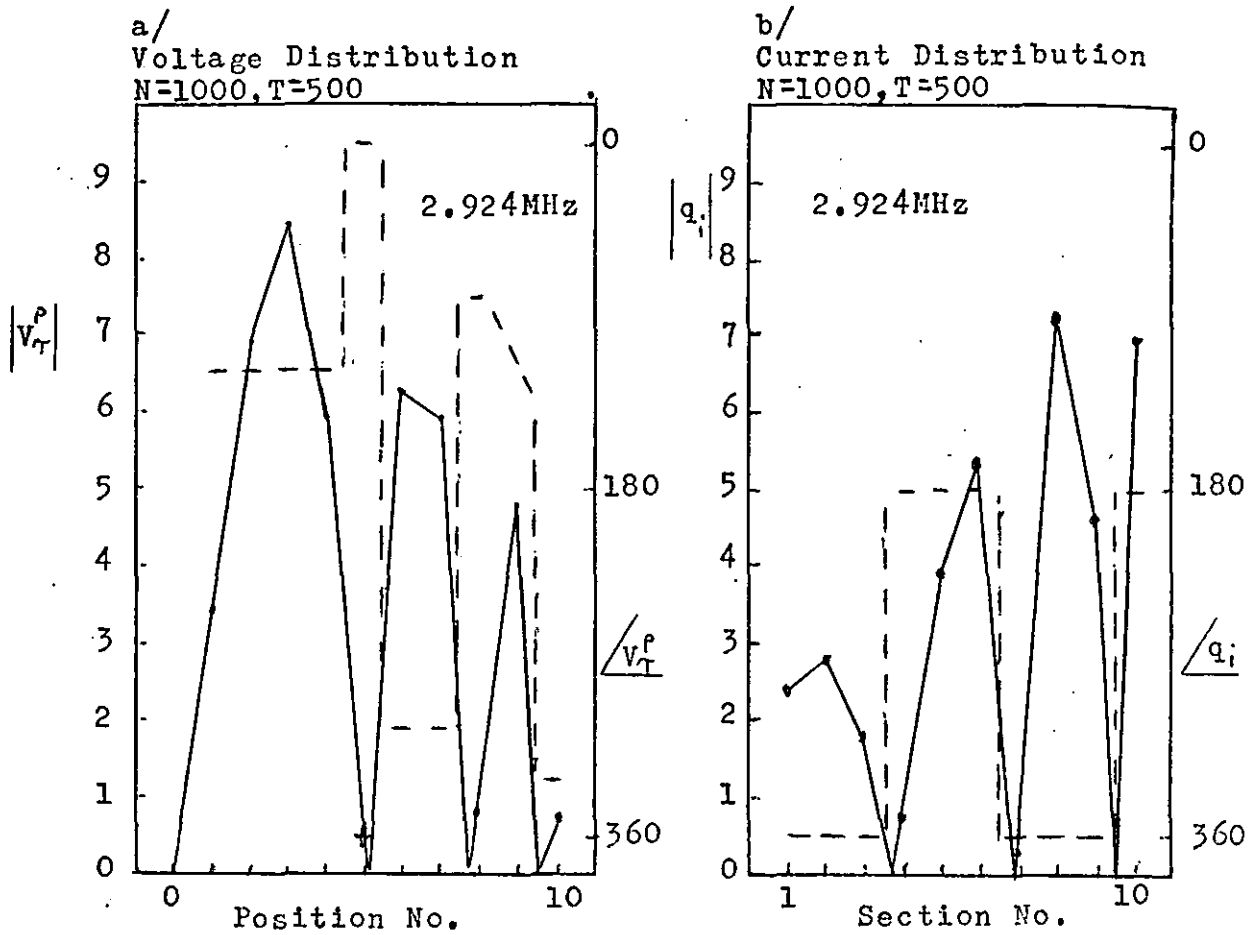

Figure 4-27

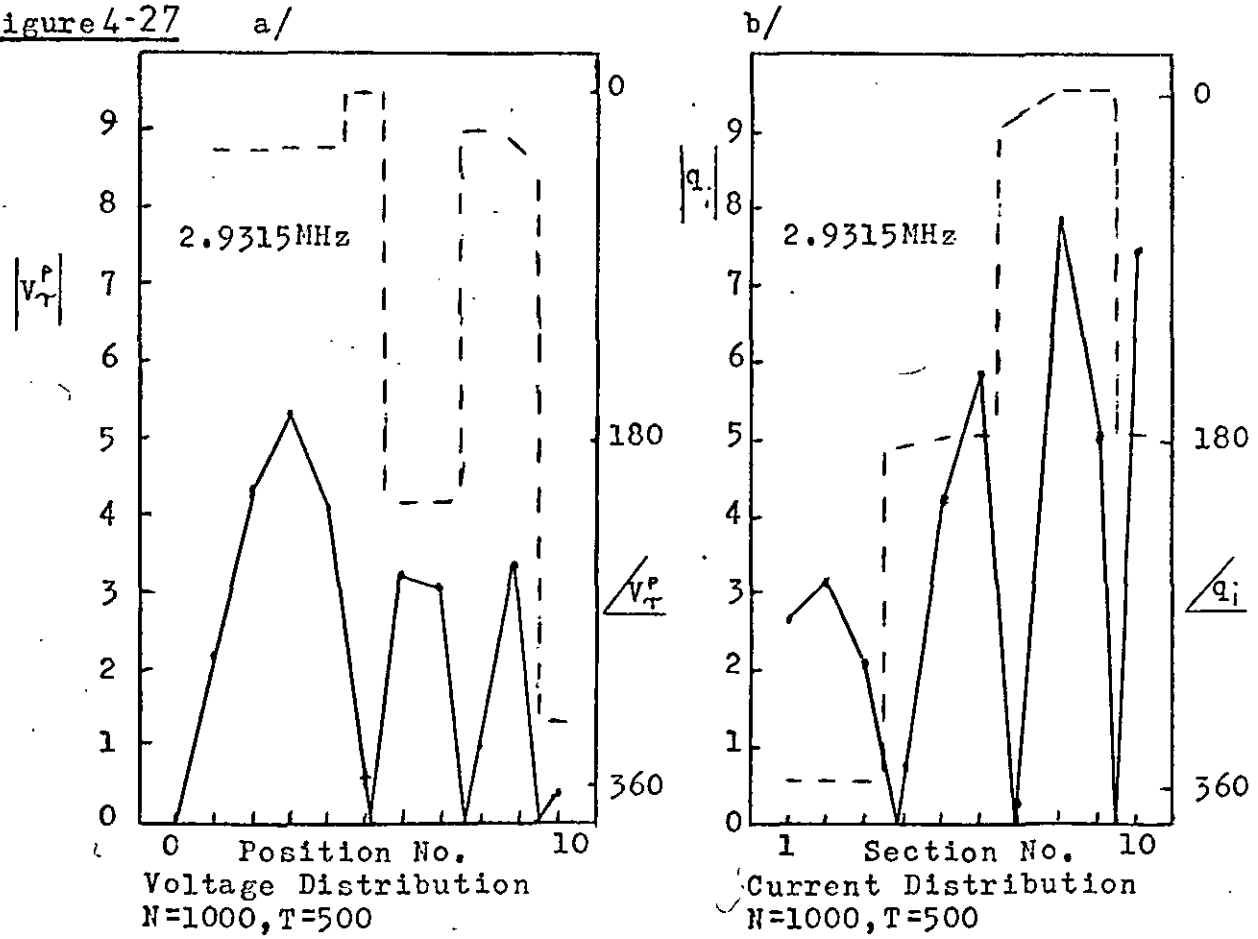

+Input Voltage ——— Magnitude — — — Phase

Figure 4-28

Comparison of the Theoretical and Experimental Relative Output Voltage Responses of the 1000 Turn Tapped Foil Wound Inductor with T=500

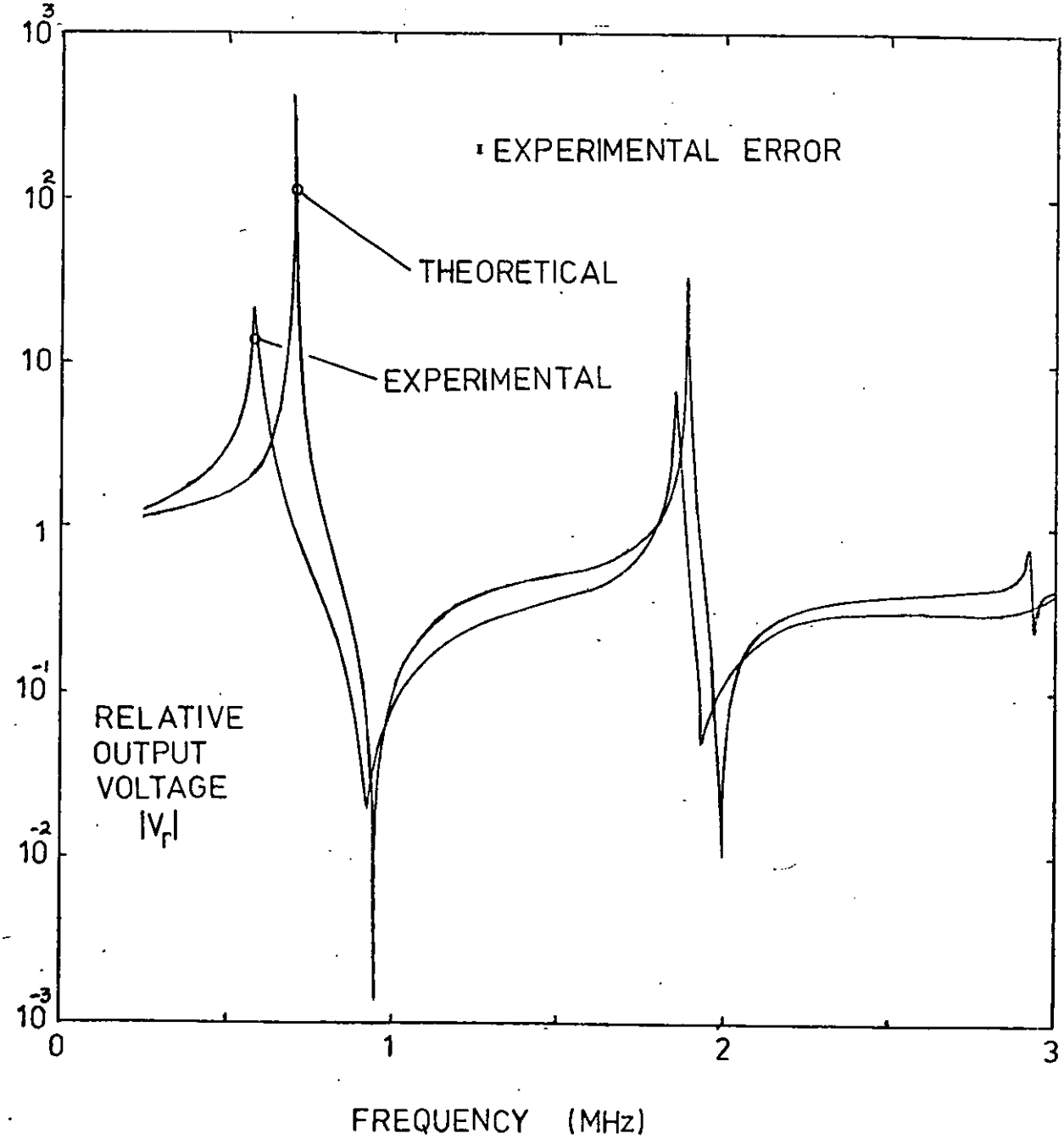

Figure 4-29

Comparison of the Theoretical and Experimental Resonant Frequencies of the Output Voltage Response of the 1000 Turn Tapped Foil Wound Inductor

First Maximum Input Connection	Experimental Resonant Frequency MHz	Theoretical Resonant Frequency MHz	Percentage Difference
T = 900	1.069 ±2KHz	1.073 ±250Hz	+0.37
T = 800	0.890 "	0.945 "	+5.9
T = 700	0.759 "	0.840 "	+9.6
T = 600	0.654 "	0.759 "	+13.8
T = 500	0.589 "	0.6975 "	+15.6
T = 400	0.527 "	0.6505 "	+19.0
T = 300	0.481 "	0.6145 "	+23.9
T = 200	0.460 "	0.5865 "	+21.9
T = 100	0.428 "	0.564 "	+24.1
Second Maximum Input Connection	**Experimental Resonant Frequency MHz**	**Theoretical Resonant Frequency MHz**	**Percentage Difference**
T = 900	2.192 ±4KHz	2.178 ±250Hz	-0.64
T = 800	2.193 "	2.181 "	-0.55
T = 700	2.150 "	2.128 "	-1.0
T = 600	2.016 "	2.0165 "	+0.25
T = 500	1.843 "	1.886 "	+2.3
T = 400	1.692 "	1.7645 "	+4.1
T = 300	1.583 "	1.625 "	+2.6
T = 200	1.507 "	1.579 "	+4.1
T = 100	1.418 "	1.511 "	+6.2
Third Maximum Input Connection	**Experimental Resonant Frequency MHz**	**Theoretical Resonant Frequency MHz**	**Percentage Difference**
T=900	2.925 ±5KHz	2.882 ±3KHz	-1.5
T=800	3.000 "	2.938 "	-2.1
T=700	3.055+ "	3.005 "	-1.7
T=600	-	3.000	-
T=500	2.990 "	2.925 "	-2.2
T=400	2.860 "	2.795 "	-2.3
T=300	2.725 "	2.660 "	-2.4
T=200	2.595 "	2.538 "	-2.2
T=100	2.470 "	2.435 "	-1.4

+ This resonance is visible as a phase change only.
- This resonance is not visible.

Figure 4-30

Comparison of the Theoretical and Experimental Resonant Frequencies of the Output Voltage Response of the 1000 Turn Tapped Foil Wound Inductor

First Minimum Input Connection	Experimental Resonant Frequency MHz	Theoretical Resonant Frequency MHz	Percentage Difference
T = 900	1.173 ±2KHz	1.142 ±250Hz	-2.7
T = 800	1.124 "	1.086 "	-3.5
T = 700	1.080 "	1.0345 "	-4.4
T = 600	1.039 "	0.9895 "	-5.0
T = 500	1.000 "	0.951 "	-5.2
T = 400	0.963 "	0.919 "	-4.8
T = 300	0.927 "	0.8925 "	-3.9
T = 200	0.903 "	0.872 "	-3.6
T = 100	0.893 "	0.858 "	-4.1
Second Minimum Input Connection	**Experimental Resonant Frequency MHz**	**Theoretical Resonant Frequency MHz**	**Percentage Difference**
T = 900	2.170 ±5KHz	2.156 ±250Hz	-0.67
T = 800	2.171 "	2.155 "	-0.74
T = 700	2.126 "	2.1155 "	-0.54
T = 600	2.059 "	2.058 "	-0.04
T = 500	1.978 "	2.000 "	+1.1
T = 400	1.913 "	1.9425 "	+1.5
T = 300	1.849 "	1.8955 "	+2.5
T = 200	1.842 "	1.858 "	+0.86
T = 100	1.783 "	1.8325 "	+2.8
Third Minimum Input Connection	**Experimental Resonant Frequency MHz**	**Theoretical Resonant Frequency MHz**	**Percentage Difference**
T = 900	3.016 ±10KHz	2.929 ±3KHz	-3.0
T = 800	3.041 "	2.948 "	-3.2
T = 700	3.075+ "	2.985 "	-3.0
T = 600	-	2.979 "	-
T = 500	3.048 "	2.932 "	-4.0
T = 400	2.966 "	2.870 "	-3.3
T = 300	2.919 "	2.808 "	-4.0
T = 200	2.891 "	2.759 "	-4.8
T = 100	2.858 "	2.725 "	-4.9

+ This resonance is visible as a phase change only.
- This resonance is not visible.

output voltages of the 1000 turn tapped foil wound inductor with $T = 500$ is shown in Fig. 4-28 from 200 KHz to 3 MHz. This shows general agreement between the theoretical and experimental responses, with the exception of the Q values of the resonances, which is to be expected.

A comparison is shown in Figs. 4-29 and 4-30 between the theoretical and experimental resonant frequencies for the first three maxima and minima in the relative output voltage response of the 1000 turn tapped foil wound inductor for all possible values of T. The theoretical and experimental values compare well, with a maximum error of $\pm 6.2\%$, except for the first maximum resonance. The error in this case rises from $+0.37\%$ at $T = 900$ to $+24.1\%$ at $T = 100$. This error increase may be due to the impedance of the probe.

6) Investigation of the Probe Impedance

To examine the effect of the load impedance theoretically a computer program was written to solve the complex matrix equation formed by equations 4-3-5, 4-3-6 and 4-3-8. These equations describe the equivalent circuit of Fig. 4-7, which includes the load impedance. The form of the load impedance is shown in Fig. 4-31. R_p and C_p are the input resistance and capacitance of the F.E.T. probe. C_l is an added external capacitance. If C_l is large enough then any stray capacitance can be swamped. Z_l has the form

$$Z_l = \frac{R_p}{1 + j\omega R_p(C_p + C_l)} \qquad 4\text{-}6\text{-}1$$

Figure 4-31

Composition of the Load Impedance Z_l of Figure 3-4

C_p and R_p represent the impedance of the probe.

C_l represents any added capacitive load.

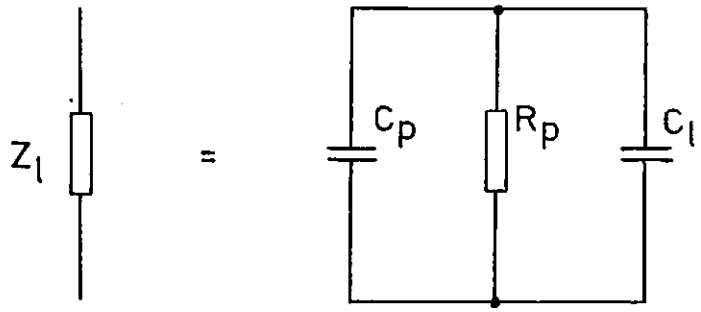

Figure 4-32

Variation of the Theoretical and Experimental Fundamental Resonant Frequency of the 1000 Turn Tapped Foil Wound Inductor (T = 400) with C_l

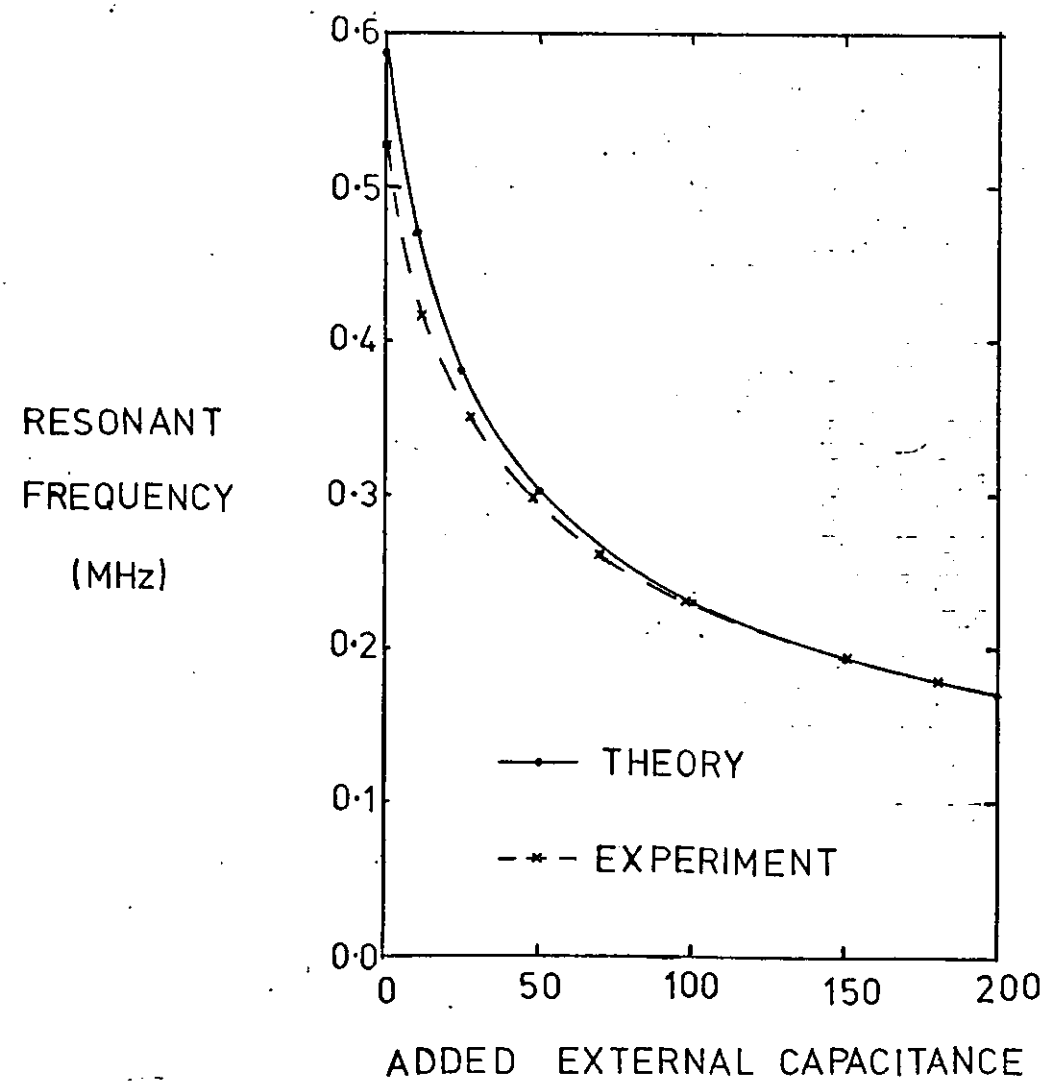

Initially only the load imposed by the F.E.T. probe, which consisted of 1 Mega-Ohm in parallel with 3.5 pF, was considered. Taking one particular resonance, that of the 1000 turn tapped foil wound inductor with $T = 400$ at 0.527 MHz; the simple model neglecting the probe load predicts a resonant frequency of 0.6505 MHz, taking the probe load into consideration reduces this predicted frequency to 0.5858 MHz, a reduction in the error from 19.0% to 10.0%. Another effect of considering the probe impedance was to reduce the predicted maximum value of V_r from 398 to 98.7: compared with an experimental value of 44.

Adding the probe capacitance of 3.5 pF to the equivalent circuit has reduced the error in the calculated resonant frequency by almost half. This suggests that the resonant frequency of this order of resonance is sensitive to the load capacitance. Therefore any stray capacitance can have a marked effect on the experimental resonant frequency. Adding a capacitive load to the output from the tapped foil wound inductor would reduce the significance of any stray capacitance.

Consider again the resonance in the output voltage response of the 1000 turn tapped foil wound inductor with $T = 400$ at 0.527 MHz. Ceramic capacitors, with measured capacitances between 12 pF and 200 pF, were added across the output in parallel with the probe and the resonant frequency measured. The variation of both the theoretical and experimental resonant frequencies with the added capacitance is shown in Fig. 4-32. The two curves converge as as the capacitance increases, until at a capacitance of 150 pF the difference between the theoretical and experimental resonant frequencies is only +0.2%. Clearly the add-

ition of a relatively large external capacitance has swamped any stray capacitance and any errors in the calculated sectional capacitances.

7) Conclusion

Although it was not possible to measure directly the voltage distribution within a foil wound inductor, it has been possible to infer the existance of various orders of voltage resonance within a tapped foil wound inductor by observing their effect on the output voltage response when the coil is connected as an auto-transformer.

Chapter 5 Voltage Resonances in Foil Wound Transformers

1) Introduction

The study of tapped foil wound inductors in chapter 4 has shown that voltage resonances can occur in foil wound devices. Therefore it is reasonable to suppose that voltage resonances can also occur in foil wound transformers.

A foil wound transformer can be wound in a number of ways. However due to the limitations of the coil winding machine available this study had to be limited to one form, in which the primary is wound on top of the secondary or vice-versa, with a gap filled with insulating film between them. The end view of a transformer wound in this manner is shown in Fig. 5-1. This study is also limited to air-cored transformers of small dimensions wound from thin foil. However the results from this study can be applied to some of the other winding forms.

Two foil wound transformers were made for this study, one with two windings each of 100 turns and the other with two windings each of 200 turns. The other dimensions of these transformers are given in Figs. 5-2 and 5-3. The transformers were heat treated in the manner described in section 2-2. The terminals on the transformers were made in the usual way by placing strips of 50 μm thick aluminium foil into the winding at the appropriate points.

2) Experimental Arrangement

The apparatus used to investigate the output voltage response of the transformers is shown in Fig. 5-4. The arrange-

Figure 5-1

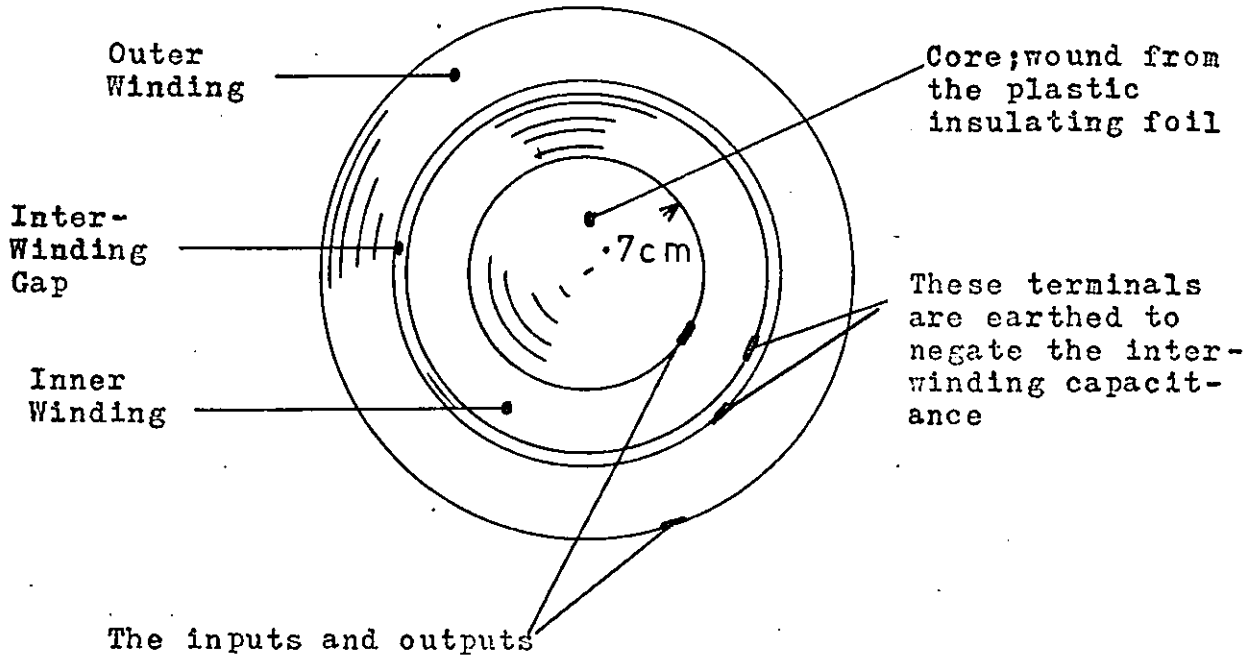

End on View of a Foil Wound Transformer

Figure 5-2

Physical Parameters and Dimensions of the 100+100 Turn Foil Wound Transformer	
Number of Turns on the Outer Winding	100 Turns
Number of Turns on the Inner Winding	100 "
Number of Turns of Insulating Foil in the Inter-Winding Gap	10 "
Core Radius	0.7 cm
Type of Metal Foil	Aluminium
Thickness of Metal Foil	5.0 μm
Width of Metal Foil	3.9cm
Type of Plastic Foil	Polypropylene
Thickness of Plastic Foil	12.5 μm

Figure 5-3

Physical Parameters and Dimensions of the 200 + 200 Turn Foil Wound Transformer	
Number of Turns on the Outer Winding	200
Number of Turns on the Inner Winding	200
Number of Turns of Insulating Foil in the Inter-Winding Gap	20
Core Radius	0.7 cm
Type of Metal Foil	Aluminium
Thickness of Metal Foil	5.0 μm
Width of Metal Foil	3.9 cm
Type of Plastic Film	Polypropylene
Thickness of Plastic Film	12.5 μm

Figure 5-4

Experimental Arrangement used to Measure the Output Voltage Response of the Foil Wound Transformers

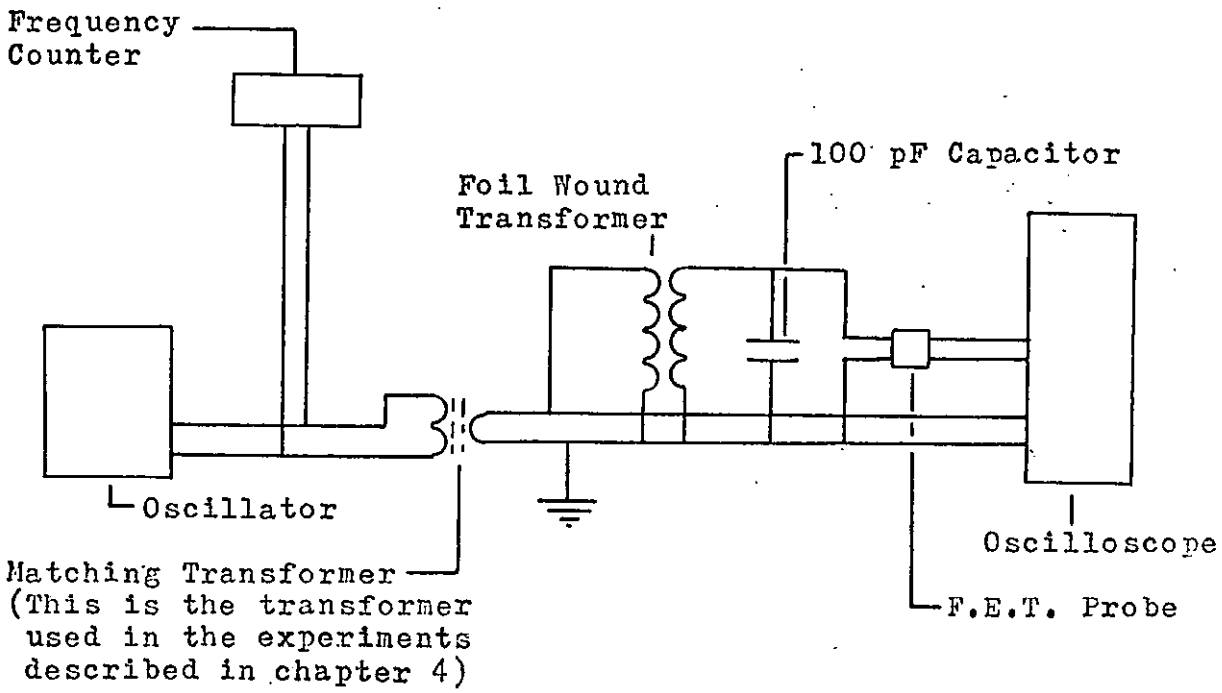

Figure 5-5

Connections to the Foil Wound Transformer

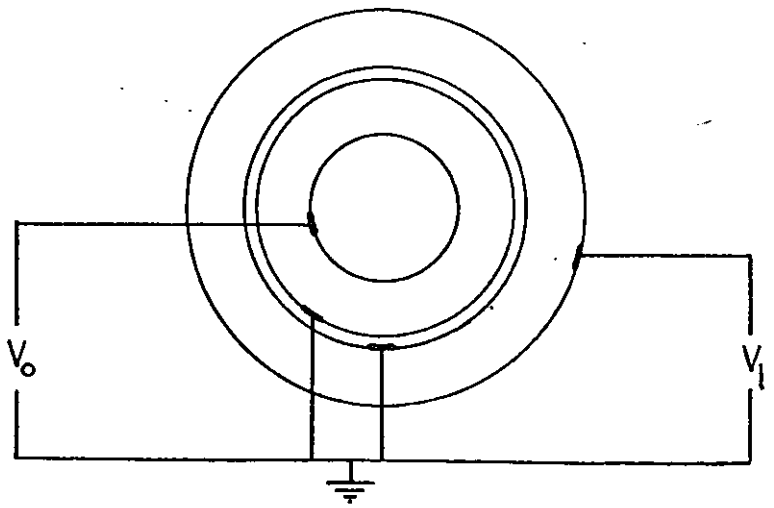

ment is very similar to that of chapter 4. The differences are in the connections to the transformer and the addition of a capacitor across the output of the transformer. To negate the inter-winding capacitance the transformer was connected in the manner shown in Fig. 5-5. The adjacent terminals on either side of the inter-winding gap are connected to earth. There are two methods of connecting the transformer; one with the inner winding as the primary and the other with the outer winding as the primary. In this study the convention was adopted of using the inner winding as the primary. A 100 pF ±0.5 pF ceramic capacitor was placed across the secondary of the transformer to swamp any stray capacitance.

The relative output voltage V_N , which is normalised with respect to the input voltage and the number of turns on the primary and secondary windings, is given by

$$V_N = \frac{V_l N_p}{V_o N_s} \qquad 5\text{-}2\text{-}1$$

Where V_o is the input voltage, V_l is the output voltage, N_p the number of turns on the primary winding and N_s the number of turns on the secondary winding.

The measured relative output voltage response of the 100+100 turn transformer is shown in Fig. 5-6 plotted on a log scale against frequency from 50 KHz to 6 MHz. V_N has a low-frequency value of 1, then rises to a value of 37 ±1.0 at 2.66 MHz ±0.005 MHZ and falls off at higher frequencies.

3) Analysis of the Equivalent Circuit

The lumped-element equivalent circuit of a foil wound

Figure 5-6

Experimental Output Voltage Response of the 100 + 100 Turn Foil Wound Transformer

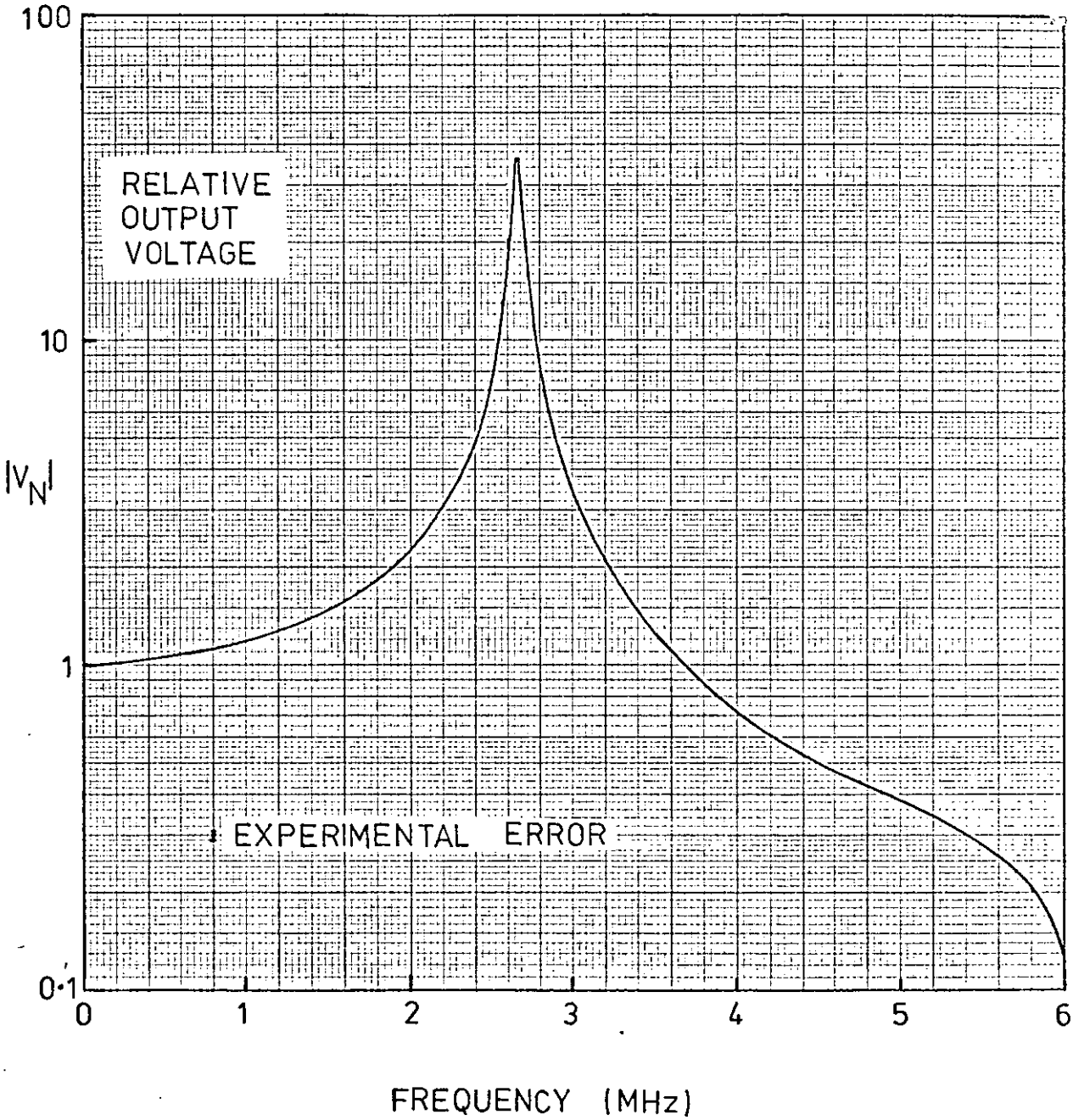

transformer is shown in Fig. 5-7. The primary has been split into S_p sections and the secondary into S_s sections. A total of S sections ($S = S_p + S_s$). It has been assumed that the inter-winding capacitance can be neglected, as the appropriate terminals at the ends of sections S_p and $S_p + 1$ have been earthed. The beginning of section 1 lies at the centre of the coil and the end of section 10 lies at the edge of the coil.

This equivalent circuit can be described by $S+1$ mesh equations, S_p of the form

$$(R_i + j\omega L_i + \frac{1}{j\omega C_i})q_i + \sum_{k\neq i}^{S} j\omega M_{i,k} q_k = \frac{1}{j\omega C_i} \qquad 5\text{-}3\text{-}1$$

$$1 \leqslant i \leqslant S_p$$

S_s of the form

$$(R_i + j\omega L_i + \frac{1}{j\omega C_i})q_i + \sum_{k\neq i}^{S} j\omega M_{i,k} q_k - \frac{q_{S+1}}{j\omega C_i} = 0 \qquad 5\text{-}3\text{-}2$$

$$S_p < i \leqslant S$$

Where $q_i = \frac{I_i}{I_o}$, $q_k = \frac{I_k}{I_o}$ and $q_{S+1} = \frac{I_l}{I_o}$. The mesh equation round the load loop is given by

$$Z_l q_{S+1} + \sum_{k=S_p+1}^{S} \frac{(q_{S+1} - q_k)}{j\omega C_k} = 0 \qquad 5\text{-}3\text{-}3$$

The input impedance Z_o can be obtained from

$$\frac{V_o}{I_o} = Z_o = \sum_{k=1}^{S_p} \frac{(1 - q_k)}{j\omega C_k} \qquad 5\text{-}3\text{-}4$$

Equations 5-3-1, 5-3-2 and 5-3-3 form an $S+1 \times S+1$ complex matrix equation of the same form as equation 2-4-10. In this equation Re[A] is an $S+1 \times S+1$ matrix of the form

Figure 5-7

Lumped-Element Equivalent Circuit for a Foil Wound Transformer

All inductors are coupled by positive mutual-inductances.

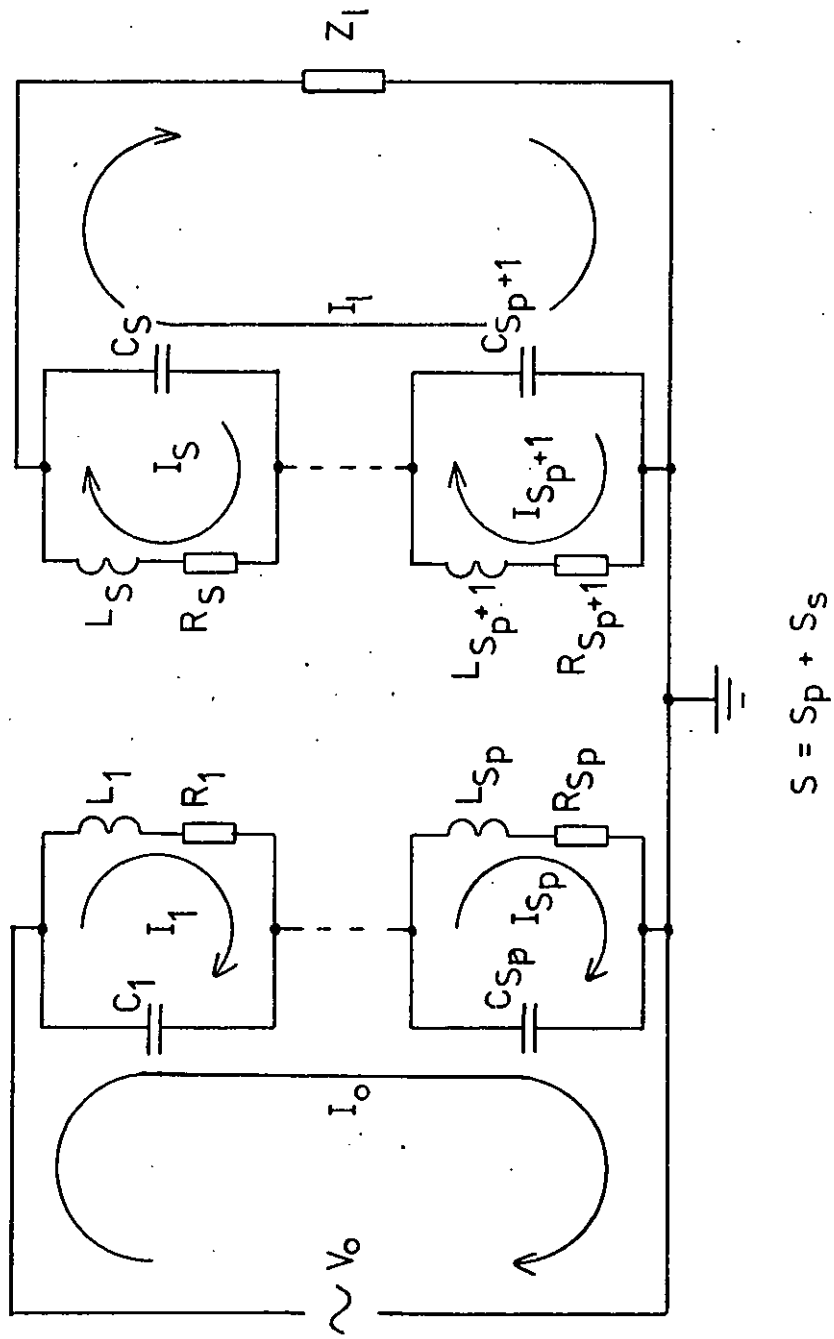

$$\begin{bmatrix} R_1 & \cdot & \cdot & \cdot & \cdot \\ \cdot & R_2 & \cdot & \cdot & \cdot \\ \cdot & \cdot & - & \cdot & \cdot \\ \cdot & \cdot & \cdot & R_S & \cdot \\ \cdot & \cdot & \cdot & \cdot & \mathrm{Re}(Z_l) \end{bmatrix} \qquad 5\text{-}3\text{-}5$$

Im[A] is an $S+1 \times S+1$ matrix of the form

$$\begin{bmatrix} \omega L_1 - \frac{1}{\omega C_1} & - & \cdot & \omega M_{1,S_{p+1}} & \cdot & - & \cdot \\ - & - & - & - & - & - & \cdot \\ \omega M_{S_{p+1},1} & - & \cdot & \omega L_{S_{p+1}} - \frac{1}{\omega C_{S_{p+1}}} & - & \frac{-1}{\omega C_{S_{p+1}}} & \\ - & - & - & - & - & - & \\ \cdot & \cdot & \cdot & \frac{-1}{\omega C_{S_{p+1}}} & - & \mathrm{Im}[Z_l] - \sum_{k=S_{p+1}}^{S} \frac{1}{\omega C_k} & \end{bmatrix} \qquad 5\text{-}3\text{-}6$$

The complex matrix [B] is composed of the left hand sides of equations 5-3-1, 5-3-2 and 5-3-3.

Once the matrix equation has been solved using the Gaussian Elimination program of Appendix 1, the matrix of the unknowns [Q] can be inserted into equation 5-3-4 to obtain the input impedance of the transformer.

In the same manner as equation 4-3-13 an expression for V_N can be derived; this expression has the form

$$V_N = \frac{V_l N_p}{V_o N_s} = \frac{Z_l q_{S+1} N_p}{Z_o N_s} \qquad 5\text{-}3\text{-}7$$

An alternative expression for V_N can be derived from equation 5-3-3. This has the form

$$V_N = \frac{N_p}{Z_o N_s} \sum_{k=S_p+1}^{S} \frac{(q_k - q_{S+1})}{j\omega C_k} \qquad 5\text{-}3\text{-}8$$

Once the input impedance Z_o has been obtained it can be inserted into either equation 5-3-7 or 5-3-8, together with the appropriate relative current or currents, to obtain the relative output voltage.

The load impedance is described by the circuit in Fig. 4-31 and Z_l has the same form as equation 4-6-1.

The sectional inductances, capacitances and resistances were derived in the same manner as the sectional inductances, capacitances and resistances described in sections 2-6, 2-7 and 2-8. Obviously the use of the D.C. resistance will lead to errors in the calculated Q values of the resonances.

4) Comparison of Theory and Experiment

The theoretical relative output voltage response of the 100+100 turn foil wound transformer was calculated, based on a model of 10 sections each of 20 turns, 5 sections to the primary winding and 5 sections to the secondary winding. This response together with the experimental relative output voltage response of the same transformer is shown in Fig. 5-8. The theoretical resonant frequency is 2.834 MHz ±1 KHz compared with an experimental resonant frequency of 2.66 MHz ±5 KHz, a difference of +6.5%. The predicted maximum value of V_N is 223 compared with an experimental value of 37 ±1.0, a factor of times 6 difference.

A comparison the theoretical and experimental output voltage responses for the 200+200 turn foil wound transformer is

Figure 5-8 Comparison of Theory and Experiment for the 100 + 100 Turn Foil Wound Transformer

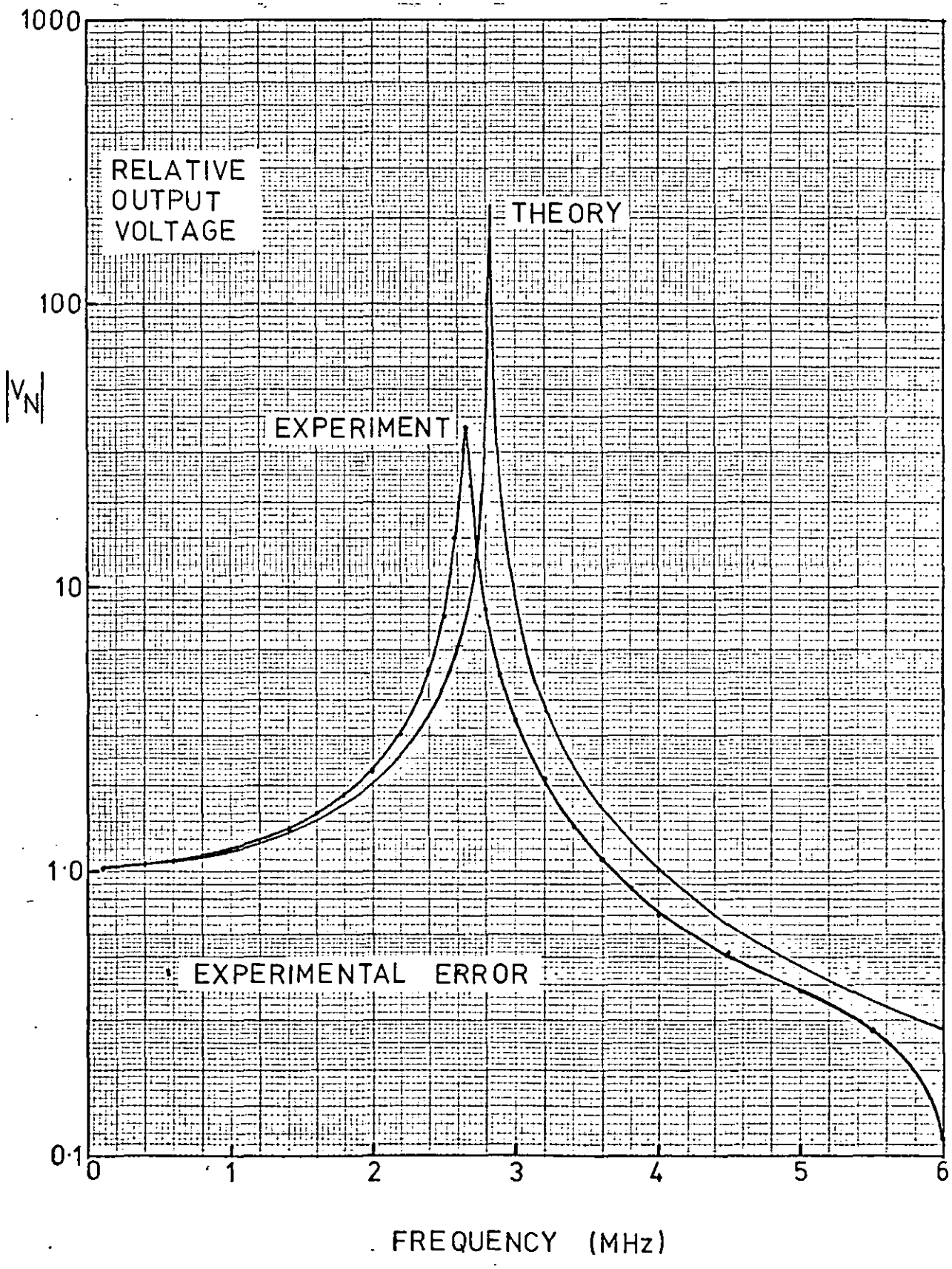

shown in Fig. 5-9 from 100 KHz to 2 MHz and in Fig. 5-10 from 100 KHz to 8 MHz, in both cases plotted on a log scale. In Fig. 5-9 the experimental resonance occurs at 997 KHz ± 1 KHz and the theoretical resonance occurs at 1.0594 MHz ± 200 Hz, a difference between theory and experiment of -5.9%. The observed maximum value of $|V_N|$ for this resonance is 59. ± 1, compared with the predicted value of 228.3 ± 0.5. Fig. 5-10 shows that at higher frequencies the 200 + 200 turn transformer multiply resonates. There is a second maximum in $|V_N|$ which occurs theoretically at 6.590 MHz ±5 KHz and experimentally at 6.523 MHz ± 5 KHz, a difference of - 1%. The minimum in $|V_N|$ which experimentally occurs at 4.80 MHz ± 10 KHz has a predicted frequency of 5.630 MHz ± 5 KHz a difference of-14.7%. In the case of the secondary maximum the difference between the predicted and observed values of $|V_N|$ is a factor of times 3.4. However in the case of the minimum in $|V_N|$ the difference between the predicted and observed values of $|V_N|$ is a factor of times 0.046.

5) Conclusion

It has been shown that for one particular type of air-cored foil-wound transformer the lumped-element equivalent circuit analysis can predict the form of the output voltage response with reasonable accuracy. Skin effect, proximity effect and width effect have all been neglected in the theoretical analysis therefore the predicted Q values will be in error.

Figure 5-9 Comparison of Theory and Experiment for the 200 + 200 Turn Foil Wound Transformer

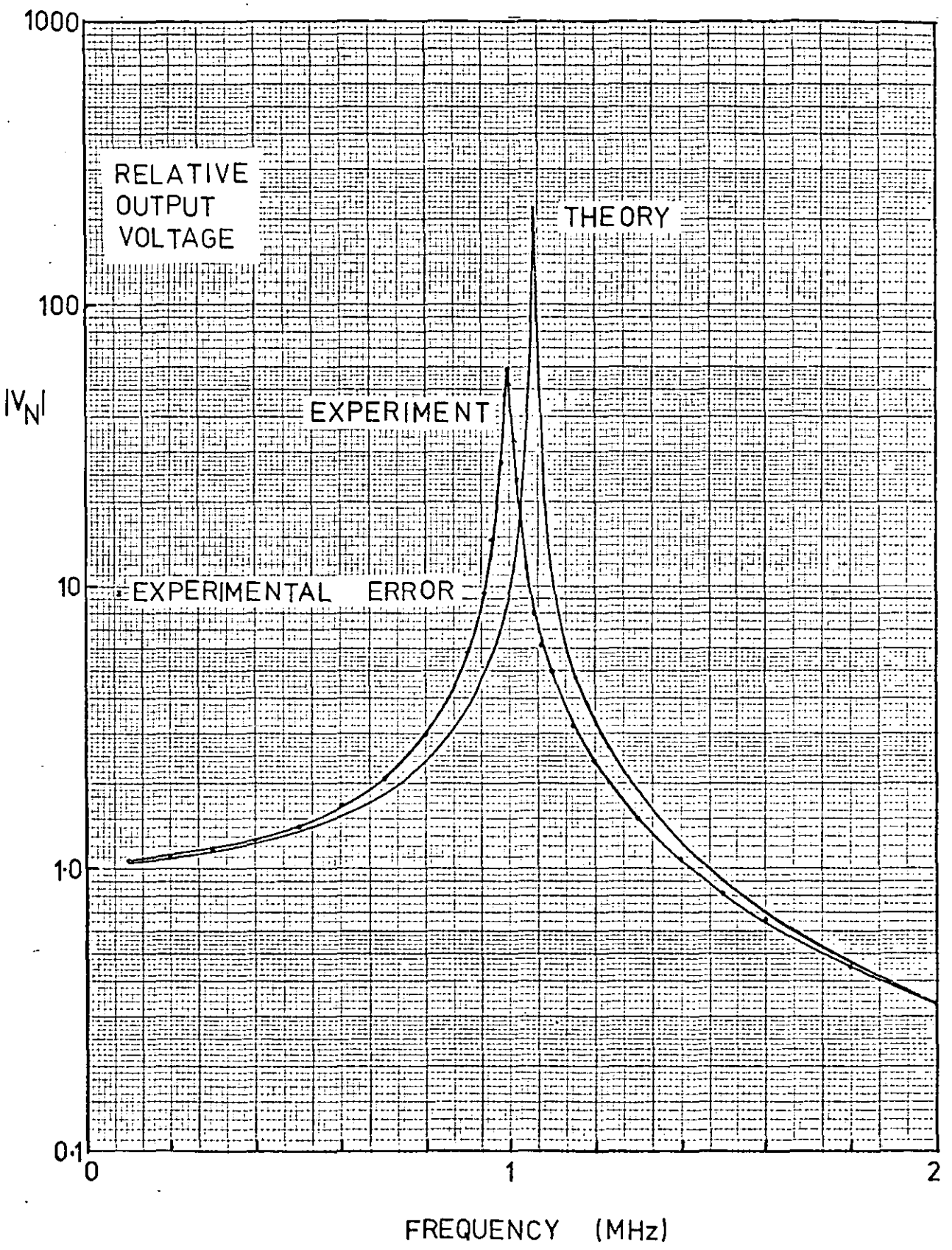

Figure 5-10

Comparison of Theory and Experiment for the 200+200 Turn Foil Wound Transformer Showing Secondary Resonances

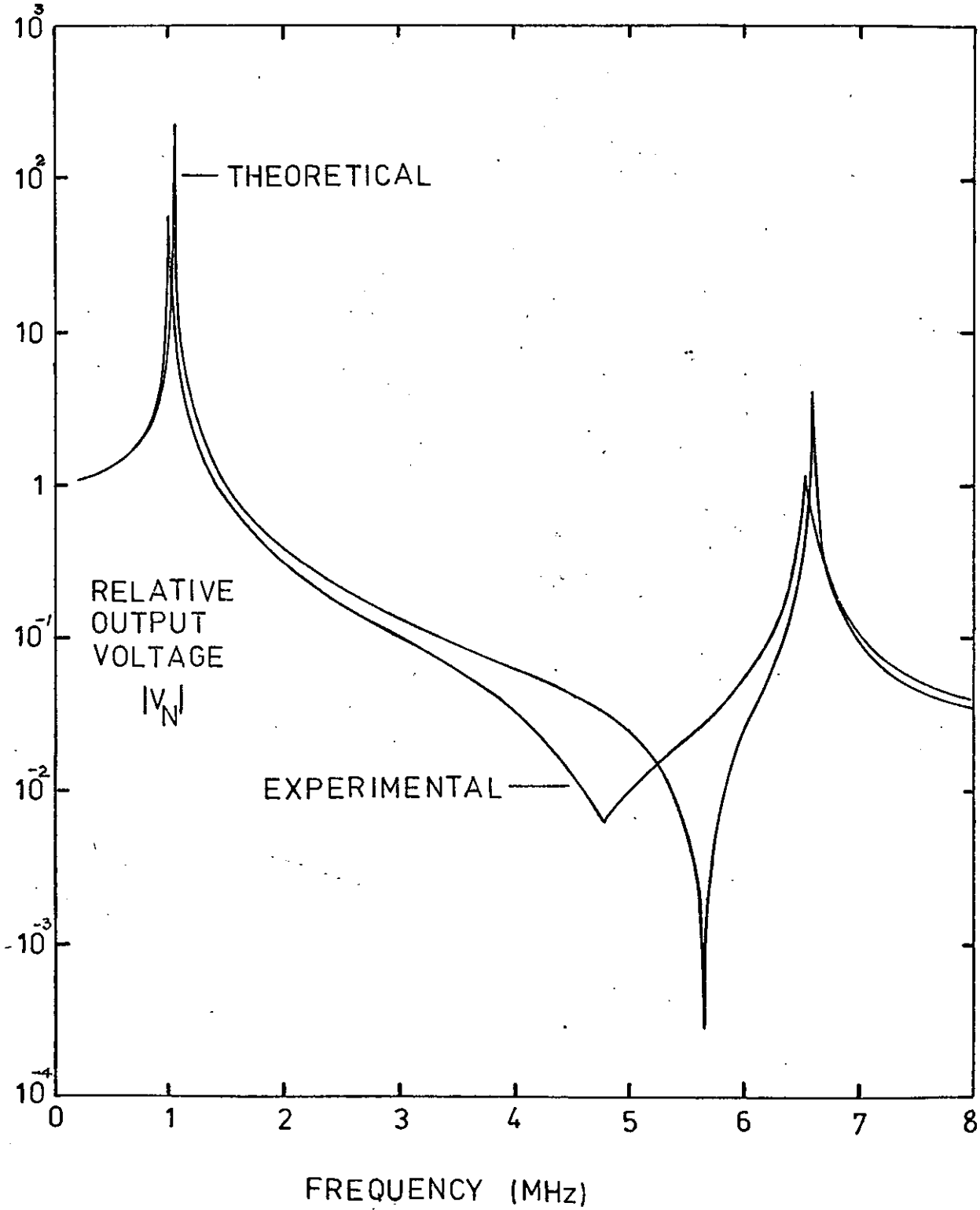

Chapter 6 Devices with Two Foils

1) Introduction

The simplest and commonest application for a device with two foils is that of the wound foil capacitor. This device takes a large number of forms, but in all except a very few of these forms the manufacturer is concerned with reducing the self-inductance of the capacitor he makes. This concern with the minimisation of the self-inductance has in the past led to a neglect of the other devices that can be manufactured from two or more foils.

From the preceding chapters it should be clear that a capacitor manufactured by the embedded lug method, in which two or more terminals are placed in the winding rather than solder all the turns of one foil together to form a terminal, should have self-inductance. The terminals in an embedded lug capacitor are normally placed to minimise the self-inductance, but equally the terminals could be placed to maximise the self-inductance. This chapter is concerned with devices that use this self-inductance.

A simple lumped element equivalent circuit for two identical spiral wound foils is shown in Fig. 6-1. These foils could have the four terminals placed at any points along the winding, but for simplicity they have been placed at the ends of the windings, Each foil has an inductance L , which has been split into two identical inductances of magnitude $\frac{L}{4}$ coupled by a mutual-inductance M . In a small tightly wound device the mutual inductance M can be approximated to $\frac{L}{4}$ without

Figure 6-1

Simple Equivalent Circuit of a Device Made From Two Identical Foils

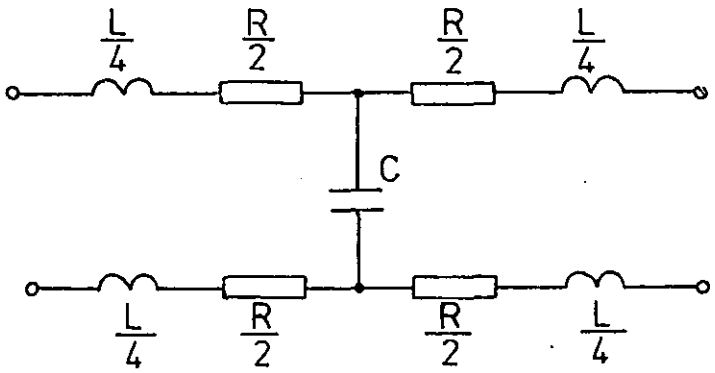

All inductors are coupled by a mutual inductance.

Figure 6-2

Two Terminal Connection: Capacitive

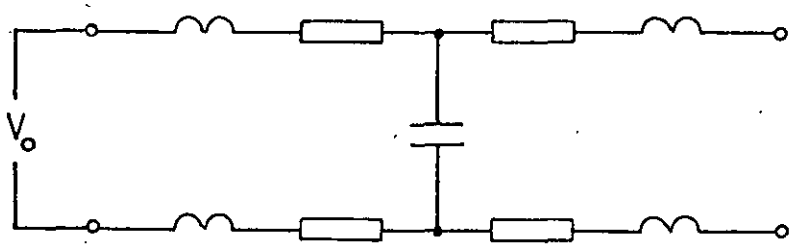

Figure 6-3

Two Terminal Connection: Resonant

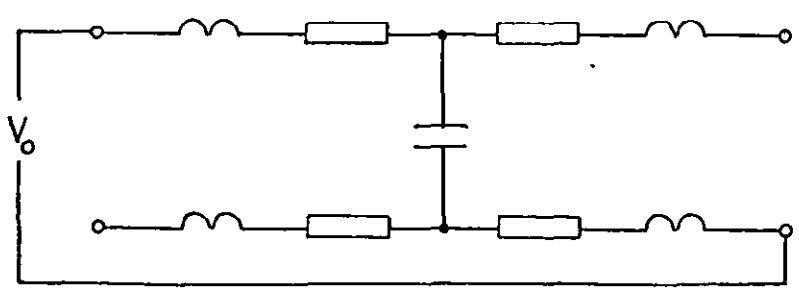

departing from reality too far. The D.C. resistance of the foil R has been split into two separate resistances $\frac{R}{2}$. The total capacitance between the two foils is represented by C. Obviously this equivalent circuit will only be valid at low frequencies.

2.) Two Terminal Devices

There are three different ways of connecting Fig. 6-1 as a two terminal device. The first method is shown in Fig. 6-2. This arrangement has an input impedance of the form

$$Z_o = j\frac{\omega L}{4} - j\omega M + \frac{R}{2} + \frac{R}{2} + j\frac{\omega L}{4} - j\omega M + \frac{1}{j\omega C}$$

$$= j\frac{\omega L}{2} - 2j\omega M + R + \frac{1}{j\omega C} \qquad 6\text{-}2\text{-}1$$

With the approximation $M = \frac{L}{4}$ this becomes

$$Z_o = R + \frac{1}{j\omega C} \qquad 6\text{-}2\text{-}2$$

When the resistance is neglected the input impedance Z_o is purely capacitive. When the inductances $\frac{L}{4}$ are tightly coupled this terminal arrangement gives a low-inductance capacitance. At high frequency Morley (37) has shown that this terminal arrangement behaves as a transmission line.

The second method is shown in Fig. 6-3 and has an input-impedance of the form

$$Z_o = j\frac{\omega L}{2} + 2j\omega M + R + \frac{1}{j\omega C} \qquad 6\text{-}2\text{-}3$$

With the approximation $M=\frac{L}{4}$ this becomes

$$Z_o = j\omega L + R + \frac{1}{j\omega C} \qquad 6\text{-}2\text{-}4$$

At a critical frequency $\omega_o = \frac{1}{\sqrt{LC}}$ the input impedance Z_o falls to $Z_o = R$. At frequencies $\ll \omega_o$ the impedance is inductive and at frequencies $\gg \omega_o$ the impedance is capacitive. In reality the author discovered that at frequencies $\gg \omega_o$ this terminal arrangement of a two foil device will multiply resonate in the same manner as the foil wound inductors investigated in chapter 2. Wilson (38) used this arrangement of the two foil device, which he termed the "Inductive Capacitor", as a resonator in a delay line to form high-current pulses and as the primary of a transformer to generate high voltage pulses.

The third method is shown in Fig. 6-4 and has an input-impedance of the form

$$Z_o = j\frac{\omega L}{2} + 2j\omega M + R \qquad 6\text{-}2\text{-}5$$

This impedance is inductive and at high frequencies behaves in the same manner as the foil wound inductors investigated in chapter 2.

3) Four Terminal Devices

There are three ways of connecting the two foils as a four terminal device. The first method is shown in Fig. 6-5 and the output voltage for this arrangement is given by

$$V_1 = \frac{V_o}{1 + j\omega CR} \qquad 6\text{-}3\text{-}1$$

assuming that $M = \frac{L}{4}$

Figure 6-4

Two Terminal Connection: Inductive

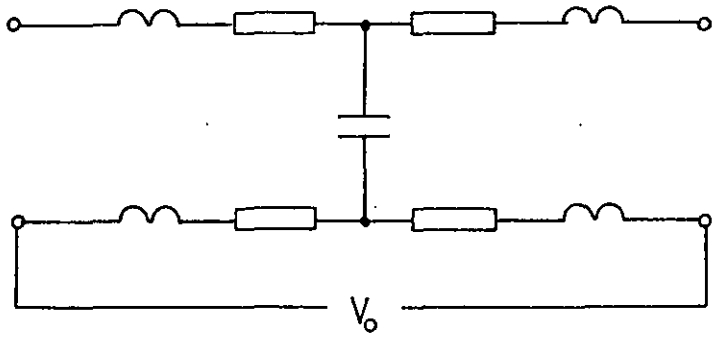

Figure 6-5

Four Terminal Connection: Capacitive

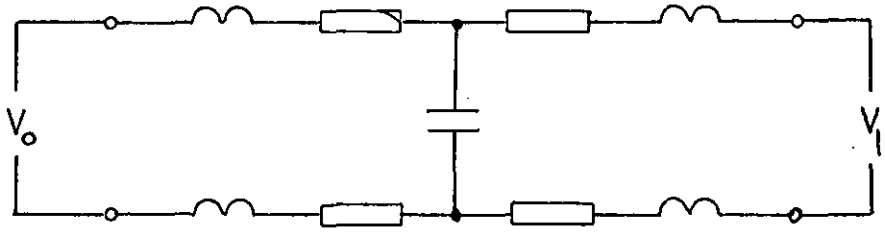

Figure 6-6

Four Terminal Connection: Transformer

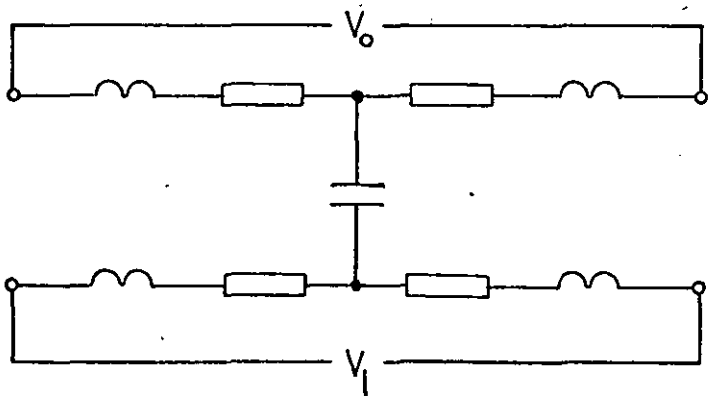

At frequencies $\ll \frac{1}{CR}$ the output voltage equals the input voltage and at frequencies $\gg \frac{1}{CR}$ the output voltage is given by

$$V_1 \simeq \frac{V_o}{j\omega CR} \qquad 6\text{-}3\text{-}2$$

This terminal arrangement acts as a filter.

The second method is shown in Fig. 6-6. In this case the output voltage is given by

$$V_1 = \frac{4j\omega M V_o}{j\omega \frac{L}{2} + 2j\omega M + R} \qquad 6\text{-}3\text{-}3$$

This terminal arrangement acts as a transformer.

The third method is shown in Fig. 6-7. With no load impedance connected the output voltage is given by

$$V_1 = \frac{V_o\left(\frac{1}{j\omega C} - 4j\omega M\right)}{\left(j\omega \frac{L}{2} + 2j\omega M + R + \frac{1}{j\omega C}\right)} \qquad 6\text{-}3\text{-}4$$

With the approximation $M = \frac{L}{4}$ this equation becomes

$$V_1 = \frac{V_o\left(\frac{1}{j\omega C} - j\omega L\right)}{j\omega L + R + \frac{1}{j\omega C}} \qquad 6\text{-}3\text{-}5$$

At a critical frequency $\omega_o = \frac{1}{\sqrt{LC}}$ the output voltage is given by

$$V_1 = \frac{2V_o}{jR}\sqrt{\frac{L}{C}} \qquad 6\text{-}3\text{-}6$$

At frequencies $\ll \omega_o$ the output voltage is given by

$$V_1 = V_o \qquad 6\text{-}3\text{-}7$$

At frequencies $\gg \omega_o$ the output voltage is given by

$$V_1 = -V_o \qquad 6\text{-}3\text{-}8$$

Figure 6-7

Four Terminal Connection: Resonant

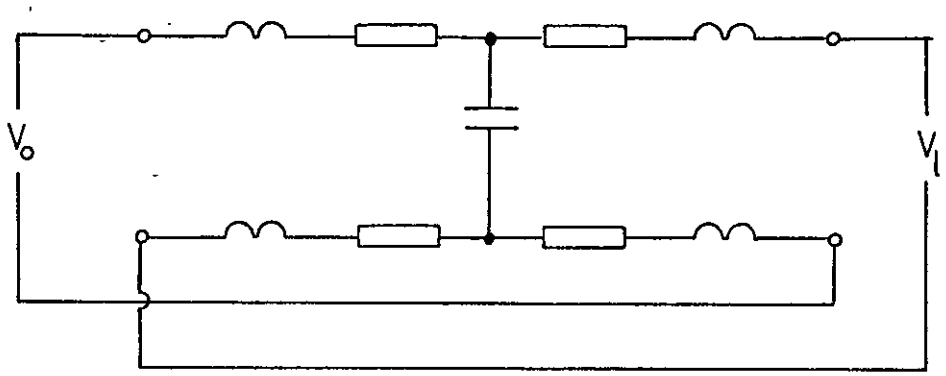

Figure 6-8

Resonant Four Terminal Connection with Load Impedance Z_1

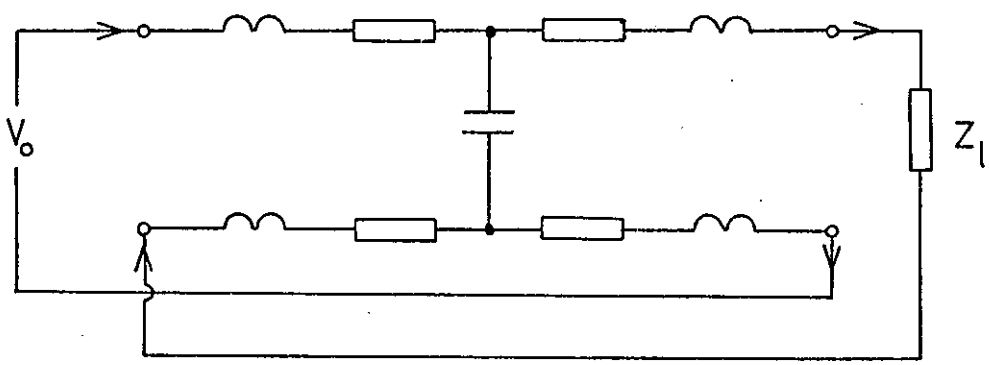

Figure 6-9

Fig. 6-8 Rearranged for Mesh Analysis

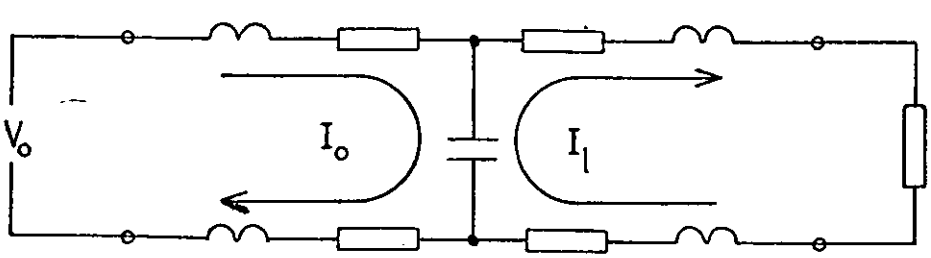

This terminal arrangement has been termed by Reeves the " Inductor-Capacitor Hybrid" (39,40). This device resonates at a frequency of $\omega_o = \frac{1}{\sqrt{LC}}$ and at this frequency: $V_1 = \frac{2QV_o}{j}$, when there is no load connected. Q is given by the normal expression, which is

$$Q = \frac{1}{R}\sqrt{\frac{L}{C}} \qquad 6\text{-}3\text{-}9$$

4) Inductor-Capacitor Hybrid

Reeves' theory of the Inductor-Capacitor Hybrid (40) turns on the assumption that the resistance of the metal foils is negligibly small. The theory predicts that if operated at its resonant frequency the hybrid supplies the same current into any load resistance (39). It will be shown in this section that this difficulty can be avoided if the hybrid is modelled by discrete elements, including finite resistance for the metal foils. For a full analysis a load impedance must be included in the description.

The lumped circuit model including the load impedance is shown in Fig. 6-8. In Fig. 6-9 the circuit has been re-arranged to facilitate a mesh analysis, as follows.

$$V_o = j\omega\frac{L}{2}I_o + 2j\omega MI_o + 4j\omega MI_1 + RI_o + \frac{(I_o - I_1)}{j\omega C} \qquad 6\text{-}4\text{-}1$$

$$0 = Z_1I_1 + j\omega\frac{L}{2}I_1 + 2j\omega MI_1 + 4j\omega MI_o + RI_1 + \frac{(I_1 - I_o)}{j\omega C} \qquad 6\text{-}4\text{-}2$$

With the approximation $M = \frac{L}{4}$ these equations reduce to

$$V_o = AI_o - BI_1 \qquad 6\text{-}4\text{-}3$$

$$I_o B = (Z_1 + A)I_1 \qquad 6\text{-}4\text{-}4$$

Where

$$A = j\omega L + R + \frac{1}{j\omega C} \qquad 6\text{-}4\text{-}5$$

$$B = \frac{1}{j\omega C} - j\omega L \qquad 6\text{-}4\text{-}6$$

At resonance we have $B = -j2\omega_o L$ and $A = R$.

The principal equations given by Reeves to describe the currents and voltages in the hybrid appear as special cases of 6-4-3 and 6-4-4 when R is set to zero.

The output current of the device is given by

$$I_1 = \frac{BV_o}{Z_1 A + A^2 - B^2} \qquad 6\text{-}4\text{-}7$$

At the resonant frequency and letting R go to zero we obtain Reeves' result,

$$I_1 = \frac{V_o}{j\,2\omega_o L} \qquad 6\text{-}4\text{-}8$$

In this expression the current is independent of the load. However if we keep R finite and let Z_1 become large we obtain

$$I_1 = -\frac{j2\omega_o L V_o}{Z_1 R} \qquad 6\text{-}4\text{-}9$$

which decreases with increasing load.

The input current is given by

$$I_o = \frac{(Z_1 + A)V_o}{Z_1 A + A^2 - B^2} \qquad 6\text{-}4\text{-}10$$

Again at the resonant frequency and letting R go to zero, we find

$$I_o = \frac{Z_1 V_o}{(2\omega_o L)^2} \qquad 6\text{-}4\text{-}11$$

For a resistive load this agrees with Reeves' result and shows that if the same current is to be delivered into increasingly large loads, the input current must rise in proportion to the load. If we keep R finite and let Z_1 become large we find

$$I_o = \frac{V_o}{R} \qquad 6\text{-}4\text{-}12$$

indicating that the input current is limited by the foil resistance.

The low-frequency behaviour of the hybrid is completely described by equations 6-4-3, 6-4-4, 6-4-5 and 6-4-6 subject to the approximations stated. Hybrids can multiply resonate at high frequency (40). A more complex equivalent circuit would be required to describe this behaviour.

The application of hybrids to the ignition of gas-discharge lamps was proposed by Reeves (39). By designing a hybrid capable of resonating at 50 Hz it is possible to provide ignition, current limiting and phase correction within the one device rather than using two or three separate components. The large

iron-cored device shown in the photograph in Fig. 6-10 is designed to operate in this manner and was used in Hybrid research at Loughborough University.

A summary of the equivalent circuit analysis of the Inductor-Capacitor Hybrid appears in a paper by Murgatroyd and Walker which is reproduced as Appendix 5.

Figure 6-10

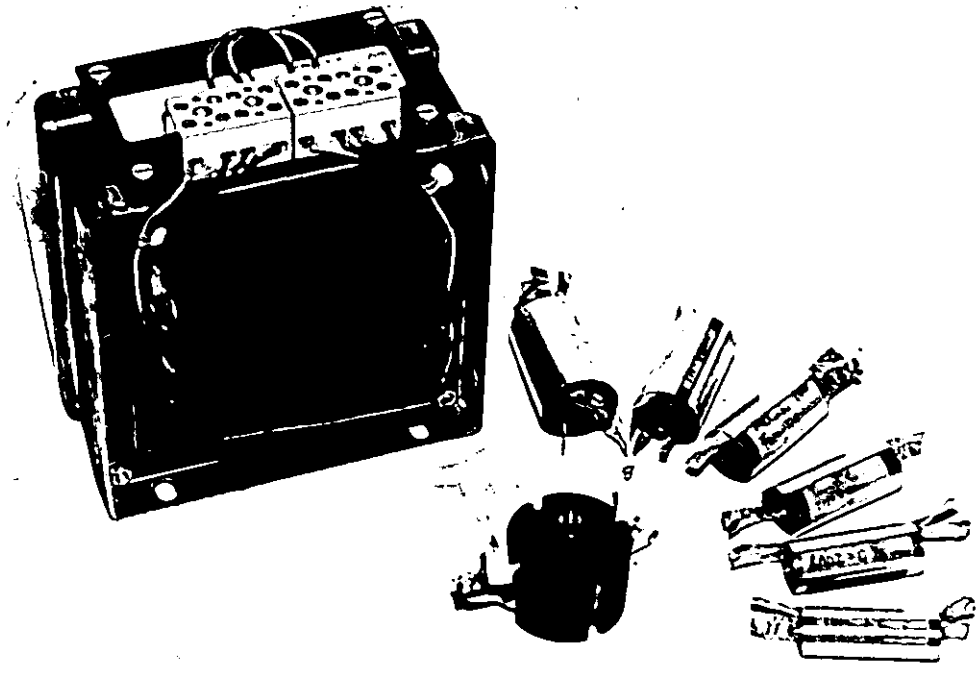

Eight Two Foil Devices
The large iron cored device and the smaller ferrite cored device were used in Inductor-Capacitor Hybrid research at Loughborough University.
The line on the photograph is 10 cm long.

Chapter 7 Conclusion

1) General

This thesis has been concerned with the application of lumped-element equivalent circuits to foil wound devices, in particular the foil wound inductor. Fig. 2-1 gives the normal high frequency equivalent circuit of an inductor, which is composed of an inductor and a resistor in series both shunted by a capacitor. In most cases although the inductance and the resistance can be calculated from the fundamental field equations the addition of the capacitance is simply a model: it explains the observed behaviour of the inductor although it cannot be calculated. The reason for this is simply that the capacitance scheme within most inductors is too complex for analysis and in any case it is far easier just to measure the equivalent capacitance. With foil wound inductors the capacitance scheme within the device is not complex; nearly all the capacitance is from turn-to-turn and very little to any of the other turns. This fact permits an analysis based not on a model which mimics the impedance of the device, but on the fundamental field equations. Such an analysis can provide an insight into the current and voltage distributions within the device.

The use of lumped-element equivalent circuits may be thought a substitute for a complete field theory solution of the problem, but the problems of finding an analytic solution to the field equations in all but the simplest cases means that approximations would have to be made. The approximation method

could take two forms: either the field equations could be simplified by approximation until an analytic solution was reached or a numerical approximation method could be used. The equivalent circuit approach can be regarded as a combination of both methods. Murgatroyd (26) has shown that the field equations can with certain approximations be reduced to the equivalent circuit of Fig. 2-11. This equivalent circuit can be reduced until it will yield manageable analytic solutions. However such simplified circuits consisting of one two or three sections would only be able to predict the impedance of the coil up to the second or third resonance, clearly larger circuits are required to calculate the impedance/frequency spectrum of Fig. 2-9. These circuits are too large to handle on an analytic basis, therefore a numerical computational method has to be employed.

Inherent in this equivalent circuit approach is the concept that the capacitance of a foil wound inductor is as important a part of the characteristic of the device as the inductance. In most applications a pure inductance or a pure capacitance is required. However it is not possible to separate these characteristics in real components. Indeed it is possible to construct devices that use this duality; such as the inductor capacitor hybrid (40) and the inductive capacitor (38).

2) Particular

The lumped-element equivalent circuit when applied to a 1000 turn foil wound inductor (Fig. 2-2) could quite accurately predict the frequencies of the first three resonances (Fig. 2-23), although the predicted frequencies of the higher order resonances were much less accurate. The number of sections used in these

calculations was 10, therefore the theory is accurate up to the frequency of the resonance whose order is given approximately by the number of sections divided by three. It can be seen from the comparison in Fig. 2-22 that Q values of the resonances cannot be predicted with accuracy, this is due to the use of the D.C. resistance of the metal foil in deriving the sectional resistances in section 2-7. It is not yet possible to calculate the A.C. resistance of a foil wound inductor over the frequency range investigated in chapter 2.

In chapter 3 the lumped element equivalent circuit was applied to another field theory problem; that of the current distribution across the width of a foil conductor loop. Again the method proved successful, although the success is limited in terms of application to physical devices and frequency range. The range of application is limited by the approximations needed to derive a usable theory and by the assumption that the current distribution varies across the width of the foil and not the thickness. These are the fundamental limitations to the application of the theory, but there is also the limitation imposed by the finite width of the strips.

Chapters 4 and 5 are devoted to one of the predictions of the theoretical analysis of chapter 2. The theory predicts that at certain frequencies current and voltage standing waves can exist within a foil wound inductor. The existence of the current standing waves can be proved directly by examining the external AC magnetic field of a large foil wound inductor (32,33). However the voltage standing waves could not be observed directly,

their presence had to be inferred from the output voltage responses of tapped foil wound inductors and foil wound transformers.

The very simple lumped element equivalent circuit analysed in chapter 6 is that of a two foil device. Depending on the terminal connections to the device it can exhibit capacitance, inductance or resonance. This analysis shows that even simple circuits can yield useful analytic results under certain circumstances.

References

1) Anon. World production of non-ferrous metals. Metallurgia 75 (448), Feb. 1967, 76

2) McNally, D.P. Aluminium's role in the electrical industry. Elect. Engineer, 46 (5), May 1969, 30

3) Miller, J.P. Metal resources. Part 1: Aluminium J. Metals, May 1973, 13

4) Pelikan, T. Modern distribution transformers with aluminium foil windings. Brown Boveri Review, 54 (7), July 1967, 376

5) Vidmar, M. Der aluminium-transformator. Electrotech und Masch, 35, 1917, 321

6) Daguet, R. Use of aluminium in AC machines. Rev. Aluminium, 30 (200), 1953, 236

7) Maione, G. Design of transformers with aluminium windings. Elettrotecnica, 27, Jan. 1940, 35

8) Di Stefano, R. Static transformers with aluminium windings. Elettrotecnica, 26, Dec. 1939, 718

9) Anon. Anodised aluminium strip for electrical windings. Machinery Lloyd, 31 (6), 1959

10) Bennett, D.A. Aluminium winding foil for electrical coils. Electrical Times, 162 (4220), Mar. 1973, 15

11) Chapman, D.F. Enamelled aluminium wire for small coil windings, Electrical Rev. (GB), 196 (6), Feb. 1975, 183

12) Owen, O. Solving transformer problems with aluminium foil. Electrical Equipment, Mar. 1971

13) Bode, H. Spingler, H. Scrap-core reactor with an aluminium foil winding. Siemens Review, 37 (7), July 1970, 408

14) Lee, J.J. Aluminium foil and strip for electrical windings Electrical Rev., 10th April 1959

15) Novak, W.J. Pahel, W.M. Why strip conductor and why aluminium. Proc. Amer. Power Conf., 25, 1963, 932

16) Massey, S.N. The ten year revolution-The important conversion to aluminium in power transformer sizes. Proc. Amer. Conf., 30, 1968, 1191

17) Anon. Aluminium in electrical engineering. Electrical Eng. (Australia), 45 (5), 1968, 5

18) Shobe, D.W. Aluminium replacing copper in electrical transformers. Modern Metals, 26 (4), 1970, 37

19) Green, H.E. Aluminium in the electrical industry. Electronics and Power, 1st Nov. 1973

20) Treanor, E.D. Broverman, M. On distribution transformer design. Electric Light and Power, Feb. 1955

21) Saravya, S.T.D. Care to be taken while using aluminium in place of copper in electrical engineering field. Electrical India, 14 (13), July 1974, 21

22) Lemke, T. Terminating aluminium conductors. Machine Design, 31st Aug. 1967

23) Husain, I.M.A. Work performed at the Plessey Company, Bathgate, Lothian, Scotland

24) Welsby, V.G. The theory and design of inductance coils. Macdonald (London), 1960, 31, 144

25) Murgatroyd, P.N. Walker, N.J. Frequency-dependent inductance and resistance of foil conductor loops. Proc. IEE, 124 (5), May 1977, 493

26) Murgatroyd, P.N. Field and circuit models for the wound

foil inductor. Electrocomponent Science and Technology, 3, 1976, 97

27) Froberg, C. Introduction to numerical analysis. Addison-Wesley (New York), 1965, 73

28) Nottingham Algorithms Group, Document Number 367, 1972

29) Bleaney, B.I. Bleaney, B. Electricity and Magnetism. Oxford University Press (London), 1965, 149

30) Petit-Bois, G. Tables of indefinite integrals. Dover (London), 51, 69

31) Kemp, R.J. Murgatroyd, P.N. Walker, N.J. Self resonance in foil inductors. Electronics Letters, 2 (15), July 1975

32) Kemp, R.J. Final Year Project. Loughborough University, 1973

33) Walker, N.J. Multiple resonance in foil wound inductors. MSc. Thesis, Loughborough University, 1975

34) Reeves, R. Work performed at the Plessey Company, Bathgate, Lothian, Scotland

35) Grover, F.W. Inductance calculations. Van Nostrand, 1947

36) Mullineux, N. Reed J.R. Whyte, I.J. Current distribution in sheet and foil-wound transformers. Proc. IEE, 116 (1), Jan. 1969, 127

37) Morley, A. Aluminium foil in dry capacitors. BAFRA Conf. on Aluminium foil in the Electrical and Electronic Industry, University of Aston, Sept. 1974

38) Wilson, G.E. The theory and applications of the inductive capacitor. MSc. Thesis, University of Leeds, 1964

39) Reeves, R. Choke-capacitor hybrid as a fluorescent lamp ballast. Proc. IEE, 122 (10), 1975, 1151

40) Reeves, R. Inductor-capacitor hybrid. Proc. IEE, 122 (11), 1975, 1323

41) McCraken, P.D. Dorn, W.S. Numerical methods and fortran programming with applications in engineering and science. Wiley (New York), 1964

Appendix 1 Gaussian Elimination

The Gaussian elimination method of solving simultaneous equations was chosen in preference to the other methods available because it could be applied to the matrix equations studied over the full frequency range of interest. The Gaussian elimination method is in essence simple and is dealt with specifically in many books, eg (41). If we have a set of equations 1, 2 and 3, Then we multiply equation 1 by m_2 and subtract it from equation 2.

$$a_{1,1}q_1 + a_{1,2}q_2 + a_{1,3}q_3 = b_1 \qquad 1$$

$$a_{2,1}q_1 + a_{2,2}q_2 + a_{2,3}q_3 = b_2 \qquad 2$$

$$a_{3,1}q_1 + a_{3,2}q_2 + a_{3,3}q_3 = b_3 \qquad 3$$

m_2 is equal to $a_{2,1}/a_{1,1}$, therefore equation 2 becomes

$$(a_{2,1} - a_{2,1})q_1 + (a_{2,2} - a_{1,2}m_2)q_2 + (a_{2,3} - a_{1,3}m_2)q_3 = b_2 - b_1m_2 \qquad 4$$

Setting m_3 equal to $a_{3,1}/a_{1,1}$ and repeating the above procedure with equation 3 gives

$$(a_{3,1} - a_{3,1})q_1 + (a_{3,2} - a_{1,2}m_3)q_2 + (a_{3,3} - a_{1,3}m_3)q_3 = b_3 - b_1m_3 \qquad 5$$

Put

$$a'_{2,2} = a_{2,2} - a_{1,2}m_2 \quad , \quad a'_{2,3} = a_{2,3} - a_{1,3}m_2$$

$$b'_2 = b_2 - b_1m_2 \qquad 6$$

$$a'_{3,2} = a_{3,2} - a_{1,2}\, m_3 \quad , \quad a'_{3,3} = a_{3,3} - a_{1,3}\, m_3$$

$$b'_3 = b_3 - b_1 m_3 \qquad (7)$$

The above proce dure results in a modified set of equations

$$a_{1,1}q_1 + a_{1,2}q_2 + a_{1,3}q_3 = b_1 \qquad (8)$$

$$a'_{2,2}q_2 + a'_{2,3}q_3 = b'_2 \qquad (9)$$

$$a'_{3,2}q_2 + a'_{3,3}q_3 = b'_3 \qquad (10)$$

Multiplying equation 9 by $m'_3 = a_{3,2}/a_{2,2}$ and subtracting it from eqation 10 gives

$$a''_{3,3}\, q_3 = b''_3 \qquad (11)$$

Where

$$a''_{3,3} = a'_{3,3} - a'_{2,3}\, m'_3 \quad , \quad b''_3 = b'_3 - b'_2 m'_3 \qquad (12)$$

Back substituting q_3 into equation 9, and q_3 and q_2 into equation 8 gives

$$q_3 = \frac{b''_3}{a''_{33}} \qquad (13)$$

$$q_2 = (b'_2 - a'_{2,3}q_3)/a_{2,2} \qquad (14)$$

$$q_1 = (b_1 + a_{1,2}q_2 + a_{1,3}q_3)/a_{11} \qquad 15$$

The solution is given by equations 13, 14 and 15 .However,if the matrix elements $a_{1,1}$ or $a_{2,2}$ are small,then the corresponding multipliers m_2, m_3 and m'_3 will be large.Clearly this would give rise to large errors or totally meaningless answers. Therefore the technique of Partial Pivoting is used.This involves hunting the column to be eliminated for the largest element,and using the row containing this element as the eliminating row.

The flow diagrems for eliminating a real matrix equation of size H and form

$$\left[\ a\ \right]\left[x\right] = \left[b\right] \qquad 16$$

are shown in Figs. 1, 2 and 3.

Figure 1 Elimination

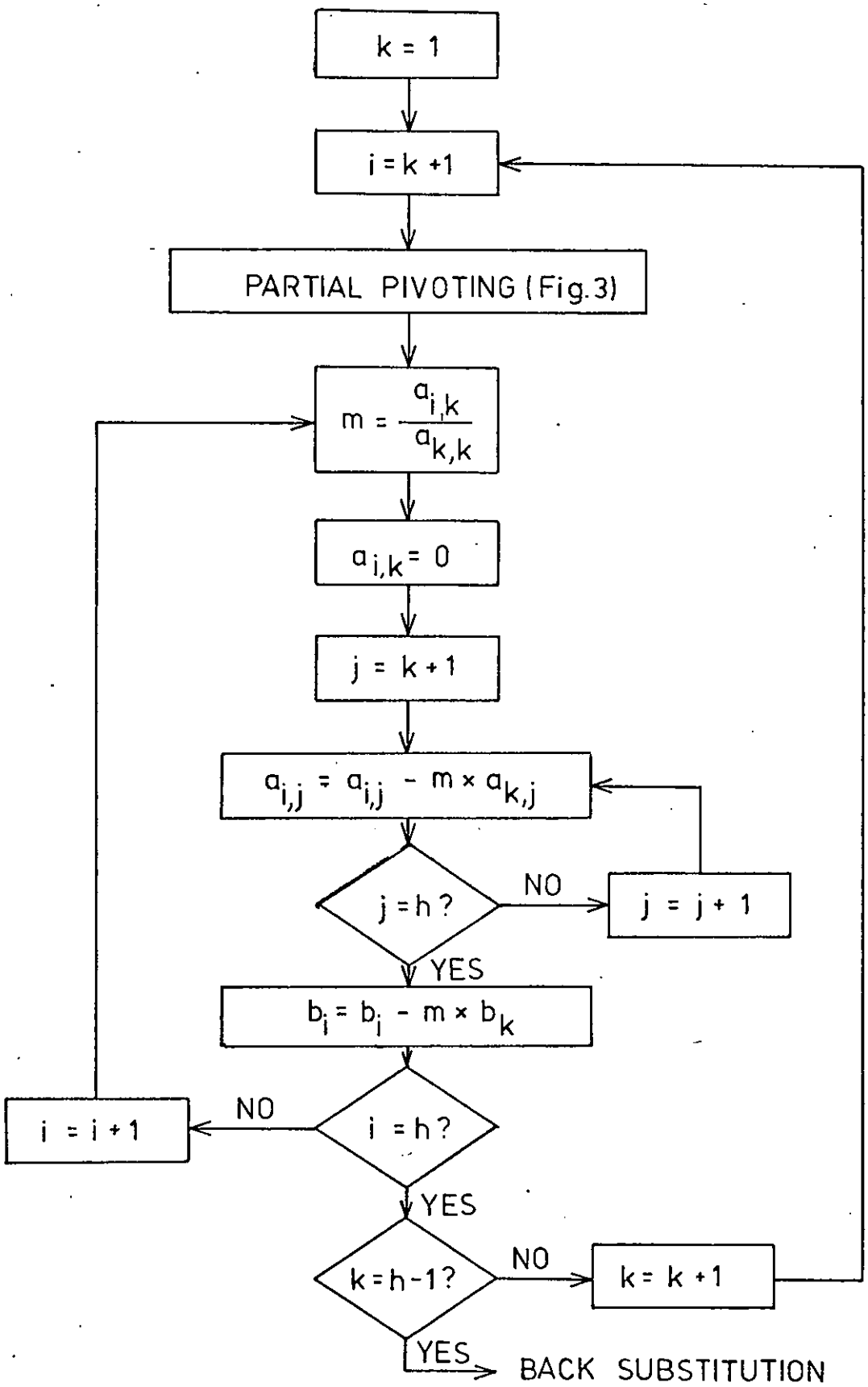

Figure 2 Back Substitution

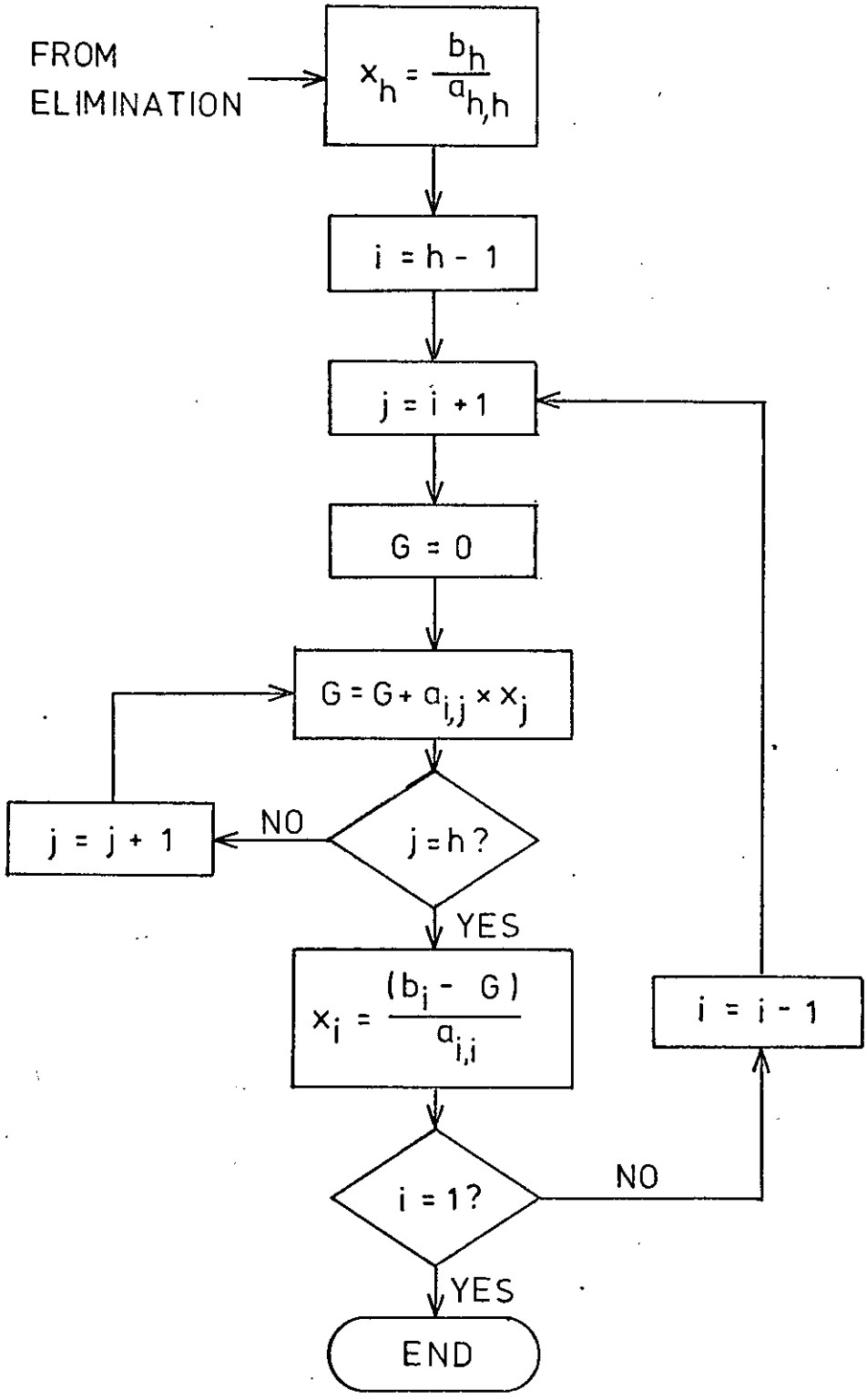

Figure 3 Partial Pivoting

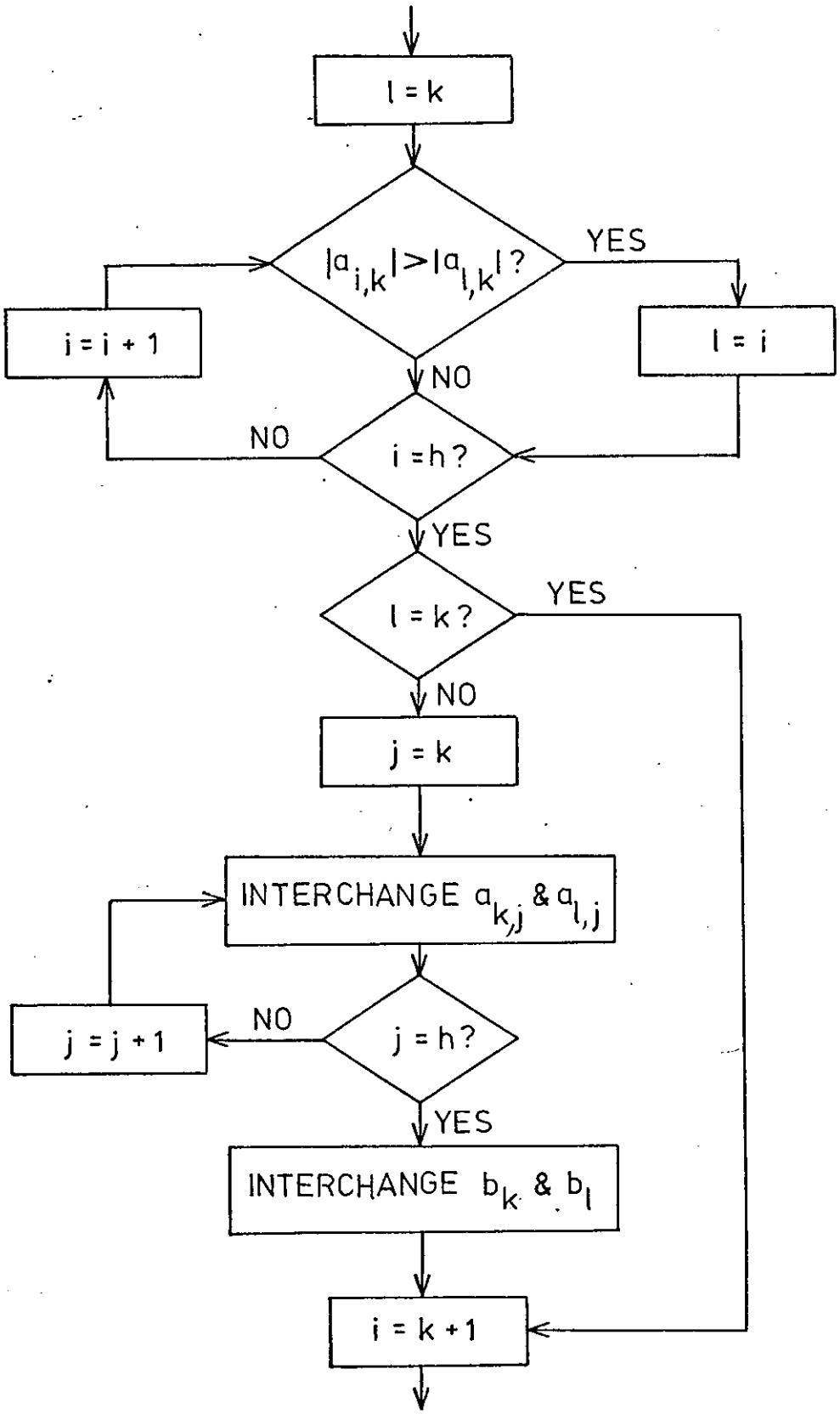

Appendix 2

Kemp, R.J. Murgatroyd, P.N. Walker, N.J. Self resonance in foil inductors. Electronics Letters, 11 (15), July 1975

SELF RESONANCE IN FOIL INDUCTORS

Indexing terms: Circuit resonance, Equivalent circuits, Inductors

Coils having aluminium-foil windings exhibit multiple self-resonant behaviour in the range 0·5–20 MHz. The dependence of resonance frequencies on number of turns is reported, and a lumped circuit model which accounts approximately for the effects is presented.

The phenomenon of self resonance in wire coils is well known, yet is poorly understood in detail. Welsby[1] describes how the impedance of a coil may be represented by a circuit comprising a resistance and an inductance in series, both shunted by an effective capacitance. This circuit has an impedance maximum when the inductance resonates with the capacitance, and, above this frequency, the impedance falls, approaching the behaviour of the capacitance alone. This is what usually happens in practice. However, depending on the way the coil is wound, the impedance may have other resonances at frequencies above the first;[1] these are said to occur because, if loosely coupled, the coil may behave as a transmission line.

Recent work at Loughborough has shown complicated self-resonant behaviour in foil coils. These coils are made from a single strip of aluminium foil and a slightly wider strip of plastics foil, wound together on a core of the plastics foil, using a capacitor-winding machine. The method of construction and the principal dimensions are shown in Fig. 1

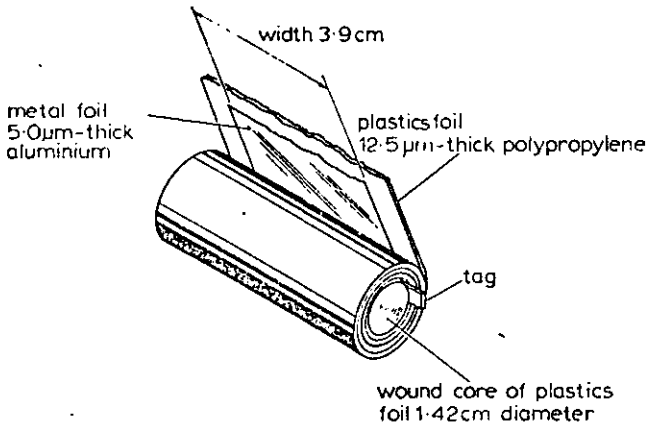

Fig. 1 *Construction of foil inductors*
N turns, 10 < *N* < 1000

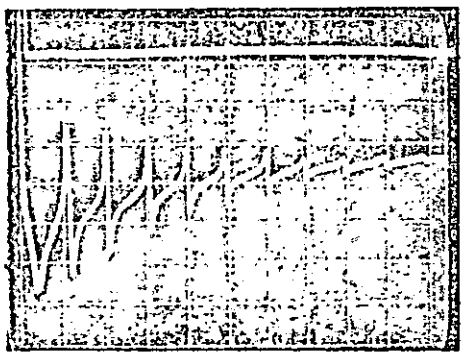

Fig. 2 *Noise attenuation measured with 1000-turn foil inductor*
Abscissa: 1 MHz per square, range 0–10 MHz
Ordinate: 10 dB attenuation per square, zero at top

Compared with a wire coil with the same number of turns, we would expect self-resonant behaviour to be more pronounced and to occur at lower frequencies, as all turn-to-turn capacitances are much higher. The impedance of a typical experimental foil coil is shown in Fig. 2. The coil was connected in series with a white-noise generator* and a spectrum analyser†, which gives the 20 Hz to 20 MHz spectrum flat to within ± 1·5 dB. The horizontal line at the top of Fig. 2 is the noise spectrum measured with the coil out of circuit. The jagged trace below is the spectrum observed with a 1000-turn coil in series with the noise generator. Noise minima, hence impedance maxima, occur at 0·49, 1·3, 2·18 MHz etc., and noise maxima, hence impedance minima, occur at 1·18, 2·1, 3·12 MHz etc.

* General Radio 1383

† Hewlett-Packard, sections 8553B, 8552B and 14T

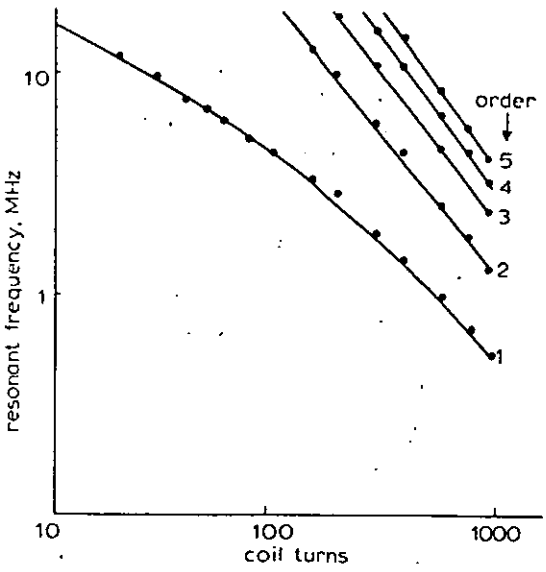

Fig. 3 *Dependence of the first five resonance frequencies on number of turns*

Fig. 3 shows how the frequencies of the impedance maxima depend on the number of turns, for a series of coils having the same core size and wound with the same materials. For each order of resonance there is a clear decreasing trend of frequency with increasing number of turns. The graph for the first resonance has a gradient of −0·53, for coils having less than 50 turns. This seems to fit a simple model, which depends on the thickness of winding being small compared with the radius of the core. We suppose that all turns are perfectly coupled to each other, and that all turns have identical self inductance L and interturn capacitance C. The total inductance is $L_T = N^2L$ and the total capacitance $C_T = C/N$, where N is the number of turns. Then

$$\omega_1 = \frac{1}{\sqrt{(L_T\, C_T)}} = \frac{1}{\sqrt{(NLC)}} \quad . \quad . \quad . \quad . \quad . \quad (1)$$

For more than 50 turns the gradient steepens and the coil can no longer be considered as perfectly coupled.

To account fully for the multiple-resonance properties we expect that a field analysis is needed. However, rather than attempt this formidable task, we have examined an extension of the simple model mentioned. The coil is divided into S subsections, within which phase shifts are deemed negligible. The uth subsection is then considered to have a self inductance L_u, a self capacitance C_u, a resistance R_u, and a mutual inductance M_{uv} with the vth subsection. This gives the circuit in Fig. 4. The self inductances L_u can be estimated by assuming that the current is uniform across the width of the foil and that $L_u = n_u^2\, l_u'$ where l_u' is the self inductance of a single turn at the centre of the subsection which has n_u turns. A similar procedure gives the mutual inductances. The capacitances C_u can be found by treating each turn and its neighbour as a parallel plate capacitor and the mid-section value is c_u, thus $C_u = c_u/N_u$. The a.c. resistance cannot be found without assuming that the current does not vary in phase through the coil, so in this initial study the d.c. resistance R_u was used.

The circuit in Fig. 4 results in S mesh equations, where S is the number of subsections, of the form

$$j\omega M_{1,u} P_1 + j\omega M_{2,u} P_2 + \ldots + (1/j\omega\, C_u + j\omega L_u + R_u)\, P_u + \ldots + j\omega M_{S,u} P_S = 1/j\omega\, C_u \qquad u = 1, 2, \ldots, S \quad . \quad . \quad (2)$$

where ω is the angular frequency and $P_u = I_u/I_0$ is the ratio fo the current in the uth subsection to the external current I_0.

For the external circuit,

$$V_0/I_0 = Z_0 = \sum_{u=1}^{u=S} (1 - P_u)/j\omega C_u \quad . \quad . \quad . \quad . \quad . \quad (3)$$

The S equations of the form of eqn. 2 can be written in matrix form as

$$[A]\,[P] = [b] \quad . \quad . \quad . \quad . \quad . \quad . \quad . \quad . \quad . \quad (4)$$

where $[A]$ is the complex matrix of the coefficients from the left-hand side eqn. of 2, $[P]$ is the vector of the complex unknowns and $[b]$ is the vector of terms $1/j\omega C_u$. Eqn. 4 can be expanded into a $S \times S$ real matrix equation of the form

$$\begin{bmatrix} \mathrm{Re}\,A & -\mathrm{Im}\,A \\ \mathrm{Im}\,A & \mathrm{Re}\,A \end{bmatrix} \begin{bmatrix} \mathrm{Re}\,P \\ \mathrm{Im}\,P \end{bmatrix} = \begin{bmatrix} \mathrm{Re}\,b \\ \mathrm{Im}\,b \end{bmatrix} \quad . \quad . \quad . \quad (5)$$

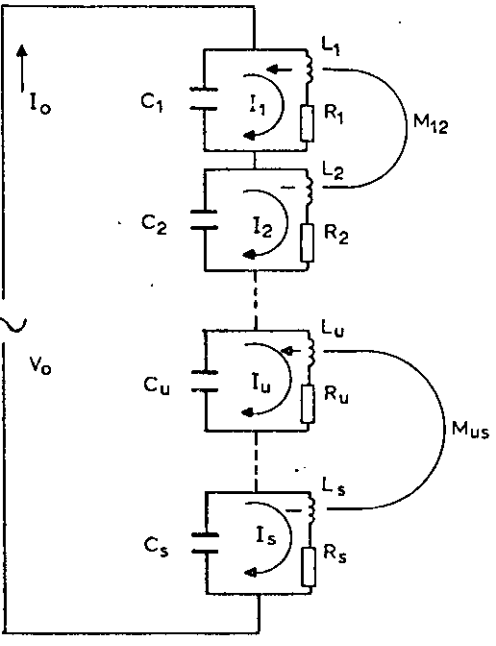

Fig. 4 *Equivalent circuit model*
All inductors are mutually coupled to each other

In this study, eqn. 5 is solved numerically using a Gaussian elimination method[2] for a range of frequencies ω. This method, although not ideally suited to the solution of large matrices, was used because problems were encountered with the convergence of iterative methods. Once evaluated, the reduced currents P_u were inserted in eqn. 2 to find the impedance, and, by plotting $|Z_0|$ against ω, the spectrum was obtained. Table 1 shows the results, for the first four resonances, of a study of one of the coils in Fig. 3, the 300-turn coil divided into 10 (S) equal sections. The discrepancy between the predicted and the observed frequencies varies from 4 to 11% and increases with the order of resonance, for the example presented here. However, the theory includes approximations which may account for the discrepancy, and the agreement with experiment is sufficient to suggest that the lumped-circuit model is broadly appropriate.

Table 1 COMPARISON OF THEORY AND EXPERIMENT FOR MAXIMUM IMPEDANCE RESONANCES

Order of resonance	1	2	3	4
Theory, MHz	1·82	5.8	10·1	14·5
Experiment, MHz	1·94	6·15	11·3	16·25

Improvements are at present being made to the approximations used in the calculation of the L_u and M_{uv}, and account will be taken of the a.c. resistance.

R. J. KEMP‡
P. N. MURGATROYD
N. J. WALKER§

19th June 1975

Department of Electronic & Electrical Engineering
Loughborough University, Leics., England

References

1 WELSBY, V. G.: 'The theory and design of inductive coils' (Macdonald, 1960), chap. 2, pp. 31–39, chap. 8, pp. 144–151
2 FROBERG, C.: 'Introduction to numerical analysis' (Addison-Wesley, 1965), chap. 4, pp. 73–76

‡ R. J. Kemp is now with the British Post Office Corporation

§ The work of N. J. Walker is supported by the Plessey Company Ltd.

Appendix 3

Murgatroyd, P.N. Walker, N.J. Frequency-dependent inductance and resistance of foil conductor loops. Proc. IEE, 124 (5), May 1977, 493

Frequency-dependent inductance and resistance of foil conductor loops

P.N. Murgatroyd, B.Sc., Ph.D., F.S.S., M.Inst. P., C.Eng., M.I.E.E., and N.J. Walker, M.Sc.

Indexing terms: Coils, Inductance, Resistance (electric)

Abstract

For both economic and technical reasons, flat thin conductors are of increasing interest in coil-winding. A problem is that at relatively low frequencies the current flow may may be nonuniform over the conductor cross-section. Both inductance and resistance of coils become frequency dependent. We have developed a new and general calculation of these effects, using a circuital model, for a single turn of a foil coil. The nonuniform current flow is described. We show that the extra losses due to this increase with the square of frequency, and that there is a small fall of inductance with increasing frequency.

List of symbols

a = radius of foil loop
c = axial length of foil loop
t = foil thickness
N = number of strips
w = width of strip
ρ = resistivity of metal
μ_0 = free-space permeability = $4\pi \times 10^{-7}$ Hm^{-1}
ω = angular frequency of applied voltage
ζ = dimensionless angular frequency
δ = nominal skin depth
R_0 = d.c. resistance of foil loop
L_0 = d.c. inductance of foil loop
R_{AC} = additional a.c. resistance of foil loop
L_{AC} = frequency-dependent inductance of foil loop
R = d.c. resistance of one strip
L = self-inductance of one strip
α, β = suffices denoting strips
$M_{\alpha\beta}$ = mutual inductance of two strips
$M_{\alpha\beta}$ = matrix of mutual inductances
$K_{\alpha\beta}$ = coupling coefficient of two strips
$K_{\alpha\beta}$ = matrix of coupling coefficients
F = shape factor in self inductance
$G_{\alpha,\beta}$ = shape factor in mutual inductance
I_0 = total current to foil loop
V_0 = applied voltage
Z_0 = impedance of foil loop
I_α = current in strip α
ϕ_α = flux threading one strip
$S(\zeta)$ = loop admittance, frequency dependent
t_α = dimensionless admittance of strip α
$j = \sqrt{-1}$

1 Introduction

For most applications, copper is the preferred material for conductors. Silver has a marginal advantage in conductivity but this is normally outweighed by greater cost. Aluminium has a definite cost advantage, but this has only rarely been exploited because the conductivity is lower. From time to time, and especially during wars[1] or other periods of uncertain supply of copper, the relative cheapness of aluminium has stimulated new development.[2] Particularly in some power transformers,[3–5] aluminium sheet or strip windings have been used for at least twenty years. At present, interest in aluminium is increasing, and projections of world reserves and consumption[6] suggest that a long-term trend away from copper is inevitable.

The technical problem is not simply one of substitution of aluminium round wires for copper round wires. If this were done, all windings would need larger cross-sections to compensate the lower conductivity, and in many applications there would not be enough room. Aluminium can be rolled, more easily than copper, into wide flat foils. Because such conductors pack closely together, and also because the insulation must withstand one rather than many inter-turn voltages, it is possible to utilise space more efficiently in foil coils than in round-wire coils. Also, the heat-dissipation properties of foil coils tend to be superior, because, in spiral or clockspring windings, every foil provides its own all-metal heat path to the outside.

The change to foil windings introduces two new problems of electrical origin. Firstly the turn-to-turn capacitance is large compared with that of adjacent round wires. This may be useful in some applications,[7] though possibly a nuisance in others because radio-frequency resonances[8] can occur. Secondly, the wide section of the foil, even though the area may be little greater than that of the round wire of equal d.c. resistance, is vulnerable to enhanced losses with a.c. due to nonuniform current flow over the cross-section.

It is the latter problem, which we term width effect, that is the main subject of this paper. Two examples illustrate the problem. In foil coils,[8,9] the resonant frequencies can be predicted with fair accuracy, but if d.c. resistance is used, the calculated Q turns out to be at least an order of magnitude greater than the measured Q. Detailed understanding of this is a long way off, but we are sure that nonuniform current flow is the basic cause. A simple experiment* using fine-wire search coils leaved into a foil inductor during original winding has confirmed this qualitatively. For our second example we comment on the properties of some air-cored chokes wound from thick aluminium foils for use in power system applications. It is found that the (additional) a.c. resistance rises rapdily with frequency, possibly as the square. This is particularly important when spiky waveforms are present, because of the high harmonic content. A report that a coil of like construction failed due to overheating near the edge of the windings, and not as one might expect near the middle of the foils, again suggests that the current density may be largest near the foil edges.

To calculate the complete current flow in a foil inductor of many turns is a formidable problem for future work. As a first step we have analysed the flow in a single foil turn, using a circuital model. By considering the turn as a number of narrow coils in parallel, we are able to calculate the current distribution, and show how it changes in amplitude and phase across the foil as the frequency is increased. We show how the effective resistance and inductance, respectively, rise and fall with increasing frequency, and that at low frequencies the additional a.c. resistance rises with the square of the frequency.

2 Current flow in a foil turn

A single foil turn is shown in Fig. 1*a*. It is made from material of uniform thickness t, width c, formed to mean radius a, and always $t \ll a$. The large hypothetical busbars are shown to emphasise that the connections to the turn are equipotentials, and we then expect, and hereafter assume, that all current flow in the turn is purely circumferential.

To examine the variation of current density within the cross-section of the foil, we now divide it into strips in the axial direction, as shown in Fig. 1*B*. It is convenient to have N strips of equal width w, so $Nw = c$ (though in principle all strip widths could be different) and w must be chosen so the expected variation of current density within is small. What the model seeks to do, therefore, is represent what must be a continuous variation by a finite number of steps.

Without knowing the answer in advance, the choice of w is to some extent arbitrary. Clearly, however, w need not be much smaller than the nominal skin depth δ, i.e.

$$w \lesssim \delta = \sqrt{\frac{2\rho}{\mu_0 \omega}}$$

Paper 7867S, first received 2nd August and in revised form 8th December 1976

Dr. Murgatroyd and Mr. Walker are with the Department of Electronic and Electrical Engineering, Loughborough University of Technology, Loughborough, Leicestershire LE11 3TU England

* REEVES, R.: Unpublished work at the Plessey Company Ltd., Bathgate, Lothian, Scotland.

here ρ is the material resistivity. At sufficiently high frequencies ere could be current density variations within the thickness of the il, but we shall exclude these by only considering low frequencies

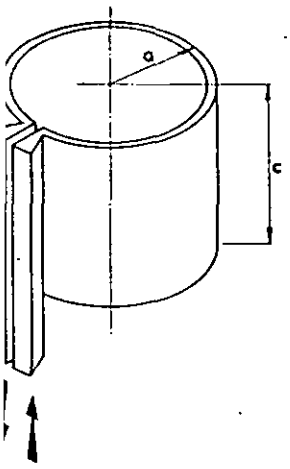

g. 1A
ngle foil turn with equipotential connecting bars

ich that $t \ll \delta$. The highest frequency for which our calculation ould be a valid approximation would be given by $t = w \sim \delta$. The d.c. sistance of a strip is given by

$$R = \frac{2\pi a\rho}{wt} \tag{2}$$

id the d.c. resistance of the complete turn is $R_0 = R/N$. The induc- nce of a strip is given by[10]

$$L = \mu_0 a\left[\log\frac{\delta a}{w} - \frac{1}{2}\right] = \mu_0 aF \tag{3}$$

hich is calculated on the assumptions of t negligible and uniform irrent density within w. The mutual inductance between any pair of rips can be calculated[10] using the formula appropriate for coaxial rcular filaments. It has the form

$$M_{\alpha,\beta} = \mu_0 a G_{\alpha,\beta}. \tag{4}$$

here $G_{\alpha\beta}$ is a dimensionless factor dependent on the ratio d_a, where is the axial separation of the filaments denoted by subscripts α and

The complete foil turn is represented by the equivalent circuit Fig. C. Each strip is represented by a constant (d.c. value) resistance in eries with an inductance, and all the inductances are mutually coup- d together. The width effect can be predicted at once from the llowing physical argument. Suppose as a first approximation that ie currents I_α in all strips are equal. Each current is driven by the me applied voltage, but opposed by a different set of inductive back m.f.s. A strip at, or near, the foil edge has all or most of the outer rips to one side, and hence its neighbours are on average further way than are the neighbours of a strip at or near midfoil. Therefore, wards the edge, the total of back e.m.f.s is less than near midfoil id so as a first correction the currents near the edge will be greater ian those in midfoil.

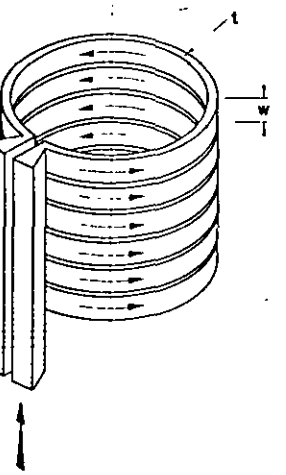

ig. 1B
ngle foil turn divided into equal parallel strips

3 Circuit equations

The equivalent circuit Fig. 1C is to be analysed. The external current I_0 is the sum of the strip currents I_α:

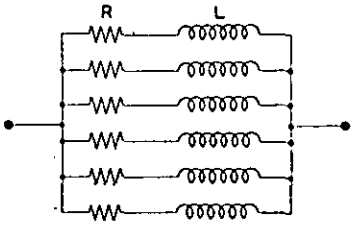

Fig. 1C
Equivalent circuit of divided turn (all inductors are mutually coupled)

$$I_0 = \sum_{\alpha=1}^{\alpha=N} I_\alpha \tag{5}$$

The circuit impedance is given by

$$Z_0 = \frac{V_0}{I_0} \tag{6}$$

The currents are found by solving the N simultaneous equations

$$V_0 = I_\alpha R + j\omega L I_\alpha + \sum_{\beta\neq\alpha} j\omega I_\beta M_{\alpha\beta} \tag{7}$$

We are here assuming all strips have equal width and hence equal R and L, though the calculations are readily generalised for all widths different.

To solve the equations it is convenient and efficient to reduce the problem to dimensionless form as follows. A generalised frequency ξ is defined by

$$\xi = \frac{\omega L}{R} \tag{8}$$

and a generalised admittance for strip α:

$$t_\alpha = \frac{RI_\alpha}{V_0} \tag{9}$$

The matrix of mutual inductances $M_{\alpha\beta}$ is replaced by a matrix of coupling coefficients $K_{\alpha\beta}$ where $K_{\alpha\beta} = M_{\alpha\beta}/L$. For coils having different radii but the same shape and divided into the same number of strips, $K_{\alpha\beta}$ is the same, and though the matrix has N^2 elements of which in general $1/2\ (N^2 + 1)$ values must be supplied, when the filaments are equally spaced only N distinct values are needed and in $K_{\alpha\beta}$ all elements equidistant from the diagonal are identical.

With the above transformations we are now required to solve the equations

$$t_\alpha(1 + j\xi) + j\xi\sum_{\beta\neq\alpha} t_\beta K_{\alpha\beta} = 1 \tag{10}$$

and the complete foil admittance will be given by

$$S(\xi) = \frac{1}{NR}\sum_{\alpha=1}^{N} t_\alpha \tag{11}$$

Since the t_α are complex we can re-organise eqn. 10 as $2N$ real equations. A number of methods of solution are available: we used Gaussian elimination in a Fortran program on the ICL 1904 S computer at Loughborough University.

4 Results

We have calculated the width effect for foil turns of about the size and shape used in power-frequency aluminium chokes. With $a = 5$ cm, $c = 5$ cm, and $N = 20$, we have $w = 0{\cdot}25$ cm. For aluminium the maximum frequency allowed by the criterion eqn. 1 is about 6400 Hz, which amply covers high harmonics of power frequencies. The same criterion may be used to set a maximum for the frequency variable ξ: there is no point in extending the dimensionless calculations beyond the region of physical validity. Using eqn. 2 and 3 with eqn. 8 we find

$$\xi_{max} = \frac{t}{w}\frac{F}{\pi} \tag{12}$$

and in the example above $\xi_{max} = 0{\cdot}36$ for $t = 0{\cdot}1$ cm

The nonuniform current distribution, and its dependence on fre-

quency, are shown in Fig. 2. In the particular example given, the magnitude of current flowing in midfoil strips is well below half that in the edge strips for $\xi = 1$, so a significant increase of effective resistance is expected. There is a variation of phase across the foil width, as shown in the Argand diagram, Fig. 3. Each solid line represents the fan of vectors $I_k(\omega t_k)$. As ξ increases the average phase of the fan

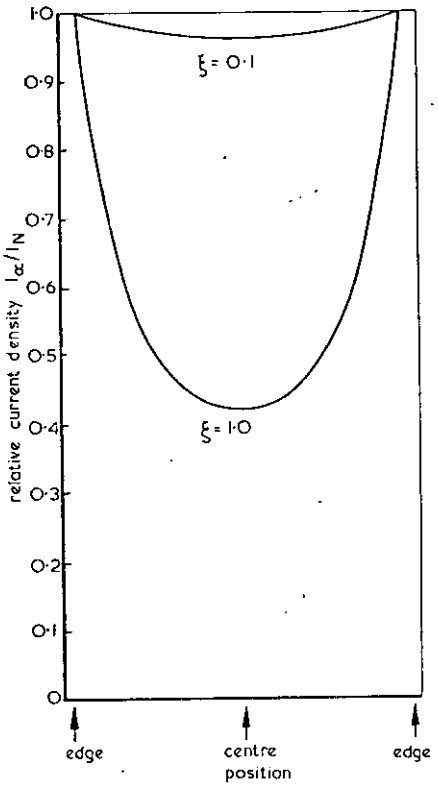

Fig. 2
Plot of relative magnitude of current density across foil width as a function of frequency (a = c)

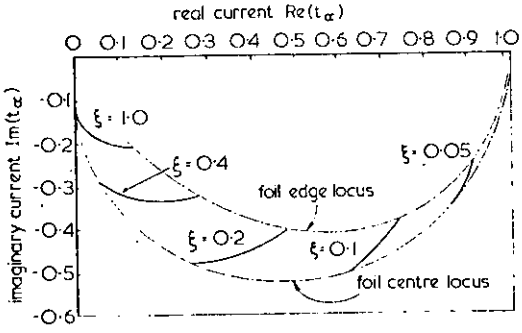

Fig. 3
Argand diagram showing phase and amplitude of current density across foil width, as function of frequency (a = c)

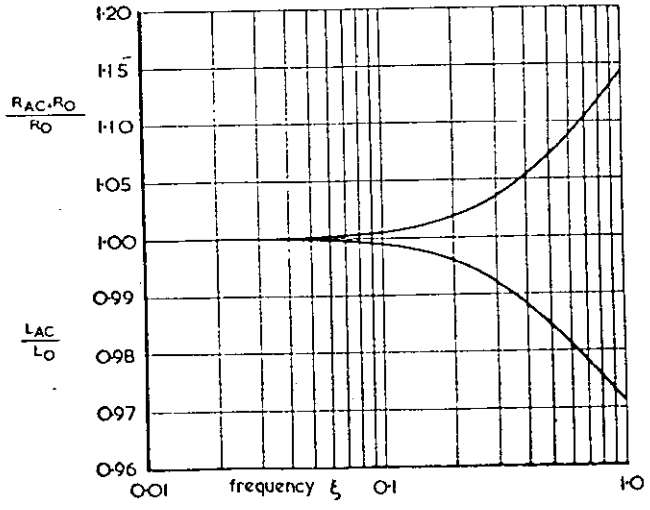

Fig. 4
Frequency dependence of resistance and inductance for single foil turn with a = c

(which is the phase of I_0 relative to V_0) has increasing lag, and the currents in midfoil always lag the larger currents near the edges.

The effective resistance and inductance of the foil turn are calculated by separating the real and imaginary parts of eqn. 11. Their variation with frequency, relative to the d.c. values, is shown in Fig. 4, for the same example. At $\xi = 1$ the fall of inductance is only 3%, and for many purposes this is negligible. The rise of resistance at 15% may need to be allowed for in foil choke design: we would anticipate somewhat larger effects in multiturn coils. Fig. 5 shows that the extra (a.c.) resistance is closely proportional to the square of the frequency. This behaviour is observed, approximately, in multiturn foil coils.

As the current profile changes with increasing frequency, we would expect the shape of the magnetic field within the coil also to change. A simple experiment, repeating the work of Reeves with a multiturn coil, showed that at low frequencies the axial flux near the centre of the coil was substantially larger than the axial flux near the edge, but as the frequency was increased these fluxes tended towards equality. Our calculations for a single turn show this effect. The strip α is threaded by flux ϕ_α given by

$$\phi_\alpha = I_\alpha L + \sum_{\beta \neq \alpha} I_\beta M_{\alpha\beta} \qquad (13)$$

Fig. 6 shows the profile of ϕ_α, as a ratio to the value at the centre of

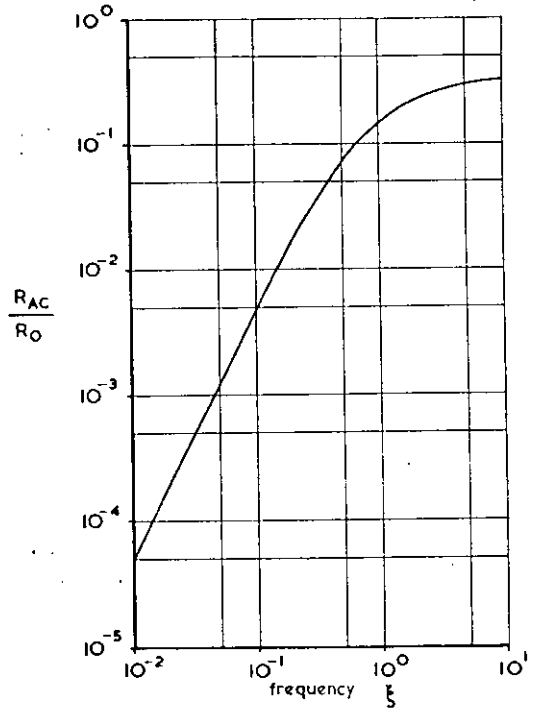

Fig. 5
Approximate square law dependence of excess a.c. resistance R_{AC}

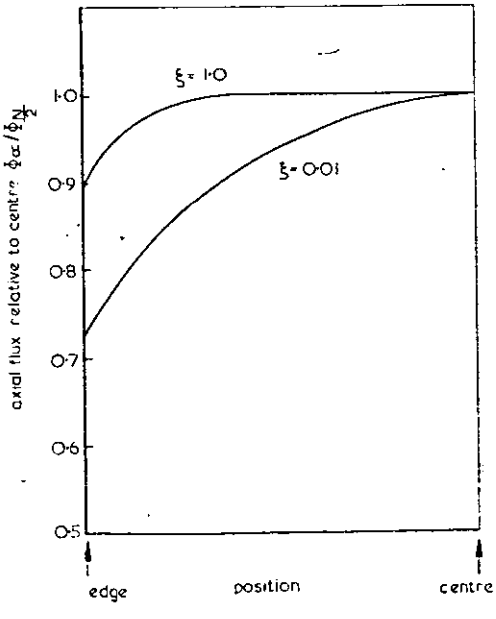

Fig. 6
Dependence of flux on axial position and frequency (a = c)

e turn, for two values of ξ, and the trend towards a flat profile is ar. At $\xi = 1{\cdot}0$, the curve is virtually flat over more than three-fifths the turn length. If we examine eqn. 7 in the limit of large frencies, and neglect the resistive term, we may then substitute from n. 13 and obtain

$$V_0 = j\omega\phi_\alpha \tag{14}$$

r all α. So the mathemetical limit gives equal flux through all secons. As the limit is approached, the shape of the current profile will ange no further, and for fixed V_0 the current amplitudes will all y in the same proportions. This regime was evident in our calcuions, though at frequencies above the range of interest, where we und that the increasing resistance and decreasing inductance both nded to approach limiting values as the frequency was increased. owever, we would expect in practice that these extremes would not observed due to other effects not included in the width-effect lculation (for example variations of current density across the thickss of the conductor in the manner of skin-effect in a single conctor) intervening at lower frequencies.

Treatment of the foil as a finite number of strips is an approxation, and some interest attaches to choosing a number that strikes acceptable compromise between accuracy and cost of computation. our particular example we studied the same shape of foil ($a = c$) th various N. With $N = 20$ and $N = 10$ there is negligible difference the calculated resistance and inductance at $\xi < 0{\cdot}5$, but with $N = 5$ e resistance value is low by about 3%. As a general rule such discrepcies increase as ξ increases, with larger N always giving somewhat rger resistance and smaller inductance. This is perhaps to be expecd, for narrower strips will more closely describe the regions near the il edges where the current density varies steeply. The recommended ocedure, adequate for most practical values of ξ, is to choose a value N, do the calculations for both N and $N/2$, and accept the two sults up to such frequency that the differences between them are gligible.

The width effect has also been investigated for coils with different lues of the ratio a/c. For the same frequency the added a.c. resistance tends to be larger, and the fall of inductance smaller, as a/c increases, i.e. the foil is relatively narrower. We expect that full details of this will be published soon.

5 Conclusion

It has been shown that the inductance and resistance of a single foil turn are expected to vary with frequency due to nonuniform current profiles across the foil width. The calculation uses a minimal set of dimensionless variables to give results in the most general form possible. Our example shows that the 'width effect' will have to be taken into account in the design of aluminium foil chokes at power frequencies.

6 Acknowledgment

The work of N.J. Walker is supported by a scholarship from the Science Research Council.

7 References

1 PELIKAN, T.: 'Modern distribution transformers with aluminium foil windings', *Brown Boveri Rev.*, 1967, 54, pp. 376–381
2 WITZIG, H., and BENNETT, D.A.: 'Coil winding with aluminium – recent alloy and foil developments'. Coil Winding International Convention, London, March 1974
3 OWEN, E.: 'Solving transformer problems with aluminium foil', *Electr. Equip.*, March 1971
4 GREEN, H.E.: 'The economics of aluminium for power transformer windings', *Electr. Rev.*, 1973, pp. 631–632
5 GREEN, H.E.: 'Aluminium windings in large transformers', *Electr. Export Rev.*, 1974, 3, pp. 52–55
6 TAYLOR, G.R.: 'How to avoid the future' (Secker and Warburg, 1975)
7 REEVES, R.: 'Choke-capacitor hybrid as a fluorescent lamp ballast', *Proc. IEE*, 1975, 122, (10), pp. 1151–1152
8 KEMP, R.J., MURGATROYD, P.N., and WALKER, N.J.: 'Self resonance in foil inductors', *Electron. Lett.*, 1975, 11, (15), pp. 337–338
9 WALKER, N.J.: M.Sc. thesis, Loughborough University, 1975
10 GROVER, F.W.: 'Inductance calculations' (Van Nostrand, 1947), Chaps. 11 and 16

Appendix 4

Murgatroyd, P.N. Walker, N.J. The frequency dependence of resistance in foil-wound inductors. Electrocomponent Science and Technology, 5, 1979, 219

Electrocomponent Science and Technology
1979, Vol. 5, pp. 219–222

THE FREQUENCY DEPENDENCE OF RESISTANCE IN FOIL-WOUND INDUCTORS†

P. N. MURGATROYD and N. J. WALKER

Department of Electronic and Electrical Engineering,
Loughborough University of Technology, Leicestershire, England

(Received June 1, 1978; in final form August 1, 1978)

Foil wound air-cored inductors are widely used in power electronics applications, and often exhibit power dissipation much greater than can be accounted for by the d.c. resistance. This is shown to be due to non-uniform current flow. A scaling rule, relating the effects to turns and frequency, is demonstrated. The general principle of equal current sharing can be satisfied in a toroidal system.

1. INTRODUCTION

For some years aluminium foil or thin sheet has been used to wind air-cored inductors for power-electronics applications. The inductors are relatively easy to make and are structurally simple and strong. The foil is wound, together with a slightly wider insulating sheet of (say) melinex, usually on a cylindrical former. Compared with a copper winding with the same rating and inductance, an aluminium foil inductor tends to be slightly bulkier, considerably lighter, and probably somewhat cheaper in material costs. If the comparison is made between a conventional multi-layer wire coil and a foil coil of similar electrical properties, the latter tends to have better thermal dissipation because every turn provides its own all-metal heat path to the outside.

We became interested in foil coils at Loughborough about five years ago, initially not through their importance in power electronics, but as a vehicle to study self-resonance in capacitors. Using an equivalent circuit model[1] we were able to calculate the self-resonant frequencies of foil coils,[2] which are due to the large turn-to-turn capacitance, but through using the d.c. foil resistance we always seriously over-estimated the coil Q's. Our explanation was non-uniform current flow, and we began to study the theory of a one-turn foil coil.[3] It was shown that the resistance of foil coils increases with frequency, and this "width effect" contributes to the overheating observed in some power electronics systems, particularly as chopper frequencies are increased, even though the inductors are apparently correctly rated.

This paper will describe the main features of the "width effect," and also suggest that a further non-uniformity of current flow, across the thickness of the foils, is important at the higher frequencies.

2. WIDTH EFFECT

This term describes the tendency of the current in a foil coil to flow more densely near the edges of the foil than in the centre, as the frequency is raised. The detailed solution is given elsewhere,[3] but the problem may be understood physically from the single-turn model of Figure 1. Let this turn be divided into equal strip-coils, such that in each one the current density is effectively uniform. The turn may now be represented by an equivalent circuit, Figure 2, of identical inductors, all in parallel and all mutually coupled. When the applied voltage amplitude is V, the currents are given by equations (one for each strip) of the form

$$V = I_\alpha R + j\omega L_\alpha I_\alpha + j\omega \sum_{\beta \neq \alpha} M_{\alpha\beta} I_\beta \qquad (1)$$

So the current I_α in strip α is related to the currents I_β in all the others.

To understand the width effect physically, first suppose that all the currents are equal. Then any inductor representing a strip near the middle of the foil is subject to strong mutual couplings from near-neighbours on both sides, whereas a strip at the edge has near-neighbours on only one side, so the total inductive back-voltage there is less. Therefore

†This paper is based upon a lecture given by Dr. Murgatroyd to the Institution of Electrical Engineers colloquium on "Trends in Forced Commutation Components", on 12th January 1978.

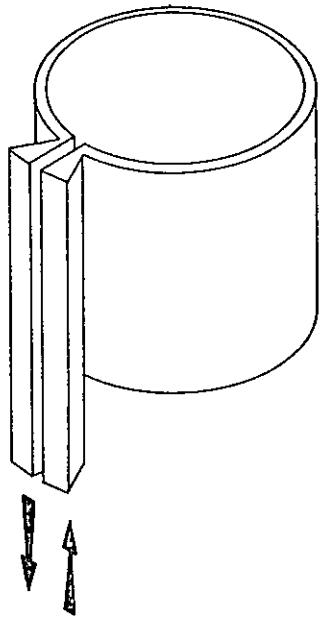

FIGURE 1 One-turn foil coil with torus-bars to maintain equipotential connections.

the currents cannot all be equal, and must therefore be larger near the edge than in the middle.

Our calculations used 40 equal strips to represent the turn. The current profile is clearly symmetrical, but this still leaves 20 complex unknowns, so requires the inversion of 40 x 40 matrices. For a given turn geometry the calculation is repeated for a range of frequencies. For increasing frequency, the following general results are obtained:

1) The current density at the centre decreases and lags in phase relative to that at the edge.

2) The turn inductance decreases, and the turn resistance increases somewhat faster, and the extra resistance is initially proportional to the square of frequency.

3) The axial magnetic field becomes increasingly uniform.

4) Within the model of "width effect," all the foregoing effects do not increase indefinitely with frequency, but approach a limit. Just as at d.c. the current profile across the width is uniform and is completely controlled by the foil resistances, there is in the high frequency limit another current profile that is completely controlled by the foil inductances. (This means that the known high-frequency properties of some coils cannot be due to "width effect" alone).

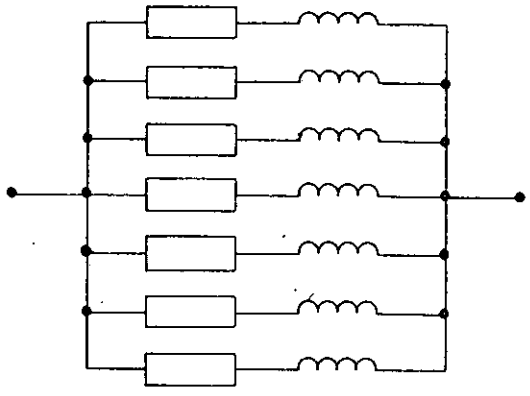

FIGURE 2 Equivalent circuit to represent "width effect" in a one-turn foil coil.

These results have been checked experimentally by bridge measurements over a range of frequencies.[4] It was not possible to do this with a one-turn coil: we used sets of N-turn coils (N = 25, 50, 100) made with thin foil such that the buildup of turns was small compared with the internal diameter. In this instance the theory indicates a scaling rule for the "width effect": the proportional changes of inductance and resistance in a one-turn coil at frequency F will occur in an N-turn coil at frequency F/N. This rule is demonstrated in Figure 3: the coils were made from foil 60 mm wide, 50 μm thick, on an internal diameter of 64 mm. The rule predicts that with the abscissal scale of turns x frequency, results for different coils must superpose, and this happens reasonably well. There is however a significant departure from the "width effect" theory at higher frequencies: theory predicts a levelling off, but in practice the resistance continues to rise with frequency. This is believed to be due to another effect, current non-uniformity across the foil thickness, and will be discussed.

Unlike our coils, which were specially made to test the theory, the commercial coils for use in thyristor circuits usually have a much larger build-up, to perhaps a square cross-section of windings, and foils perhaps as thick as 1·5 mm are used. Calculations for this type of coil have been done[5] by an essentially similar method, except that the coil is divided into subsections along the foil length as well as axially. The equivalent circuit then has the form of Figure 4, and it allows for the possibility that the current density profile across the width may itself be dependent on radius. Small differences were calculated. The overall resistance increases calculated

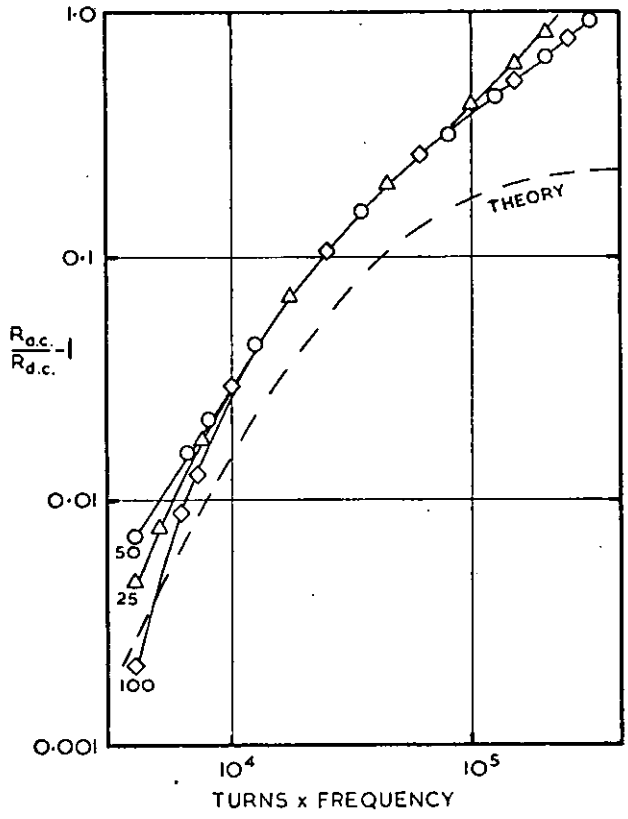

FIGURE 3 Resistance vs. Turns-frequency product in multiturn foil coils, demonstrating scaling.

were 19% and 23% for two particular cases, and most of the calculations were for a fixed frequency of 50 Hz. This is an important limitation, for thyristor chopper circuits at over 500 Hz are now in use, and the waveforms have a high harmonic content. Our measurements have shown resistance increases of over 300% in thin foil coils, and much more in thick foil coils. The conclusion drawn is that while calculations of "width effect" are moderately successful at low frequencies, they eventually fail, and it is believed that the current density profile must also become non-uniform across the foil thickness.

3. THICKNESS LOSSES

It might perhaps be thought that provided the penetration depth δ, given by the standard formula, is large compared with the foil thickness λ, then no appreciable non-uniformity is possible. However, every foil is subject to the axial field of all the others: this collective field acts most strongly in the innermost and outermost turns. A simple theory suggests the formula

$$R_{a.c.} = R_{d.c.}\left(1 + \frac{N^2}{72}\frac{\lambda^4}{\delta^4}\right) \tag{2}$$

This formula depends on rather sweeping assumptions and is not accurate. However the number 72 is an upper limit, so thickness losses will probably be worse than the formula suggests, and are additional to "width effect." The corresponding formula for skin effect in a single foil is

$$R_{a.c.} = R_{d.c.}\left(1 + \frac{1}{45}\frac{\lambda^4}{\delta^4}\right) \tag{3}$$

so the collective effect of N-turns is clear.

The formula may possibly explain a curious observation. In a particular invertor application, a coil ran hot, and was replaced by another with thicker foil conductors and presumably higher current rating. However the new coil ran even hotter. The decrease of d.c. resistance may well have been overtaken by the dependence on λ^4 in the thickness losses. The formula in Eq. (2) also may explain why our measurements, shown in Figure 3, still obeyed the turns-frequency rule at large departures from the "width effect" theory. Since N^2/δ^4 is proportional to $N^2\omega^2$ the rule still holds.

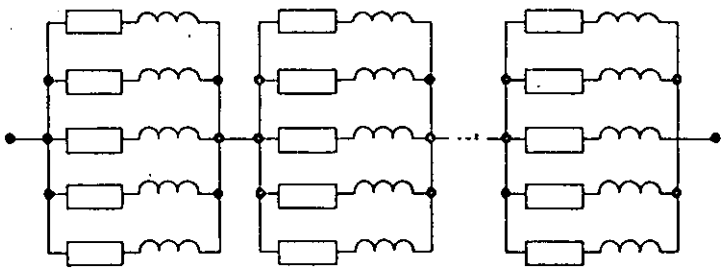

FIGURE 4 Equivalent circuit to represent "width effect" in a multiturn foil coil.

4. APPROACHES TO OPTIMUM DESIGN

There are a number of possible criteria for optimum design of foil coils, depending on their applications. The optimum shapes have been calculated[5] for best Q, against "width effect" losses. However these shapes are only likely to be valid at quite low frequencies. In applications involving pulsed currents, hence high harmonics, it is likely that the thickness losses will be important, and ought to be considered in any situations where the effective a.c. resistance is more than 50% greater than the d.c. resistance.

A general principle for design is evident in Figure 2 and Figure 4. If it can be arranged that, for every inductor in each one-turn circuit, the sum of the mutual inductances with *all* other inductors in the circuit is a constant, then the current is equally shared and the "width effect" is eliminated.
A geometry that has this property is shown in Figure 5. The torus is to be considered as complete, the break is only for purposes of illustration.
Clearly in this one-turn foil coil all current paths round the minor circumference, from one bus-ring to the other, are geometrically identical to each other and in their relation to the coil as a whole.
The authors do not imagine that such a construction, especially with many turns, is a practical or commercial proposition. However the basic principle of current sharing, together with the fact that toroidal coils enclose their flux and so do not create eddy currents and interference elsewhere, suggest that for the most demanding applications an approach to toroidal design, perhaps in paralleled sub-sections, will be required.

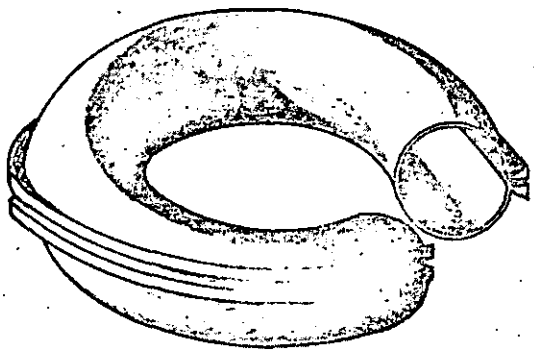

FIGURE 5 The one-turn foil torus (cut away drawing): an optimum design against "width effect."

ACKNOWLEDGEMENTS

We wish to thank Mr. B. Martindale of Aluminium Inductors Ltd. for supplying test devices, and Mr. P.G. LeGood of Loughborough University for his telepathic artwork.

REFERENCES

1 P. N. Murgatroyd, Field and circuit models for the wound foil inductor, *Electrocomp. Sci. and Technol.*, 3, 97–102 (1976).
2. R. J. Kemp, P. N. Murgatroyd and N. J. Walker, Self-resonance in foil inductors, *Electron. Lett.*, 11, 337–8 (1975).
3. P. N. Murgatroyd and N. J. Walker, Frequency-dependent inductance and resistance of foil conductor loops, *Proc. I.E.E.*, **124**, 493–6 (1977).
4. N. J. Walker, Ph.D. Thesis, Loughborough University.
5. M. M. El-Missiry, Calculation of current distribution and optimum dimensions of foil-wound air-cored reactors, *Proc. I.E.E.*, **124**, 1073–7 (1977).

Appendix 5

Murgatroyd, P.N. Walker, N.J. Lumped-circuit model for inductor-capacitor hybrid. Electronics Letters, 12 (1), Jan. 1976

LUMPED-CIRCUIT MODEL FOR INDUCTOR-CAPACITOR HYBRID

Indexing terms: Capacitors, Distributed-parameter networks, Equivalent circuits, Inductors, Lumped-parameter networks

The inductor–capacitor hybrid described by Reeves is analysed by a lumped-circuit model, in which the metal foils in the device have finite resistance. The earlier theory appears as a special case of the model, and some difficulties at the principal resonance are removed.

In recent papers,[1, 2] Reeves has described a hybrid inductor–capacitor device made by winding alternate layers of paper and aluminium foil on a ferromagnetic former. The theory of the device[2] rests on the assumption that the resistance of the metal foils is negligibly small. The theory predicts, *inter alia*, that if operated at its resonance frequency the hybrid supplies the same current into any load resistance.[1] Although this may be approximately so if the load resistance is small, it cannot be reasonable to expect the device to deliver ever increasing power as larger and larger resistances are connected. We show that this difficulty does not appear if the hybrid is modelled by discrete elements, including finite resistance for the metal foils.

The lumped circuit model is shown in Fig. 1. Each metal foil is notionally divided into two parts connected in series, each half having inductance L and resistance R in series. The capacitance of the hybrid is represented, in this simplest of models, by a single capacitance C connected between the midpoints of the foils. It suffices here to assume that all the

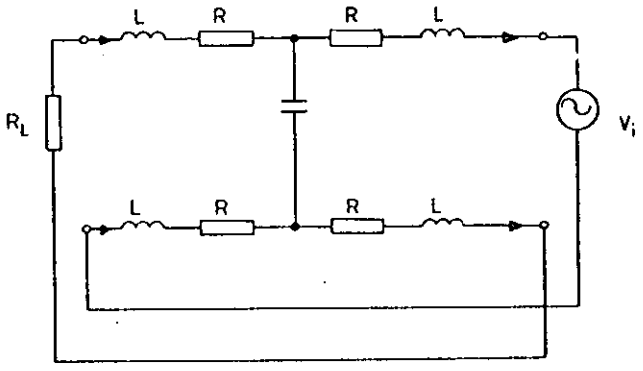

Fig. 1 *Equivalent circuit of hybrid showing current flow at low frequency*
All possible pairs of inductances have mutual coupling M

inductors and all the resistors are equal, and also that each inductor has mutual inductance M to all the others; owing to the stacking of foils these equalities will not be exact in

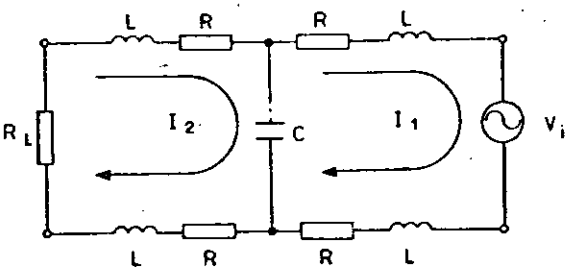

Fig. 2 *Redrawn circuit for mesh analysis*
All possible pairs of inductances have mutual coupling M

practice. In Fig. 2 the circuit has been rearranged to facilitate a mesh analysis, as follows:

$$V_i = 2RI_1 + (I_1 - I_2)/j\omega C + 2I_1\, j\omega L + 2I_1\, j\omega M + 4I_2\, j\omega M \quad (1)$$

$$0 = I_2 Z_L + 2RI_2 + (I_2 - I_1)/j\omega C + 2I_2\, j\omega L + 2I_2\, j\omega M + 4I_1\, j\omega M \quad (2)$$

These equations simplify to

$$V_i = I_1 T - I_2 S \quad . \quad . \quad . \quad . \quad . \quad . \quad . \quad . \quad . \quad . \quad (3)$$

$$I_1 S = I_2(Z_L + T) \quad . \quad . \quad . \quad . \quad . \quad . \quad . \quad . \quad . \quad . \quad (4)$$

where

$$S = 1/j\omega C - 4j\omega L \quad . \quad . \quad . \quad . \quad . \quad . \quad . \quad . \quad . \quad (5)$$

$$T = 2R + 4j\omega L + 1/j\omega C \quad . \quad . \quad . \quad . \quad . \quad . \quad . \quad . \quad (6)$$

and we have now assumed perfect coupling, $M = L$. We define a resonance frequency ω_0 by the equation $4\omega_0^2 LC = 1$. At resonance we have $S = -8j\omega_0 L$ and $T = 2R$.

We note that, since Reeves[2] denotes by L the inductance of a complete foil, which is four times the inductance of half a foil, which we call L, our frequency ω_0 is the same as Reeves's.

The principal equations given by Reeves to describe the currents and voltages in the hybrid appear as special cases of eqns. 3 and 4 when R is set to zero.

The output current of the device is given by

$$I_2 = \frac{V_i S}{Z_L T + T^2 - S^2} \quad . \quad . \quad . \quad . \quad . \quad . \quad . \quad . \quad . \quad (7)$$

At the resonance frequency, and letting R go to zero, we obtain Reeves's result:

$$I_2 = \frac{V_i}{8j\omega_0 L} \quad . \quad . \quad . \quad . \quad . \quad . \quad . \quad . \quad . \quad . \quad (8)$$

i.e. the current is independent of the load. If, however, we keep R finite and let Z_L become large, we obtain

$$I_2 = -\frac{4j\omega_0 LV_i}{Z_L R} \quad . \quad . \quad . \quad . \quad . \quad . \quad . \quad . \quad . \quad (9)$$

which decreases with increasing resistive loads. When the output to the hybrid is open circuit, the voltage multiplication ratio $|V_0/V_i|$ has a maximum value of $2Q$ at resonance, where $Q = R^{-1}(L/C)^{\frac{1}{2}}$.

The input current is given by

$$I_1 = \frac{V_i(Z_L + T)}{Z_L T + T^2 - S^2} \quad . \quad . \quad . \quad . \quad . \quad . \quad . \quad . \quad . \quad (10)$$

Again, at the resonance frequency, and letting R go to zero, we find

$$I_1 = \frac{V_i Z_L}{(8\omega_0 L)^2} \quad . \quad . \quad . \quad . \quad . \quad . \quad . \quad . \quad . \quad . \quad (11)$$

For a resistive load this agrees with Reeves's result, and shows that, if the same current is indeed to be delivered into increasingly large loads, the input current must rise in proportion to the load. Returning to eqn. 10, if we keep R finite and let Z_L become large, we find

$$I_1 = \frac{V_i}{2R} \quad . \quad . \quad . \quad . \quad . \quad . \quad . \quad . \quad . \quad . \quad . \quad (12)$$

indicating that the input current is, in fact, limited by the foil resistance.

In conclusion, we remark that the behaviour of the hybrid is completely described by eqns. 3, 4, 5 and 6 subject to the assumptions stated and provided the frequency is not too high. The second resonance of the hybrid[2] we suggest is due to a failure of the 'short' assumption. A multiple lumped equivalent circuit,[3] in which each foil is described by a number of inductive sections crossconnected by subdivisions of the complete capacitance, may be required to describe such behaviour.

Acknowledgment: The work of N. J. Walker is supported by the UK Science Research Council.

P. N. MURGATROYD
N. J. WALKER

1st December 1975

Department of Electronic & Electrical Engineering
Loughborough University, Leics. LE11 3TU, England

References

1 REEVES, R.: 'Choke-capacitor hybrid as a fluorescent lamp ballast', *Proc. IEE*, 1975, 122, (10), pp. 1151–1152.
2 REEVES, R.: 'Inductor-capacitor hybrid', *ibid.*, 1975, **122**, (11) pp. 1323–1326
3 KEMP, R. J., MURGATROYD, P. N., and WALKER, N. J.: 'Self resonance in foil inductors', *Electron. Lett.*, 1975, 11, pp. 337–338